AWARD NUMBER: W81XWH-14-1-0625

TITLE: Plasticity and Activation of Spared Intraspinal Respiratory Circuits Following Spinal Cord Injury

PRINCIPAL INVESTIGATOR: Paul J. Reier, Ph.D.

CONTRACTING ORGANIZATION: University of Florida
Gainesville, FL 32611

REPORT DATE: December 2017

TYPE OF REPORT: Final

PREPARED FOR: U.S. Army Medical Research and Materiel Command
Fort Detrick, Maryland 21702-5012

REPORT DOCUMENTATION PAGE

Form Approved
OMB No. 0704-0188

1. REPORT DATE	2. REPORT TYPE	3. DATES COVERED
DECEMBER 2017	Final	29Sept2014 – 28Sept2017

4. TITLE AND SUBTITLE
"Plasticity and Activation of Spared Intraspinal Respiratory Circuits Following Spinal Cord Injury"

5a. CONTRACT NUMBER

5b. GRANT NUMBER
W81XWH-14-1-0625

5c. PROGRAM ELEMENT NUMBER

6. AUTHOR(S)
Paul J. Reier, Ph.D.

E-Mail: reier@ufl.edu

5d. PROJECT NUMBER

5e. TASK NUMBER

5f. WORK UNIT NUMBER

7. PERFORMING ORGANIZATION NAME(S) AND ADDRESS(ES)

University of Florida
Gainesville, FL 32611

Division of Sponsored Research
219 Grinter Hall
P.O. Box 115500
Gainesville, FL. 32611-5500

8. PERFORMING ORGANIZATION REPORT NUMBER

9. SPONSORING / MONITORING AGENCY NAME(S) AND ADDRESS(ES)

U.S. Army Medical Research and Materiel Command
Fort Detrick, Maryland 21702-5012

10. SPONSOR/MONITOR'S ACRONYM(S)

11. SPONSOR/MONITOR'S REPORT NUMBER(S)

12. DISTRIBUTION / AVAILABILITY STATEMENT

Approved for Public Release; Distribution Unlimited

13. SUPPLEMENTARY NOTES

14. ABSTRACT
The goal of this project is to determine whether electrical stimulation of the spinal cord can reduce respiratory dysfunctions occurring after mid-to-high cervical spinal cord injuries (cSCI). Our primary emphasis is on intraspinal microstimulation (ISMS) of the phrenic circuit using physiologically-appropriate, endogenous respiratory signals to trigger activation of the phrenic motoneuron (PhMN) pool following a cSCI above the level of the phrenic nucleus at spinal levels C3-C5/6 in adult rats. A major accomplishment of our studies is demonstration of proof-of-concept for our closed-loop strategy before and after a spinal hemisection at C2 which results in immediate paralysis of the ipsilateral hemidiaphragm. Our studies have established that ISMS at the level of the PhMN can effectively activate diaphragm motor units following high cSCI even beyond when stimulation ended. Per comments from our proposal's initial review, we also began looking at the efficacy of high frequency (open-loop) spinal (epidural) stimulation. Our data indicate this approach is not as effective at selectively activating inspiratory diaphragm (phrenic) motor units. These and other areas of progress lend considerable initial strength to the potential therapeutic value of closed-loop ISMS activation of respiratory circuits caudal to SCI.

15. SUBJECT TERMS
respiration, cervical spinal cord injury, intraspinal microstimulation, epidural stimulation, Neurochip, neural interface, neuroplasticity, diaphragm

16. SECURITY CLASSIFICATION OF:			17. LIMITATION OF ABSTRACT	18. NUMBER OF PAGES	19a. NAME OF RESPONSIBLE PERSON
a. REPORT	b. ABSTRACT	c. THIS PAGE			USAMRMC
Unclassified	Unclassified	Unclassified	Unclassified	89	19b. TELEPHONE NUMBER *(include area code)*

Table of Contents

1. INTRODUCTION:

Compromised breathing (i.e., respiratory insufficiency) is one of the more devastating and potentially life-threatening consequences of spinal cord injury (SCI) at mid- to upper-neck (i.e., cervical) levels due to disrupted connections between respiratory centers in the brainstem and circuits controlling ventilatory muscles in the spinal cord. Lesions at or above C4 often result in severely, if not completely, reduced diaphragm function. This muscle, which is often considered the primary muscle of inhalation, receives its motor innervation from the phrenic nucleus primarily located at spinal C3-C5. Depending upon the severity and symmetry of the injury, descending inspiratory drive from the brainstem to the phrenic nucleus can result in uni- or bilateral paralysis of the diaphragm. Severe impairment of diaphragm function requires individuals to receive some form of assisted ventilatory support (e.g., mechanical, phrenic nerve, or diaphragm pacing). Even if some individuals are weaned, patterns of breathing rarely approximate normal, and pulmonary infection-related hospitalizations and deaths remain common. A need thus exists for interventions that can lead to a greater and more normal restoration of diaphragm and other respiratory muscle functions. Studies being conducted under this Department of Defense award are based upon increasing evidence showing that electrical stimulation of the injured spinal cord can elicit some degree of motor function (e.g., standing, limb movements) in animals and humans even with motor complete SCIs. The most common strategy involves epidural stimulation in which an electrical current is delivered to an electrode array placed on the surface of the spinal cord. Other studies are now emerging, however, which show that insertion of tiny microwires directly into spinal cord tissue (intraspinal microstimulation, ISMS) may produce more natural motor improvements. Epidural high frequency spinal stimulation has been shown to offer potential for improving aspects of respiratory function, but it is still dependent upon delivery of programmed signals (i.e., open-loop). We are now proposing to explore the capacity of ISMS to improve diaphragm function when delivered to phrenic circuitry. An innovative feature of our approach is a custom-designed circuit that will be used to capture signals from unaffected respiratory muscles. Those signals will then be used to stimulate the phrenic circuit in a natural and physiologically appropriate fashion under normal and more demanding ventilatory conditions. The intriguing possibility also exists this type of closed-loop strategy may lead to persistent recovery by directing functional and anatomical circuit remodeling and long-term effects no longer dependent upon stimulation. We will also determine differences in outcomes via epidural vs. ISMS. Overall, we are proposing the first investigation of a promising approach for stimulating respiratory circuits in two SCI models involving lesions above or within the phrenic circuit. Success of this project can lead to a significant shift in current approaches for managing respiratory dysfunction following cervical SCI. Knowledge obtained from this study also may have broader implications related to the use of ISMS for treating other aspects of SCI alone or in combination with other interventions.

2. KEYWORDS:

respiration
cervical spinal cord injury
intraspinal microstimulation
epidural stimulation
Neurochip
phrenic nucleus
phrenic motoneurons
phrenic neurograms
hypoglossal nerve
hypercapnia
hypoxia
neuroplasticity
C2 hemisection
mid-cervical contusion injury
interneurons
closed-loop stimulation
open-loop stimulation

3. ACCOMPLISHMENTS:

Major Goals of the Project:

This Final Report is based upon the summary presented at the In-Progress Review meeting of SCIRP Funded (Unclassified) Research convened September 26, 2017 at Fort Detrick, MD.

The following Specific Aims were proposed for this project:

Aim 1: To determine whether physiologically-based ISMS (intraspinal microstimulation) below a C3/4 lateralized contusion or C2 hemisection will enhance the activity of phrenic motoneurons (PhMNs) and the diaphragm.

This aim was to be addressed by Major Tasks 1 and 2 which involved mapping phrenic circuit discharge patterns and obtaining a terminal electrophysiological comparison of epidural stimulation and ISMS after chronic C2Hx. Also, included was Major Task 3 to analyze tissue responses to microwire implantation. This effort, however, seemed more appropriate under experiments in Aim 2 and was thus not immediately pursued beyond some initial experiments. The main part of this aim was to be addressed by Major Task 5 that was designed to obtain proof-of-concept for closed-loop ISMS of PhMNs and thereby obtain a lead-in to Aim 2. It should be noted that focus of all our lesion studies was the C2 hemisection (C2Hx) model. With prior DOD approval, the contusion injury was dropped from the study for multiple practical and logistical reasons. Foremost was the injury model and resulting deficits needed further development based upon conflicting findings in the literature, whereas the C2Hx model was far more established. Studies were conducted as part of a University of Florida and University of Washington collaboration which essentially replicated UF results.

Aim 2: To demonstrate with neuroanatomical and electrophysiological methods that patterned electrical stimulation of spinal circuitry, caudal to the site of injury, will promote altered connectivity in conjunction with changes in PhMN and diaphragm function.

This aim identified with Major Tasks 6-11 which were to test open- and closed-loop ISMS in awake, freely-behaving C2Hx rats. Replication of the most promising stimulation approach was to be pursued with follow-up neuroanatomical studies. This aim, unfortunately, could not be completed as intended as the protocols needed to perform these experiments involved complex surgeries and more technical refinement than envisioned for the original proposal. Nevertheless, progress did continue, and this aim represents a control for two recently funded proposals based upon work carried out during this DOD award period. Some initial findings showing diaphragm responses in awake C2Hx rats are presented at the end of this report.

Specific Accomplishments of the Project:

Table 1 (Appendix) presents a summary of the status of work that was originally listed in our Statement of Work. The detailed descriptions below, reflect the more natural progression of research directed at the main objectives of the supported research – namely to obtain insights regarding the potential of intraspinal microstimulation for improving respiratory outcomes following cervical spinal cord injury. Accordingly, several major tasks were either fused by virtue of the focus of the individual experiments or overlapped in varying degrees.

Study (Major Tasks 2 and 7): Terminal electrophysiological analysis of affected hemidiaphragm function after C2Hx and respiratory-triggered intraspinal microstimulation (ISMS). As noted above, one of the primary objectives of Aim 1 was to obtain proof-of-concept for physiologically-triggered ISMS serving to restore diaphragm function below a high cervical injury. The results of that study were published in the *J. Neurophysiology* (see Item 6) and a copy of that article is appended to this Report.

In brief, the design of that study entailed animals being maintained under tightly controlled physiological conditions with regard to temperature and blood gases especially. Mechanical ventilation was employed to remove fluctuations in Pa_{O2} and Pa_{CO2}. End-tidal CO_2 was continuously monitored. Genioglossus EMGs were used as a physiological trigger for ISMS since the tongue moves in synchrony with inspiratory activation of the diaphragm. ISMS stimulation involved a continuous 250ms train and 0.3 ms pulses at 100Hz

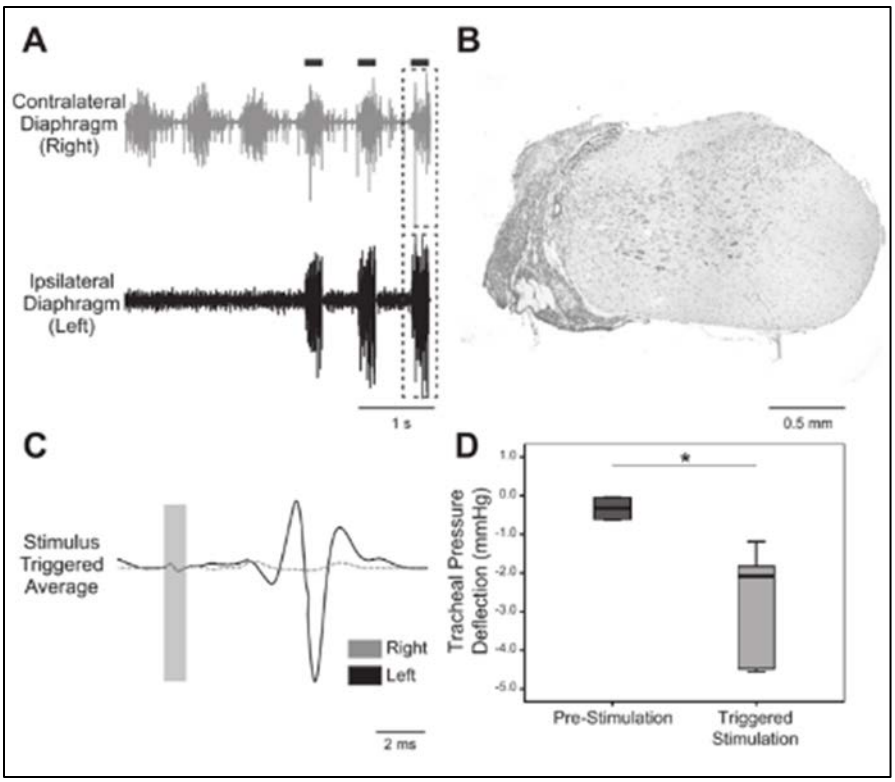

Figure 1. Figure from Mercier LM, et al. *J Neurophysiol 117: 767-776, 2017.*

and 100µA. Three groups of rats were tested with this protocol: spinal intact, acute C2Hx, and subacute C2Hx (5-21d post-injury). Figure 1 illustrates the major outcome of the study. In a subacute C2Hx animal, the hemidiaphragm ipsilateral to a histologically verified complete hemisection (Fig. 1B) is paretic but becomes activated by genioglossus-triggered ISMS was delivered during the breaths marked by the black bars. (Fig. 1A). Stimulus-triggered averages from the ipsilesional (solid line) and contralesional diaphragm (dashed line) were obtained from the period indicated by the dashed boxes in Fig. 1A. These traces illustrate activation of the diaphragm restricted ipsilateral to the C2Hx lesion. Tracheal pressures were evaluated to explore the potential of a biomechanical impact of ISMS-induced muscle contract-ion. Negative pressure swings in tracheal pressure would be expected in this preparation if diaphragm contraction is altering the dimensions of the thoracic cavity. Figure 1 D shows average change in tracheal pressure during lung inflation at pre-stimulation baseline and during ISMS. *P < 0.05.

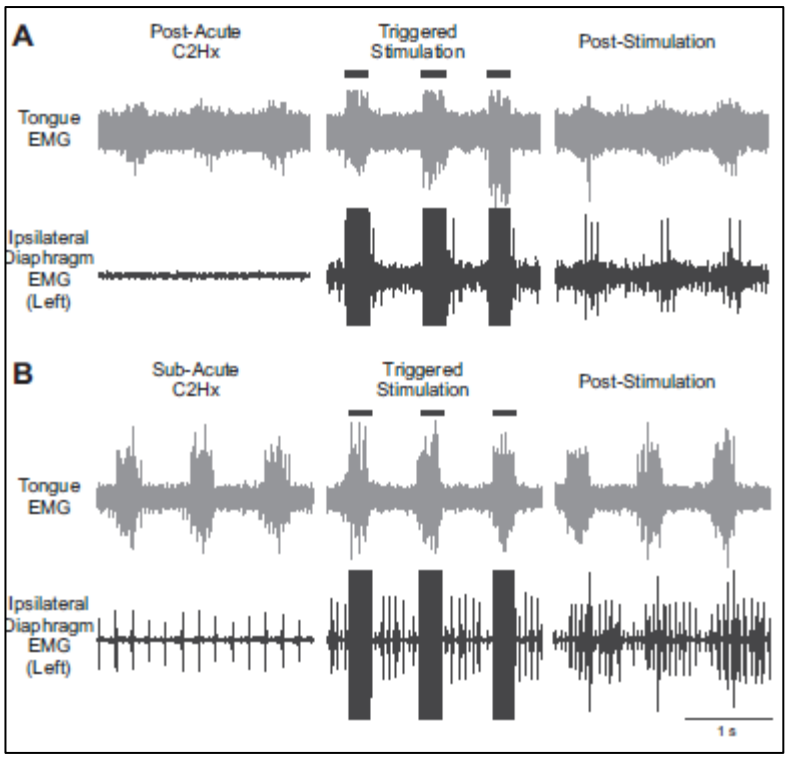

Figure 2. From Mercier et al. *J. Neurophysiol*. 117:767-776, 2017.

Collectively, this study demonstrated the feasibility of using intra-spinal microstimulation (ISMS) of the cervical spinal cord to evoke diaphragm activity ipsilateral to acute and subacute hemisection of the upper cervical spinal cord of the rat. In addition, these data provide proof-of-concept for the efficacy of diaphragm activation using an upper airway respiratory EMG signal to trigger ISMS at the level of the ipsilesional phrenic nucleus during acute and advanced post-injury intervals.

Even more interesting was that the lasting effect of ISMS as shown in Figure 2 by recordings that illustrate persistence of ipsilateral diaphragm EMG activity following ISMS. Figure 2A shows tongue and ipsilateral (left) diaphragm EMG activity after acute C2Hx, during ISMS, and immediately after cessation of ISMS. Note that clear phasic (inspiratory) activity can be seen after ISMS, whereas the baseline showed no such activity. A similar response can be observed in a subacute C2Hx animal. In these examples, the ISMS was triggered by the inspiratory genioglossus EMG signal and was delivered at 100 Hz for 1 min of respiratory efforts. This potentially important observation was not part of our original hypothesis. Persistence of inspiratory bursting in the hemiparetic diaphragm for several respiratory cycles

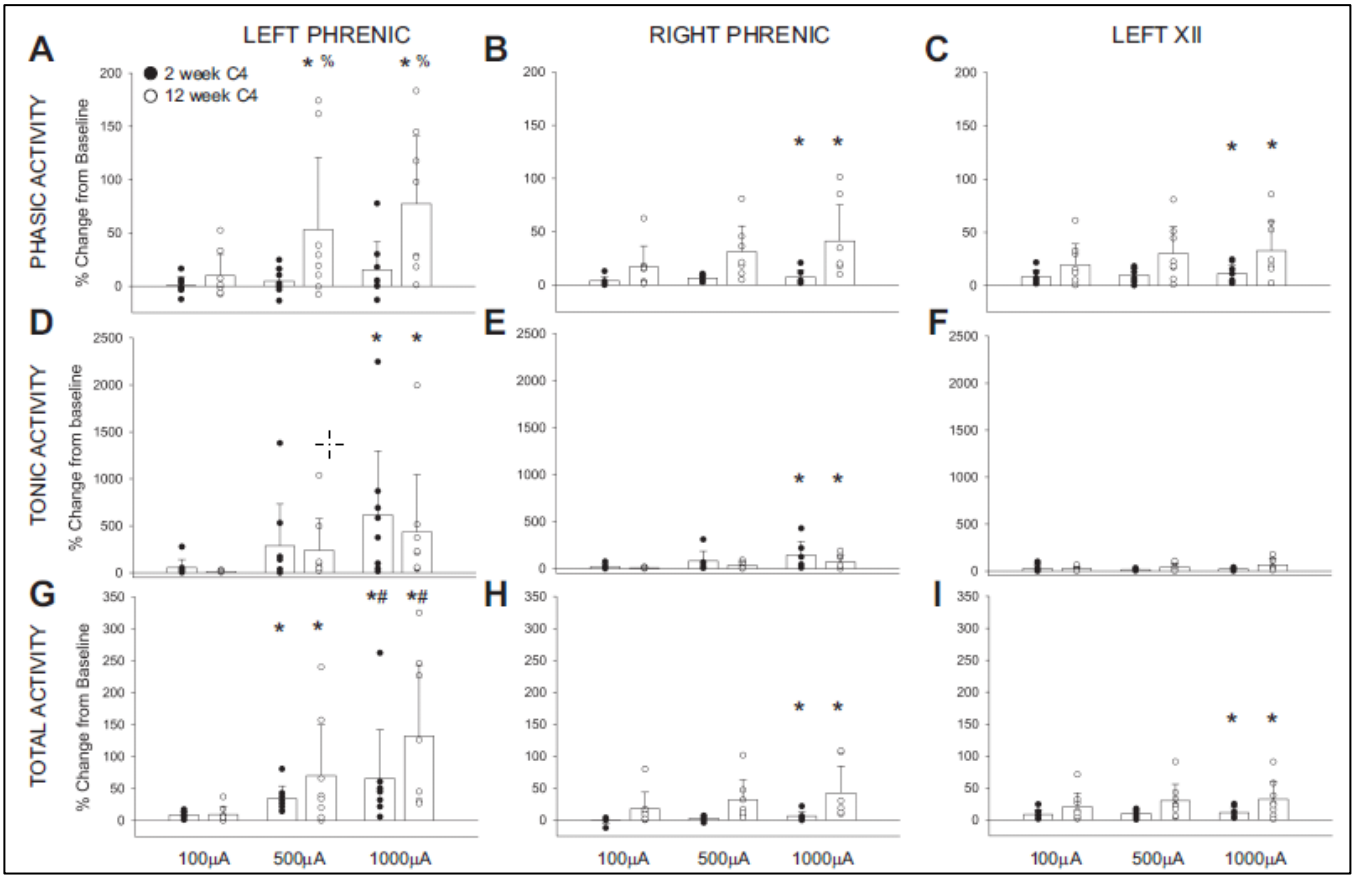

Figure 3. Average changes in phrenic and hypoglossal nerve activity following C4 HF-ES. Depicted are changes in phasic (A–C), tonic (D–F), and total (G–I) phrenic and hypoglossal nerve activity following HF-ES of the C4 spinal cord, delivered at 2 and 12 weeks post-injury. Data were calculated over the 3 min following each bout of stimulation and are represented as % change from baseline activity. HF-ES delivered to the C4 spinal cord at 12 weeks post-C2Hx resulted in an increase in phasic phrenic activity. No other group differences were observed, although dose-dependent increases in amplitude (%change above baseline) were observed following HF-ES across both groups, with the greatest amplitude changes occurring following the highest stimulation intensities (e.g., 500 and 1,000 µA). Note that profound increases in tonic activity comprised much of the increase in total activity and that the ipsilateral phrenic nerve demonstrated the most dramatic changes in nerve amplitude relative to baseline. *P< 0.05, different from 100 µA. #P < 0.05, different from 500 µA. %P 0.05, different from 2 wk at same stimulus current. Data were evaluated using 2-way repeated-measures ANOVA with Holm-Sidak post hoc tests for individual comparisons (groups: 2-wk C4, n = 8; 12-wk C4, n= 8).

after cessation of the stimulation occurred in the majority of acute and subacute C2Hx lesions and is similar to the previously described phenomenon of respiratory short-term potentiation (STP), which is manifested as a progressive enhancement of activity followed by a slow decline to baseline levels after removal of a stimulus. We previously demonstrated that hypoxia can induce STP of phrenic motor output in rats with subacute C2Hx, and the response is greater in the nerve ipsilateral vs. contra-lateral to the lesion (Lee et al. 2015). The STP in C2Hx rats appeared to reflect recruitment of a population of phrenic motoneurons that had been silenced by injury, which continued to burst beyond the period of hypoxic stimulation. This increased phrenic bursting after cessation of ISMS also may be analogous to longer-duration functional recoveries others have observed with chronic ISMS in other motor systems.

Study (Major Task 2, 5): Epidural Stimulation and Respiratory Function Following C2Hx. This study was included in the Statement of Work per recommendation of the reviewers of our proposal. The basic goal was to obtain some comparative information relative to what could be achieved by ISMS versus a less invasive form of spinal cord stimulation. The publication resulting from this study (Gonzalez-Rothi et al., 2017) is appended. The hypothesis tested was that high frequency epidural stimulation (HF-ES) would potentiate ipsilateral phrenic output after subacute and chronic C2Hx. We thus investigated whether applying HF-ES with a continuous paradigm similar to stimulation studies targeting increased limb muscle activation, can induce phrenic motor plasticity on short timescales in rats with subacute (2 weeks) or chronic (12 weeks) C2Hx.

For this study HF-ES (300 Hz) was applied to the ventrolateral C4 (Fig. 3) or T2 (Fig. 4) spinal cord ipsilateral to C2Hx in anesthetized and mechanically ventilated adult rats. Stimulus duration was 60-sec and currents ranged from 100-1000 µA. Bilateral phrenic nerve and ipsilateral hypoglossal nerve activity were recorded before and after HF-ES. This study is the first to explore the impact of HF-ES on phrenic and XII motor output after subacute and chronic incomplete cervical SCI.

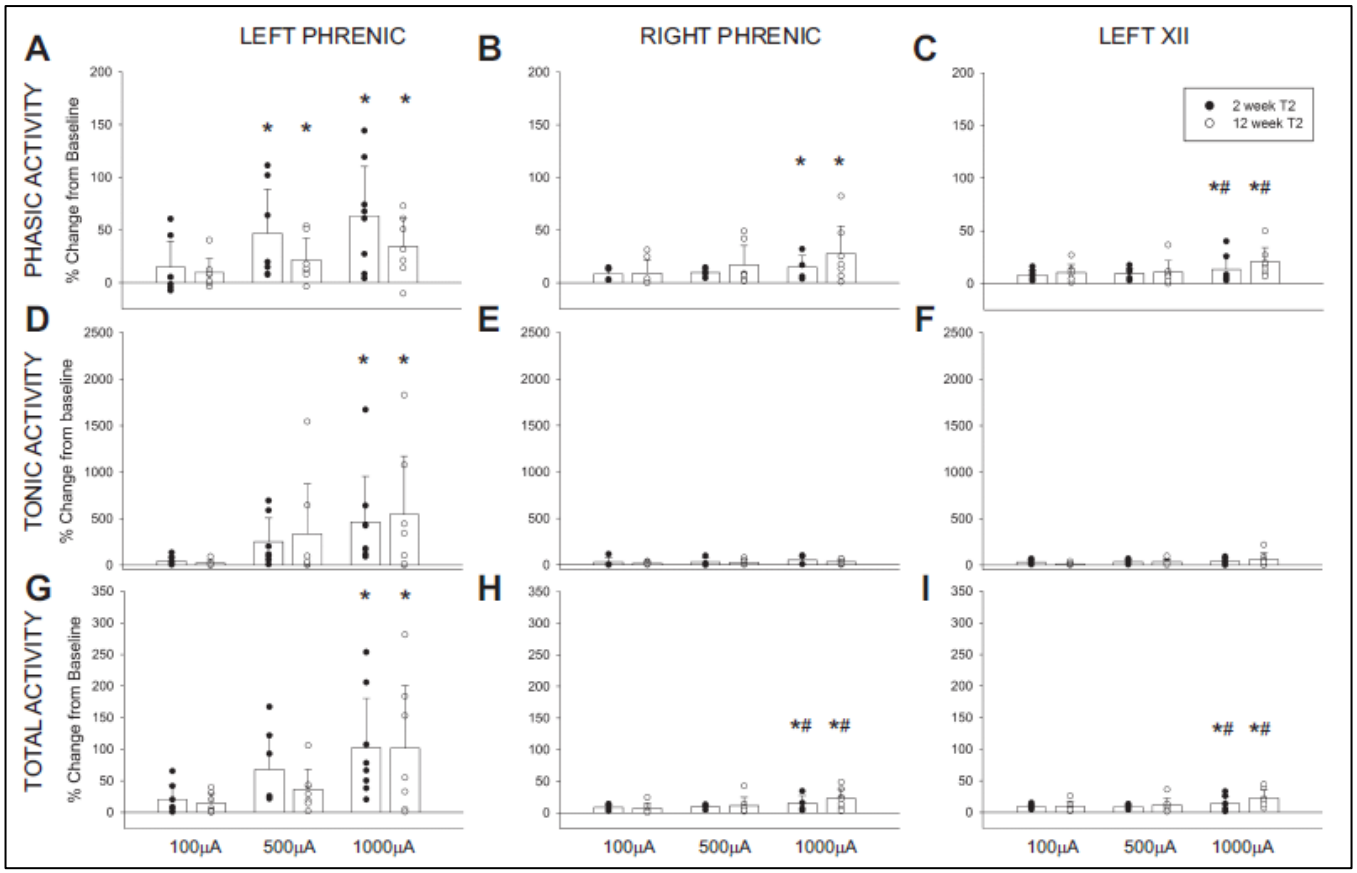

Figure 4. Average changes in phrenic and hypoglossal nerve activity following T2 HF-ES. Shown are changes in phasic (*A–C*), tonic (*D–F*), and total (*G–I*) phrenic and hypoglossal nerve activity following HF-ES of the T2 spinal cord, delivered at 2 and 12 weeks post-injury. Data were calculated over the 3 min following each bout of stimulation and are represented as %change from baseline activity. A dose-dependent increase in amplitude (%change above baseline) was observed in all nerves (**P*< 0.05, different from 100µA; #*P* <0.05, different from 500 µA) across all outcomes (phasic, tonic, and total nerve activity), with the greatest amplitude changes occurring following the highest stimulation intensities. Note that profound increases in tonic activity comprised much of the increase in total activity and that the ipsilateral phrenic nerve demonstrated the most dramatic changes in nerve amplitude relative to baseline. No significant group differences were observed in any nerve in any of the outcomes assessed. Data were evaluated using 2-way repeated-measures ANOVA with Holm-Sidak post hoc tests for individual comparisons (groups: 2-weeks T2, *n* =7; 12-weeks T2, *n*= 7).

Higher T2 stimulus currents potentiated ipsilateral phasic inspiratory activity at both 2 and 12 weeks post-C2Hx (Fig. 4), whereas higher stimulus currents delivered at C4 (Fig. 3) potentiated ipsilateral phasic phrenic activity only at 12 weeks (P <0.028, Figs. 3 and 4, from Gonzalez-Rothi et al., 2017). Meanwhile, tonic output in the ipsilateral phrenic nerve reached 500% of baseline values at the high currents with no difference between 2 and 12 weeks. HF-ES did not trigger inspiratory burst-frequency changes. Similar responses occurred following T2 HF-ES (Fig. 4, from Gonzalez-Rothi, 2017). Increases in contralateral phrenic and XII nerve output were induced by C4 and T2 HF-ES at higher currents, but the relative magnitude of these changes was small compared with the ipsilateral phrenic response.

We conclude that following incomplete cervical spinal cord injury, HF-ES of the ventrolateral mid-cervical or thoracic spinal cord can potentiate efferent phrenic motor output with little impact on inspiratory burst frequency. However, the substantial increases in tonic output indicate that the uninterrupted 60s stimulation paradigm is unlikely to be useful for respiratory muscle activation after spinal cord injury.

Study (Major Task 1): Mapping respiratory-related circuitry in the intact spinal cord of the adult rat. Part A.

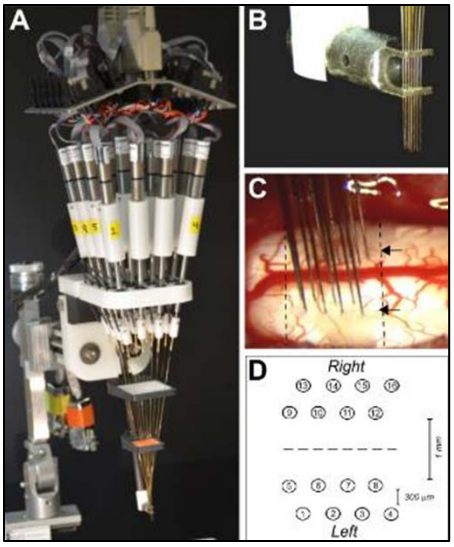

Figure 5. From Streeter et al. 2017

A fundamental question related to most, if not all, approaches to spinal cord stimulation is what is being stimulated. In addition, it may become extremely useful to have a perspective regarding neural substrate changes occurring after spinal cord injury (SCI). As a prelude to a detailed mapping study of respiratory-related circuitry (now in progress) following SCI, two studies were carried out involving spinal-intact rats in which we first wanted to demonstrate an ability to identify multielectrode array (MEA) recording sites and then use MEAs to study respiratory-modulated interneurons which we would ultimately wish to target with ISMS. The first study involved development of a silver labeling approach which was described in a publication listed in Item 6 and appended to this Report (Streeter et al., 2017a)

Figure 5A shows the MEA consisting of 16 fine tungsten wire electrodes each controlled by micromotors and held in place by the array guide. The electrode tips maintained in a "fixed matrix" by the array guide (Fig. 5B). For recording, the electrodes are positioned in the dorsal C4 spinal cord at the dorsal root entry zone (e.g., black arrows, Fig. 5C). Figure 5D shows a schematic of the recording matrix consisting of 8 electrodes arranged in 2 rows of 4. The inner distance between the 2 sets of 8 electrodes was ~1 mm, and the distance between electrodes within each row was ~300 µm.

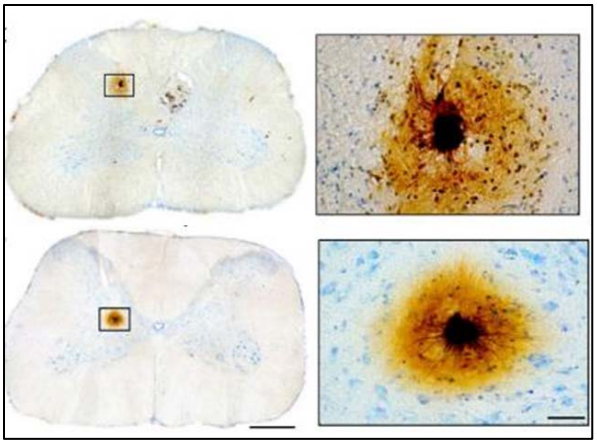

Figure 6. Representative histological sections from the cervical spinal cord containing silver-labeled sites counterstained with cresyl violet

We delivered 100-nA currents to electroplate silver onto and subsequently deposit silver from electrode tips after obtaining mid-cervical (C3–C5) recordings using an MEA in anesthetized and ventilated adult rats. Histological studies verified that the silver deposition method discretely labeled (50µm resolution) spinal recording locations between laminae IV and X in cervical segments C3-C5 (Fig. 6). Using correlative techniques, we next tested the hypothesis that mid-cervical neuronal discharge patterns are temporally linked. Cross-correlation histograms produced few positive peaks (5.3%) in the range of 0–0.4 ms, but 21.4% of neuronal pairs had correlogram peaks with a lag of ~0.6 ms.

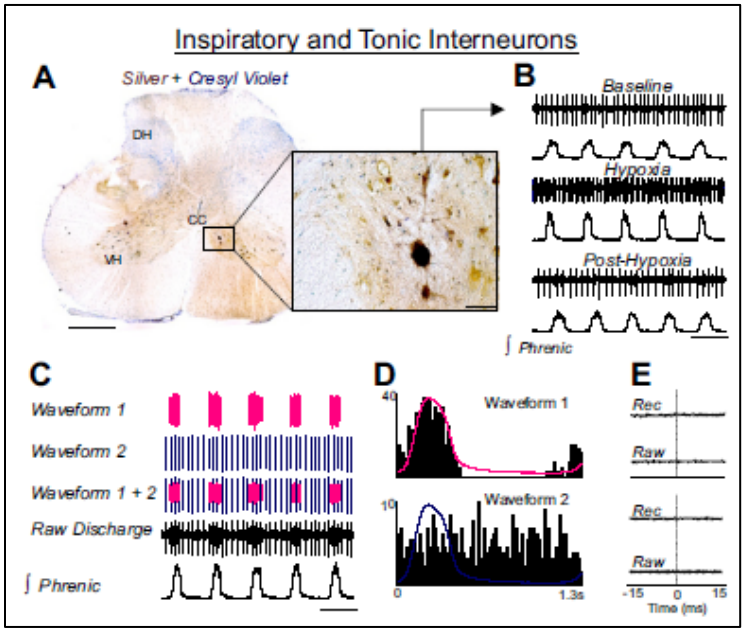

Figure 7. Silver labeling of mid-cervical spinal interneurons. A: representative C4 section containing a silver-labeled site counterstained with cresyl violet and high-resolution image containing the silver-labeled site (callout). B: corresponding neuronal output and integrated phrenic output during baseline, hypoxia, and post-hypoxia depicting a single tonic firing neuron at baseline and recruitment of a phasic inspiratory neuron during hypoxia and post-hypoxia. C: integrated phrenic output, raw neuronal discharge, and sorted spikes (waveforms) during hypoxia. D: cycle-triggered histograms of both neurons during 50 consecutive breaths overlaid with the average integrated phrenic waveform during hypoxia. E: spike-triggered average of the raw and rectified phrenic nerve depicting a lack of positive features.

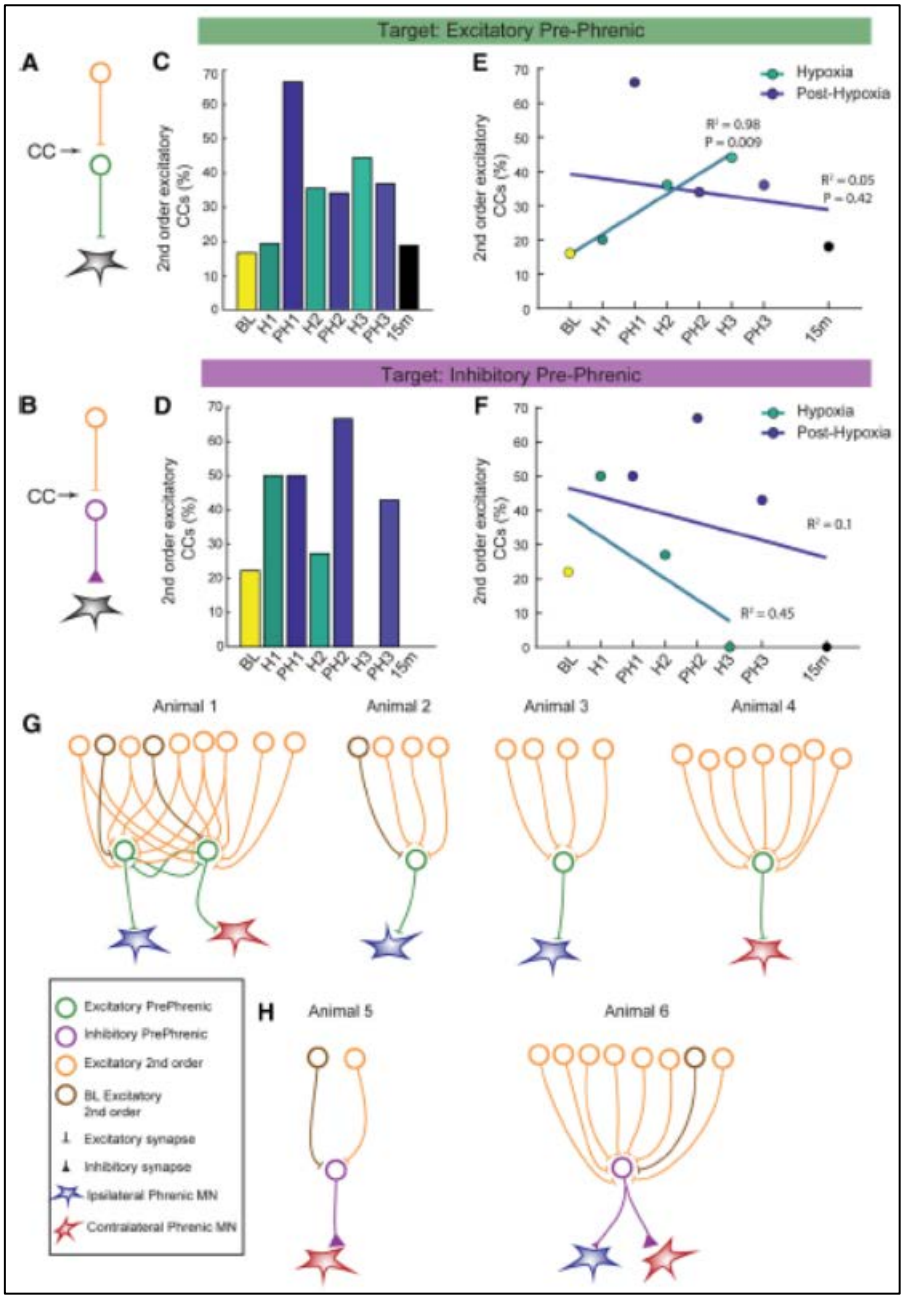

Figure 8. C-INs temporally linked to pre-phrenic neurons before, during, and following acute intermittent hypoxia. A, B, Schematic of second-order excitatory C-IN projecting to excitatory pre-phrenic (A) and inhibitory pre-phrenic C-IN (B). C,D, Excitatory C-INs (as a percentage of possible connections) temporally linked to excitatory pre-phrenic C-INs (C) and inhibitory (D) pre-phrenic C-INs. E, F, Linear regression analysis of the proportion of second-order excitatory connections to excitatory (E) and inhibitory (F) pre-phrenic C-INs. G, H, Schematic summarizing second-order excitatory C-INs projecting to excitatory (G) and inhibitory (H) pre-phrenic interneurons at BL (brown) and recruited (orange) during intermittent hypoxia. (From Streeter et al., 2017b).

Accordingly, we identified inspiratory (Fig. 7) and expiratory (not shown, see publication) interneuronal populations. These results are consistent with synchronous discharge involving mono- and polysynaptic connections among mid-cervical neurons. We conclude that there is a high degree of synaptic connectivity in the mid-cervical spinal cord and that the silver-labeling method can reliably mark metal electrode recording sites and “map” interneuronal populations, thereby providing a low-cost and effective tool for use in MEA experiments. We suggest that this method will be useful for further exploration of mid-cervical network connectivity.

Study (Major Task 1): Mapping respiratory-related circuitry in the intact spinal cord of the adult rat. Part B.

The above study was followed up by a more detailed analysis of phrenic neural circuitry using the MEA approach described. In addition, we added intermittent hypoxia (IH) to the recording protocols to demonstrate respiratory-modulated interneuronal connectivity. IH is becoming recognized as a viable rehabilitative strategy for improving respiratory function and may be coupled with other interventions such as ISMS. Acute intermittent hypoxia (AIH) can trigger spinal plasticity associated with sustained in-creases in respiratory, somatic, and/or autonomic motor output. However, the impact of AIH on cervical spinal interneuron (C-IN) discharge and connectivity is unknown. Thus, we were in-terested in gaining insights into the connectivity of respiratory-modulated spinal interneurons and how that might be affected by IH. Accordingly, bilateral phrenic nerve activity was recorded in anesthetized and ventilated adult male rats and a multielectrode array was used to record C4/5 spinal discharge before [baseline (BL)], during, and 15 min after three 5 min hypoxic episodes (11% O_2 , H1–H3). The published paper (Streeter et al., 2017b) is appended in Item 6.

We found that most C-INs (94%) responded to hypoxia by either increasing or decreasing firing rate. Functional connect-ivity was examined by cross-correlating C-IN discharge. Cor-relograms with a peak or trough were taken as evidence for ex-citatory or inhibitory connectivity between C-IN pairs. We further identified C-INs that were functionally connected to pre-phrenic C-INs (ideal targets for ISMS); these neurons were operationally defined as "second order" (Fig. 8). The relationship between the number of excitatory connections from second-order C-INs to either excitatory pre-phrenic neurons or inhibitory pre-phrenic neurons was quantified (Fig. 8C, D), and examined using linear regression (Fig. 8E,F). A strong, positive relationship was present between the number of excitatory connections (n = 24) from second order neurons to excitatory pre-phrenic interneurons (n = 5) during (R^2 = 0.982; $p < 0.0091$), but not after hypoxia (R^2 = 0.048; $p<0.7211$; Fig. 8E). We did not detect a sufficient number of inhibitory pre-phrenic interneurons (n=2) to enable a similar statistical test, but data are shown in Figure 8F.

These results provide evidence that the number of excitatory connections between C-INs and excitatory pre-phrenic interneurons is enhanced during hypoxia (summarized by Figs. 8 G and H). Thus, we conclude that C-INs are an integral part of the neural network that controls the diaphragm, and that the strength of synaptic connections in this network may be altered during and after AIH. Similar mapping experiments are currently in progress to see how these patterns of connectivity and effects of AIH are altered by C2Hx. That study will cap off this Major Task of the Statement of Work.

University of Washington Subcontract: Chet Moritz, Ph.D. (Subcontract P.I.)

Additional Mapping Data and Replication: Major Tasks 1 and 8

The above mapping studies were reproduced at the University of Washington, and the manuscript to *Exp. Neurol.* has just been accepted with very minor revision (Sunshine et al., In Press). A next-to-final draft is appended (Item 6).

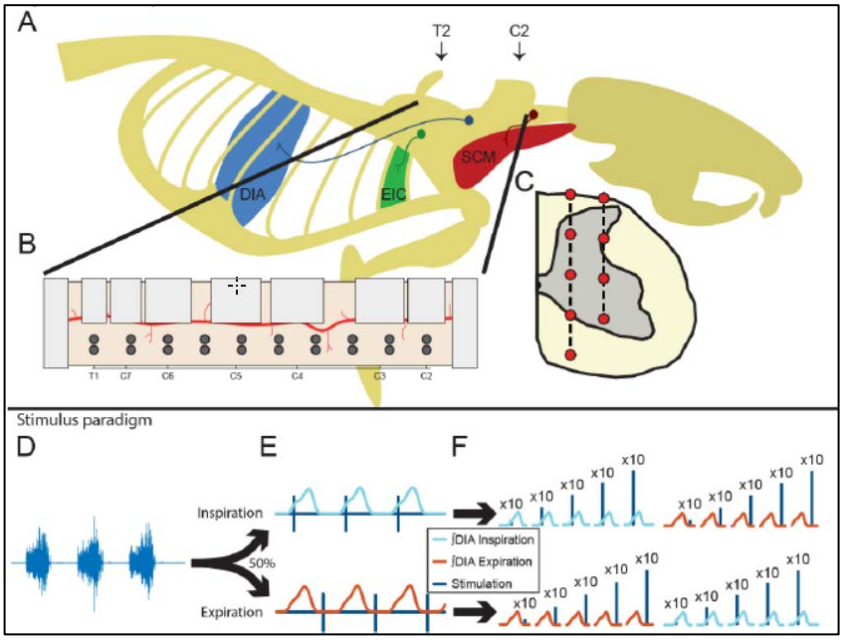

Figure 9. Experimental set-up. A) Rodent respiratory anatomy including schematic of spinal innervation to key respiratory muscles. EMG recording electrodes were placed in the Diaphragm (DIA), External Intercostal (EIC) and Sternocleidomastoid (SCM) muscles. B) Dorsal view of the exposed spinal cord. Grey circles indicate the position where each of the 20 stimulation tracks began on the dorsal surface of the spinal cord in an example animal. C) Coronal view illustrating electrode tracks (dashed lines) and stimulus locations (red circles). Stimulus paradigm. D) Diaphragm EMG prior to the start of stimulation. E) Diaphragm EMG is rectified and integrated with a sliding-average window. For each stimulation site, there was a 50% probability of first triggering stimulation during either inspiration or expiration. F) Ten stimuli delivered at 10-90μA in steps of 20μA. After all stimulus intensities are delivered during one phase of respiration, stimulation is then delivered during the opposite respiratory phase at each intraspinal location. (From Sunshine et al., In Press).

As noted above, a complex propriospinal network is synaptically coupled to phrenic and intercostal motoneurons which makes it difficult to predict how gray matter intraspinal microstimulation (ISMS) will recruit respiratory motor units. Using acute electrodes to apply ISMS (Fig. 9), we mapped the cervical and high thoracic gray matter at locations which ISMS activates diaphragm (DIA) and external intercostal (EIC) motor units. Respiratory muscle electromyography (EMG) was recorded in anesthetized female spinal-intact adult rats while a stimulating electrode was advanced ventrally into the spinal cord in 600 μm increments. At each depth, single biphasic stimuli were delivered at 10-90μA during both the inspiratory and expiratory phase independently. Twenty electrode tracks were made from C2-T1 at medial and lateral gray matter locations.

Figure 10 shows the impact of electrode location and respiratory phase on ISMS-induced respiratory muscle activation. We noted first that the anatomical locations at

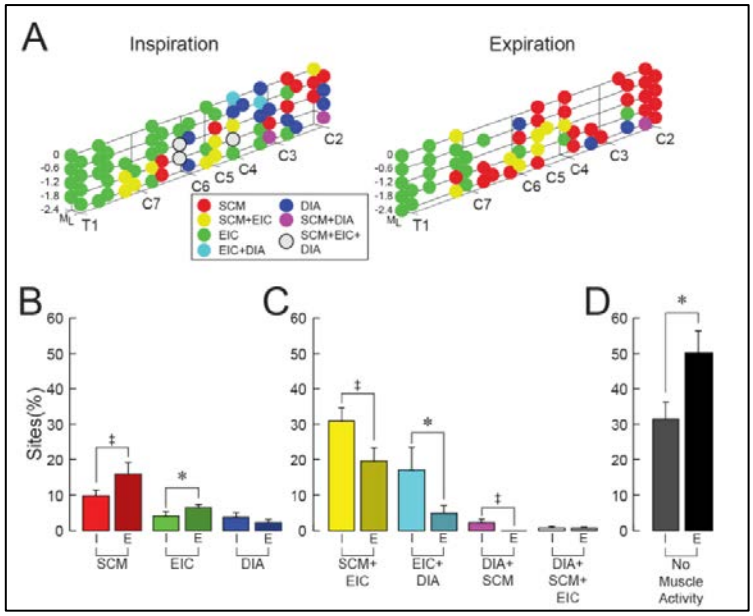

Figure 10. ISMS-evoked respiratory muscle activation & co-activation. A) Stimulus locations activating respiratory muscles during inspiration (left) and expiration (right) at the lowest stimulus current to elicit EMG activity in a representative animal, the center of the vertebral bones is noted along the x-axis. Colors denote individual muscles or combinations of muscles. Abbreviations as in Figure 2. B-D) EMG response observed as a percentage of the total sites tested at the lowest current to elicit EMG activity in any muscle (mean ± SEM). Each figure displays the type of muscle activity or co-activity during inspiration ('I'; light shading) and expiration ('E'; dark shading). ‡ denotes p <0.1, *denotes p<0.05. Diaphragm (DIA), External Intercostal (EIC) and Sternocleidomastoid (SCM). (From Sunshine et al., In Press)

which ISMS activated a muscle tended to cluster across multiple segments. Independent muscle activation (i.e., without any co-activation) occurred at a relatively low number of locations, and was more likely to occur during expiratory *vs.* inspiratory phase ISMS (Fig. 10B). Overall, significantly more sites elicited independent muscle activation during expiratory (25±8%) compared to inspiration triggered ISMS (18±4%; p = 0.03). In contrast, activating two muscles via a single ISMS pulse (i.e., co-activation) was more likely to occur during the inspiratory phase (51±12% of sites) as compared to the expiratory phase (25±11%; p<0.001). The mean co-activation data are shown in Fig. 10C. Note that significantly greater co-activation of all muscle pairs occurred during inspiratory *vs*. expiratory stimulation. We also observed a considerable number of ISMS locations at which no muscle activation could be evoked, and as shown in Fig. 10D this was more prominent during expiration when approximately 50% of locations failed to evoke muscle activity. The average stimulation threshold to evoke a response ranged from 46-55Ma, and this value was not different between muscles, nor was it altered by the respiratory phase (two-way ANOVA interaction p = 0.4492).

The latencies of recorded evoked responses (n=3187 across experiments) are summarized in Fig. 11. The plot in Fig. 11A indicates a multi-modal distribution of activation latency with the earliest detectable EMG responses occurring 1.2 ms after the stimulus. The latency distributions were next used to classify the activation of individual muscles during inspiratory- (Fig. 11B) and expiratory-phase ISMS (Fig. 11C). During inspiration, the average number of short latency (<2.6 ms) diaphragm activations was relatively low. The greatest number of diaphragm activations occurred at latencies ~ 3.9 ms (Fig. 11B). In contrast to the diaphragm, both the external

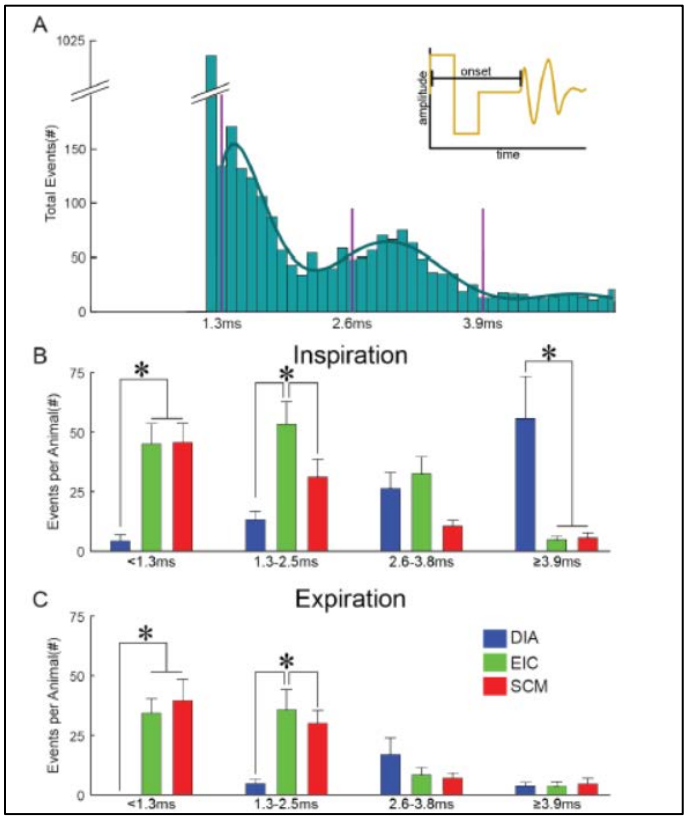

Figure 11. **Synaptic delays following ISMS stimulation** A) Pooled data from all trials with ISMS-evoked EMG responses (3187/16200). Histogram (0.1ms resolution) demonstrates the quantal pattern of synaptic delays. Dark green line indicates polynomial fit, purple lines indicate how data were divided into putative direct, monosynaptic, disynaptic and polysynaptic activations. B) Muscle activation synaptic delays resulting from stimulation delivered during the inspiratory phase. C) Muscle activation synaptic delays resulting from stimulation delivered during the expiratory phase. (* denotes p<0.05). Diaphragm (DIA), External Intercostal (EIC) and Sternocleidomastoid (SCM). (From Sunshine et al., In Press).

intercostal and sternocleidomastoid muscles were more likely to be activated at latencies ~2.5 ms (Fig. 8B).

Replication of University of Florida Terminal ISMS Results (Abecassis and Moritz, In Preparation) (Major Tasks 4, 5 and 9)

Basic Methods/Design: Adult rats were anesthetized with Isoflurane. After a midline laparotomy, bilateral diaphragm muscles were visualized and implanted with two Tungsten electromyography (EMG) leads. Intra-operative electrophysiological monitoring was used to confirm appropriate lead position with adequate signal to noise ratio. The animal was then positioned prone, a midline incision made, and muscular dissection carried down to expose the suboccipital region, and the spinous processes of C1-

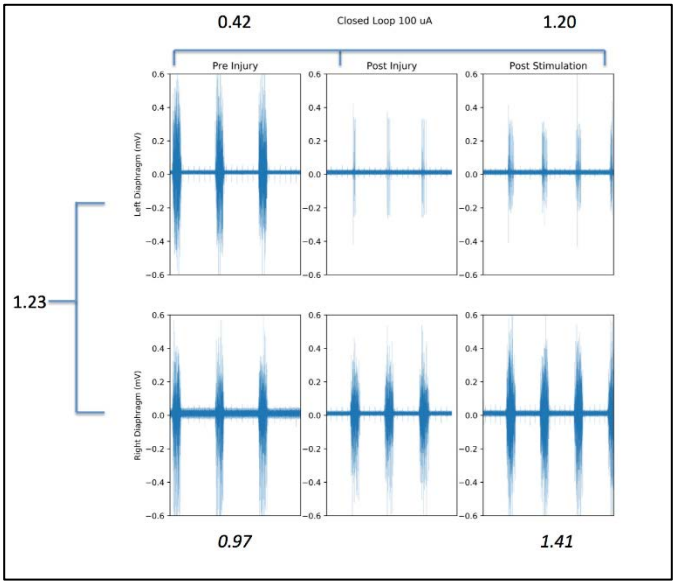

Figure 12. Left (top) and right (bottom) diaphragm EMG activity. Note that after stimulation at threshold, there was 1.20x the amount of total EMG activity in the injured (left) diaphragm.

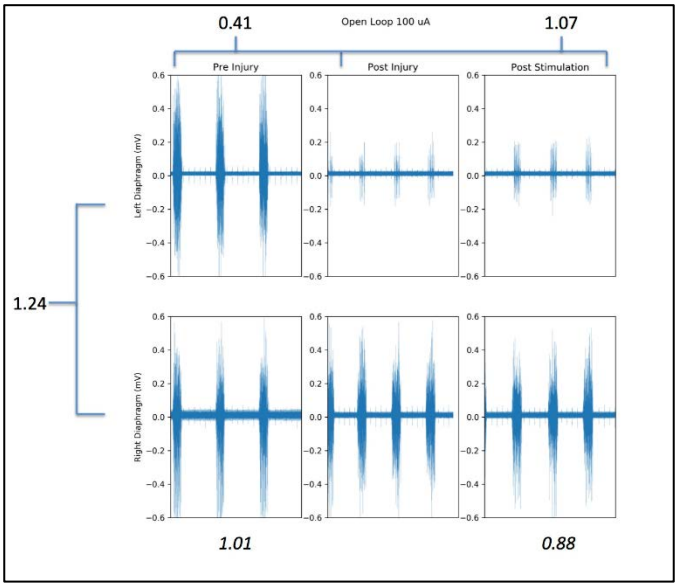

Figure 13. Open loop stimulation. Note a smaller increase in after-effect (1.07) in the top row. For this figure and Figs. 12 and 14 The number on the far left of the screen is the ratio of L to R diaphragm EMG signal before any experiments. Top left number is the ratio of post SCI EMG signal to PRE injury (i.e. how much signal remained after a near-complete C2 hemisection). Bottom left number is for uninjured side (control). Top right is the ratio of post-stimulation EMG signal to pre-stimulation, bottom is for uninjured side.

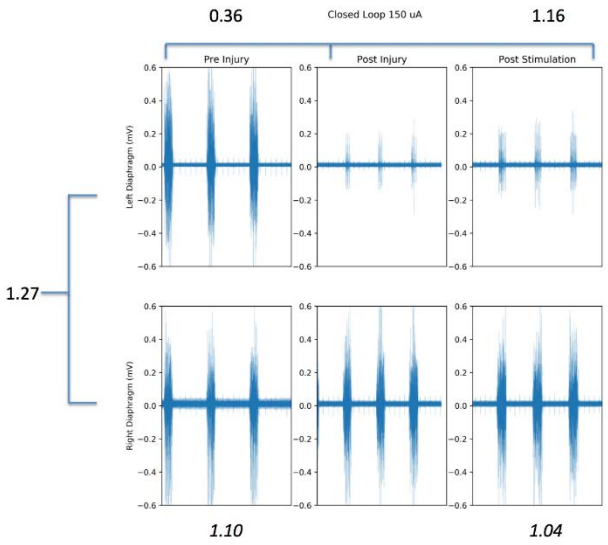

Figure 14. Closed loop stimulation at 1.5x threshold for current amplitude. Note that there is not any improvement in the amount of after-effect (1.16) from threshold (Figure 12, 1.20).

T2. Left hemi-laminectomies were performed at C2 and C4, followed by a left C2 hemisection injury, until near-complete loss of ipsilateral EMG signal was observed. A stimulating electrode was stereotaxically positioned within the spinal cord, where ISMS was delivered based on ongoing contralateral diaphragm activity.

Main Findings: Activation of hemidiaphragm activity after an acute C2Hx was demonstrated as shown in Mercier et al. (2017). In addition, an even more robust persistence of effect was observed following cessation of stimulation. After testing the effects of ISMS in 10 animals, there was an "after-effect" in diaphragmatic EMG activity ipsilateral to the SCI in 5 of the animals (50%). This effect appeared to rely on a closed-loop pattern of stimulation triggered by respiratory phase (Fig. 12), with little effect observed in an open-loop setting when stimulation was unrelated to respiratory phase (Fig. 13). Additionally, it appears that increasing the

current of stimulation above threshold did not increase the amount of after-effect (Fig. 14). An incomplete C2Hx is required to enhance the chances of obtaining any sort of persisting effect.

Our initial hypothesis is that the stimulation (particularly after incomplete injury) causes a release of 5-HT in the immediate vicinity of the phrenic motoneurons which may thereby account for the facilitation seen after stimulation. However, it may be that the potentiation observed is a slow decay of output (similar to STP, which is not 5-HT dependent) or it is a sustained response (similar to respiratory long-term facilitation, which is 5-HT dependent). Regardless of the mechanism, such closed-loop stimulation appears promising as a potential therapy, and merits further investigation.

Major Tasks 8-11: Studies of ISMS and Epidural Stimulation on Recovery of Diaphragm Function and Neural Circuit Plasticity Following C2Hx in Awake, Freely-Behaving Rats.

The last phase of this project was to carry forward with our terminal proof-of-concept ISMS study (Mercier et al., 2017) in chronic ISMS animals and compare results with chronic epidural stimulation. Based on earlier results and the labor-intensive nature of the overall project, epidural stimulation was not pursued. In addition, we wanted to investigate whether functional outcomes were related to anatomical plasticity. For various logistical reasons mentioned below (Item 5), progress was limited. However, towards the end of the DoD funding period, two new awards were obtained for which this part of the proposal represents the control data. Accordingly, this effort will be completed.

One of the reasons for not completing this phase of the project was the fact that effort and technical requirements for chronic ISMS in anaesthetized, freely-behaving animals exceeded what was originally envisioned when the proposal was submitted. Nevertheless, essential technical progress was made that demonstrated not only feasibility, but also initial data demonstrating ISMS has potential for improving diaphragm function in the awake animal.For the ISMS experiment, the approach involved working out a complex surgical protocol like that described by **McPherson et al. (2015,** Targeted, activity-dependent spinal stimulation produces long-lasting motor recovery in chronic cervical spinal cord injury. *PNAS* 112: 12193-12198). This entails implanting chronic EMG recording electrodes into each hemidiaphragm (DIA, Fig. 15). The leads (green lines, Fig. 15) are then run in a silicone tube subcutaneously to a head connector which relays signals to a neural interface (Neurochip-2). The Neurochip is then programmed to send a stimulus back through the connector and unto the ISMS site in the cervical spinal cord (red lines, Fig. 15).

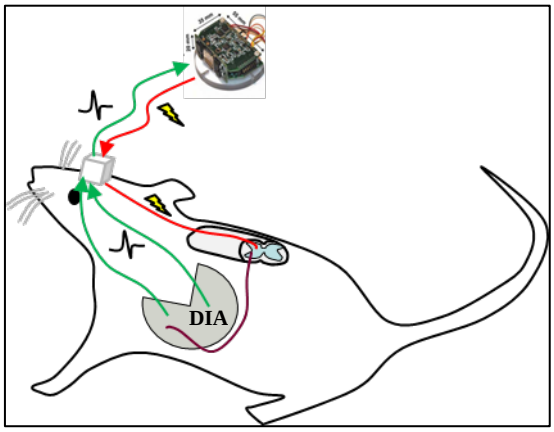

Figure 15. Graphic Based On: McPherson et al., 2015

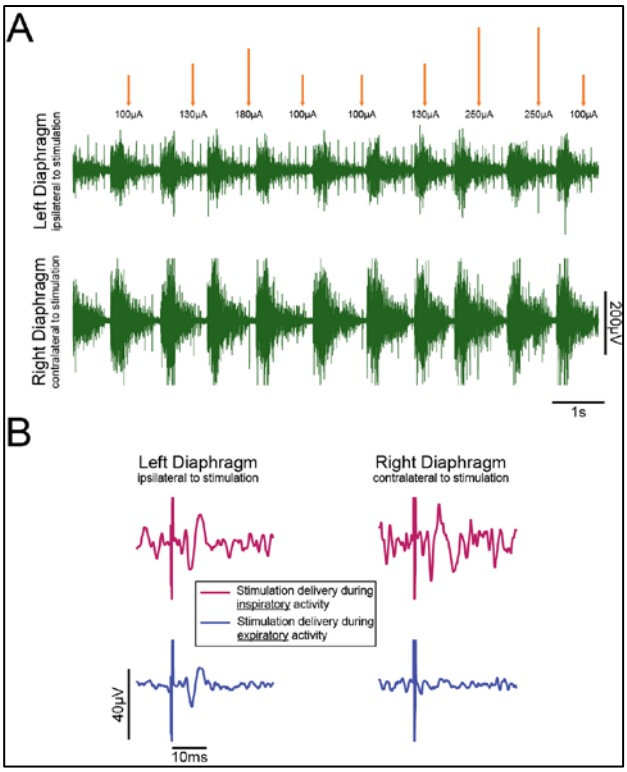

Figure 16. Open loop intraspinal microstimulation delivery one week post implant. A) Example traces of diaphragm activity recorded from implanted diaphragm EMG wires. Orange arrows indicate timing and amplitude of intraspinal stimulation. B) Stimulus triggered averages from 250µA stimulation. Stimulation was separated into inspiratory delivered (pink) and expiratory delivered (blue) offline. Note: stimulation was delivered on the left side only but when stimulation was delivered during inspiration there was an evoked potential on both sides of the diaphragm.

Our initial feasibility test involved an open-loop stimulus delivery (i.e., stimulus not triggered by DIA EMGs) in an anesthetized, spinal-intact rat (Fig. 16). Consistent with our mapping studies, left side stimulation evoked a response in both the left and right diaphragm when stimulation was delivered during Inspiratory phase (panel B, red traces). This likely reflects activation of interneurons, although that will need to be evaluated with more rats. When delivered during Expiration, left side stimulation could only produce an evoked potential in the left diaphragm (panel B, blue traces).

Results of a more recent experiment further confirm feasibility and provide an initial demonstration for cervical ISMS serving to restore hemidiaphragm function ipsilateral to an acute C2Hx (Fig. 17). In that study, contralateral EMG activity was used to trigger ISMS (Fig. 17A) thus approximating a closed-loop system. These were limited trials and thus not chronic deliveries. Accordingly, we are not yet able to conclude anything about persistence of effect as others have described for ISMS and forelimb function in rats. Nevertheless, the feasibility of a closed-loop ISMS approach for improving breathing is clearly indicated. We are currently pursuing ISMS in animals with subacute C2Hx (i.e., ~5-7d post-injury). Based upon our earlier proof-of-concept publication (Mercier et al., 2017), the prediction would be that the success of ISMS in an acute C2Hx (Fig. 17) will carry over to the more chronic lesion condition. Figure 18 confirms that supposition (see legend for details).

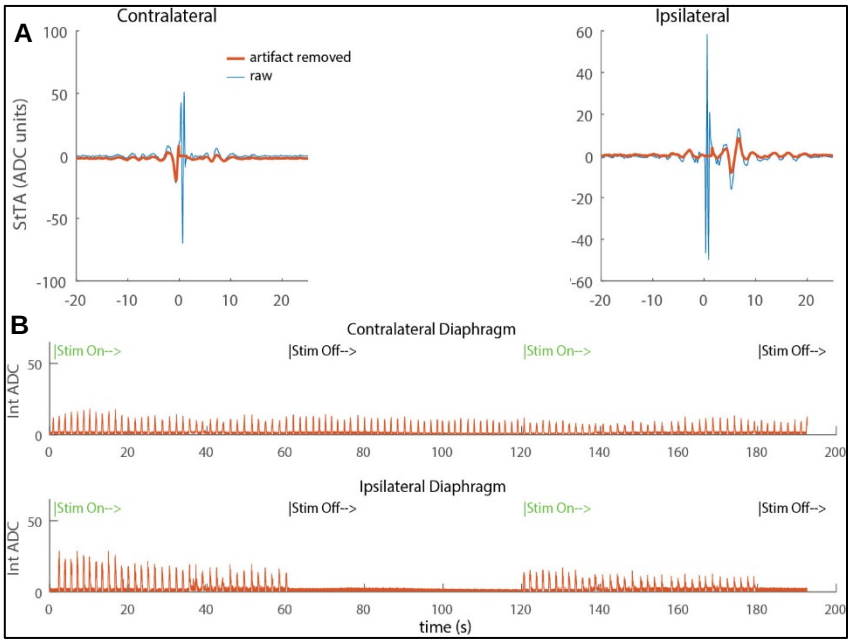

Figure 17. ISMS restoration of hemidiaphragm function in an acute C2Hx rat. **Panel A** shows spike-triggered averaged (StTA) contralateral and ipsilateral diaphragm EMG waveforms to illustrate ipsilateral activity being triggered in relation to natural EMG activity on the contralateral (spinal-intact) side. Blue lines at 0 indicate ISMS (200uA) delivery in register with spared respiratory activity. Thus, a defined action potential can be seen ipsilaterally after stimulus delivery via the Neurochip. **Panel B** shows recordings of contra- and ipsilateral diaphragm activity. Note silence of the diaphragm when no stimulation is being delivered.

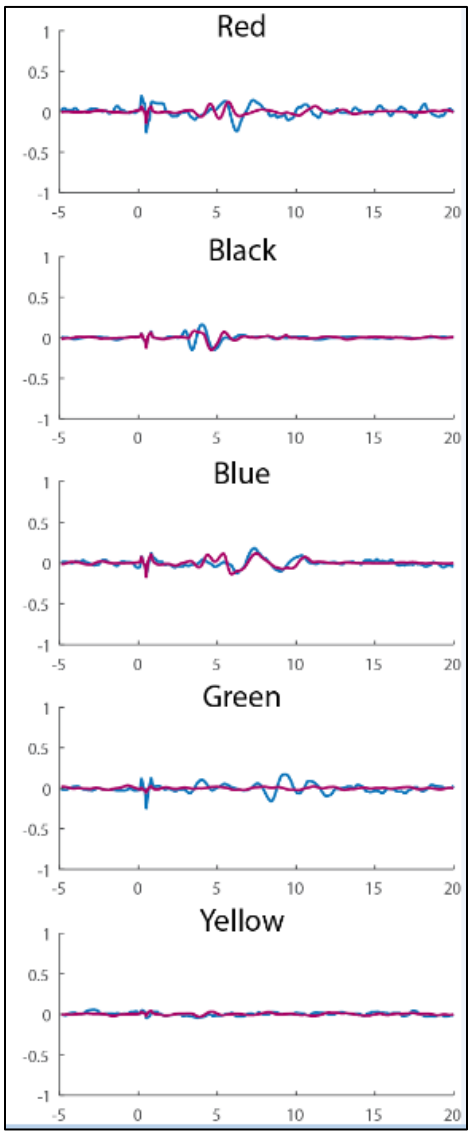

Figure 18. Ipsilateral diaphragm motor evoked potentials following ISMS stimulation via five different spinal electrodes in a rat with a C2Hx made one week prior to implantation of the spinal electrode array. Stimulus intensity = 200uA. Morning recordings (blue), evening (red). Responses are seen on four of the five channels with repeated morning/evening stimulations.

We are now in the process of instrumenting a larger-scale study under recently obtain private funding in which chronic stimulation and its effect on neuronal plasticity in the phrenic circuit will be investigated as part of a program looking at ISMS coupled with neural tissue transplantation.

What opportunities for training and professional development has the project provided?

Training. Portions of this project involved close training interactions between Drs. David Baekey and Kristi Streeter (Post-Doctoral Fellow) through which Dr. Streeter gained additional experience in respiratory neurophysiology and multi-electrode array recordings (Dr. Baekey's expertise). Ms. Lynne Mercier, a fourth year graduate student during this project, also worked under the guidance of Drs. Baekey and Fuller and gained respiratory neurobiology and electrophysiology experience. She is now training at Emory University in the Nurse Anesthesiology program.

Mr. Michael Sunshine (previously Univ. Washington in Dr. Moritz's laboratory) visited the Gainesville campus and learned new surgical procedures and was interacting closely on experimental design with Drs. Fuller and Moritz. He is now in the Fuller laboratory at the University of Florida and enrolled in the Physical Therapy graduate program.

Professional Development. Drs. Streeter and Mercier participated in several national meetings where they presented posters related to the DoD effort described above.

How were the results disseminated to communities of interest?
Nothing to Report.

What do you plan to do during the next reporting period to accomplish the goals?
Nothing to Report as this is the Final Report

4. IMPACT:

What was the impact on the development of the principal discipline(s) of the project?

Spinal cord stimulation (SCS) has been extensively investigated and applied for purposes of improving bladder function and modulating spasticity, as well as pain, following SCI. However, SCS has become an approach of increasing interest in recent years based on animal and human studies demonstrating that SCS can facilitate volitionally-initiated movements in SCI subjects classified as AIS A (i.e., motor and sensory complete). Epidural and more recently, percutaneous, stimulation of the spinal cord have attracted considerable attention based on the minimally or virtually non-invasive nature of the approaches, respectively. On the other hand, more invasive ISMS currently offers other advantages including a tight temporal precision of stimulus delivery. Whether one approach is universally or conditionally better than the other remains to be determined as much remains to be learned about the logistics and mechanisms associated with SCS.

High-frequency, epidural SCS (HF-SCS) has been investigated for improving respiratory function via the activation of intercostal muscles. This method also may provide alternatives to diaphragm pacing, although separate electrodes for intercostal and diaphragm activation would be required. Beyond those studies (see appended Sunshine et al., In Press for references), relatively little effort has been given to concerted investigations of SCS for improving respiratory function and plasticity. In that regard, the studies described above have broken new ground with respect to the feasibility and potential of ISMS for promoting improved diaphragm function. In addition, one of the major issues related to SCS is what is the substrate actually being stimulated. The work undertaken by the University of Florida and the University of Washington has led to fundamental insights that will likely lead to future mechanistic investigations.

We showed via an initial proof-of-concept study the feasibility of using intraspinal microstimulation (ISMS) of the cervical spinal cord to evoke diaphragm activity ipsilateral to acute and subacute hemisection of the upper cervical spinal cord of the rat. Accordingly, we demonstrated the efficacy of diaphragm activation, using an upper airway respiratory EMG signal to trigger ISMS at the level of the ipsilesional phrenic nucleus during acute and advanced post-injury intervals. This opens the possibility of using spared, accessory respiratory function to trigger ISMS in a more appropriate physiological way even in a severely injured, cervical SCI individual. That approach may also be employed to complement HF-SCS approaches. The feasibility and efficacy of ISMS for respiration also has been independently replicated at the University of Washington via this award's subcontract. Our proof-of-concept findings

have now begun to move forward in application to non-anesthetized, freely-behaving rats with acute and subacute C2Hx injuries.

As mentioned, a central issue related to any form of ISMS is what is the nature of the neural substrate being stimulated? Considerable independent efforts were devoted to this question at the Universities of Florida and Washington. We first described a method that reliably identified the locations of multielectrode array (MEA) recording sites while preserving the surrounding tissue for immunohistochemistry. To our knowledge, this is the first cost-effective method to identify the anatomical locations of neuronal ensembles recorded with a MEA during acute preparations without the requirement of specialized array electrodes. In addition, evaluation of activity recorded from silver-labeled sites revealed a previously unappreciated degree of connectivity between mid-cervical interneurons. We followed this up at the University of Florida with a more detailed mapping study that implicated cervical interneurons (C-Ins) as candidates for ISMS-induced modulators of phrenic motoneuron activity impacting on diaphragm function. Even more importantly, we found that recruitment of C-INs can be achieved with acute intermittent hypoxia thereby introducing the possibility of combining a rehabilitation approach with ISMS. To our knowledge, this is the first demonstration that AIH induces plasticity within a propriospinal network that appears to impact upon respiratory function.

These findings were expanded upon by our colleagues at the University of Washington who conducted the first comprehensive mapping of ISMS locations in the cervical and high thoracic spinal cord contributing to evoked respiratory muscle responses. Their findings first demonstrate that respiratory phase is a fundamentally important consideration when designing ISMS protocols and suggest ISMS-induced activation of polysynaptic spinal pathways can effectively recruit inspiratory muscles. Also consistent with polysynaptic (i.e., interneuronal) pathway activation was that diaphragm activation was a long-latency response. Collectively, our combined findings point to ISMS having impact on a complex interneuronal circuitry that ultimately affects the phrenic circuit leading to diaphragm activation. Future use of phase-dependent ISMS to activate respiratory circuits in a synergistic and context-dependent manner may provide functional activation of respiratory muscles and aid in ventilator weaning.

In view of various R&D elements of this project, a detailed comparison of epidural SCS vs. ISMS was beyond the scope of the work proposed and budget. Also, such was not a central goal of what was proposed. Nevertheless, we did find in one of our published studies that HF-SCS had some potential for inducing short-term potentiation analogous to what we saw with ISMS; however, that approach also resulted in increased tonic phrenic motoneuron excitability which would have adverse impact on respiratory muscle activation.

What was the impact on other disciplines?
Nothing to Report

What was the impact on technology transfer?
Nothing to Report

What was the impact on society beyond science and technology?
Nothing to Report

5. CHANGES / PROBLEMS

The most significant change was removing the contusion injury model and replacing it with the C2Hx lesion. That modification, however, was done prior to initiation of the project and with CMRP approval. The major problem with completion of Aim 2 centered largely on personnel availability and the labor-intensive nature of the approach. During the course of this project, the UF laboratory (Dr. Reier) underwent multiple changes in technical staff. In addition, use of the Neurochip interface required significantly more expertise than envisioned initially. The addition of Mr. Michael Sunshine later in this project facilitated the early data presented for ISMS in awake animals. He originally worked as a technician in Dr. Chet Moritz's lab and has considerable experience with the surgery required and use of the Neurochip interface. His ability to devote more time to this project was limited by coursework and other considerations related to his graduate student status.

6. PRODUCTS:

Nothing to Report

Publications, conference papers, and presentations

Journal publications.

Mercier LM, Gonzalez-Rothi EJ, Streeter KA, Posgai SS, Poirier AS, Fuller DD, Reier PJ, and Baekey DM. Intraspinal microstimulation and diaphragm activation after cervical spinal cord injury. *J Neurophysiol 117* (2017)*: 767-776. Federal Support Acknowledged*

Streeter KA, Sunshine MD, Patel SR, Liddell SS, Denholtz LE, Reier PJ, Fuller DD, and Baekey DM. Coupling multielectrode array recordings with silver labeling of recording sites to study cervical spinal network connectivity. *J Neurophysiol 117* (2017a)*: 1014-1029. Federal Support Acknowledged*

Gonzalez-Rothi EJ, Streeter KA, Hanna MH, Stamas AC, Reier PJ, Baekey DM, and Fuller DD. High frequency epidural stimulation across the respiratory cycle evokes phrenic short-term potentiation after incomplete cervical spinal cord injury. *J Neurophysiol jn 00913 02016* (2017)*. Federal Support Acknowledged*

Streeter KA, Sunshine MD, Patel S, Gonzalez-Rothi EJ, Reier PJ, Baekey DM, and Fuller DD. Intermittent Hypoxia Enhances Functional Connectivity of Midcervical Spinal Interneurons. J Neurosci 37 (2017b): 8349-8362. *Federal Support Acknowledged*

Sunshine,M.D., Ganji,C.N., Reier, P.J., Fuller, D.D., Moritz, C.T. Intraspinal microstimulation for respiratory muscle activation. *Exp. Neurol.* (In Press). *Federal Support Acknowledged*

Books or other non-periodical, one-time publications.

None

7. PARTICIPANTS & OTHER COLLABORATING ORGANIZATIONS

What individuals have worked on the project?

Name: ***Paul J. Reier, Ph.D.***
Project Role: *Principal Investigator*
Researcher Identifier (e.g. ORCID ID): https://orcid.org/0000-0003-2319-0575
Nearest person month worked: *3*
Contribution to Project: *Dr. Reier was the overall project coordinator who was involved with maintaining emphasis on the overall goal of this research. He was involved in data analysis, preparation of manuscripts, writing of progress reports, communication with the University of Washington subcontract director, and budgetary oversight.*
Funding Support: *None*

Name: ***Chet Moritz, Ph.D.***
Project Role: *University of Washington Subcontract Principal Investigator*
Researcher Identifier (e.g. ORCID ID): https://orcid.org/0000-0002-3559-9442, www.linkedin.com/in/chet-moritz-9908a2142/
Nearest person month worked: *2*
Contribution to Project: Dr. Moritz was responsible for overseeing studies performed at the University of Washington. He provided routine updates to Dr. Reier and was involved in one publication and another one currently in preparation.
Funding Support: *None*

Name: ***David D. Fuller, Ph.D.***
Project Role: *Co-Investigator*
Researcher Identifier (e.g. ORCID ID): -
Nearest person month worked: *2*

Contribution to Project: *Dr. Fuller was the key respiratory neurophysiology expert who advised on technical matters and, along with Dr. Reier, developed experimental designs and was intimately associated with manuscript preparations.*
Funding Support: *None*

Name: ***David Baekey, Ph.D.***
Project Role: *Co-Investigator*
Researcher Identifier (e.g. ORCID ID): *https://www.linkedin.com/in/david-m-baekey-9488138/*
Nearest person month worked: *1*
Contribution to Project: *Dr. Baekey assisted with directing multiarray recordings performed by Drs. Kristi Streeter and the proof-of-concept ISMS study performed by Lynne Mercier.*
Funding Support: *None*

Name: ***Kristi Streeter, Ph.D.***
Project Role: *Post-Doctoral Fellow*
Researcher Identifier (e.g. ORCID ID):
Nearest person month worked: *5*
Contribution to Project: *Dr. Streeter carried out the MEA mapping studies of Major Task I.*
Funding Support: *None*

Name: ***Elisa Gonzalez-Rothi***
Project Role: *Post-Doctoral Fellow/Res. Asst. Professor*
Researcher Identifier (e.g. ORCID ID):-
Nearest person month worked: *3*
Contribution to Project: *Dr. Gonzalez-Rothi carried out the epidural stimulation study which was published. Due to other career objectives, she became more removed from this project but has recently returned to it and has been integral to the development of the chronic ISMS stimulation studies that are on-going. She also made substantive contributions to other publications which emerged via this award.*
Funding Support: *None*

Name: ***Lynne Mercier (Ph.D.)***
Project Role: *Graduate Student*
Researcher Identifier (e.g. ORCID ID): -
Nearest person month worked: *10*
Contribution to Project: *As a graduate student, she was the lead investigator on the proof-of-concept ISMS paper that was published which also represented a part of her dissertation. She subsequently received her Ph.D. and is now enrolled in the Nurse Anesthesiologist Program at Emory University.*
Funding Support: *None*

Name: ***Michael Sunshine***
Project Role: *Graduate Student*
Researcher Identifier (e.g. ORCID ID): -
Nearest person month worked: 12 to *3* more recently
Contribution to Project: *Primary person responsible for carrying out U. Washington studies. He has now come to the Univ. Florida to pursue graduate studies and is credited for launching the initial chronic ISMS experiments in awake animals. His past experience with the surgical procedures required and technical aspects of the Neurochip interface have been crucial. While at the University of Washington, he devoted full-time effort to the project. However, due to other demands of early graduate school, his effort had to be reduced significantly.*
Funding Support: *None*

Name: ***Lucy Denholtz***
Project Role: *Technician/Laboratory Manager*
Researcher Identifier (e.g. ORCID ID): -
Nearest person month worked: *12*

Contribution to Project: *Basic surgical and histological assistance. She has subsequently obtained employment at Columbia University.*
Funding Support: *None*

Name: ***Savannah Posgai***
Project Role: *Laboratory Assistant*
Researcher Identifier (e.g. ORCID ID): -
Nearest person month worked: *12*
Contribution to Project: *General technical assistance for ~ one year before leaving to enroll in medical school at the University of Florida.*
Funding Support: *None*

Name: ***Joey Tringali***
Project Role: *Laboratory Assistant*
Researcher Identifier (e.g. ORCID ID): -
Nearest person month worked: *5*
Contribution to Project: *He replaced Ms. Posgai for ~ 5 mos. before leaving to pursue medical school.*
Funding Support: *None*

Name: ***Robin Zimmer***
Project Role: *Laboratory Technician*
Researcher Identifier (e.g. ORCID ID):*1234567*
Nearest person month worked: *~3*
Contribution to Project: *She replaced Ms. Denholtz. However, for administrative reasons and insufficient experience, her employment had to be terminated.*
Funding Support: *None*

Name: ***Orinda Hobson***
Project Role: *Laboratory Assistant/Current Laboratory Manager*
Researcher Identifier (e.g. ORCID ID):*1234567*
Nearest person month worked: *12*
Contribution to Project: *Ms. Hobson replaced Mr. Tringali and after Ms. Zimmer left the laboratory, Ms. Hobson began assuming more technical and day-to-day management responsibilities in the laboratory. She is now effectively interfacing with Dr. Gonzalez-Rothi and Mr. Sunshine on the chronic ISMS studies that are continuing.*
Funding Support: *None*

Name: ***Isaac Josh Abecassis, M.D.***
Project Role: *Resident Dept. Neurological Surgery, Univ. Washington*
Researcher Identifier (e.g. ORCID ID):*1234567*
Nearest person month worked: *5*
Contribution to Project: *He replaced Mr. Sunshine at the University of Washington and has been pursuing ISMS studies as described above.*
Funding Support: *None*

Has there been a change in the active other support of the PD/PI(s) or senior/key personnel since the last reporting period?

Two foundation awards were received towards the end of the Extension Without Funds year of this award. Those projects build upon the ISMS approach developed under auspices of the DOD award, but do not overlap or in any other way conflict with the DOD Statement of Work in terms of design or execution. However, the controls for those new projects, which involve intraspinal neural tissue transplantation, build upon Major Tasks 8-11. In effect, therefore, that part of the DoD proposal will be carried out and partial DoD support of that part of the future studies will be acknowledged based upon history.

What other organizations were involved as partners?
Nothing to Report

8. SPECIAL REPORTING REQUIREMENTS:

COLLABORATIVE AWARDS: N/A

QUAD CHARTS: Included in appendices

9. APPENDICES:

Table 1			
Major Task	**Current Status**	**Publication(s)**	**Explanation**
#1: To determine chronic changes in neuronal discharge patterns within the phrenic circuit region following a C2 hemisection (C2Hx) lesion.	Partially Completed	Streeter et al., 2017a, b Sunshine et al., in press	The paper was based on normal, spinal-intact animals. The data for comparison with chronic injuries has been collected and is undergoing analysis.
#2: Terminal electrophysiological comparison of epidural and ISMS stimulation on activation of the phrenic motor circuit after chronic C2Hx (one month post-SCI).	Completed	Mercier et al., 2017 Gonzalez-Rothi et al., 2017	We did not make a head-to-head comparison based on budgetary and personnel considerations. However, the results of the two papers indicated more promise for ISMS.
#3: Analysis of Tissue Responses to microwire implantation.	Not Completed		Made more sense to do this after chronic stimulation (SOW #10). Some initial results of inactive wire implants were presented in an earlier Progress Report. However, we got better with introducing microwires over time.
#4: Prepare for respiratory studies.	Completed by Univ. Wash. researchers		
#5: Conduct Phase I of closed-loop intraspinal stimulation of PhMNs (phrenic motoneurons) after C2Hx. Contralateral diaphragm EMG triggers ISMS of PhMNs.	Partially Completed; Study still in progress at Univ. Wash.		Personnel changes at Univ. Washington affected progress
#6: University of Florida replication of closed-loop/C2Hx (contralateral diaphragm triggered stimulus) results at U.W. and comparison with epidural stimulation.	Not Completed		Dependent on SOW #6 which is still ongoing. Comparison with epidural is not relevant as each may be more suited to some conditions than another.
#7: Conduct Phase II of closed-loop intraspinal stimulation of PhMNs. Contralateral intercostal EMG triggers ISMS of PhMNs.	Completed	Mercier et al., 2017	For this SOW item, we used the hypoglossal nerve as the source of the EMG trigger for technical reasons. The principle is the same since hypoglossal nerve activity also is in relative synchrony with diaphragm activity.
#8: Conduct Open-loop intraspinal stimulation of PhMNs. Average respiratory activity recorded in Phase I & II triggers ISMS.	Partially completed	Sunshine et al., In Press	All subtasks of this SOW Item could not be completed as stated due to personnel changes at the Univ. Washington. However, the main objective was achieved in that we determined ISMS efficacy was dependent upon respiratory phase in spinal-intact animals. Such information is vital to SOW Item 10.
#9: Conduct Phase III of closed-loop intraspinal stimulation of PhMNs. Repeat most promising closed-loop method (Diaphragm or intercostal triggered ISMS) using the C2Hx model.	Not completed, but in progress		The progression of work on this project was such that UF took the lead in first demonstrating proof-of-concept for ISMS impact on respiration (SOW #2). Dr. Moritz's lab at the Univ. Washington has preliminary data replicating the UF results. Work is continuing to expand on those initial findings.
#10: U.F. replication of most efficacious closed- or open-loop ISMS treatment in rats with chronic C2Hx.	Not completed		This part of the SOW involves a challenging technical approach in order to provide chronic ISMS to spinal-injured animals. Personnel to carry this out did not become available until late in the funding period, and considerable efforts were required to become fully instrumented to perform these studies. Preliminary data are shown in the final report demonstrating we are not in a closer position to perform these studies which will be continued under other funding mechanisms. However, initial publications will cite CDMRP funding.
#11: Neuroanatomical studies to on closed-loop and open-loop ISMS treated rats.	Not completed		Studies dependent on SOW 10 and will be done under new funding mechanisms.

Table 1. Note that C3-4 contusions stated in the original SOW text has been replaced by the C2Hx injury per approval prior to the initiation of this project.

J Neurophysiol 117: 767–776, 2017.
First published November 23, 2016; doi:10.1152/jn.00721.2016.

RESEARCH ARTICLE | *Spinal Control of Motor Outputs*

Intraspinal microstimulation and diaphragm activation after cervical spinal cord injury

L. M. Mercier,[1] E. J. Gonzalez-Rothi,[2] K. A. Streeter,[2] S. S. Posgai,[1] A. S. Poirier,[2] D. D. Fuller,[2] P. J. Reier,[1] and D. M. Baekey[3]

[1]*Department of Neuroscience, University of Florida, Gainesville, Florida;* [2]*Department of Physical Therapy, University of Florida, Gainesville, Florida; and* [3]*Department of Physiological Sciences, University of Florida, Gainesville, Florida*

Submitted 6 September 2016; accepted in final form 21 November 2016

Mercier LM, Gonzalez-Rothi EJ, Streeter KA, Posgai SS, Poirier AS, Fuller DD, Reier PJ, Baekey DM. Intraspinal microstimulation and diaphragm activation after cervical spinal cord injury. *J Neurophysiol* 117: 767–776, 2017. First published November 23, 2016; doi:10.1152/jn.00721.2016.—Intraspinal microstimulation (ISMS) using implanted electrodes can evoke locomotor movements after spinal cord injury (SCI) but has not been explored in the context of respiratory motor output. An advantage over epidural and direct muscle stimulation is the potential of ISMS to selectively stimulate components of the spinal respiratory network. The present study tested the hypothesis that medullary respiratory activity could be used to trigger midcervical ISMS and diaphragm motor unit activation in rats with cervical SCI. Studies were conducted after acute (hours) and subacute (5–21 days) C_2 hemisection (C2Hx) injury in adult rats. Inspiratory bursting in the genioglossus (tongue) muscle was used to trigger a 250-ms train stimulus (100 Hz, 100–200 μA) to the ventral C_4 spinal cord, targeting the phrenic motor nucleus. After both acute and subacute injury, genioglossus EMG activity effectively triggered ISMS and activated diaphragm motor units during the inspiratory phase. The ISMS paradigm also evoked short-term potentiation of spontaneous inspiratory activity in the previously paralyzed hemidiaphragm (i.e., bursting persisting beyond the stimulus period) in ~70% of the C2Hx animals. We conclude that medullary inspiratory output can be used to trigger cervical ISMS and diaphragm activity after SCI. Further refinement of this method may enable "closed-loop-like" ISMS approaches to sustain ventilation after severe SCI.

NEW & NOTEWORTHY We examined the feasibility of using intraspinal microstimulation (ISMS) of the cervical spinal cord to evoke diaphragm activity ipsilateral to acute and subacute hemisection of the upper cervical spinal cord of the rat. This proof-of-concept study demonstrated the efficacy of diaphragm activation, using an upper airway respiratory EMG signal to trigger ISMS at the level of the ipsilesional phrenic nucleus during acute and advanced postinjury intervals.

phrenic motor nucleus; rat; respiration; hypoglossal respiratory activity; diaphragm function

SEVERE RESPIRATORY COMPROMISE often occurs after spinal cord injury (SCI) at upper cervical to midcervical spinal levels (Mansel and Norman 1990; Winslow and Rozovsky 2003). When independent breathing is not possible, positive-pressure mechanical ventilation is often used to sustain alveolar ventilation, but at the risk of potentially rapid diaphragm atrophy, atelectasis, and respiratory tract infections (Bezzant and Mortensen 1994; Laghi et al. 2003; Smuder et al. 2016). Diaphragm and phrenic nerve pacing options are clinically available (DiMarco et al. 2005; Glenn and Phelps 1985; Onders et al. 2009), and recent preclinical work has begun exploring high-frequency epidural stimulation of the spinal cord to activate the diaphragm (DiMarco and Kowalski 2013, 2015; Kowalski et al. 2013).

Another approach that may effectively activate respiratory muscles after SCI is intraspinal microstimulation (ISMS). Implementation of this method in motor systems has been demonstrated (Giszter 2015; Kasten et al. 2013; McPherson et al. 2015; Tator et al. 2012), but applications to respiratory motor output after cervical SCI have not been investigated. Potential advantages of ISMS include the ability to deliver currents over a relatively wide range of intensities and with high selectivity for specific motor systems (Mondello et al. 2015; Mushahwar et al. 2000; Sunshine et al. 2013).

The present study was therefore designed to obtain proof-of-concept evidence in support of cervical ISMS as a means of activating diaphragm motor units after cervical SCI. To move toward a "closed-loop-like" design for ISMS, we recorded the inspiratory output of an upper airway muscle (the genioglossus, innervated by cranial nerve XII) and used that signal to trigger stimulation. Thus cervical ISMS was activated by endogenous inspiratory drive. The data show that a physiologically relevant medullary inspiratory output can be used to trigger cervical ISMS and that this approach can effectively activate diaphragm motor units after acute and subacute SCI.

MATERIALS AND METHODS

Thirteen female Sprague-Dawley rats (255 ± 16 g; Harlan, Indianapolis, IN) were distributed between two experimental groups: *1*) ISMS after acute SCI, tested before and immediately after lateral hemisection of the spinal cord at C_2 (C2Hx) ($n = 8$), and *2*) ISMS after subacute SCI, tested 5–21 days after C2Hx ($n = 5$). All data were collected in terminal procedures using protocols approved by the Institutional Animal Care and Use Committee at the University of Florida and the US Army Medical Research and Materiel Command Animal Care and Use Review Office.

Address for reprint requests and other correspondence: D. M. Baekey, Dept. of Physiological Sciences, PO Box 100144, Gainesville, FL 32610-0144 (e-mail: dbaekey@ufl.edu).

C2Hx surgery. For survival surgery, rats were initially anesthetized with isoflurane (3–5% in O_2) in a closed chamber and then anesthesia was maintained via nosecone (1.5–3% in O_2). A dorsal incision was made over the cervical spine, followed by a C_2 laminectomy and durotomy. For acute C2Hx, resection lesions were performed with a needle-blade microknife (Fine Science Tools, Foster City, CA). Subacute C2Hx resection lesions were made with microscissors and fine forceps followed by gentle aspiration of tissue to complete the hemisection (Fuller et al. 2008). The dura and overlying muscles were closed and lactated Ringer solution (5 ml sc) and buprenorphine were administered (0.03 mg/kg sc.; Hospira, Lake Forest, IL). Postoperative care consisted of daily lactated Ringer solution (5 ml/day sc) and oral nutritional supplement (1–3 ml/day; Nutrical, Webster Veterinary). Buprenorphine was given at ~12-h intervals for 2 days after surgery.

General neurophysiology protocols. Rats were anesthetized as above. Rectal temperature was maintained at ~37.5°C by a heating pad (CWE, Ardmore, PA). A femoral artery was catheterized (PE-50) for blood pressure measurements (Statham P-10EZ pressure transducer, CP122 AC/DC strain gauge amplifier; Grass Instruments, West Warwick, RI) and arterial blood samples. The femoral vein of the same hindlimb was also catheterized (PE-50) for supplemental fluid administration and conversion from isoflurane to urethane anesthesia (1.7 g/kg iv; Sigma, St. Louis, MO). Animals received a tracheotomy and were mechanically ventilated (50–65% O_2, balance N_2; 6–7 ml/kg volume; 70–72 bpm frequency; Harvard Apparatus, Holliston, MA) throughout the experimental procedures. Since spontaneously breathing anesthetized rats can rapidly become hypercapnic, we elected to employ mechanical ventilation for these initial experiments in order to keep blood gases stable and remove Pa_{O_2} and/or Pa_{CO_2} fluctuations as confounding variables.

End-tidal CO_2 (Capnogard 1265; Respironics, Wallingford, CT) was continuously monitored, and arterial blood gases (iSTAT1; Abbott, Princeton, NJ) were periodically assessed from 0.1-ml arterial samples. On the basis of these measures, the inspired CO_2 content was adjusted to maintain Pa_{CO_2} at 40 mmHg. If base excess was greater than −3 meq, this was corrected with intravenous administration of sodium bicarbonate solution [8.4%, Hospira; dose (ml) = 0.3·weight (kg)·standard base excess].

Recordings of EMG activity from respiratory-related muscles (i.e., diaphragm, genioglossus, and intercostal) and an off-target, nonrespiratory muscle [i.e., extensor carpi radialis longus (ECR)] were obtained with pairs of Teflon-coated tungsten hooked wires (A-M Systems, Sequim, WA). Recordings of the genioglossus muscle were obtained at the base of the tongue (Fuller et al. 1999; Fuller and Fregosi 2000) and exhibited a centrally driven inspiratory rhythm that was used to trigger ISMS. For intercostal EMG recordings, a small incision lateral to the sternum was made at the T_2 level and wires were placed 1–1.5 cm lateral to the midline.

The spinal cord was exposed via a cervical middorsal incision followed by laminectomy and durotomy from C_2 to C_5. Raw EMG signals were amplified at 100-10K, band-pass filtered at 100 Hz–10 kHz (A-M Systems, Carlsborg, WA), and, in the case of the genioglossus EMG recording, passed through a moving time averager (50 ms time constant; CWE, Ardmore, PA). The moving time average signal was used to trigger the stimulator for ISMS. All EMG signals were digitized at 25 kHz (CED Power 1401) and recorded (Spike2 v8; CED, Cambridge, UK) to a PC and then analyzed off-line.

ISMS at midcervical spinal cord. A tungsten microwire electrode (FHC, Bowdoin, ME) was mounted in a stereotaxic micromanipulator (David Kopf Instruments, Tujunga, CA). The microwire had a 100-μm segment at the tip stripped of all insulation. The electrode was placed above the C_4 segment with the dorsal root entry zone as the lateral anatomical landmark. Electrical activity was initially recorded via the stimulating electrode and assessed visually with Spike2 software and audibly with an AM8 Audio Monitor (Grass Technologies, Quincy, MA). The software program simultaneously displayed the inspiratory diaphragm EMG recording; these procedures enabled placement of the stimulating electrode tip in proximity to inspiratory neurons (i.e., targeting phrenic motoneurons). Inspiratory bursting was absent in rats with subacute C2Hx injury. Therefore, a stimulator and constant-current stimulus isolation unit (S88X and SIU-C; Grass Technologies, Warwick, RI) were used to deliver single pulses (0.3 ms duration) during electrode descent with gradually decreasing currents (200, 100, 50 μA). This approach allowed us to determine a location for ISMS that evoked left diaphragm activation.

Stimulation of the spinal cord was initiated (triggered) with the EMG signal recorded from the genioglossus muscle. Specifically, a "threshold crossing" was established such that when the inspiratory integrated EMG burst (50 ms time constant) reached a preset amplitude the spinal cord was stimulated. All stimulations during the inspiratory phase were made at the onset of the genioglossus inspiratory burst, while stimulations made during expiratory periods were accomplished by adding a 400-ms delay to the trigger.

Experimental group 1: ISMS before and after acute C2Hx. The genioglossus EMG signal was used to trigger ISMS during two consecutive inspiratory cycles, followed by ISMS delivered during two consecutive expiratory cycles. In both cases, repeated 250-ms stimulus trains (200 μA) were delivered with 0.3 ms pulse duration and 100 Hz stimulus frequency. Once these initial stimulations were complete, ISMS was delivered during the inspiratory cycle for 1 min. All of the aforementioned ISMS was done with the spinal cord intact. After C2Hx, the ISMS protocol was repeated, as described above. Subsequent to protocols performed with spinal cord intact or after C2Hx, an additional bout of ISMS was administered after neuromuscular blockade via intravenous pancuronium bromide (2.5 mg/kg; Hospira) to confirm unequivocally that the evoked activity was not contaminated by a stimulus artifact.

Selection of stimulus parameters. Pilot experiments were done with a manually triggered, open-loop approach in spinal-intact animals. Repeated 250-ms trains of ISMS were targeted to the left phrenic motor nucleus, and EMG activity was recorded in both hemidiaphragms, the genioglossus, and ipsilateral intercostal and forelimb (ECR) muscles (see, e.g., Fig. 1). A range of stimulation frequencies (50, 100, 200, 300 Hz) and currents (50–200 μA) were tested to optimize parameters for eliciting compound motor unit action potentials (MUAPs) in the left diaphragm. Activation of the ipsilateral hemidiaphragm was more pronounced when 100-Hz stimulation was used, with stimulation frequencies above 200 Hz producing large contractions of nonrespiratory muscles. Preliminary experiments also indicated that progressive attenuation of ISMS-induced phrenic MUAP amplitude occurred during sustained stimulation (e.g., 1 min) at 200 Hz but not at lower stimulus frequencies (50 Hz, 100 Hz). In the first series of experiments, a stimulus current of 200 μA was used to activate the ipsilateral diaphragm.

Experimental group 2: ISMS after subacute C2Hx. The intraspinal electrode placement was determined as described above. Triggered ISMS was then delivered during two consecutive expiratory periods, followed by one continuous minute of stimulation during the inspiratory phase. In both cases, a continuous 250-ms train was delivered with 0.3-ms pulses at 100 Hz and 100 μA. Stimulations also were repeated after neuromuscular blockade as described above.

Consistent with other reports, we used cessation of the ipsilateral diaphragm inspiratory EMG burst and histology as functional and anatomical verification, respectively, of the subacute C2Hx lesions (Goshgarian 1981). After the electrophysiology protocols, the animals were perfused with saline followed by 4% paraformaldehyde (Sigma). The cervical spinal cords from the subacute C2Hx animals were subsequently harvested, and a tissue block including the C_2 region was paraffin embedded, sectioned (8 μm), and counterstained with cresyl violet.

Biomechanical impact of ISMS. Changes in tracheal pressure were assessed as a crude indicator of the biomechanical impact of ISMS. It should be noted, however, that this was not considered to be a primary

outcome variable but rather an accessory measurement intended to provide some insight regarding the functional impact of spinal stimulation. The pressures associated with lung inflation and deflation were measured at the tracheal cannula. Measurements were taken continuously and used to compare baseline conditions to stimulation periods. For each period of interest, tracheal pressure deflections for 20 consecutive breaths were averaged and presented in a box and whisker plot (SPSS; IBM, Armonk, NY). Passive tracheal pressure values during exhalation were obtained in each preparation after neuromuscular blockade and thus provided a baseline measurement that was devoid of any respiratory contribution from the animal (for additional details, see RESULTS).

Data acquisition and analyses. For the first group of experiments, results from the spinal-intact condition were compared to data collected 10 min after acute C2Hx. In addition to the evoked responses (i.e., response during ISMS), we also evaluated the impact of the ISMS on spontaneous EMG activity (i.e., following the period of stimulation). To assess ISMS-entrained activation of motor units, the EMG signals were averaged with respect to stimulus pulses within each trial. The resulting stimulus-triggered average (McPherson et al. 2015; Moritz et al. 2007) served to minimize activity unrelated to ISMS. The resultant waveform averages represented ISMS-entrained MUAPs. All data were collected with a CED Spike2 data acquisition system and subsequently analyzed with Spike2 v8 software on a standard PC. Values are reported as means ± SD.

Statistics. A one-way repeated-measures ANOVA followed by the Tukey post hoc test (SigmaPlot; Systat Software, San Jose, CA) was used to compare data collected during baseline vs. ISMS. Dependent variables included the amplitude of MUAPs and spontaneous EMG burst amplitude, blood pressure, tracheal pressure, heart rate, and blood gas data. A "detectability index" statistical test (Aertsen and Gerstein 1985) was used to compare ISMS-evoked MUAP amplitude to background activity in the EMG recordings. We used the modified version of this test with a more stringent value of $D \geq 3$ to prevent "false positives" (Melssen and Epping 1987).

RESULTS

ISMS with spinal cord intact. A representative example of triggered cervical ISMS during the inspiratory phase is provided in Fig. 1. Note that compound MUAPs in the left diaphragm are clearly discernible (Fig. 1*C*) and are entrained to each stimulation pulse (e.g., Fig. 1*D*). In this example, the average latency between stimulus artifact and MUAP peak is

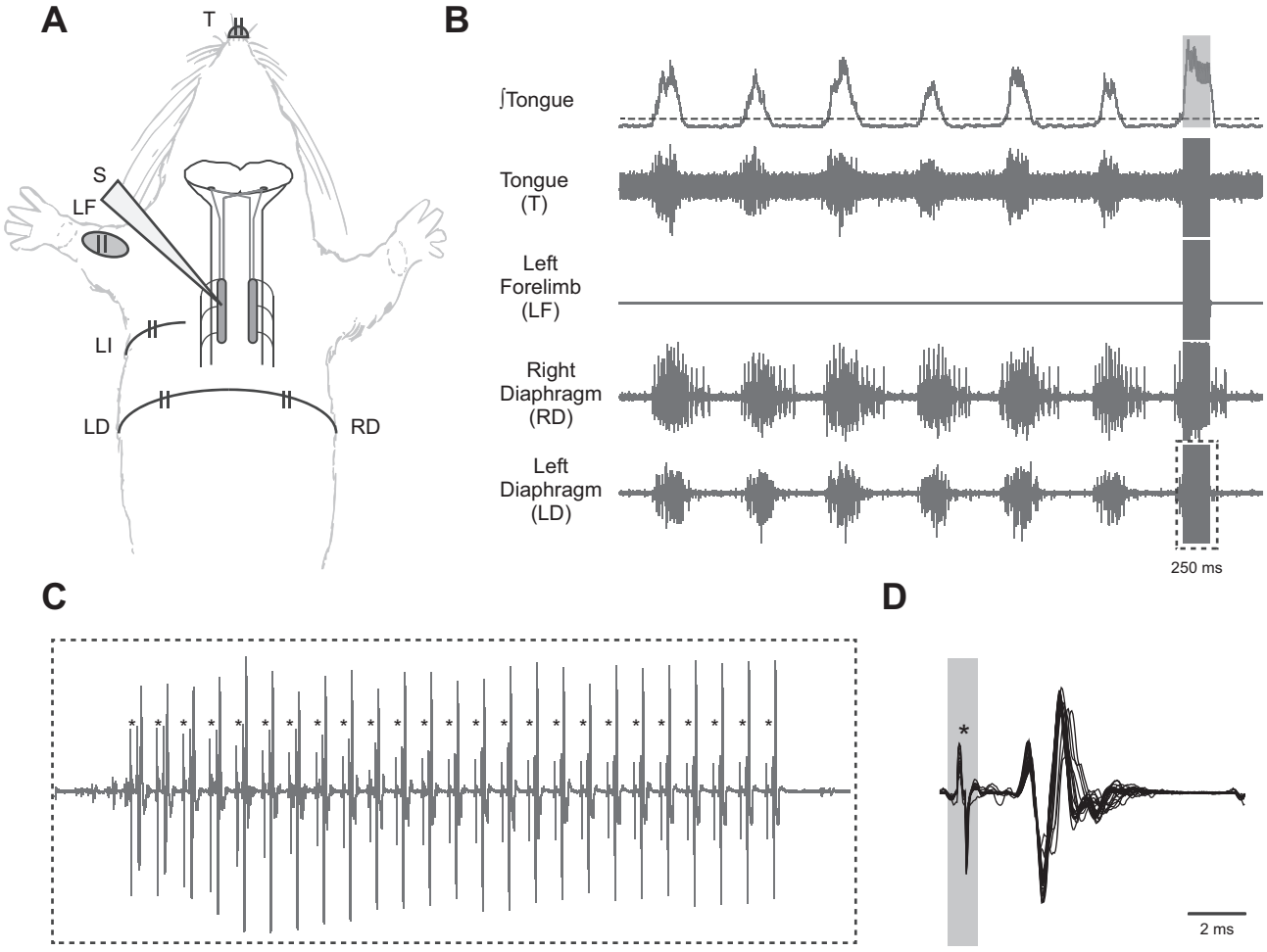

Fig. 1. Cervical ISMS activates the ipsilateral diaphragm *A*: schematic diagram illustrates the EMG recording sites relative to the placement of the stimulating electrode (S). The stimulating electrode was placed in the immediate vicinity of the phrenic motor nucleus, and ISMS was initiated via a trigger signal based on inspiratory tongue (genioglossus) EMG activity. LI, left intercostal. *B*: pre-C2Hx representative EMG recordings from the genioglossus, extensor carpi radialis (ECR), and both sides of the diaphragm showing baseline (prestimulation) activity and a period of genioglossus-triggered cervical ISMS (100 Hz, 200 μA; 0.3-ms pulse duration, 250-ms train duration) represented by a gray box in the ∫tongue trace. *C*: expanded trace of the EMG recording from the left diaphragm during the period of ISMS shows each stimulus artifact, indicated by asterisks, and each subsequent MUAP. *D*: overlay of each elicited MUAP, aligned by the stimulus artifact, demonstrates constant latency and amplitude.

2.14 ± 0.05 ms, which is consistent with a synaptic delay before motor unit activation. An example of ISMS delivered during the expiratory phase is provided in Fig. 2. In the absence of spontaneous inspiratory EMG activity, it can be appreciated that ISMS targeting the left phrenic motor nucleus evoked a marked response in both the ECR and diaphragm but had minimal impact on the left tongue or right diaphragm. To confirm that the very small-amplitude EMG signals in the tongue, diaphragm, and intercostals represented activation of motor units, we employed a previously published "detectability index" for evoked potentials (Aertsen and Gerstein 1985; Melssen and Epping 1987). This assessment indicated that ISMS evoked a small but statistically significant increase in entrained and averaged EMG activity in the tongue (5 of 8 animals), left intercostal (8 of 8 animals), and right diaphragm (8 of 8 animals). It should be noted, however, that the amplitudes of these off-target evoked potentials were modest compared with those of the left diaphragm and ECR muscles. Neuromuscular blockade eliminated evoked potentials, as expected (Fig. 2*C*).

ISMS after high cervical SCI. Experiments were performed immediately after C2Hx (acute injury) and also in rats that were 5–21 days post-C2Hx (subacute injury). These temporally advanced lesion experiments were performed to determine whether degenerative processes triggered by C2Hx (e.g., axonal retraction) prevented or mitigated the impact of ISMS on diaphragm activation. The general experimental paradigm is illustrated in Fig. 3*A*.

In the acute C2Hx experiments, diaphragm MUAPs were first evaluated with the spinal cord intact (Fig. 3*B*). The ISMS-evoked potentials in the spinal-intact condition were similar to those described in the preceding section. Acute C2Hx abolished spontaneous inspiratory EMG activity in the ipsilateral hemidiaphragm in all animals (Fig. 3*C*). However, cervical ISMS still produced clear MUAPs in the ipsilateral diaphragm after the acute lesion (Fig. 3*D*). Before C2Hx, the average latency from stimulus to the peak of the MUAP was 1.99 ± 0.25 ms. After C2Hx the value tended to be reduced (1.69 ± 0.57 ms), but this did not approach statistical significance ($P = 0.190$). In seven of eight experiments, the amplitude of the ISMS-evoked MUAP remained relatively consistent after the acute C2Hx, ranging from 80% to 124% of the preinjury value, with a mean of 94 ± 15% ($P = 0.065$ vs. pre-C2Hx). There was one significant outlier rat (confirmed with Grubbs' outlier test, $P < 0.05$) that demonstrated a profound reduction in MUAP amplitude after acute C2Hx, with

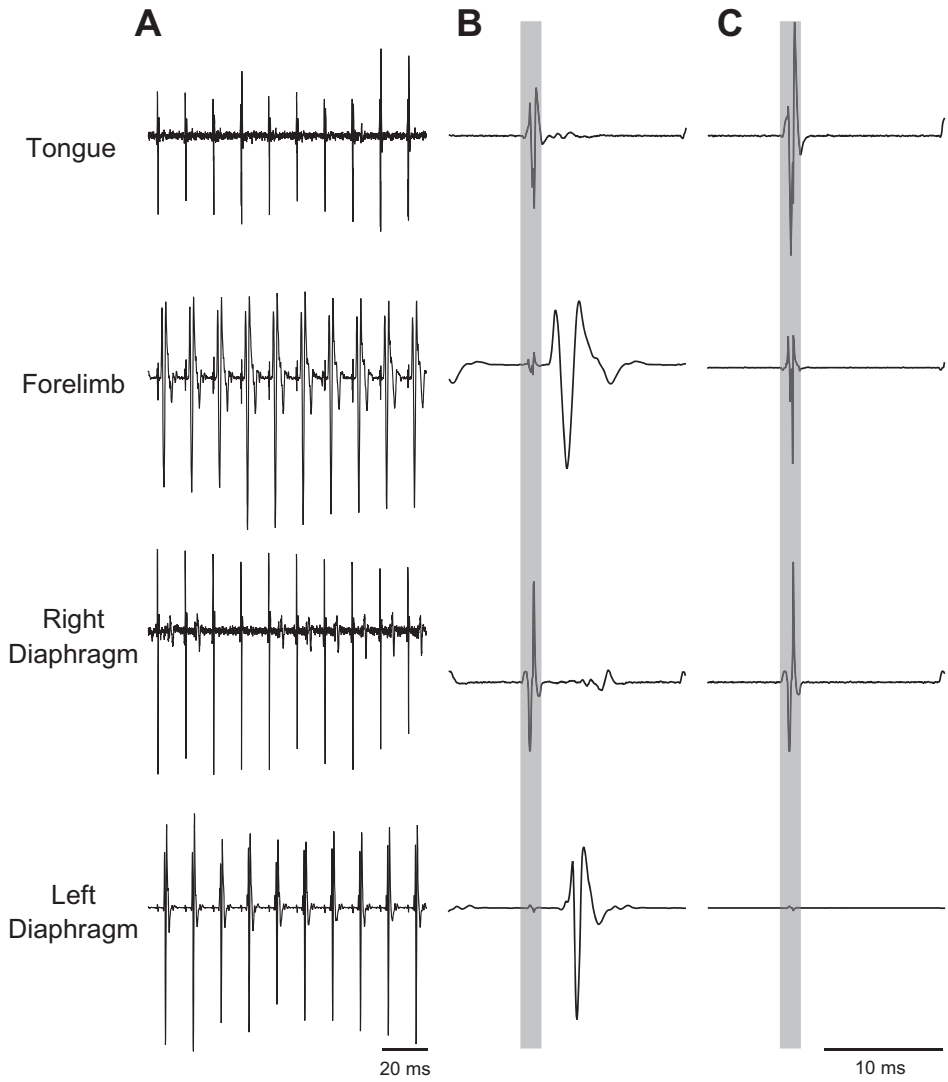

Fig. 2. Examples of raw EMG activity recorded in the tongue (genioglossus), forelimb (ECR), and the left and right hemidiaphragm during ISMS. *A*: representative examples before C2Hx. *B*: stimulus-triggered averages of EMG activity show prominent MUAPs in the forelimb and ipsilateral diaphragm. *C*: stimulus-triggered averages of EMG activity after neuromuscular blockade. In *B* and *C*, the stimulus artifact is highlighted by the gray boxes. Stimulus-triggered averages were scaled to the same values and represent 25 stimulus triggers. In these examples, ISMS was delivered at 100 Hz and 200 μA during expiration.

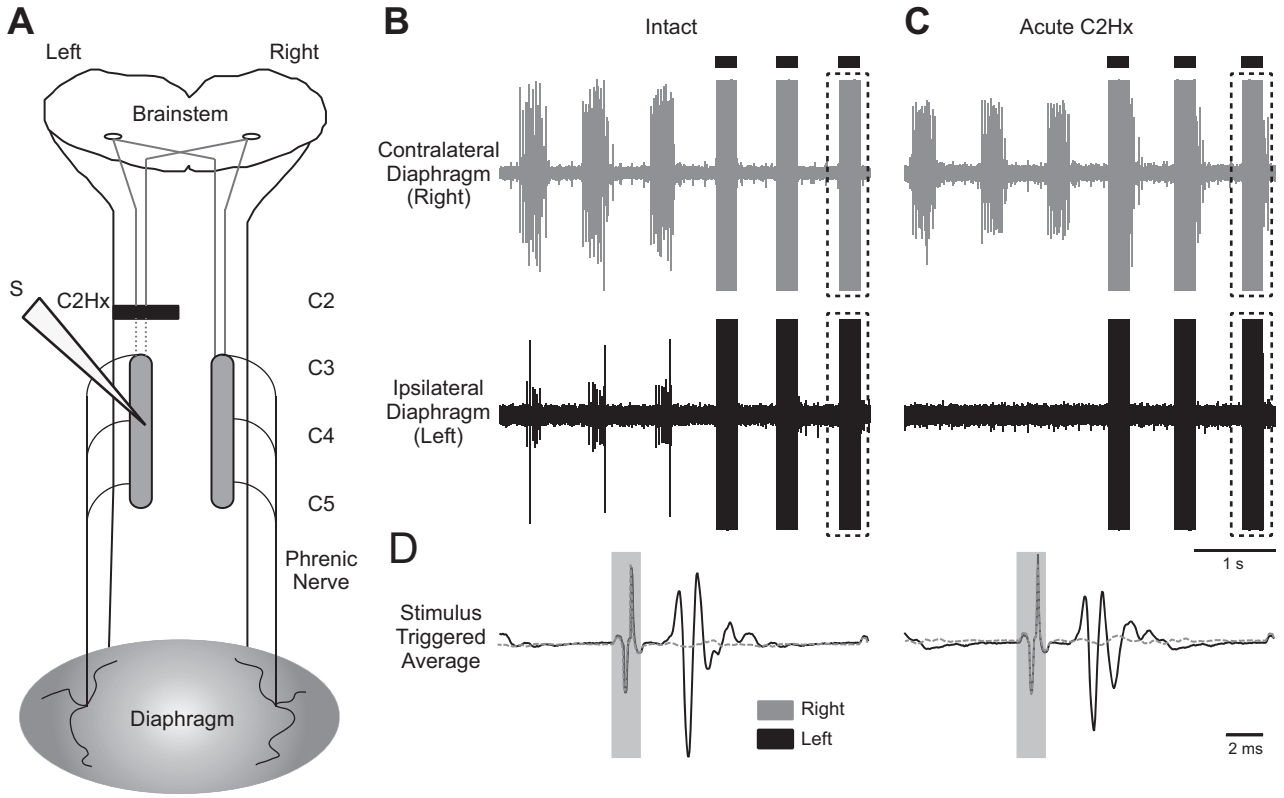

Fig. 3. ISMS after acute C2Hx. *A*: illustration of the electrode placement relative to the C2Hx lesion. The solid dark bar represents the injury site; the dashed lines represent severed pathways. *B*: examples of EMG activity in the right and left diaphragm before C2Hx. *C*: examples of left and right diaphragm EMG activity after acute C2Hx. Note that activity is abolished in the left diaphragm. In *B* and *C*, 3 spontaneous breaths are shown followed by 3 breaths during triggered cervical ISMS (solid bars; 100 Hz, 200 μA). *D*: stimulus-triggered averages of right and left diaphragm EMG activity obtained from the period of ISMS highlighted by dashed boxes in *B* and *C*. Stimulus-triggered averages were scaled to the same values and represent 25 stimulus triggers. In *D*, the stimulus artifact is highlighted by the gray boxes.

evoked responses reaching only 8% of the preinjury amplitude. If that particular data point is included in the calculation of the overall mean the values after acute C2Hx are 83 ± 35% of the preinjury condition, but the added variance actually produces a higher P value ($P = 0.139$ vs. preinjury). Collectively, the data are consistent with a slight reduction in cervical ISMS-evoked MUAP amplitude in most animals after acute C2Hx. The off-target impact of ISMS after C2Hx (i.e., evoked activity in ECR, tongue, and right diaphragm) was indistinguishable from that reported above for the spinal-intact condition (data not shown).

Tracheal pressures were evaluated to explore the potential of a biomechanical impact of ISMS-induced muscle contraction (Fig. 4, *A* and *B*). Negative pressure swings in tracheal pressure would be expected in this preparation if diaphragm contraction is altering the dimensions of the thoracic cavity. In the spinal-intact condition, genioglossus-triggered cervical ISMS caused a significant negative deflection in tracheal pressure ($P = 0.02$ vs. baseline; Fig. 4*C*), as expected. The acute C2Hx injury resulted in a small, but statistically significant, change in the tracheal pressures that were recorded during ventilator-induced lung inflation (i.e., independent of ISMS; $P = 0.028$; Fig. 4*C*). After acute C2Hx, ISMS also induced a change in tracheal pressure ($P = 0.005$ vs. baseline), thus suggesting a biomechanical impact of the stimulation. However, the relative magnitude of ISMS-induced changes in tracheal pressure were attenuated after C2Hx ($P = 0.038$; Fig. 4*C*).

Spontaneous ipsilateral diaphragm EMG activity was absent in rats studied 5–21 days after C2Hx (Fig. 5*A*), and subsequent histological evaluation of the spinal cord indicated anatomically complete hemilesion in all animals (Fig. 5*B*). The ISMS procedure evoked clearly discernible MUAPs in the ipsilateral (paralyzed) hemidiaphragm (Fig. 5*C*). Compared with the acute injury group, the only apparent difference in the ISMS responses in the animals with the subacute lesions was a trend for more variable and longer latencies. On average, however, there were no statistical differences between the groups for latency (acute C2Hx: 1.69 ± 0.57 ms, subacute C2Hx: 2.50 ± 0.67 ms), but the increase in latency in the subacute group was close to threshold for significance ($P = 0.065$). The MUAP amplitude was variable, but with no evidence for a difference between the two groups (acute C2Hx: 1.62 ± 1.45 mV, subacute C2Hx: 1.76 ± 2.65 mV, $P = 0.833$). ISMS caused the expected negative deflection in tracheal pressure in the subacute C2Hx animals, thus confirming that there was a biomechanical impact of the stimulation (Fig. 5*D*). The off-target muscle activation was similar to what was obtained in the spinal-intact and acute C2Hx animals. Thus very small but statistically significant changes in EMG activity during ISMS were detected in the tongue (4/5 animals), intercostal (3/4 animals), and right diaphragm (4/5 animals). The left ECR showed greater EMG responses in five of five animals.

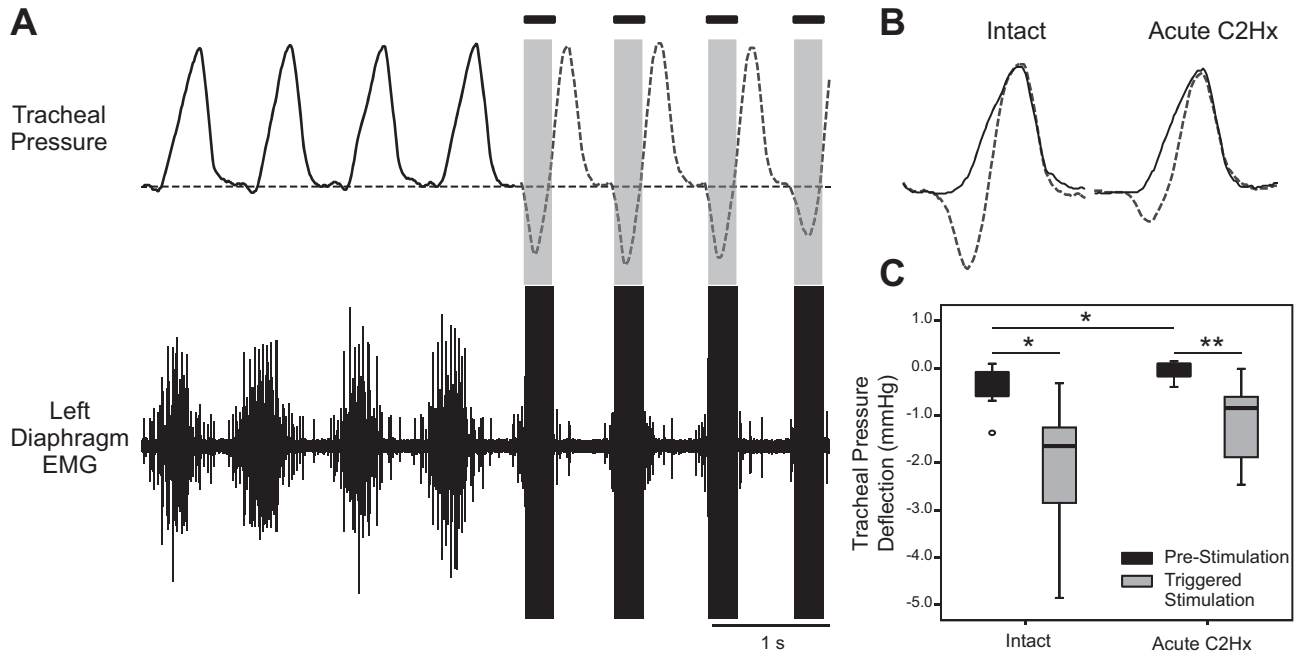

Fig. 4. Impact of ISMS on tracheal pressure. *A*: representative examples of tracheal pressure and left diaphragm EMG activity before and during cervical ISMS (100 Hz, 200 μA). The period of ISMS is indicated by the solid bars. Note the negative deflection in tracheal pressure during ISMS. *B*: overlay plot further illustrates the tracheal pressure before stimulation (solid line) and during ISMS (dashed line). *C*: average change in tracheal pressure during lung inflation at prestimulation baseline and during ISMS. Data are shown for the spinal-intact condition (*left*) and after acute C2Hx (*right*). $*P < 0.05$, $**P < 0.005$.

Inspiratory-related diaphragm EMG bursting is enhanced after ISMS. While our primary intent was to determine whether ISMS evoked diaphragm activity during the period of stimulation, we noted that spontaneous diaphragm EMG activity often was present after the stimulus was turned off. Thus, in six of eight animals after acute C2Hx, the hemidiaphragm that was electrically silent before ISMS showed both tonic and inspiratory-related activity during and after the 1-min period of stimulation (Fig. 6*A*). In these experiments, "activity" was defined as one or more clearly discernible motor unit potentials that were discharging phasically during the inspiratory period. The duration of the effect was variable and did not persist beyond 2 min in any experiment. On average, ISMS-induced spontaneous diaphragm motor unit activity lasted for 43 ± 38

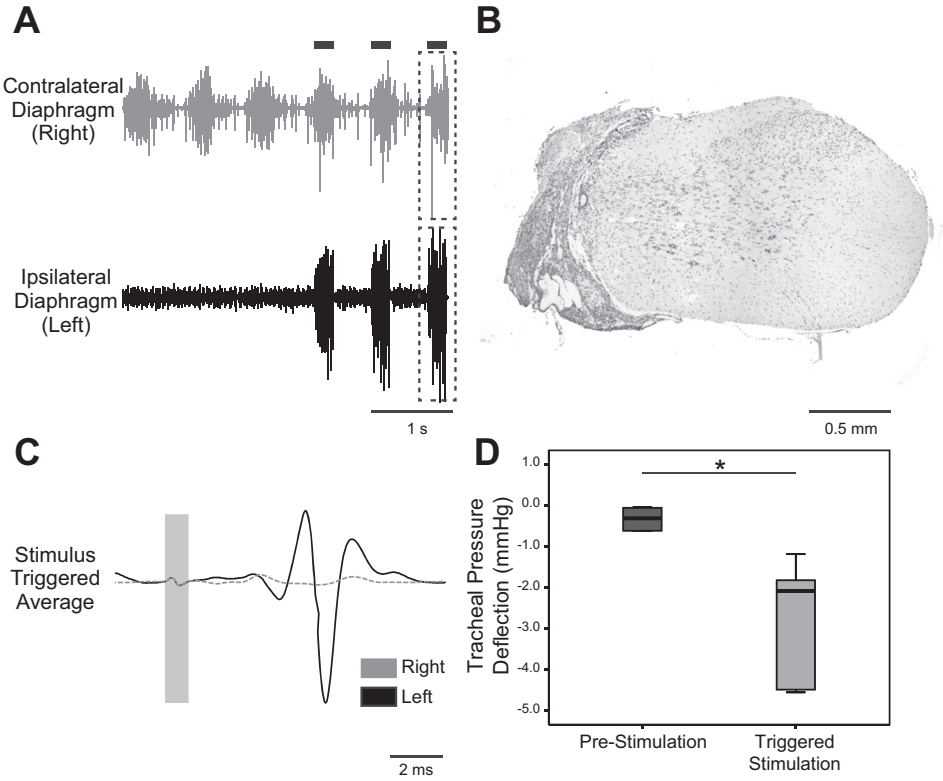

Fig. 5. ISMS after subacute C2Hx. *A*: representative diaphragm EMG activity after subacute C2Hx. In the example traces, genioglossus-triggered ISMS was delivered during the breaths marked by the black bars. *B*: histological section of the C_2 spinal cord stained with cresyl violet. The example demonstrates an anatomically complete hemilesion extending to the midline of cervical cord. *C*: stimulus-triggered averages from the ipsilesional (solid line) and contralesional diaphragm (dashed line); data were obtained from the period indicated by the dashed boxes in *A*. These traces illustrate activation of the diaphragm ipsilateral to the C2Hx lesion. *D*: average change in tracheal pressure during lung inflation at prestimulation baseline and during ISMS. $*P < 0.05$.

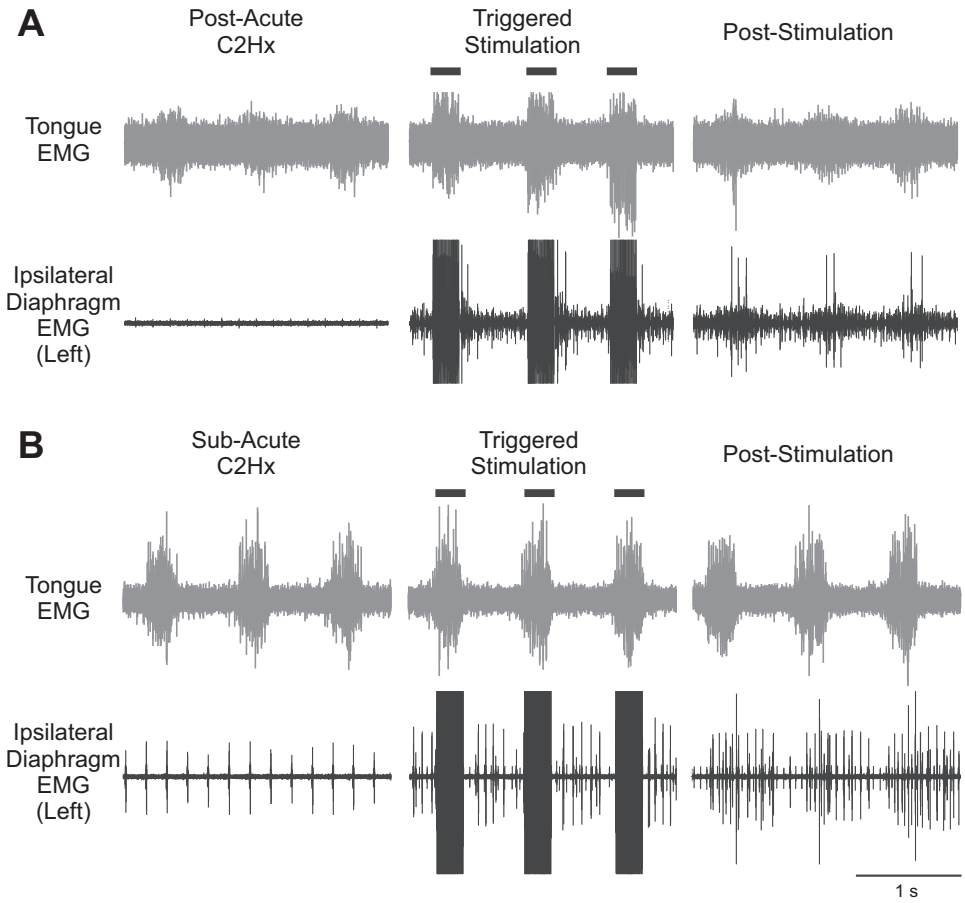

Fig. 6. Example recordings illustrate short-term potentiation of ipsilateral diaphragm EMG activity following ISMS. *A*: tongue and ipsilateral (left) diaphragm EMG activity after acute C2Hx, during ISMS, and immediately after cessation of ISMS. Note that clear phasic (inspiratory) activity can be seen after ISMS, whereas the baseline showed no such activity. *B*: a similar response can be observed in a subacute C2Hx animal. In these examples, the ISMS was triggered by the inspiratory genioglossus EMG signal and was delivered at 100 Hz for 1 min of respiratory efforts.

respiratory cycles after ISMS was terminated. The first breath immediately after cessation of ISMS typically demonstrated the greatest amount of motor unit recruitment, and this was followed by a gradual decrease in motor unit activity over subsequent respiratory cycles. In addition, we noted an increase in tonic activity (i.e., activity persisting across the entire respiratory cycle) after ISMS that followed a time course similar to the phasically active motor units. A similar response to ISMS was observed in three of five rats after subacute C2Hx injury (Fig. 6*B*).

DISCUSSION

This study has demonstrated the feasibility of using endogenous medullary output to trigger ISMS to the midcervical spinal cord. The ISMS paradigm was successful in recruiting diaphragm motor units in spinal-intact animals and also after both acute and subacute interruption of bulbospinal inspiratory drive to the phrenic motoneuron pool following high cervical SCI. Further refinement of this approach may enable development of a "respiratory neuroprosthesis" that, by virtue of the endogenous trigger, could adapt to temporally changing metabolic demands.

Endogenously triggered ISMS induces diaphragm activation. The approach used in this study was a "closed-loop-like" strategy for activating phrenic motoneurons in the cervical spinal cord. As an initial proof of concept, cervical ISMS was triggered from EMG signals recorded from the base of the tongue. Such recordings consist largely of activity from the primary tongue protrudor muscle, the genioglossus (Fuller et al. 1998). Respiratory-related activation of the genioglossus occurs in humans (Mateika et al. 1999; Saboisky et al. 2007) and animal models (Bailey et al. 2005; Fregosi and Fuller 1997) and acts to stiffen and/or dilate the oropharyngeal airway and thus preserve upper airway patency during breathing. The respiratory-related discharge of genioglossus motor units increases during chemoreceptor stimulation in a manner similar to respiratory pump muscles such as the diaphragm (Bailey 2011; Fuller et al. 1998). Genioglossus and tongue muscle output is also subject to vagal modulation, with progressive inhibition occurring as the lung inflates (Bailey et al. 2001; Fukuda and Honda 1982). Collectively, the literature establishes that a complex but coordinated interaction between the genioglossus and the respiratory pump muscles is important for optimizing airway resistance across the respiratory cycle and maintaining upper airway patency. For the present study, the most salient point is that an inspiratory signal was recorded from the genioglossus that provided a marker for the endogenous respiratory rhythm. Thus the animals' own "decision to breathe" triggered the cervical ISMS.

The genioglossus EMG-triggered cervical ISMS approach resulted in diaphragm motor unit activation after both acute (i.e., minutes) and subacute (i.e., days-weeks) C2Hx injury. It was important to repeat the studies under these advanced lesion settings because severed descending pathways have not undergone degeneration after acute injury and therefore could still be capable of conducting action potentials during stimulation

(Gandevia and Kirkwood 2011; Kowalski et al. 2013) as seen in other experimental conditions (Moldovan et al. 2009). Indeed, the latencies of the diaphragm MUAPs in the acute condition (i.e., >1.6 ms) were not consistent with direct phrenic motoneuron activation, and therefore it is likely that synaptic inputs to the phrenic motoneuron pool were being activated via ISMS. Accordingly, it was uncertain if the ISMS approach would be effective at later C2Hx postinjury intervals when degeneration of severed bulbospinal respiratory axons would be well underway. The results showed that diaphragm MUAPs could still be effectively evoked after subacute injury but with a trend toward longer and more variable diaphragm MUAP latencies compared with acute C2Hx animals. In addition, the biomechanical impact of the ISMS (indirectly inferred from changes in tracheal pressure) also appeared to be reduced after subacute vs. acute injury. Refinement of the ISMS method to enable direct phrenic motoneuron stimulation will likely be necessary to optimize diaphragm activation after long-term cervical SCI.

An interesting and potentially important observation that was not part of our original hypothesis was that ISMS-induced inspiratory bursting in the hemiparetic diaphragm persisted for several respiratory cycles after cessation of the stimulation. This occurred in the majority of acute and subacute C2Hx lesions and is similar to the previously described phenomenon of respiratory short-term potentiation (STP) (Lee et al. 2015). Exposure to brief periods of reduced oxygen (hypoxia) triggers phrenic STP, which is manifested as a progressive enhancement of activity followed by a slow decline to baseline levels after removal of the hypoxic stimulus (Lee et al. 2009; Powell et al. 1998). We previously demonstrated that hypoxia can induce STP of phrenic motor output in rats with subacute C2Hx, and the response is greater in the nerve ipsilateral vs. contralateral to the lesion (Lee et al. 2015). The STP in C2Hx rats appeared to reflect recruitment of a population of phrenic motoneurons that had been silenced by injury, which continued to burst beyond the period of hypoxic stimulation. It may be that ISMS can trigger similar STP-like mechanisms of short-term plasticity and ultimately have value in the context of neurorehabilitation. This increased phrenic bursting after cessation of ISMS also may be analogous to longer-duration functional recoveries others have observed with chronic ISMS in other motor systems (Kasten et al. 2013; McPherson et al. 2015).

Methodological caveats including off-target effects of cervical ISMS. The method described here is not truly a "closed-loop" system because the ISMS intensity did not vary with the relative strength of endogenous "respiratory drive." Varying the stimulus intensity or duration in proportion to the relative magnitude of the EMG burst used to trigger ISMS (vs. a simple "onset trigger") could potentially address that issue, but this could also prove problematic since ISMS needs to occur at the onset (vs. peak) of the inspiratory effort. Another caveat is that rats were mechanically ventilated because in our experience spontaneously breathing and anesthetized rats rapidly develop arterial hypercapnia and respiratory acidosis. However, mechanical ventilation will impact endogenous respiratory drive and thereby alter the interactions between spontaneous and ISMS input to the phrenic region. It should also be noted that tongue EMG activity is unlikely to provide an effective ISMS trigger signal in the vagally intact and spontaneously breathing rodent or human. It is possible to record inspiratory-related discharge from the tongue muscles in the awake human and rodent, but available data indicate that tongue EMG may not provide a consistent inspiratory trigger signal (Bailey 2011; Sood et al. 2005). In the present experiments on anesthetized rats, however, the tongue EMG output enabled a rigorous test of the fundamental hypothesis, and we suggest that future work should focus on additional potential sources of respiratory output to serve as endogenous trigger signals or alternative detection algorithms (Dow et al. 2006).

Neural substrate considerations. One of the more challenging issues related to electrical stimulation of the spinal cord is identification of the neural substrate being affected directly or indirectly. Here our immediate goal was to target ISMS of gray matter at the level of the phrenic motor nucleus. Whether phrenic motoneurons are being directly activated by ISMS cannot be determined from the present findings, although latencies in the range of 1.5–2.5 ms suggest indirect stimulation via polysynaptic pathways. In the subacute C2Hx group, stimulation of ipsilateral bulbospinal inputs to phrenic motoneurons can be effectively ruled out because these pathways will be undergoing degeneration. It is possible that ISMS activated commissural bulbospinal projections from the contralateral cord [i.e., pathways associated with the "crossed phrenic phenomenon" (Goshgarian 2003; Goshgarian et al. 1991)]. However, past studies in which intraspinal stimulation of the cervical cord was used to activate crossed phrenic pathways reported latencies of <1 ms (Fuller et al. 2003), and these are considerably shorter than the values reported here. Collectively, the evidence is most consistent with indirect activation of phrenic motoneurons via ISMS, possibly via spinal prephrenic interneurons (Lane 2011) or even ascending afferent projections originating below the injury (Decima and von Euler 1969).

ISMS is capable of discrete activation of circuitry with minimal undesired physiological effects (Pikov et al. 2007). Here we observed clear responses in the ipsilateral diaphragm, as intended, but also off-target motor unit recruitment. Very small and inconsistent activation of the contralateral diaphragm, intercostal muscles, and genioglossus were present during ISMS. This indicates current spread beyond the target region or activation of other circuits via interneurons (Perlmutter et al. 1998). For example, in the case of ISMS-evoked responses in the contralateral diaphragm and intercostal muscles, our previous transneuronal tracing studies provide an interneuronal basis for those off-target responses (Lane et al. 2008). Intercostal and/or contralateral diaphragm recruitment could in fact be advantageous when cervical SCIs involve much larger-scale compromise of diaphragm and inspiratory intercostal function compared with C2Hx. Activation of the genioglossus was barely above the threshold for detection and probably reflected activation of ascending projections to medullary respiratory control neurons. For example, we previously reported that some cervical interneurons associated with the phrenic motor circuit have ascending projections to the medulla (Lane et al. 2008).

The relatively stronger coactivation of forelimb muscles induced by ISMS presents a more challenging technical issue. As with the ipsilateral diaphragm, constant-latency entrainment occurred in the forelimb, and this may reflect overlap of phrenic and forelimb circuits along the rostro-caudal axis

(Gonzalez-Rothi et al. 2015). ECR motoneurons, however, appear to occupy a more dorso-lateral position than the phrenic motoneuron pool (Tosolini and Morris 2012). This raises the possibility that even if ISMS was precisely restricted to phrenic motoneurons, concomitant excitation of ECR axons as they course toward their ventral roots could still occur. Further investigations are needed to sort out the neuroanatomical basis for direct vs. indirect effects of ISMS. The latter may be especially beneficial by activating desired motoneuron pools in a more natural order than achieved with direct stimulation.

Conclusions. Previous studies directed at spinal cord stimulation and the respiratory system after SCI have focused on epidural stimulation as a means of enhancing abdominal or phrenic motor output. Epidural stimulation has been successful at recruiting diaphragm motor units in animal studies (DiMarco and Kowalski 2009, 2011; Kowalski et al. 2013) and has been used to enhance cough in spinally injured humans (DiMarco et al. 2014). Epidural stimulation also shows promise in the context of locomotor function after SCI in both animals and humans (Edgerton and Harkema 2011; Rejc et al. 2015). Despite these successes, there is unquestionably a need for improvement and refinement of spinal cord stimulation methods. In that regard, the initial findings from our study raise the possibility of utilizing endogenous, physiologically relevant respiratory signals, which entail peripheral and chemosensory feedback, for triggering neuromodulation of the phrenic motor circuit and alleviation of ventilatory insufficiency following mid- to high-cervical SCI. Many ISMS parameters (Bamford and Mushahwar 2011; Giszter 2015; Tator et al. 2012) must be refined, however, before the benefits of invasive ISMS protocols to promote respiratory improvements after cervical SCI can be fully evaluated or compared with other approaches, high-frequency epidural stimulation (Kowalski et al. 2013) in particular. It also is possible that a given spinal stimulation approach will be better suited for some SCI cases than another. Future investigations involving awake, spontaneously breathing animals will be crucial for determining whether chronic ISMS delivery will function solely as a neuroprosthetic or can be used short term to promote functional and anatomical neuroplasticity (Moritz et al. 2007) alone or in combination with other therapeutic approaches leading to long-lasting improvement in respiratory function.

ACKNOWLEDGMENTS

We thank Dr. Danielle Meola, L. Emma Denholtz, Amy Poirier, Sarah El-Azab, and Alexis Caballero for their technical contributions.

GRANTS

This work was funded by awards from the Department of Defense (W81XWH-14-1-0625; P. J. Reier), the National Institutes of Health (NIH) [R01 NS-054025 (P. J. Reier), R01 NS-080180 (D. D. Fuller)], and the State of Florida Brain and Spinal Cord Injury Research Trust Fund (P. J. Reier, D. D. Fuller, D. M. Baekey). The authors also express their appreciation for the generous support received from the Fraternal Order of Eagles Aerie #3496. L. M. Mercier was supported by a NIH T32 training grant (HD-043730).

DISCLOSURES

No conflicts of interest, financial or otherwise, are declared by the author(s).

AUTHOR CONTRIBUTIONS

L.M.M. and E.J.G.-R. performed experiments; L.M.M., K.A.S., S.S.P., and A.S.P. analyzed data; L.M.M., D.D.F., P.J.R., and D.M.B. interpreted results of experiments; L.M.M. prepared figures; L.M.M. and D.M.B. drafted manuscript; L.M.M., E.J.G.-R., K.A.S., S.S.P., A.S.P., D.D.F., P.J.R., and D.M.B. approved final version of manuscript; D.D.F., P.J.R., and D.M.B. edited and revised manuscript; D.D.F., P.J.R., and D.M.B. conceived and designed research.

REFERENCES

Aertsen AM, Gerstein GL. Evaluation of neuronal connectivity: sensitivity of cross-correlation. *Brain Res* 340: 341–354, 1985.

Bailey EF. Activities of human genioglossus motor units. *Respir Physiol Neurobiol* 179: 14–22, 2011.

Bailey EF, Janssen PL, Fregosi RF. PO_2-dependent changes in intrinsic and extrinsic tongue muscle activities in the rat. *Am J Respir Crit Care Med* 171: 1403–1407, 2005.

Bailey EF, Jones CL, Reeder JC, Fuller DD, Fregosi RF. Effect of pulmonary stretch receptor feedback and CO_2 on upper airway and respiratory pump muscle activity in the rat. *J Physiol* 532: 525–534, 2001.

Bamford JA, Mushahwar VK. Intraspinal microstimulation for the recovery of function following spinal cord injury. *Prog Brain Res* 194: 227–239, 2011.

Bezzant TB, Mortensen JD. Risks and hazards of mechanical ventilation: a collective review of published literature. *Dis Mon* 40: 581–638, 1994.

Decima EE, von Euler C. Excitability of phrenic motoneurones to afferent input from lower intercostal nerves in the spinal cat. *Acta Physiol Scand* 75: 580–591, 1969.

DiMarco AF, Kowalski KE. High-frequency spinal cord stimulation of inspiratory muscles in dogs: a new method of inspiratory muscle pacing. *J Appl Physiol (1985)* 107: 662–669, 2009.

DiMarco AF, Kowalski KE. Distribution of electrical activation to the external intercostal muscles during high frequency spinal cord stimulation in dogs. *J Physiol* 589: 1383–1395, 2011.

DiMarco AF, Kowalski KE. Spinal pathways mediating phrenic activation during high frequency spinal cord stimulation. *Respir Physiol Neurobiol* 186: 1–6, 2013.

DiMarco AF, Kowalski KE. Electrical activation to the parasternal intercostal muscles during high-frequency spinal cord stimulation in dogs. *J Appl Physiol (1985)* 118: 148–155, 2015.

DiMarco AF, Kowalski KE, Hromyak DR, Geertman RT. Long-term follow-up of spinal cord stimulation to restore cough in subjects with spinal cord injury. *J Spinal Cord Med* 37: 380–388, 2014.

DiMarco AF, Onders RP, Ignagni A, Kowalski KE, Mortimer JT. Phrenic nerve pacing via intramuscular diaphragm electrodes in tetraplegic subjects. *Chest* 127: 671–678, 2005.

Dow DE, Mantilla CB, Zhan WZ, Sieck GC. EMG-based detection of inspiration in the rat diaphragm muscle. *Conf Proc IEEE Eng Med Biol Soc* 1: 1204–1207, 2006.

Edgerton VR, Harkema S. Epidural stimulation of the spinal cord in spinal cord injury: current status and future challenges. *Expert Rev Neurother* 11: 1351–1353, 2011.

Fregosi RF, Fuller DD. Respiratory-related control of extrinsic tongue muscle activity. *Respir Physiol* 110: 295–306, 1997.

Fukuda Y, Honda Y. Roles of vagal afferents on discharge patterns and CO_2-responsiveness of efferent superior laryngeal, hypoglossal, and phrenic respiratory activities in anesthetized rats. *Jpn J Physiol* 32: 689–698, 1982.

Fuller D, Mateika JH, Fregosi RF. Co-activation of tongue protrudor and retractor muscles during chemoreceptor stimulation in the rat. *J Physiol* 507: 265–276, 1998.

Fuller DD, Doperalski NJ, Dougherty BJ, Sandhu MS, Bolser DC, Reier PJ. Modest spontaneous recovery of ventilation following chronic high cervical hemisection in rats. *Exp Neurol* 211: 97–106, 2008.

Fuller DD, Fregosi RF. Fatiguing contractions of tongue protrudor and retractor muscles: influence of systemic hypoxia. *J Appl Physiol* 88: 2123–2130, 2000.

Fuller DD, Johnson SM, Olson EB Jr, Mitchell GS. Synaptic pathways to phrenic motoneurons are enhanced by chronic intermittent hypoxia after cervical spinal cord injury. *J Neurosci* 23: 2993–3000, 2003.

Fuller DD, Williams JS, Janssen PL, Fregosi RF. Effect of co-activation of tongue protrudor and retractor muscles on tongue movements and pharyngeal airflow mechanics in the rat. *J Physiol* 519: 601–613, 1999.

Gandevia SC, Kirkwood PA. Spinal breathing: stimulation and surprises. *J Neurotrauma* 589: 2661–2662, 2011.

Giszter SF. Spinal primitives and intra-spinal micro-stimulation (ISMS) based prostheses: a neurobiological perspective on the "known unknowns" in ISMS and future prospects. *Front Neurosci* 9: 72, 2015.

Glenn WW, Phelps ML. Diaphragm pacing by electrical stimulation of the phrenic nerve. *Neurosurgery* 17: 974–984, 1985.

Gonzalez-Rothi EJ, Rombola AM, Rousseau CA, Mercier LM, Fitzpatrick GM, Reier PJ, Fuller DD, Lane MA. Spinal interneurons and forelimb plasticity after incomplete cervical spinal cord injury in adult rats. *J Neurotrauma* 32: 893–907, 2015.

Goshgarian HG. The role of cervical afferent nerve fiber inhibition of the crossed phrenic phenomenon. *Exp Neurol* 72: 211–225, 1981.

Goshgarian HG. The crossed phrenic phenomenon: a model for plasticity in the respiratory pathways following spinal cord injury. *J Appl Physiol* 94: 795–810, 2003.

Goshgarian HG, Ellenberger HH, Feldman JL. Decussation of bulbospinal respiratory axons at the level of the phrenic nuclei in adult rats: a possible substrate for the crossed phrenic phenomenon. *Exp Neurol* 111: 135–139, 1991.

Kasten MR, Sunshine MD, Secrist ES, Horner PJ, Moritz CT. Therapeutic intraspinal microstimulation improves forelimb function after cervical contusion injury. *J Neural Eng* 10: 044001, 2013.

Kowalski KE, Hsieh YH, Dick TE, DiMarco AF. Diaphragm activation via high frequency spinal cord stimulation in a rodent model of spinal cord injury. *Exp Neurol* 247: 689–693, 2013.

Laghi F, Cattapan SE, Jubran A, Parthasarathy S, Warshawsky P, Choi YS, Tobin MJ. Is weaning failure caused by low-frequency fatigue of the diaphragm? *Am J Respir Crit Care Med* 167: 120–127, 2003.

Lane MA. Spinal respiratory motoneurons and interneurons. *Respir Physiol Neurobiol* 179: 3–13, 2011.

Lane MA, White TE, Coutts MA, Jones AL, Sandhu MS, Bloom DC, Bolser DC, Yates BJ, Fuller DD, Reier PJ. Cervical prephrenic interneurons in the normal and lesioned spinal cord of the adult rat. *J Comp Neurol* 511: 692–709, 2008.

Lee KZ, Reier PJ, Fuller DD. Phrenic motoneuron discharge patterns during hypoxia-induced short-term potentiation in rats. *J Neurophysiol* 102: 2184–2193, 2009.

Lee KZ, Sandhu MS, Dougherty BJ, Reier PJ, Fuller DD. Hypoxia triggers short term potentiation of phrenic motoneuron discharge after chronic cervical spinal cord injury. *Exp Neurol* 263: 314–324, 2015.

Mansel JK, Norman JR. Respiratory complications and management of spinal cord injuries. *Chest* 97: 1446–1452, 1990.

Mateika JH, Millrood DL, Kim J, Rodriguez HP, Samara GJ. Response of human tongue protrudor and retractors to hypoxia and hypercapnia. *Am J Respir Crit Care Med* 160: 1976–1982, 1999.

McPherson JG, Miller RR, Perlmutter SI. Targeted, activity-dependent spinal stimulation produces long-lasting motor recovery in chronic cervical spinal cord injury. *Proc Natl Acad Sci USA* 112: 12193–12198, 2015.

Melssen WJ, Epping WJ. Detection and estimation of neural connectivity based on crosscorrelation analysis. *Biol Cybern* 57: 403–414, 1987.

Moldovan M, Alvarez S, Krarup C. Motor axon excitability during Wallerian degeneration. *Brain* 132: 511–523, 2009.

Mondello SE, Sunshine MD, Fischedick AE, Moritz CT, Horner PJ. A cervical hemi-contusion spinal cord injury model for the investigation of novel therapeutics targeting proximal and distal forelimb functional recovery. *J Neurotrauma* 32: 1994–2007, 2015.

Moritz CT, Lucas TH, Perlmutter SI, Fetz EE. Forelimb movements and muscle responses evoked by microstimulation of cervical spinal cord in sedated monkeys. *J Neurophysiol* 97: 110–120, 2007.

Mushahwar VK, Collins DF, Prochazka A. Spinal cord microstimulation generates functional limb movements in chronically implanted cats. *Exp Neurol* 163: 422–429, 2000.

Onders RP, Elmo M, Khansarinia S, Bowman B, Yee J, Road J, Bass B, Dunkin B, Ingvarsson PE, Oddsdottir M. Complete worldwide operative experience in laparoscopic diaphragm pacing: results and differences in spinal cord injured patients and amyotrophic lateral sclerosis patients. *Surg Endosc* 23: 1433–1440, 2009.

Perlmutter SI, Maier MA, Fetz EE. Activity of spinal interneurons and their effects on forearm muscles during voluntary wrist movements in the monkey. *J Neurophysiol* 80: 2475–2494, 1998.

Pikov V, Bullara L, McCreery DB. Intraspinal stimulation for bladder voiding in cats before and after chronic spinal cord injury. *J Neural Eng* 4: 356–368, 2007.

Powell FL, Milsom WK, Mitchell GS. Time domains of the hypoxic ventilatory response. *Respir Physiol* 112: 123–134, 1998.

Rejc E, Angeli C, Harkema S. Effects of lumbosacral spinal cord epidural stimulation for standing after chronic complete paralysis in humans. *PLoS One* 10: e0133998, 2015.

Saboisky JP, Gorman RB, De Troyer A, Gandevia SC, Butler JE. Differential activation among five human inspiratory motoneuron pools during tidal breathing. *J Appl Physiol* 102: 772–780, 2007.

Smuder AJ, Gonzalez-Rothi EJ, Kwon OS, Morton AB, Sollanek KJ, Powers SK, Fuller DD. Cervical spinal cord injury exacerbates ventilator-induced diaphragm dysfunction. *J Appl Physiol (1985)* 120: 166–177, 2016.

Sood S, Morrison JL, Liu H, Horner RL. Role of endogenous serotonin in modulating genioglossus muscle activity in awake and sleeping rats. *Am J Respir Crit Care Med* 172: 1338–1347, 2005.

Sunshine MD, Cho FS, Lockwood DR, Fechko AS, Kasten MR, Moritz CT. Cervical intraspinal microstimulation evokes robust forelimb movements before and after injury. *J Neural Eng* 10: 036001, 2013.

Tator CH, Minassian K, Mushahwar VK. Spinal cord stimulation: therapeutic benefits and movement generation after spinal cord injury. *Handb Clin Neurol* 109: 283–296, 2012.

Tosolini AP, Morris R. Spatial characterization of the motor neuron columns supplying the rat forelimb. *Neuroscience* 200: 19–30, 2012.

Winslow C, Rozovsky J. Effect of spinal cord injury on the respiratory system. *Am J Phys Med Rehabil* 82: 803–814, 2003.

J Neurophysiol 118: 2344–2357, 2017.
First published June 14, 2017; doi:10.1152/jn.00913.2016.

RESEARCH ARTICLE | *Spinal Control of Motor Outputs*

High-frequency epidural stimulation across the respiratory cycle evokes phrenic short-term potentiation after incomplete cervical spinal cord injury

Elisa J. Gonzalez-Rothi,[1] Kristi A. Streeter,[1] Marie H. Hanna,[1] Anna C. Stamas,[1] Paul J. Reier,[2] David M. Baekey,[3] and David D. Fuller[1]

[1]*McKnight Brain Institute, Department of Physical Therapy, College of Public Health and Health Professions, University of Florida, Gainesville, Florida;* [2]*Department of Neuroscience, College of Medicine, University of Florida, Gainesville, Florida; and* [3]*Department of Physiological Sciences, College of Veterinary Medicine, University of Florida, Gainesville, Florida*

Submitted 29 November 2016; accepted in final form 14 June 2017

Gonzalez-Rothi EJ, Streeter KA, Hanna MH, Stamas AC, Reier PJ, Baekey DM, Fuller DD. High-frequency epidural stimulation across the respiratory cycle evokes phrenic short-term potentiation after incomplete cervical spinal cord injury. *J Neurophysiol* 118: 2344–2357, 2017. First published June 14, 2017; doi:10.1152/jn.00913.2016.—C2 spinal hemilesion (C2Hx) paralyzes the ipsilateral diaphragm, but recovery is possible through activation of "crossed spinal" synaptic inputs to ipsilateral phrenic motoneurons. We tested the hypothesis that high-frequency epidural stimulation (HF-ES) would potentiate ipsilateral phrenic output after subacute and chronic C2Hx. HF-ES (300 Hz) was applied to the ventrolateral C4 or T2 spinal cord ipsilateral to C2Hx in anesthetized and mechanically ventilated adult rats. Stimulus duration was 60 s, and currents ranged from 100 to 1,000 μA. Bilateral phrenic nerve activity and ipsilateral hypoglossal (XII) nerve activity were recorded before and after HF-ES. Higher T2 stimulus currents potentiated ipsilateral phasic inspiratory activity at both 2 and 12 wk post-C2Hx, whereas higher stimulus currents delivered at C4 potentiated ipsilateral phasic phrenic activity only at 12 wk ($P = 0.028$). Meanwhile, tonic output in the ipsilateral phrenic nerve reached 500% of baseline values at the high currents with no difference between 2 and 12 wk. HF-ES did not trigger inspiratory burst-frequency changes. Similar responses occurred following T2 HF-ES. Increases in contralateral phrenic and XII nerve output were induced by C4 and T2 HF-ES at higher currents, but the relative magnitude of these changes was small compared with the ipsilateral phrenic response. We conclude that following incomplete cervical spinal cord injury, HF-ES of the ventrolateral midcervical or thoracic spinal cord can potentiate efferent phrenic motor output with little impact on inspiratory burst frequency. However, the substantial increases in tonic output indicate that the uninterrupted 60-s stimulation paradigm used is unlikely to be useful for respiratory muscle activation after spinal injury.

NEW & NOTEWORTHY Previous studies reported that high-frequency epidural stimulation (HF-ES) activates the diaphragm following acute spinal transection. This study examined HF-ES and phrenic motor output following subacute and chronic incomplete cervical spinal cord injury. Short-term potentiation of phrenic bursting following HF-ES illustrates the potential for spinal stimulation to induce respiratory neuroplasticity. Increased tonic phrenic output indicates that alternatives to the continuous stimulation paradigm used in this study will be required for respiratory muscle activation after spinal cord injury.

spinal cord injury; epidural stimulation; phrenic, potentiation; plasticity

DELIVERY OF ELECTRICAL CURRENTS to the dorsal, lateral, or ventral spinal dura mater (i.e., "epidural stimulation") has been explored in animal models and humans following spinal cord injury (SCI). Much of that work has focused on enabling locomotor movement (Angeli et al. 2014; Harkema et al. 2011; Rejc et al. 2015; Sayenko et al. 2014), but epidural stimulation also has been used to activate respiratory muscles (DiMarco and Kowalski 2009, 2010, 2013b, 2015; DiMarco et al. 2002, 2014; Kowalski et al. 2013, 2016). Following a complete spinal transection at C1, high-frequency epidural stimulation (HF-ES) of the upper thoracic spinal cord can evoke bursting of diaphragm motor units during stimulation, but at rates (e.g., 10–50 Hz) well below the stimulus frequency of 300 Hz. With the use of this approach, recruitment of diaphragm motor units occurs during stimulation, and off-target effects appear to be minimal. The specific mechanisms underlying diaphragm motor unit recruitment during HF-ES of the transected spinal cord are unknown, but the phenomenon has been demonstrated in both rats (Kowalski et al. 2013) and dogs (DiMarco and Kowalski 2009).

Neuroplasticity in respiratory motoneurons and/or networks (Fuller and Mitchell 2017) is an important consideration in the context of epidural stimulation and SCI. For example, if the stimulation paradigm is intended to function as a "respiratory neuroprosthesis," then stimulus-induced changes in synaptic efficacy could enhance (or impair) subsequent evoked motor responses. Perhaps even more important is the potential for stimulation-induced neuroplasticity to promote motor recovery (Kasten et al. 2013; McPherson et al. 2015). Electrical stimulation of the spinal cord can alter neuronal growth (Borgens et al. 1981) and synaptic plasticity (Fetz 2015; McPherson et al. 2015; Nishimura et al. 2013; Widge and Moritz 2014) and has already been used in neurorehabilitation paradigms (Harkema et al. 2011; Rejc et al. 2015, 2017; Sayenko et al. 2015).

In the current study, we investigated whether a sustained period of HF-ES would induce neuroplastic changes in phrenic

Address for reprint requests and other correspondence: E. J. Gonzalez-Rothi, McKnight Brain Institute, Department of Physical Therapy, College of Public Health and Health Professions, University of Florida, PO Box 100154, 100 S. Newell Dr., Gainesville, FL 32610 (e-mail: elisagon@phhp.ufl.edu).

motor activity similar to the well-described short-term potentiation of phrenic nerve activity that occurs following short periods of arterial hypoxia (Lee et al. 2015). The mechanisms underlying phrenic short-term potentiation induced by hypoxia are not definitively known (Lee et al. 2015), but several studies have shown that electrically stimulating synaptic inputs to spinal respiratory motoneurons can potentiate spinal respiratory output on short timescales (Hayashi et al. 2003; Johnson and Mitchell 2002; McCrimmon et al. 1997; Mercier et al. 2017). The aforementioned epidural stimulation experiments (DiMarco and Kowalski 2009, 2010, 2013b; DiMarco et al. 2002; Kowalski et al. 2013) indicate that HF-ES robustly activates synaptic inputs to phrenic motoneurons, at least following acute spinal transection. Epidural stimulation may also activate neuromodulatory neurons (e.g., raphe-spinal projections) located in proximity to phrenic motoneurons (Kinkead et al. 1998) which have the capacity to induce respiratory neuroplasticity (Fuller and Mitchell 2017). Accordingly, in this study we hypothesized that a brief period of HF-ES in rats with incomplete cervical SCI would induce short-term potentiation in phrenic motor output. Experiments were conducted in adult rats following hemilesion of the spinal cord at C2 (C2Hx; Goshgarian 2003; Sandhu et al. 2009). The C2Hx lesion transiently eliminates ipsilateral inspiratory phrenic activity, but this is followed by a gradual and spontaneous return of a small degree of inspiratory activity (Nantwi et al. 1999; Pitts 1940) coupled with increases in tonic discharge (Fuller et al. 2008). Epidural stimulation was applied to the ventrolateral wall of the midcervical (C4) or high thoracic (T2) spinal cord, ipsilateral to C2Hx, and both phrenic and supraspinal (hypoglossal, XII) respiratory output were recorded. Experiments were conducted after both subacute (2 wk) and chronic (12 wk) injury because the spontaneous neuroplastic processes that drive phrenic motor recovery after C2Hx (Golder and Mitchell 2005) may also impact the response to HF-ES. The results indicate that HF-ES can potentiate motor output in the phrenic nerve with impaired output (i.e., ipsilateral to C2Hx), with some evidence for improved efficacy at 12 vs. 2 wk post-C2Hx. However, large increases in tonic phrenic motor output following stimulation masked the increases in phasic (inspiratory) phrenic bursting.

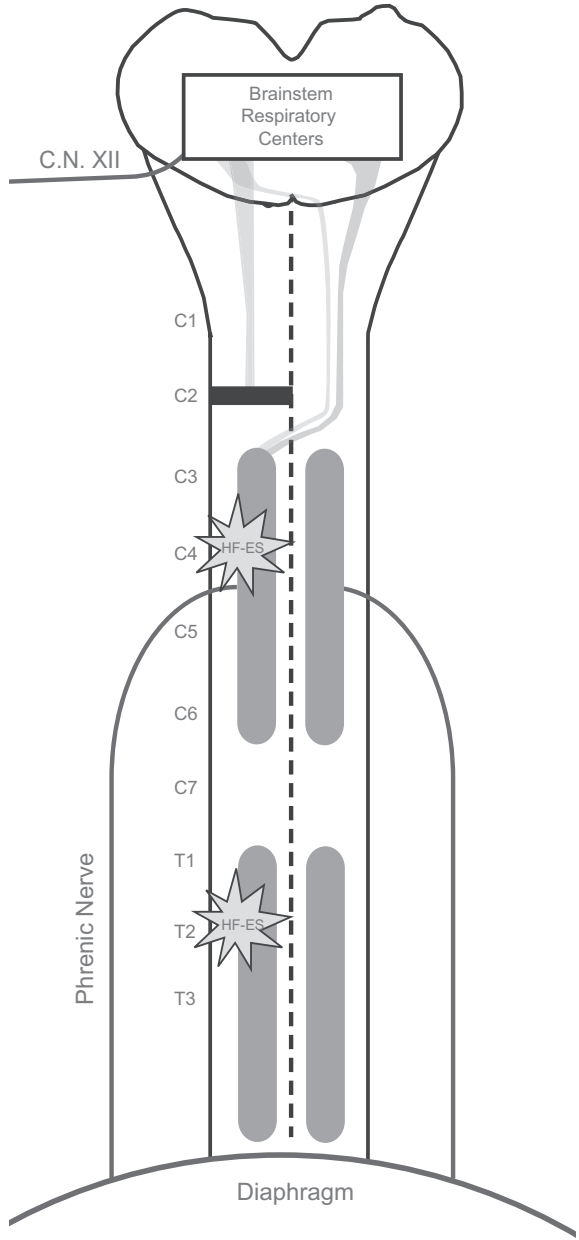

Fig. 1. Schematic diagram illustrating the experimental model. Lateral C2 spinal cord hemisection injury disrupts the descending bulbospinal projections innervating the phrenic motor pool on one side, rendering the ipsilateral hemidiaphragm paralyzed. Modest but incomplete spontaneous recovery of ipsilateral diaphragm function occurs in the weeks following injury. At either 2 or 12 wk following injury, HF-ES was delivered to the ventrolateral surface of the spinal cord at either the midcervical (C4) or upper thoracic (T2) level ipsilateral to the side of injury. C.N. XII, cranial nerve XII.

MATERIALS AND METHODS

Experiments were conducted on adult, female Sprague-Dawley rats (Harlan, Indianapolis, IN) with C2Hx injury. All rats were housed in pairs in a controlled environment (12:12-h light-dark cycles) with food and water ad libitum. The C4 or T2 spinal cord was stimulated in separate rats at either 2 or 12 wk post-C2Hx: 2-wk C4, $n = 8$; 12-wk C4, $n = 8$; 2-wk T2, $n = 7$; and 12-wk T2, $n = 7$. A summary of the experimental approach including the SCI model and location of stimulation is shown in Fig. 1. All experimental procedures were approved by the Institutional Animal Care and Use Committee at the University of Florida.

SCI surgery. Anesthesia and C2Hx methods have been previously described (Doperalski et al. 2008; Dougherty et al. 2012; Fuller et al. 2008). Rats were anesthetized by 3% isoflurane in a closed chamber and then maintained at a surgical plane by using a nose cone to inspire 1–2% isoflurane. A 1-in. dorsal midline incision was made from the base of the skull to approximately the fourth cervical segment (C4). After C2 laminectomy, a small incision was made in the dura, followed by lateral hemisection of the left spinal cord, using a microscalpel and gentle aspiration. After completeness of the lesion was verified visually, the dura was closed with interrupted 9-0 sutures. The overlying muscle was sutured in layers, and the skin was closed with surgical wound clips. Rats were given injections of buprenorphine (0.03 mg/kg sc; Hospira, Lake Forest, IL) for analgesia and sterile lactated Ringer's solution (5 ml sc) to prevent dehydration. Buprenorphine (0.03 mg/kg sc) was given at 12-h intervals for the initial 48 h. Lactated Ringer's solution (5 ml/day sc) and oral Nutri-Cal supplements (1–3 ml; Webster Veterinary Supply, Devens, MA) were given until adequate volitional drinking and eating resumed.

Phrenic and XII nerve recordings. Isoflurane anesthesia (3–4%) was induced in a closed chamber followed by intravenous infusion of

urethane (1.7–1.8 g/kg; Sigma, St. Louis, MO) via a tail vein catheter. The trachea was cannulated with polyethylene (PE-240) tubing, and rats were mechanically ventilated for the remainder of the experiment with 50% O_2. Tracheal pressure was continuously monitored with a pressure transducer (DTXPlus pressure transducer, Argon Critical Care Systems, Singapore; model TA-100 strain gauge amplifier, CWE, Ardmore, PA) connected to the tracheal cannula. The vagus nerves were sectioned in the midcervical region to prevent entrainment of phrenic motor output with the ventilator and rats were paralyzed with pancuronium bromide (2.5 mg/kg iv; Hospira) to eliminate spontaneous breathing efforts. After paralysis, arterial blood pressure and phrenic nerve response to toe pinch were monitored to ensure the depth of anesthesia, and supplemental urethane was given if indicated (0.3 g/kg iv). A femoral arterial catheter (PE-50) was inserted to measure blood pressure (DTXPlus, Argon Critical Care Systems; model TA-100 strain gauge amplifier, CWE) and end-tidal carbon dioxide partial pressure ($P_{ET_{CO_2}}$) to periodically withdraw blood samples. Heart rate was extracted from the arterial pressure trace and calculated in real time using Spike2 software (Cambridge Electronic Design, Cambridge, UK). Arterial P_{O_2} (Pa_{O_2}) and P_{CO_2} (Pa_{CO_2}) and pH were determined from 0.2-ml arterial blood samples using an i-Stat blood gas analyzer (Heska, Fort Collins, CO). Rectal temperature was maintained at 37 ± 1°C using a rectal thermistor connected to a servo-controlled heating pad (model TC-1000; CWE). The $P_{ET_{CO_2}}$ was measured using a rapidly responding mainstream CO_2 analyzer positioned a few centimeters from the tracheostomy tube (Capnogard; Novametrix Medical Systems, Wallingford, CT).

With the use of a dorsal surgical approach, the phrenic and hypoglossal nerves were isolated, cut distally, and partially desheathed (Mahamed et al. 2011). Electrical activity in the nerves was recorded using custom-made bipolar silver wire suction electrodes filled with 0.9% saline. Signals were amplified (×10,000), filtered (bandpass = 3–30 kHz), digitized (16-bit, 25-kHz sampling frequency/channel; CED Power 1401 data acquisition interface), and recorded using Spike2 software. The amplified signals were full-wave rectified in real time using Spike2 software.

Stimulation of the spinal cord. After isolation of the phrenic and XII nerves, a laminectomy was performed at either C3–C5 or T1–T3 (Fig. 1). Two Teflon-coated silver wires (diameter: 0.010 in. bare, 0.013 in. coated; A-M Systems) with 1 mm of insulation removed at the tip were used to stimulate the spinal cord. Electrode tips were separated by 1.5 mm and were slid between the dorsal roots ipsilateral to the side of injury to wrap around to the ventrolateral surface of the spinal cord. A Grass S-88 stimulator was used to pass electrical current through the wires.

Experimental protocol. Baseline conditions were established by adjusting the ventilator rate to maintain $P_{ET_{CO_2}}$ between 44 and 48 mmHg; this ensured that a robust and rhythmic inspiratory burst could be recorded in the phrenic and XII nerves. All baseline recordings were made for a minimum of 10 min, during which the burst amplitude remained consistent. The stimulation protocol consisted of three 60-s trains of high-frequency (300 Hz) stimulation delivered at 100, 500, and 1,000 μA (pulse duration = 0.2 ms). A 3-min recovery period followed each bout of stimulation. Throughout the protocol, $P_{ET_{CO_2}}$ measurements were used as a guide to help maintain Pa_{CO_2} stability; arterial blood gases were measured at baseline and after the final bout of stimulation.

Data analysis. The amplitude and frequency (burst/min) of the integrated phrenic and hypoglossal signals were quantified at baseline and after each bout of stimulation. Figure 2 provides an overview of how the phasic inspiratory-related discharge and the tonic discharge were evaluated. The integrated signals were compared with a "zero" point, which was determined at the end of the experimental protocol, when each nerve was bathed in lidocaine to silence all neural activity. Tonic activity was measured as the integrated amplitude during the expiratory phase of the respiratory cycle relative to the calculated zero. Phasic (inspiratory) activity was quantified as the peak of the integrated inspiratory burst amplitude relative to the amplitude of the expiratory phase preceding it. The total activity during the inspiratory phase was quantified as the peak of the integrated inspiratory burst amplitude relative to zero. Integrated burst amplitudes were quantified as *1*) absolute voltages (i.e., arbitrary units, a.u.), *2*) relative to the amplitude recorded during the baseline condition (% baseline), and *3*) as a "signal-to-noise" ratio, calculated to express the relationship of phasic to tonic nerve activity in a given nerve at each time point. Baseline nerve activity was calculated over a stable 3-min period just before initiation of stimulations. Poststimulation nerve activity was assessed as *1*) an average over the 3 min following termination of the stimulation, *2*) an average of the first 10 inspiratory cycles following termination of the stimulation, and *3*) the peak amplitude following termination of stimulation. Mean arterial pressure and heart rate were assessed throughout the entire protocol. Statistical analyses were performed using SigmaStat software. Comparisons of baseline blood gases, cardiovascular parameters (blood pressure, heart rate), and nerve data (frequency and amplitude) were made across groups using one-way analysis of variance (ANOVA). Changes in arterial blood gases, cardiovascular parameters, and neural output following stimulation were compared across groups using two-way repeated-measures analyses of variance (RM ANOVA) and Holm-Sidak post hoc tests. All data are means ± SE. A P value <0.05 was considered statistically significant.

RESULTS

Baseline respiratory and cardiovascular parameters. Robust inspiratory signals were recorded from the left XII nerve (ipsilateral to C2Hx) and the right (contralateral) phrenic nerve in all experiments (Fig. 3). Baseline inspiratory-related bursting in the left (ipsilateral) phrenic nerve was also present in all animals, and amplitude was attenuated by 41 ± 10% acompared with the contralateral side ($P < 0.001$; Fig. 3, *A* and *B*,

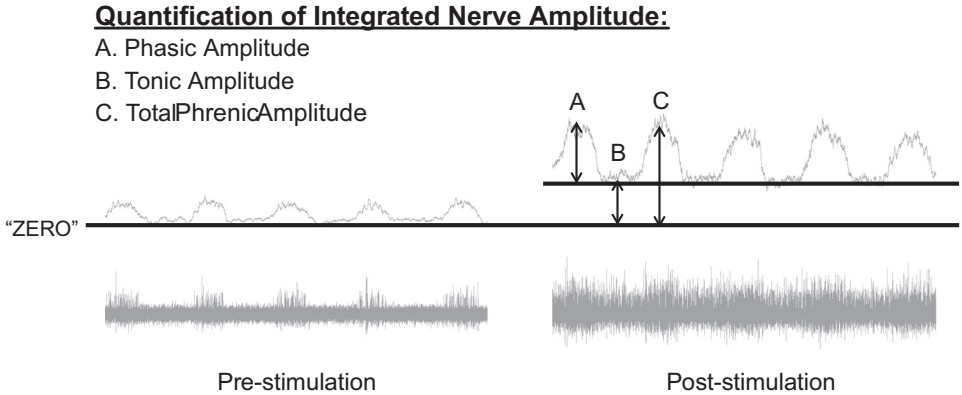

Fig. 2. Quantification of electrical activity recorded in the phrenic and XII nerves. Integrated nerve signals were compared with a "zero" point, which was determined at the end of the experimental protocol, when each nerve was bathed in lidocaine to silence all neural activity. "Phasic" amplitude (*A*) was quantified as the integrated amplitude of the inspiratory burst relative to the amplitude of the expiratory phase preceding it. "Tonic" amplitude (*B*) was quantified as the integrated amplitude during the expiratory phase relative to "zero." "Total" amplitude (*C*) was quantified as the integrated amplitude of the inspiratory burst relative to "zero."

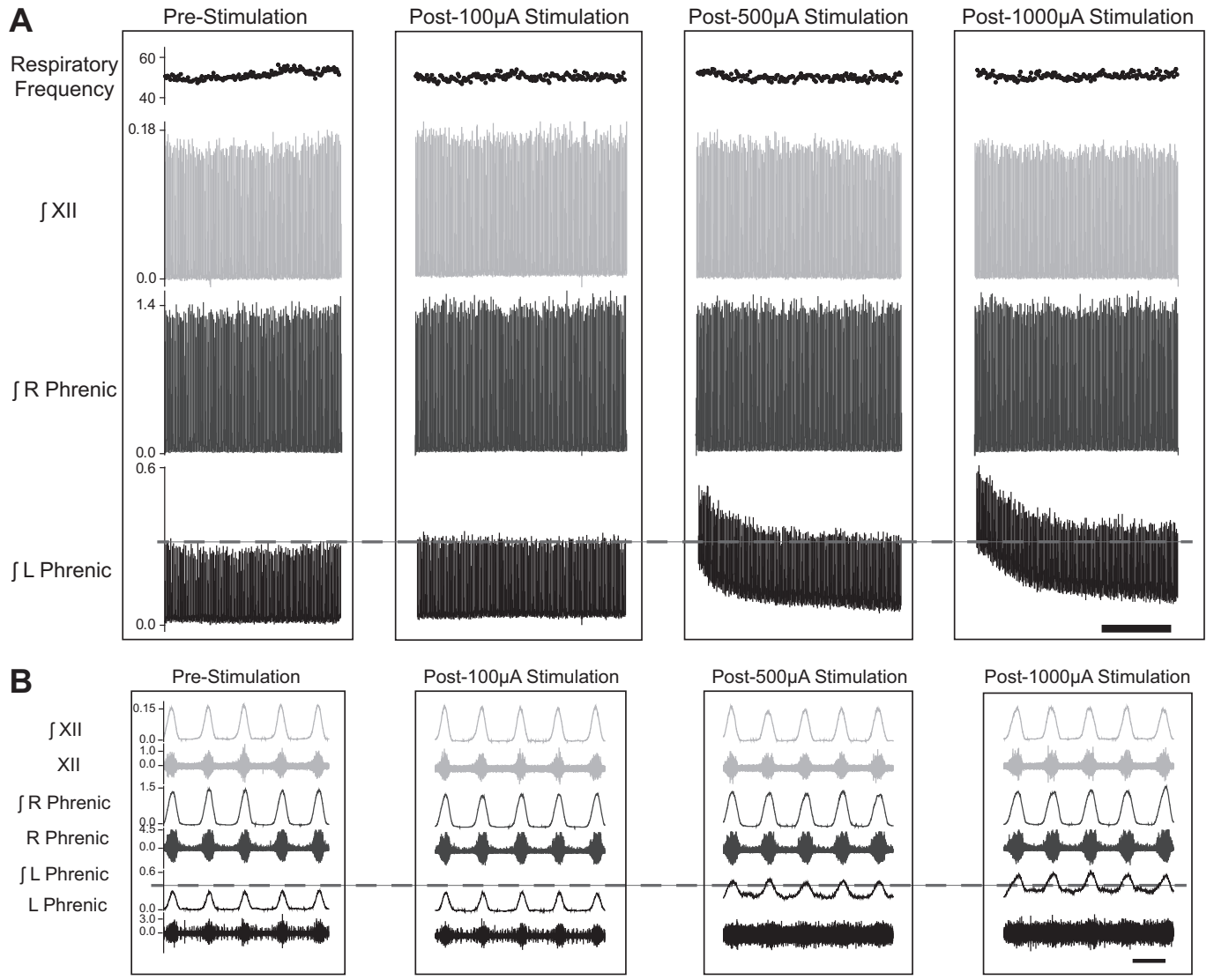

Fig. 3. Representative examples illustrating the impact of cervical HF-ES on phrenic and XII nerve activity. Following a left-sided C2 spinal cord hemisection injury, HF-ES was delivered to the ventrolateral epidural surface of the C4 spinal cord, ipsilateral to the side of injury. *A*: representative compressed traces depict integrated (∫)phrenic and hypoglossal (XII) nerve activity before and after HF-ES at 100, 500, and 1,000 μA from a rat that is 12 wk post-C2Hx. *B*: expanded traces depict both raw and integrated phrenic and hypoglossal nerve activity at baseline and following each bout of stimulation. Scale bars represent 1 min (*A*) and 1 s (*B*).

left). For each of the three motor outputs, the absolute value (mV) of the baseline burst amplitude was similar across the four experimental groups (ipsilateral phrenic: $P = 0.661$; contralateral phrenic: $P = 0.485$; XII: $P = 0.564$). The normalized ipsilateral phrenic burst showed a progressive increase in amplitude between 2 wk (19 ± 7% of the contralateral burst amplitude) and 12 wk postinjury (57 ± 14%), but the difference between these two time points was just above the threshold for statistical significance ($P = 0.061$). Inspiratory frequency (bursts/min) at baseline was similar across the four groups ($P = 0.244$; 2-wk cervical: 53 ± 2; 12-wk cervical: 48 ± 2; 2-wk thoracic: 50 ± 2; 12-wk thoracic: 51 ± 2). Baseline cardiovascular parameters including heart rate (HR), mean arterial blood pressure (MAP; Table 1), and arterial blood gases (Table 2) were also similar between the four experimental groups ($P > 0.3$ for all).

Phrenic and XII neural output following cervical HF-ES. Representative traces of phrenic and XII nerve output following brief periods of C4 epidural stimulation are provided in Fig. 3. A few features can be appreciated from these example records. First, the recording configuration precluded assessment of respiratory nerve activity during the period of stimulation due to a large stimulus artifact that obviated the underlying signal. Second, robust short-term potentiation of the ipsilateral phrenic signal is evident following HF-ES. The lowest current (100 μA) typically evoked minimal, if any, potentiation of respiratory nerve output, but stimulation at both 500 and 1,000 μA resulted in a substantial increase in the overall output of the ipsilateral phrenic nerve. In the example shown in Fig. 3 there was no appreciable impact on XII or contralateral phrenic output, even at the higher stimulus currents. Figure 4 provides an "overlay" of ipsilateral phrenic waveform averages, obtained immediately following HF-ES. The overlay plots further illustrate the potentiation of both phasic (inspiratory) and tonic phrenic output that occurred following the higher stimulus currents.

Table 1. *Cardiovascular parameters before, during, and after HF-ES*

	Mean Arterial Pressure, mmHg				Heart Rate, beats/min			
Stimulation	2-wk C4	2-wk T2	12-wk C4	12-wk T2	2-wk C4	2-wk T2	12-wk C4	12-wk T2
Baseline	100 ± 9	101 ± 5	118 ± 13	96 ± 10	409 ± 5	416 ± 9	402 ± 10	401 ± 7
100 μA	101 ± 9	101 ± 5	117 ± 13	97 ± 10	407 ± 4	416 ± 9	401 ± 9	400 ± 8
Post 100 μA	101 ± 9	101 ± 5	116 ± 13	97 ± 10	406 ± 4	417 ± 9	400 ± 9	400 ± 8
500 μA	103 ± 9*	104 ± 4	120 ± 14*	104 ± 11	405 ± 4	417 ± 8	401 ± 9	402 ± 8
Post 500 μA	102 ± 10	103 ± 5	117 ± 13	97 ± 9	405 ± 4	417 ± 8	400 ± 9	400 ± 8
1,000 μA	106 ± 10*	108 ± 4*	123 ± 13*	106 ± 11*	406 ± 4	418 ± 8	403 ± 9	402 ± 9
Post 1,000 μA	102 ± 10	102 ± 6	118 ± 14	93 ± 10	406 ± 4	420 ± 7	400 ± 9	401 ± 9

Mean arterial blood pressure was significantly increased during 500- and 1,000-μA stimulation in rats receiving stimulation at C4 and during 1,000-μA stimulation in rats receiving stimulation at T2. Heart rate was significantly increased during 1,000-μA stimulation in rats receiving HF-ES to the C4 spinal cord at 12 wk postinjury. No other statistically significant changes in cardiovascular parameters were observed during or after stimulation. *$P < 0.05$, significantly different from baseline, 100 μA, post 100 μA, post 500 μA, and post 1,000 μA. #$P < 0.05$, significantly different from T2 stimulation (2-way repeated-measures ANOVA with Holm-Sidak post hoc tests for individual comparisons).

The average changes in phasic, tonic, and total activity in the phrenic and XII nerve recordings following C4 HF-ES are presented in Fig. 5. In addition to the mean and SE, each individual data point is provided in keeping with recent recommendations for data reporting in preclinical research (Landis et al. 2012). Evaluation of phasic inspiratory activity in the left (ipsilateral) phrenic nerve revealed a statistical interaction ($P = 0.028$) between the stimulus current (i.e., 100, 500, and 1,000 μA) and the time postinjury (i.e., 2 vs. 12 wk post-C2Hx). Thus higher C4 stimulus currents evoked increases in phasic ipsilateral phrenic activity at 12 but not 2 wk following C2Hx (Fig. 5*A*). A similar response occurred in the phrenic nerve contralateral to the lesion ($P < 0.05$; Fig. 5*B*); however, neither the time postinjury ($P = 0.051$) nor the time-stimulus current interaction ($P = 0.079$) reached the threshold for statistical significance. Although there was no significant impact of time postinjury, contralateral phrenic output did increase with stimulus current ($P = 0.014$).

The C4 stimulation paradigm also influenced the medulla, as confirmed by small increases in XII motor output following HF-ES. The relative changes were small compared with the ipsilateral phrenic signal, but the XII inspiratory burst (Fig. 5*C*) increased with the stimulus current ($P = 0.027$), and potentiation of XII bursting tended to be greater at 12 vs. 2 wk post-C2Hx ($P = 0.070$).

Table 2. *Arterial blood gas parameters before and after HF-ES*

	Pa_{CO_2}, mmHg	Pa_{O_2}, mmHg	pH
2-wk C4			
Baseline	50.0 ± 2.6	171.4 ± 15.1	7.3 ± 0.0
Poststimulation	46.4 ± 2.6	162.3 ± 13.9*	7.3 ± 0.0
2-wk T2			
Baseline	51.7 ± 2.6	161.9 ± 17.8	7.3 ± 0.0
Poststimulation	51.9 ± 1.6	156.6 ± 20.2*	7.3 ± 0.0
12-wk C4			
Baseline	50.3 ± 1.0	178.6 ± 15.1	7.3 ± 0.1
Poststimulation	48.6 ± 2.8	174.6 ± 15.2*	7.3 ± 0.0
12-wk T2			
Baseline	50.5 ± 1.9	195.0 ± 19.1	7.3 ± 0.0
Poststimulation	52.4 ± 2.5	187.8 ± 20.6*	7.3 ± 0.0

Arterial partial pressure of CO_2 (Pa_{CO_2}) and O_2 (Pa_{O_2}) and pH are shown by group, before and after HF-ES. No changes in Pa_{CO_2} or pH were observed poststimulation. Although Pa_{O_2} was slightly reduced poststimulation, all animals remained well oxygenated. *$P < 0.05$, significantly different from baseline (2-way repeated-measures ANOVA with Holm-Sidak post hoc tests for individual comparisons).

The average changes in tonic neural activity following C4 stimulation are provided in Fig. 5, *D–F*. Note that the relative magnitude (%baseline) of the increased tonic discharge was considerably greater for tonic compared with phasic output. Both the left (Fig. 5*D*; $P = 0.001$) and right phrenic nerves (Fig. 5*E*; $P = 0.002$) showed increases in tonic activity as the stimulus current increased. The most robust potentiation occurred in the left phrenic nerve, with increases reaching ~500% of the baseline output at the highest stimulation intensity. There was no evidence for a time-dependent effect in either the left or right phrenic neurogram (i.e., tonic output was similar at 2 and 12 wk post-C2Hx). Tonic XII discharge tended to be greater following C4 stimulation at 12 vs. 2 wk, but this was not statistically significant (Fig. 5*F*; $P = 0.083$). Changes in total phrenic and XII activity (i.e., including both the phasic and tonic components) are presented in Fig. 5, *G–I*. All three recordings showed a progressive increase in total activity as the stimulus current was increased.

Although the XII data suggest an impact of HF-ES on medullary neurons (Fig. 5), no changes in inspiratory burst frequency were observed following stimulation of the cervical spinal cord (Table 3; $P = 0.402$).

Phrenic and XII neural output following thoracic HF-ES. The impact of thoracic (T2) stimulation on phasic, tonic, and total activity in the left and right phrenic nerves and the left XII nerve is summarized in Fig. 6. At the 100-μA stimulus current, the majority of rats showed a small increase in phasic discharge in all three motor outputs. The only exception was in the left phrenic recording at the 2-wk time point, where only 3 of 6 rats showed an increase in phasic discharge (Fig. 6*A*). The magnitude of potentiation increased with stimulus current in the left phrenic (Fig. 6*A*; $P = 0.004$), right phrenic (Fig. 6*B*; $P = 0.011$), and left XII recordings (Fig. 6*C*; $P = 0.021$). However, time-dependent effects (e.g., 2 vs. 12 wk) on phasic output were not detected for any of the recordings (all $P > 0.265$).

Tonic output was potentiated in all three nerves following T2 stimulation in nearly all experiments at both the 2- and 12-wk time points (Fig. 6, *D–F*). In the left phrenic signal, tonic discharge increased with stimulus intensity ($P = 0.004$) and reached ~500% of baseline at the highest stimulus current. Increases in tonic discharge in the right phrenic and left XII recordings were typically in the range of 50–100% (Fig. 6, *E* and *F*). Time-dependent effects on the tonic response to T2 stimulation were not statistically significant for any of the

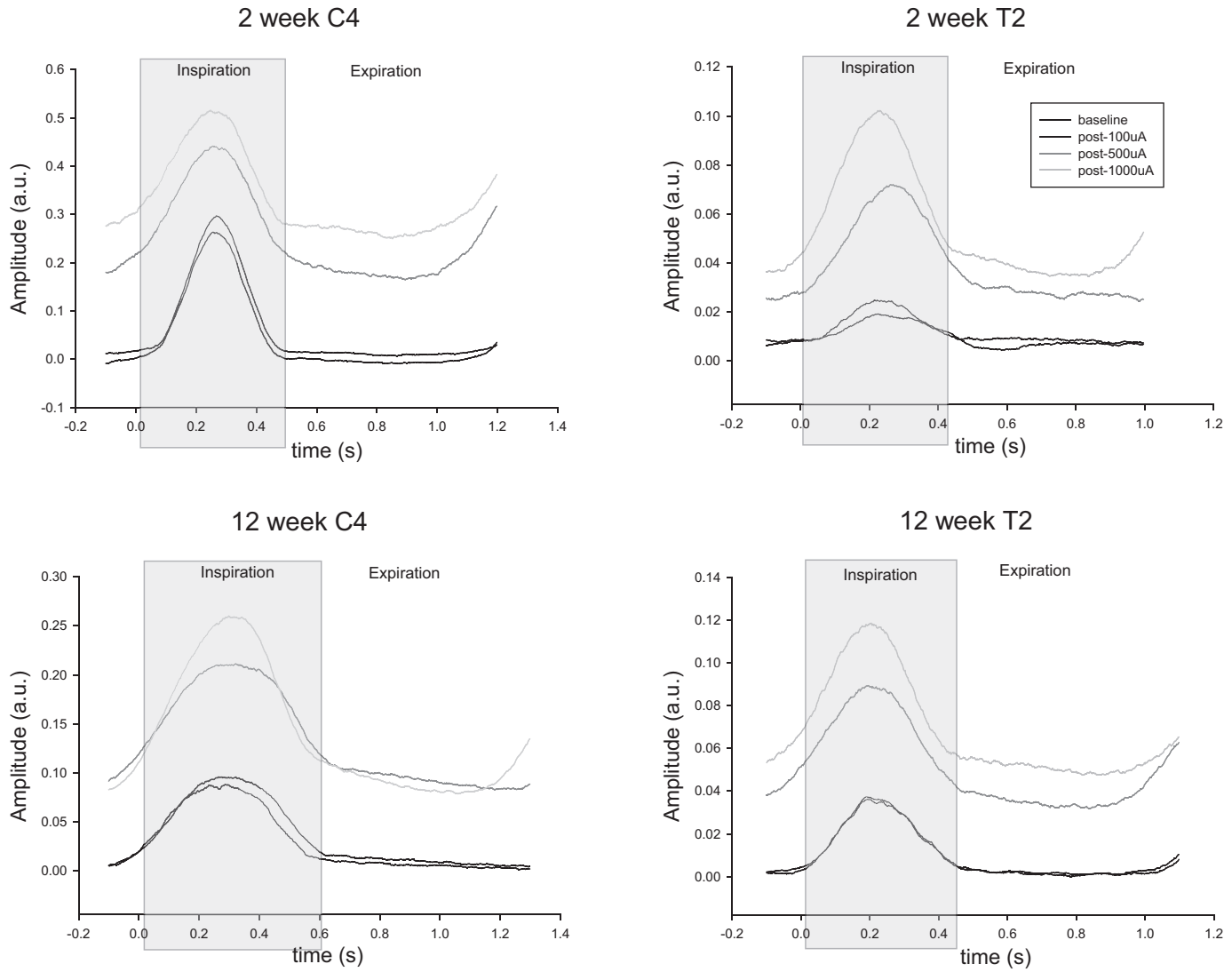

Fig. 4. Impact of HF-ES on the phrenic activity recorded ipsilateral to C2Hx. Representative traces of integrated ipsilateral phrenic waveform averages are shown from rats that were either 2 or 12 wk post-C2Hx injury and received HF-ES to either the cervical or thoracic spinal cord. Waveform averages were calculated from the 10 respiratory cycles immediately preceding the initiation of stimulation (baseline) and from the 10 cycles immediately following each bout of stimulation. For each plot, *time 0* represents the start of the inspiratory phase of the respiratory cycle, which is shaded in gray. Note the increase in tonic phrenic output in both the inspiratory and expiratory phases of the respiratory cycle following 500- and 1,000-μA stimulation (as evidenced by the upward shift in the waveform baseline).

neural outcomes assessed (all $P > 0.557$). The magnitude by which total activity was potentiated increased with stimulus intensity in all recordings (all $P < 0.007$; Fig. 6, *G–I*), and there were no significant differences in the total activity between the two time points (all $P > 0.075$).

The ratio of phasic to tonic activity within each nerve is presented in Fig. 7. For both C4 and T2 stimulation, higher HF-ES currents were associated with the most dramatic reductions in this ratio, consistent with the observed increase in tonic output relative to phasic output. Although not statistically significant, there appeared to be a greater impact of stimulation on the ratio of phasic to tonic activity at the more acute time points.

Similar to the cervical HF-ES data, changes in inspiratory burst frequency were not observed following stimulation of the thoracic spinal cord (Table 3; $P = 0.281$).

Cardiovascular parameters during and after HF-ES. Representative traces depicting the impact of C4 stimulation on HR and MAP are shown in Fig. 8, *A* and *B*; average responses along with individual data points are provided in Fig. 8, *C* and *D*. HR remained stable in all groups during and after each bout of stimulation. MAP increased during C4 stimulation at 500 ($P = 0.046$) and 1,000 μA ($P < 0.001$), but with no evidence of a time-dependent change between 2 and 12 wk ($P = 0.445$; Fig. 8*C*). MAP also increased during T2 stimulation at 1,000 μA ($P = 0.039$), but no time-dependent changes were detected ($P = 0.963$). At both 2 and 12 wk, MAP returned ack to baseline values following cessation of stimulation, regardless of the level of stimulation (all $P > 0.627$). The mean HR and MAP data are provided in Table 1.

Arterial blood was assessed for Pa_{CO_2}, Pa_{O_2}, and pH values before and after the stimulation protocol. As shown in Table 2, no group differences in Pa_{CO_2} or pH were detected at either time point (all $P > 0.38$). Despite a slight reduction in Pa_{O_2} following stimulation ($P = 0.012$), all rats remained well

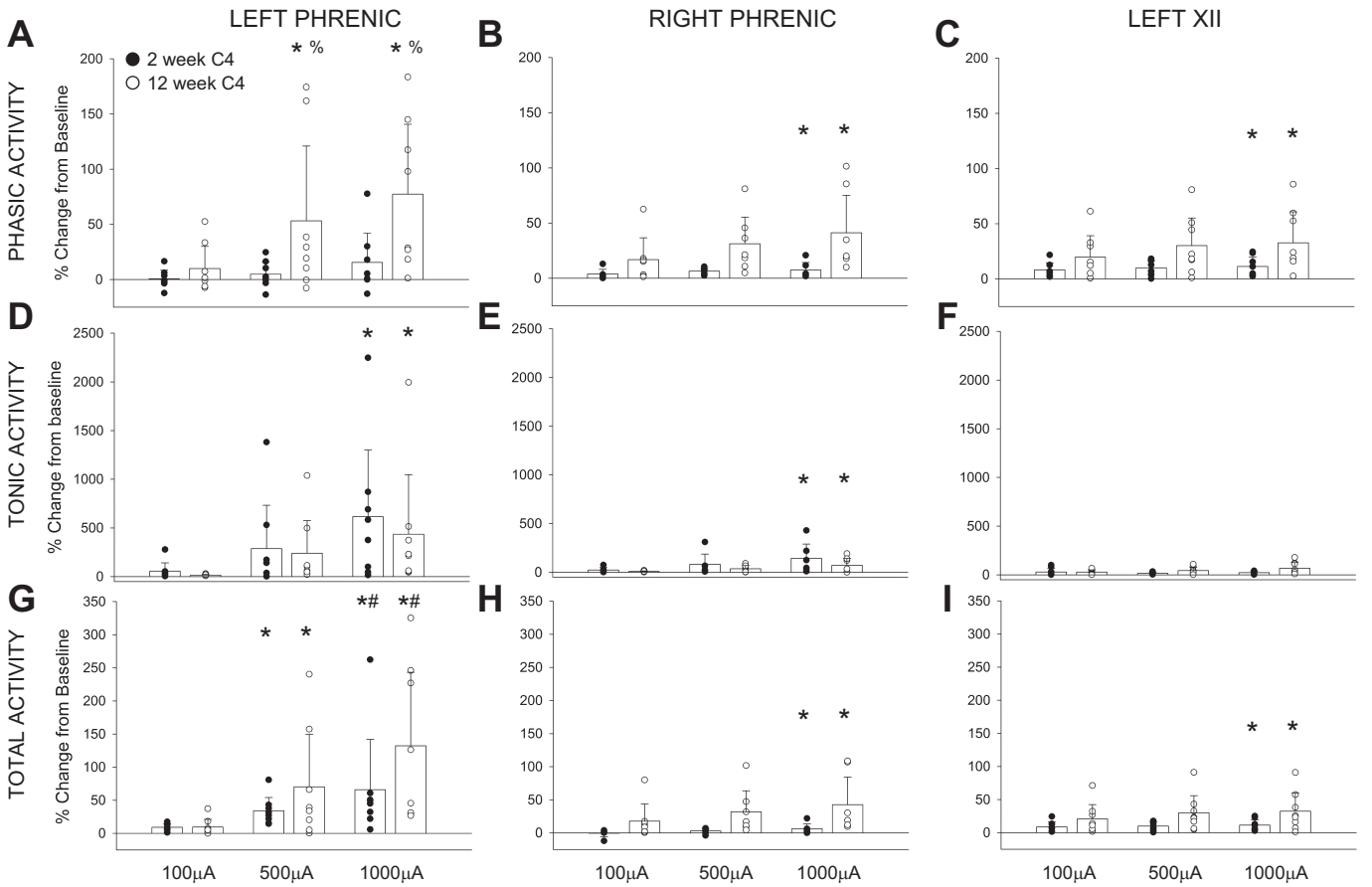

Fig. 5. Average changes in phrenic and hypoglossal nerve activity following C4 HF-ES. Depicted are changes in phasic (*A–C*), tonic (*D–F*), and total (*G–I*) phrenic and hypoglossal nerve activity following HF-ES of the C4 spinal cord, delivered at 2 and 12 wk postinjury. Data were calculated over the 3 min following each bout of stimulation and are represented as %change from baseline activity. HF-ES delivered to the C4 spinal cord at 12 wk post-C2Hx resulted in an increase in phasic phrenic activity. No other group differences were observed, although dose-dependent increases in amplitude (%change above baseline) were observed following HF-ES across both groups, with the greatest amplitude changes occurring following the highest stimulation intensities (e.g., 500 and 1,000 μA). Note that profound increases in tonic activity comprised much of the increase in total activity and that the ipsilateral phrenic nerve demonstrated the most dramatic changes in nerve amplitude relative to baseline. *$P < 0.05$, different from 100 μA. #$P < 0.05$, different from 500 μA. %$P < 0.05$, different from 2 wk at same stimulus current. Data were evaluated using 2-way repeated-measures ANOVA with Holm-Sidak post hoc tests for individual comparisons (groups: 2-wk C4, $n = 8$; 12-wk C4, $n = 8$).

oxygenated throughout the experimental protocol, with Pa_{O_2} values >98 mmHg in all cases.

DISCUSSION

In regard to respiratory muscle activation, the utility of HF-ES was first demonstrated in terminal studies in dogs and rats following complete transection at the C1 level (DiMarco and Kowalski 2009, 2011, 2013b; Kowalski et al. 2013). In the current study we tested HF-ES following an incomplete high cervical SCI that spared bulbospinal synaptic inputs to contralateral phrenic motoneurons while preserving a limited number of bulbospinal inputs to ipsilateral motoneurons via collaterals from contralateral fibers (Fuller et al. 2006; Goshgarian 2003, 2009; Goshgarian et al. 1991; Lane et al. 2008; Moreno et al. 1992; Nantwi et al. 1999). The results show that prolonged HF-ES of the ventrolateral C4 or T2 spinal cord can cause an increase in ipsilateral phrenic discharge that persists after the stimulation. This short-term potentiation of phrenic bursting illustrates the potential for spinal cord stimulation to trigger respiratory plasticity (Mercier et al. 2017), a concept that could be useful in designing neurorehabilitation paradigms (Kasten et al. 2013; McPherson et al. 2015). However, the large increases in tonic phrenic output triggered by HF-ES indicate that this particular paradigm is unlikely to have application as a "respiratory neuroprosthesis" for activation of the respiratory muscles after incomplete SCI.

Table 3. *Respiratory frequency before and after HF-ES*

	Stimulation			
	Baseline	100 μA	500 μA	1,000 μA
2-wk C4	52.5 ± 1.5	50.0 ± 1.4	51.0 ± 1.2	52.0 ± 0.7
2-wk T2	50.3 ± 1.5	47.7 ± 2.1	49.7 ± 1.8	50.9 ± 2.4
12-wk C4	47.5 ± 1.6	47.5 ± 1.6	47.0 ± 1.5	48.0 ± 1.2
12-wk T2	51.4 ± 1.9	50.9 ± 1.2	49.7 ± 1.3	48.6 ± 1.4

Average respiratory frequency (breaths per minute) are shown by group, prior to and following HF-ES. No changes in respiratory frequency were observed following stimulation (2-way repeated-measures ANOVA).

HF-ES after SCI. Application of HF-ES to the ventral spinal cord following C1 spinal cord transection can produce diaphragm and intercostal activation motor unit activation that is asynchronous relative to the stimulus (DiMarco and Kowalski

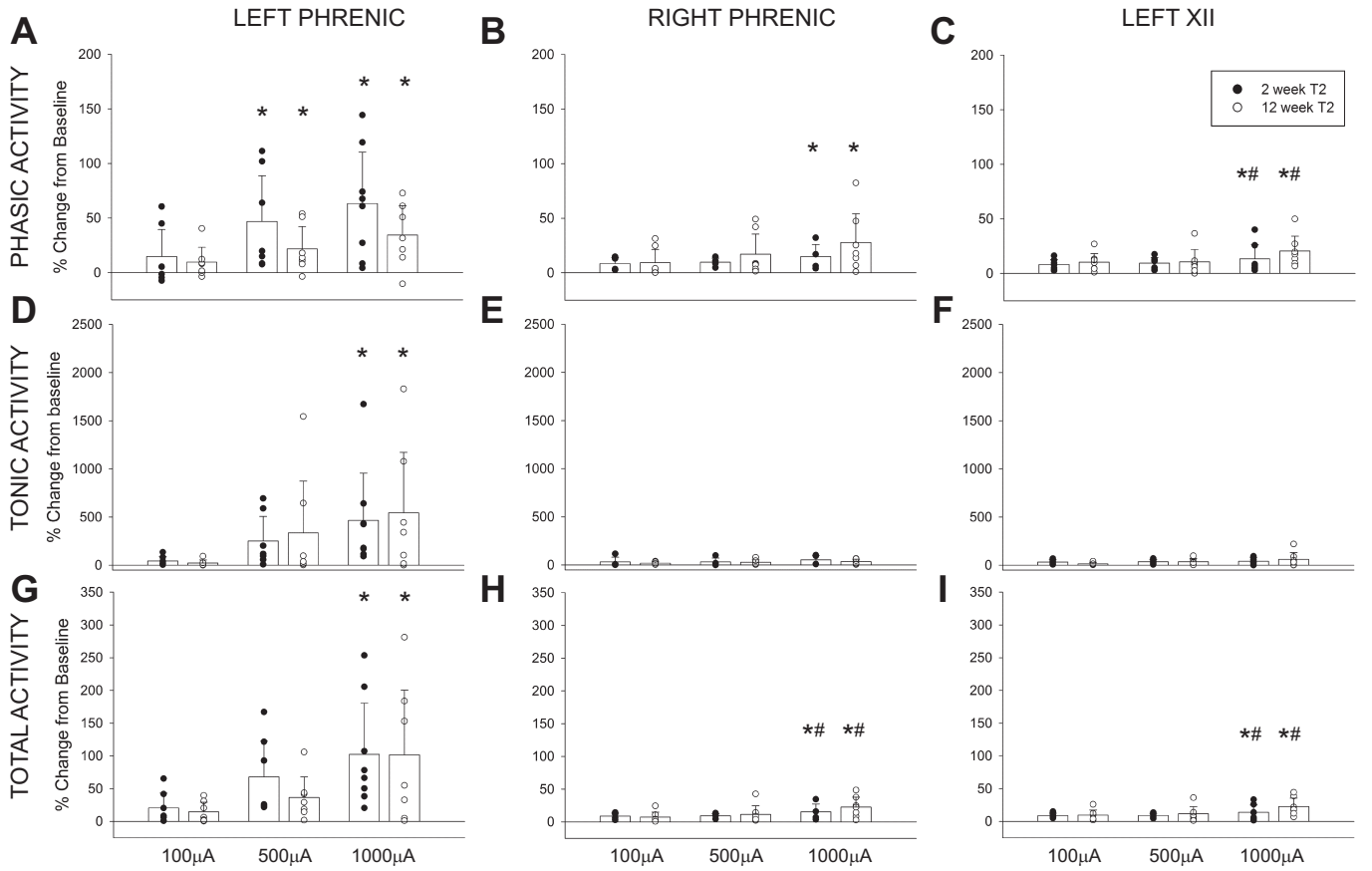

Fig. 6. Average changes in phrenic and hypoglossal nerve activity following T2 HF-ES. Shown are changes in phasic (*A–C*), tonic (*D–F*), and total (*G–I*) phrenic and hypoglossal nerve activity following HF-ES of the T2 spinal cord, delivered at 2 and 12 wk postinjury. Data were calculated over the 3 min following each bout of stimulation and are represented as %change from baseline activity. A dose-dependent increase in amplitude (%change above baseline) was observed in all nerves (*$P < 0.05$, different from 100μA; #$P < 0.05$, different from 500 μA) across all outcomes (phasic, tonic, and total nerve activity), with the greatest amplitude changes occurring following the highest stimulation intensities. Note that profound increases in tonic activity comprised much of the increase in total activity and that the ipsilateral phrenic nerve demonstrated the most dramatic changes in nerve amplitude relative to baseline. No significant group differences were observed in any nerve in any of the outcomes assessed. Data were evaluated using 2-way repeated-measures ANOVA with Holm-Sidak post hoc tests for individual comparisons (groups: 2-wk T2, $n = 7$; 12-wk T2, $n = 7$).

2009, 2010, 2011, 2013a, 2013b, 2015; Hormigo et al. 2017; Kowalski et al. 2013). In these prior reports, respiratory motor unit discharge during HF-ES occurred at rates well below the stimulation frequency, and respiratory motor unit activation resembled discharge patterns seen during spontaneous breathing. Therefore, it appears that HF-ES can activate a spinal network capable of providing "physiologically appropriate" synaptic input to respiratory motoneurons, resulting in dis-

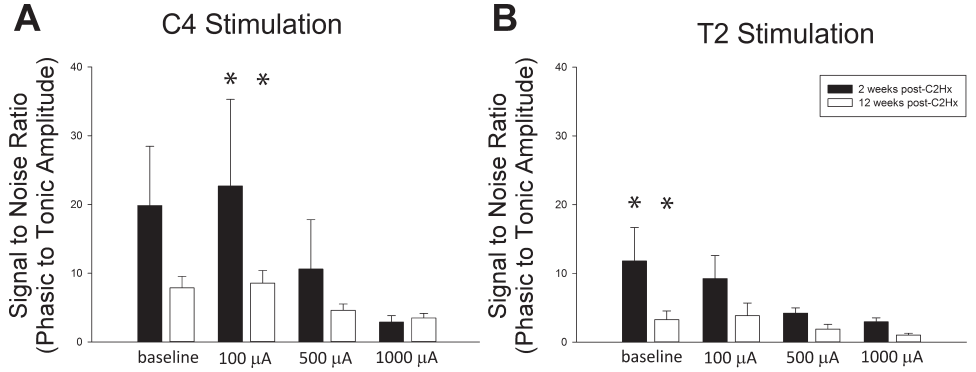

Fig. 7. Ratio of phasic to tonic ipsilateral phrenic nerve activity following C4 and T2 HF-ES. Shown are the average "signal-to-noise ratios" of phasic to tonic ipsilateral phrenic nerve activity at baseline and following each bout of HF-ES delivered to either the C4 (*A*) or T2 (*B*) spinal cord at 2 and 12 wk postinjury. A dose-dependent reduction in this ratio was observed following both C4 and T2 stimulation (*$P < 0.05$, different from 1,000 μA) across all outcomes (phasic, tonic, and total nerve activity), with the greatest reductions in this ratio occurring following the highest stimulation intensities. No significant time-dependent group differences were observed, although this ratio was consistently lower in the chronic postinjury time point, a finding that is consistent with increased baseline tonic activity in chronically injured rats. Data were evaluated using 2-way repeated-measures ANOVA with Holm-Sidak post hoc tests for individual comparisons (groups: 2-wk C4, $n = 8$; 12-wk C4, $n = 8$; 2-wk T2, $n = 7$; 12-wk T2, $n = 7$).

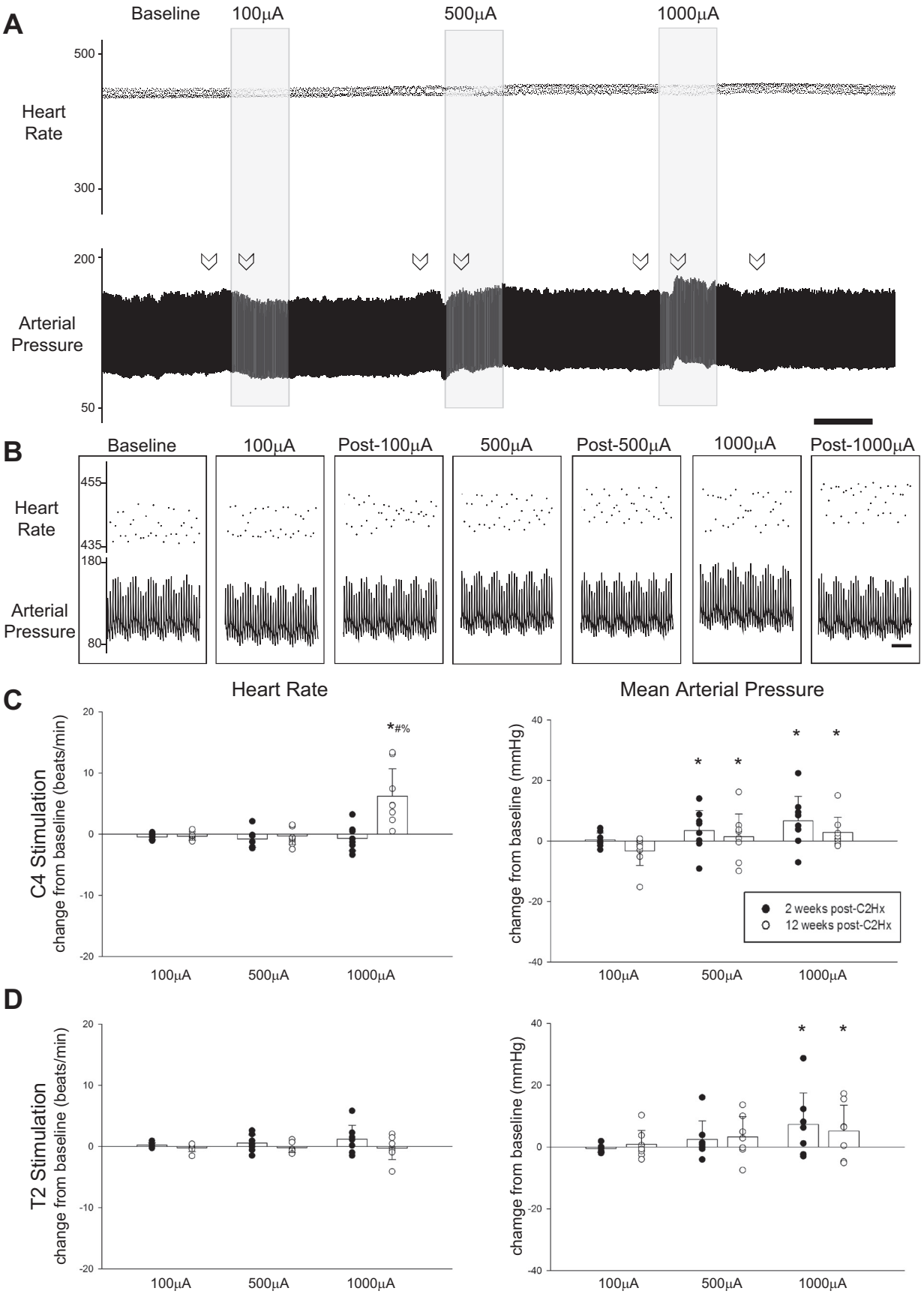

charge patterns that resemble what is observed during spontaneous breathing. In contrast, direct nerve or muscle electrical stimulation techniques (e.g., functional electrical stimulation, or FES) typically induce synchronous activation of axons within the electrical field and do not recruit motor units in an orderly fashion, which could contribute to motor unit fatigue (Levy et al. 1990). This has led to the suggestion that spinal stimulation methods may be advantageous compared with FES approaches (Bamford and Mushahwar 2011; DiMarco and Kowalski 2013a; Mondello et al. 2014; Tator et al. 2012).

The current study is the first to explore the impact of HF-ES on phrenic and XII motor output after subacute and chronic incomplete cervical SCI. We utilized a C2Hx injury, which axotomizes bulbospinal neurons projecting to the ipsilateral phrenic motor nucleus (Goshgarian 2003). The resulting paralysis of the ipsilateral diaphragm is transient, and a small but functionally relevant (Dougherty et al. 2012) return of ipsilateral diaphragm inspiratory bursting occurs over weeks to months post-C2Hx (Nantwi et al. 1999; Pitts 1940). Spontaneous activation of the ipsilateral diaphragm after C2Hx results at least in part due to activation of latent crossed bulbospinal synaptic projections to the ipsilateral phrenic motor nucleus (Goshgarian 2003, 2009). There also may be a contribution of midcervical interneurons to the "crossed phrenic pathway" (Lane 2011; Sandhu et al. 2009). Regardless of the specific neuroanatomical substrate, it is well established that crossed phrenic pathways are capable of considerable plasticity and that the relative extent of ipsilateral phrenic motor recovery after C2Hx can be enhanced (Fuller and Mitchell 2017). Treatments that can increase phrenic recovery include spinal serotonin receptor activation (Ling et al. 1994; Zhou and Goshgarian 1999, 2000), increased brain-derived neurotrophic factor availability (Gransee et al. 2013; Mantilla et al. 2013), preconditioning nerve lesions (Fuller et al. 2002; Johnson et al. 2000), and intermittent hypoxia exposure (Fuller et al. 2003; Golder and Mitchell 2005; Lovett-Barr et al. 2012). Here we investigated whether applying HF-ES with a continuous paradigm, similarly to stimulation studies targeting increased limb muscle activation (Angeli et al. 2014; Harkema et al. 2011), can induce phrenic motor plasticity on short timescales in rats with subacute (2 wk) or chronic (12 wk) C2Hx. Both thoracic and cervical HF-ES were able to potentiate phrenic bursting, but some differences were noted. With thoracic stimulation, increases in phasic (i.e., inspiratory related) activity occurred after both subacute and chronic injury. In contrast, cervical HF-ES did not increase phasic phrenic bursting at the subacute time point, but did so after chronic injury. Inflammatory processes and other aspects of "spinal shock" (Hagg and Oudega 2006) occurring in the cervical cord will be more prominent at the subacute time point, and these may limit the ability for cervical HF-ES to activate synaptic pathways to phrenic motoneurons to increase inspiratory bursting. It should be emphasized, however, that HF-ES evoked robust increases in tonic phrenic output in subacutely injured rats, similar to the tonic response after chronic injury. This differential tonic vs. phasic response at the subacute time point suggests that HF-ES is regulating these outputs via distinct mechanisms.

It is worth noting that that tonic discharge observed in our studies is similar to that in a report from Alilain et al. (2008), who used light-based activation of cervical neurons. Stimulation of the midcervical spinal cord using a channel rhodopsin method also evoked increases in phrenic bursting across the entire respiratory cycle. In that report, light-induced neuronal activation was not restricted to phrenic motoneurons, and the result was tonic phrenic motoneuron activation, similar to the current data. Regardless of the underlying mechanisms, the robust increase in tonic phrenic discharge raises concerns about the impact of this particular HF-ES paradigm on respiratory biomechanics. More specifically, the tonic activity and sustained diaphragm contraction are unlikely to facilitate lung inflation and alveolar ventilation. Accordingly, future studies of spinal epidural stimulation after incomplete SCI need to focus on the pattern of diaphragm motor unit activation both during (e.g., DiMarco and Kowalski 2009, 2011, 2013b; Kowalski et al. 2013) and after stimulation (e.g., as in the current report). Thus it appears that diffuse stimulation of the midcervical spinal cord has a high probability of evoking tonic diaphragm activation, at least after incomplete cervical SCI.

Mechanisms by which HF-ES may potentiate phasic and tonic respiratory motor output. Modeling studies indicate that epidural stimulation is not effective at direct motoneuron activation and that activation of transynaptic pathways is likely to underlie many of the observed motor responses (Capogrosso et al. 2013). In addition, the HF-ES approach used in the current study likely caused diffuse neuronal activation in the vicinity of the electrode. Accordingly, there are multiple mechanisms that may contribute to HF-ES induced short-term potentiation of ipsilateral phrenic discharge. A predominantly local (spinal) mechanism (e.g., at or near the ipsilateral phrenic motor pool) seems most likely to underlie the impact of HF-ES on ipsilateral phrenic motor output, because contralateral phrenic and XII responses were much lower. However, plasticity in respiratory premotor inputs cannot be excluded as a contributing factor, because HF-ES also induced small changes in both phasic and tonic supraspinal (XII) motor output. On the other hand, there was no sustained impact of HF-ES on brain stem processes driving the respiratory rhythm, because the frequency of breathing did not show any appreciable changes.

Activation of neuromodulatory inputs to phrenic motoneurons could have contributed to persistently increased activity following HF-ES. The caudal raphe nuclei project a dense serotonergic input to the spinal cord (Alvarez et al. 1998;

Fig. 8. Impact of HF-ES on cardiovascular parameters. *A*: representative traces depict instantaneous heart rate (HR; beats/min) and mean arterial pressure (MAP; mmHg) from a rat that received stimulation to the C4 spinal cord 2 wk postinjury. *B*: expanded traces depict instantaneous HR and MAP at baseline as well as during and after each bout of stimulation. Arrows in *A* indicate locations from which the expanded traces shown in *B* were obtained. Scale bars represent 1 min (*A*) and 1 s (*B*). *C* and *D*: stimulation-induced changes in HR and MAP for rats receiving HF-ES at either the C4 (*C*) or the T2 (*D*) spinal level. A significant increase in HR was observed following C4 stimulation in rats that were 12 wk postinjury. MAP was significantly increased relative to baseline during stimulation at both 500 (#$P < 0.05$) and 1,000 μA (*$P < 0.05$). Following T2 stimulation, MAP was only increased with stimulation at 1,000 μA (*$P < 0.05$). In all groups, HR and MAP returned to baseline following cessation of stimulation. *$P < 0.05$, different from 100 μA. #$P < 0.05$, different from 500 μA. %$P < 0.05$, different from 2 wk. Data were evaluated using 2-way repeated-measures ANOVA with Holm-Sidak post hoc tests for individual comparisons (groups: 2-wk C4, $n = 8$; 12-wk C4, $n = 8$; 2-wk T2, $n = 7$; 12-wk T2, $n = 7$).

Bowker et al. 1981a, 1981b, 1981c; Steinbusch 1981), including phrenic motoneurons (Satriotomo et al. 2012) as well as interneurons that are synaptically coupled to the phrenic motor pool (Gonzalez-Rothi EJ and Fuller DD, unpublished observations). Following C2Hx injury, there is a gradual return of serotonergic innervation to ipsilateral phrenic motoneurons (Tai et al. 1997), and the amount of serotonin immunostaining in this region correlates with the extent of phrenic recovery (Golder and Mitchell 2005). As noted above, C4 HF-ES did not increase phasic inspiratory output in the phrenic nerve ipsilateral to C2Hx at 2 wk postinjury, a time point when serotonergic innervation of ipsilateral phrenic nucleus is quite low (Golder and Mitchell 2005). On the other hand, the tonic phrenic response was very strong when HF-ES was given at the 2-wk time point. A similarly robust increase in tonic phrenic activity can be evoked by systemic delivery of the serotonin precursor molecule 5-hydroxytryptophan after both acute and chronic C2Hx injury (Ling et al. 1994; Zhou and Goshgarian 2000). Application of serotonin in an in vitro rat preparation trigger also increases tonic activity to such an extent that it can obscure rhythmic inspiratory bursting in the 4th cervical ventral root (Lindsay and Feldman 1993). The similarity between the impact of pharmacologically driven serotonin receptor activation (Ling et al. 1994; Zhou and Goshgarian 2000) and the response to HF-ES may indicate similar mechanisms are driving the increases in tonic activity.

Another possibility is that short-term potentiation of phrenic output reflected a direct impact of HF-ES on phrenic motoneuron membrane biophysical properties. For example, persistent inward currents (PICs) are possible in phrenic motoneurons, albeit extremely rare (Enríquez Denton et al. 2012). Enriquez Denton and colleagues reported that phrenic motoneurons are immunopositive for voltage-dependent calcium channels ($Ca_v1.3$), and through neurophysiological recordings they also identified a phrenic motoneuron with PIC activation. The caveat was that the PIC was only identified following interruption of bulbospinal inputs to the phrenic motoneuron pool (i.e., as occurs for ipsilateral phrenic motoneurons following C2Hx lesion). Most prominently, phrenic motoneurons showed a voltage-dependent amplification of output through NMDA receptor activation (Enríquez Denton et al. 2012). The HF-ES may have directly (or indirectly, e.g., via triggering serotonin release; Capogrosso et al. 2013) triggered motoneuron depolarization and modulation of voltage-dependent synaptic currents, or possibly even PIC activation in these spinally injured animals.

A final consideration is that high-frequency stimulation may have altered inhibitory synaptic inputs to phrenic motoneurons. Studies of deep brain stimulation have reported that stimulation frequencies greater than 50 Hz can suppress neuronal discharge (Lafreniere-Roula et al. 2010), and this inhibition can influence target/downstream neural circuits. In regard to the phrenic motor system, inhibitory inputs to phrenic motoneurons are active across the respiratory cycle (Berger 1979) and play a role in shaping the pattern of respiratory output (Marchenko et al. 2015). Thus it is plausible that HF-ES may have triggered disinhibition of phrenic motoneurons, resulting in an increase in tonic activity throughout the respiratory cycle.

C4 vs. T2 stimulation. Qualitatively similar potentiation of phrenic motor output occurred regardless of whether HF-ES was applied to the cervical or thoracic spinal cord, particularly after chronic injury. The most likely explanation is that cervical and thoracic stimulation activated the same propriospinal neurons innervating the ipsilateral phrenic motoneuron pool. Decima and colleagues (Decima and von Euler 1969a, 1969b; Decima et al. 1967, 1969) provided evidence that long propriospinal tracts connect thoracic intercostal motoneurons with cervical phrenic motoneurons, and these tracts may be activated by the HF-ES paradigm. Long propriospinal tracts also originate in the lumbar spinal cord, and traverse the thoracic spinal cord to terminate in the cervical region (Dutton et al. 2006). Indeed, in their earlier work, Dimarco and Kowalski (2013b) concluded that long propriospinal tracts located in the lateral funiculus were the likely candidate neuronal pathways mediating respiratory related activation of diaphragm motor units via HF-ES of the thoracic spinal cord.

Conclusion. We conclude that HF-ES to the ventrolateral spinal cord can potentiate ipsilateral phrenic motor output following incomplete high cervical SCI and that this appears to reflect primarily a local spinal mechanism. Similar phrenic potentiation occurred with stimulation of the midcervical or high thoracic spinal cord, indicating that a highly selective electrode placement is not needed to evoke this response. Short-term potentiation of phrenic bursting illustrates that stimulation of the injured spinal cord can trigger respiratory plasticity, and this potentially could be harnessed in the context of neurorehabilitation (Kasten et al. 2013; McPherson et al. 2015; Mercier et al. 2017). However, the substantial increases in tonic phrenic output evoked by HF-ES in our study indicate that the continuous stimulation paradigm used is unlikely to be useful for respiratory muscle activation after SCI. The increased tonic phrenic discharge highlights the need for future studies of epidural stimulation to carefully evaluate the pattern of diaphragm activation evoked by stimulation. In this regard, lower stimulation frequencies (Gad et al. 2013; Lu et al. 2016; Shah et al. 2016) may be more appropriate for activation of respiratory motor units after incomplete SCI. A recent publication explored the impact of midcervical (C3) epidural stimulation in anesthetized mice by using a relatively high current (1.5 mA) delivered at a rate of 20 Hz (Huang et al. 2016). This low-frequency paradigm did not impact tidal volume but did produce an increase in respiratory rate and also increased the occurrence of spontaneous sighs. However, we are not aware of any published reports regarding the impact of low-frequency epidural stimulation on respiratory outcomes after SCI, in either the acute or chronic setting.

GRANTS

Funding was provided by National Institutes of Health (NIH) Grants 1R01NS080180-01A1 (to D. D. Fuller), 1R01NS054025-06 (to P. J. Reier), Department of Defense Award SC120209 (to P. J. Reier), NIH Training Grant K12HDO55929 (to E. J. Gonzalex-Rothi), NIH Research Supplement to Promote Diversity NS80180 (to E. J. Gonzalez-Rothi), and the State of Florida Brain and Spinal Cord Injury Research Trust Fund (to D. D. Fuller and P. J. Reier), awarded through the McKnight Brain Institute at the University of Florida.

DISCLOSURES

No conflicts of interest, financial or otherwise, are declared by the authors.

AUTHOR CONTRIBUTIONS

E.J.G.-R., D.M.B., and D.D.F. conceived and designed research; E.J.G.-R., K.A.S., and D.M.B. performed experiments; E.J.G.-R., K.A.S., M.H.H., and

A.C.S. analyzed data; E.J.G.-R., K.A.S., P.J.R., and D.D.F. interpreted results of experiments; E.J.G.-R. prepared figures; E.J.G.-R. drafted manuscript; E.J.G.-R., K.A.S., P.J.R., D.M.B., and D.D.F. edited and revised manuscript; E.J.G.-R., K.A.S., M.H.H., A.C.S., P.J.R., D.M.B., and D.D.F. approved final version of manuscript.

REFERENCES

Alilain WJ, Li X, Horn KP, Dhingra R, Dick TE, Herlitze S, Silver J. Light-induced rescue of breathing after spinal cord injury. *J Neurosci* 28: 11862–11870, 2008. doi:10.1523/JNEUROSCI.3378-08.2008.

Alvarez FJ, Pearson JC, Harrington D, Dewey D, Torbeck L, Fyffe RE. Distribution of 5-hydroxytryptamine-immunoreactive boutons on α-motoneurons in the lumbar spinal cord of adult cats. *J Comp Neurol* 393: 69–83, 1998. doi:10.1002/(SICI)1096-9861(19980330)393:1<69::AID-CNE7>3.0.CO;2-O.

Angeli CA, Edgerton VR, Gerasimenko YP, Harkema SJ. Altering spinal cord excitability enables voluntary movements after chronic complete paralysis in humans. *Brain* 137: 1394–1409, 2014. doi:10.1093/brain/awu038.

Bamford JA, Mushahwar VK. Intraspinal microstimulation for the recovery of function following spinal cord injury. *Prog Brain Res* 194: 227–239, 2011. doi:10.1016/B978-0-444-53815-4.00004-2.

Berger AJ. Phrenic motoneurons in the cat: subpopulations and nature of respiratory drive potentials. *J Neurophysiol* 42: 76–90, 1979.

Borgens RB, Roederer E, Cohen MJ. Enhanced spinal cord regeneration in lamprey by applied electric fields. *Science* 213: 611–617, 1981. doi:10.1126/science.7256258.

Bowker RM, Steinbusch HW, Coulter JD. Serotonergic and peptidergic projections to the spinal cord demonstrated by a combined retrograde HRP histochemical and immunocytochemical staining method. *Brain Res* 211: 412–417, 1981a. doi:10.1016/0006-8993(81)90965-3.

Bowker RM, Westlund KN, Coulter JD. Origins of serotonergic projections to the spinal cord in rat: an immunocytochemical-retrograde transport study. *Brain Res* 226: 187–199, 1981b. doi:10.1016/0006-8993(81)91092-1.

Bowker RM, Westlund KN, Coulter JD. Serotonergic projections to the spinal cord from the midbrain in the rat: an immunocytochemical and retrograde transport study. *Neurosci Lett* 24: 221–226, 1981c. doi:10.1016/0304-3940(81)90160-9.

Capogrosso M, Wenger N, Raspopovic S, Musienko P, Beauparlant J, Bassi Luciani L, Courtine G, Micera S. A computational model for epidural electrical stimulation of spinal sensorimotor circuits. *J Neurosci* 33: 19326–19340, 2013. doi:10.1523/JNEUROSCI.1688-13.2013.

Decima EE, von Euler C. Excitability of phrenic motoneurones to afferent input from lower intercostal nerves in the spinal cat. *Acta Physiol Scand* 75: 580–591, 1969a. doi:10.1111/j.1748-1716.1969.tb04413.x.

Decima EE, von Euler C. Intercostal and cerebellar influences on efferent phrenic activity in the decerebrate cat. *Acta Physiol Scand* 76: 148–158, 1969b. doi:10.1111/j.1748-1716.1969.tb04459.x.

Decima EE, von Euler C, Thoden U. Spinal intercostal-phrenic reflexes. *Nature* 214: 312–313, 1967. doi:10.1038/214312a0.

Decima EE, von Euler C, Thoden U. Intercostal-to-phrenic reflexes in the spinal cat. *Acta Physiol Scand* 75: 568–579, 1969. doi:10.1111/j.1748-1716.1969.tb04412.x.

DiMarco AF, Kowalski KE. High-frequency spinal cord stimulation of inspiratory muscles in dogs: a new method of inspiratory muscle pacing. *J Appl Physiol (1985)* 107: 662–669, 2009. doi:10.1152/japplphysiol.00252.2009.

DiMarco AF, Kowalski KE. Intercostal muscle pacing with high frequency spinal cord stimulation in dogs. *Respir Physiol Neurobiol* 171: 218–224, 2010. doi:10.1016/j.resp.2010.03.017.

DiMarco AF, Kowalski KE. Distribution of electrical activation to the external intercostal muscles during high frequency spinal cord stimulation in dogs. *J Physiol* 589: 1383–1395, 2011. doi:10.1113/jphysiol.2010.199679.

DiMarco AF, Kowalski KE. Activation of inspiratory muscles via spinal cord stimulation. *Respir Physiol Neurobiol* 189: 438–449, 2013a. doi:10.1016/j.resp.2013.06.001.

DiMarco AF, Kowalski KE. Spinal pathways mediating phrenic activation during high frequency spinal cord stimulation. *Respir Physiol Neurobiol* 186: 1–6, 2013b. doi:10.1016/j.resp.2012.12.003.

DiMarco AF, Kowalski KE. Electrical activation to the parasternal intercostal muscles during high-frequency spinal cord stimulation in dogs. *J Appl Physiol (1985)* 118: 148–155, 2015. doi:10.1152/japplphysiol.01321.2013.

DiMarco AF, Kowalski KE, Hromyak DR, Geertman RT. Long-term follow-up of spinal cord stimulation to restore cough in subjects with spinal cord injury. *J Spinal Cord Med* 37: 380–388, 2014. doi:10.1179/2045772313Y.0000000152.

DiMarco AF, Kowalski KE, Supinski G, Romaniuk JR. Mechanism of expiratory muscle activation during lower thoracic spinal cord stimulation. *J Appl Physiol (1985)* 92: 2341–2346, 2002. doi:10.1152/japplphysiol.01231.2001.

Doperalski NJ, Sandhu MS, Bavis RW, Reier PJ, Fuller DD. Ventilation and phrenic output following high cervical spinal hemisection in male vs. female rats. *Respir Physiol Neurobiol* 162: 160–167, 2008. doi:10.1016/j.resp.2008.06.005.

Dougherty BJ, Lee KZ, Lane MA, Reier PJ, Fuller DD. Contribution of the spontaneous crossed-phrenic phenomenon to inspiratory tidal volume in spontaneously breathing rats. *J Appl Physiol (1985)* 112: 96–105, 2012. doi:10.1152/japplphysiol.00690.2011.

Dutton RC, Carstens MI, Antognini JF, Carstens E. Long ascending propriospinal projections from lumbosacral to upper cervical spinal cord in the rat. *Brain Res* 1119: 76–85, 2006. doi:10.1016/j.brainres.2006.08.063.

Enríquez Denton M, Wienecke J, Zhang M, Hultborn H, Kirkwood PA. Voltage-dependent amplification of synaptic inputs in respiratory motoneurones. *J Physiol* 590: 3067–3090, 2012. doi:10.1113/jphysiol.2011.225789.

Fetz EE. Restoring motor function with bidirectional neural interfaces. *Prog Brain Res* 218: 241–252, 2015. doi:10.1016/bs.pbr.2015.01.001.

Fuller DD, Doperalski NJ, Dougherty BJ, Sandhu MS, Bolser DC, Reier PJ. Modest spontaneous recovery of ventilation following chronic high cervical hemisection in rats. *Exp Neurol* 211: 97–106, 2008. doi:10.1016/j.expneurol.2008.01.013.

Fuller DD, Golder FJ, Olson EB Jr, Mitchell GS. Recovery of phrenic activity and ventilation after cervical spinal hemisection in rats. *J Appl Physiol (1985)* 100: 800–806, 2006. doi:10.1152/japplphysiol.00960.2005.

Fuller DD, Johnson SM, Johnson RA, Mitchell GS. Chronic cervical spinal sensory denervation reveals ineffective spinal pathways to phrenic motoneurons in the rat. *Neurosci Lett* 323: 25–28, 2002. doi:10.1016/S0304-3940(02)00121-0.

Fuller DD, Johnson SM, Olson EB Jr, Mitchell GS. Synaptic pathways to phrenic motoneurons are enhanced by chronic intermittent hypoxia after cervical spinal cord injury. *J Neurosci* 23: 2993–3000, 2003.

Fuller DD, Mitchell GS. Respiratory neuroplasticity - Overview, significance and future directions. *Exp Neurol* 287: 144–152, 2017. doi:10.1016/j.expneurol.2016.05.022.

Gad P, Choe J, Shah P, Garcia-Alias G, Rath M, Gerasimenko Y, Zhong H, Roy RR, Edgerton VR. Sub-threshold spinal cord stimulation facilitates spontaneous motor activity in spinal rats. *J Neuroeng Rehabil* 10: 108, 2013. doi:10.1186/1743-0003-10-108.

Golder FJ, Mitchell GS. Spinal synaptic enhancement with acute intermittent hypoxia improves respiratory function after chronic cervical spinal cord injury. *J Neurosci* 25: 2925–2932, 2005. doi:10.1523/JNEUROSCI.0148-05.2005.

Goshgarian HG. The crossed phrenic phenomenon: a model for plasticity in the respiratory pathways following spinal cord injury. *J Appl Physiol (1985)* 94: 795–810, 2003. doi:10.1152/japplphysiol.00847.2002.

Goshgarian HG. The crossed phrenic phenomenon and recovery of function following spinal cord injury. *Respir Physiol Neurobiol* 169: 85–93, 2009. doi:10.1016/j.resp.2009.06.005.

Goshgarian HG, Ellenberger HH, Feldman JL. Decussation of bulbospinal respiratory axons at the level of the phrenic nuclei in adult rats: a possible substrate for the crossed phrenic phenomenon. *Exp Neurol* 111: 135–139, 1991. doi:10.1016/0014-4886(91)90061-G.

Gransee HM, Zhan WZ, Sieck GC, Mantilla CB. Targeted delivery of TrkB receptor to phrenic motoneurons enhances functional recovery of rhythmic phrenic activity after cervical spinal hemisection. *PLoS One* 8: e64755, 2013. doi:10.1371/journal.pone.0064755.

Hagg T, Oudega M. Degenerative and spontaneous regenerative processes after spinal cord injury. *J Neurotrauma* 23: 263–280, 2006. doi:10.1089/neu.2006.23.263.

Harkema S, Gerasimenko Y, Hodes J, Burdick J, Angeli C, Chen Y, Ferreira C, Willhite A, Rejc E, Grossman RG, Edgerton VR. Effect of epidural stimulation of the lumbosacral spinal cord on voluntary movement, standing, and assisted stepping after motor complete paraplegia: a case study. *Lancet* 377: 1938–1947, 2011. doi:10.1016/S0140-6736(11)60547-3.

Hayashi F, Hinrichsen CF, McCrimmon DR. Short-term plasticity of descending synaptic input to phrenic motoneurons in rats. *J Appl Physiol (1985)* 94: 1421–1430, 2003. doi:10.1152/japplphysiol.00599.2002.

Hormigo KM, Zholudeva LV, Spruance VM, Marchenko V, Cote MP, Vinit S, Giszter S, Bezdudnaya T, Lane MA. Enhancing neural activity to

drive respiratory plasticity following cervical spinal cord injury. *Exp Neurol* 287: 276–287, 2017.

Huang R, Baca SM, Worrell JW, Liu X, Seo Y, Leiter JC, Lu DC. Modulation of respiratory output by cervical epidural stimulation in the anesthetized mouse. *J Appl Physiol (1985)* 121: 1272–1281, 2016. doi:10.1152/japplphysiol.00473.2016.

Johnson RA, Okragly AJ, Haak-Frendscho M, Mitchell GS. Cervical dorsal rhizotomy increases brain-derived neurotrophic factor and neurotrophin-3 expression in the ventral spinal cord. *J Neurosci* 20: RC77, 2000.

Johnson SM, Mitchell GS. Activity-dependent plasticity in descending synaptic inputs to respiratory spinal motoneurons. *Respir Physiol Neurobiol* 131: 79–90, 2002. doi:10.1016/S1569-9048(02)00039-3.

Kasten MR, Sunshine MD, Secrist ES. Therapeutic intraspinal microstimulation improves forelimb function after cervical contusion injury. *J Neural Eng* 10: 044001, 2013. doi:10.1088/1741-2560/10/4/044001.

Kinkead R, Zhan WZ, Prakash YS, Bach KB, Sieck GC, Mitchell GS. Cervical dorsal rhizotomy enhances serotonergic innervation of phrenic motoneurons and serotonin-dependent long-term facilitation of respiratory motor output in rats. *J Neurosci* 18: 8436–8443, 1998.

Kowalski KE, Hsieh YH, Dick TE, DiMarco AF. Diaphragm activation via high frequency spinal cord stimulation in a rodent model of spinal cord injury. *Exp Neurol* 247: 689–693, 2013. doi:10.1016/j.expneurol.2013.03.006.

Kowalski KE, Romaniuk JR, Brose SW, Richmond MA, Kowalski T, DiMarco AF. High frequency spinal cord stimulation-New method to restore cough. *Respir Physiol Neurobiol* 232: 54–56, 2016. doi:10.1016/j.resp.2016.07.001.

Lafreniere-Roula M, Kim E, Hutchison WD, Lozano AM, Hodaie M, Dostrovsky JO. High-frequency microstimulation in human globus pallidus and substantia nigra. *Exp Brain Res* 205: 251–261, 2010. doi:10.1007/s00221-010-2362-8.

Landis SC, Amara SG, Asadullah K, Austin CP, Blumenstein R, Bradley EW, Crystal RG, Darnell RB, Ferrante RJ, Fillit H, Finkelstein R, Fisher M, Gendelman HE, Golub RM, Goudreau JL, Gross RA, Gubitz AK, Hesterlee SE, Howells DW, Huguenard J, Kelner K, Koroshetz W, Krainc D, Lazic SE, Levine MS, Macleod MR, McCall JM, Moxley RT III, Narasimhan K, Noble LJ, Perrin S, Porter JD, Steward O, Unger E, Utz U, Silberberg SD. A call for transparent reporting to optimize the predictive value of preclinical research. *Nature* 490: 187–191, 2012. doi:10.1038/nature11556.

Lane MA. Spinal respiratory motoneurons and interneurons. *Respir Physiol Neurobiol* 179: 3–13, 2011. doi:10.1016/j.resp.2011.07.004.

Lane MA, White TE, Coutts MA, Jones AL, Sandhu MS, Bloom DC, Bolser DC, Yates BJ, Fuller DD, Reier PJ. Cervical prephrenic interneurons in the normal and lesioned spinal cord of the adult rat. *J Comp Neurol* 511: 692–709, 2008. doi:10.1002/cne.21864.

Lee KZ, Sandhu MS, Dougherty BJ, Reier PJ, Fuller DD. Hypoxia triggers short term potentiation of phrenic motoneuron discharge after chronic cervical spinal cord injury. *Exp Neurol* 263: 314–324, 2015. doi:10.1016/j.expneurol.2014.10.002.

Levy M, Mizrahi J, Susak Z. Recruitment, force and fatigue characteristics of quadriceps muscles of paraplegics isometrically activated by surface functional electrical stimulation. *J Biomed Eng* 12: 150–156, 1990. doi:10.1016/0141-5425(90)90136-B.

Lindsay AD, Feldman JL. Modulation of respiratory activity of neonatal rat phrenic motoneurones by serotonin. *J Physiol* 461: 213–233, 1993. doi:10.1113/jphysiol.1993.sp019510.

Ling L, Bach KB, Mitchell GS. Serotonin reveals ineffective spinal pathways to contralateral phrenic motoneurons in spinally hemisected rats. *Exp Brain Res* 101: 35–43, 1994. doi:10.1007/BF00243214.

Lovett-Barr MR, Satriotomo I, Muir GD, Wilkerson JE, Hoffman MS, Vinit S, Mitchell GS. Repetitive intermittent hypoxia induces respiratory and somatic motor recovery after chronic cervical spinal injury. *J Neurosci* 32: 3591–3600, 2012. doi:10.1523/JNEUROSCI.2908-11.2012.

Lu DC, Edgerton VR, Modaber M, AuYong N, Morikawa E, Zdunowski S, Sarino ME, Sarrafzadeh M, Nuwer MR, Roy RR, Gerasimenko Y. Engaging cervical spinal cord networks to reenable volitional control of hand function in tetraplegic patients. *Neurorehabil Neural Repair* 30: 951–962, 2016. doi:10.1177/1545968316644344.

Mahamed S, Strey KA, Mitchell GS, Baker-Herman TL. Reduced respiratory neural activity elicits phrenic motor facilitation. *Respir Physiol Neurobiol* 175: 303–309, 2011. doi:10.1016/j.resp.2010.12.005.

Mantilla CB, Gransee HM, Zhan WZ, Sieck GC. Motoneuron BDNF/TrkB signaling enhances functional recovery after cervical spinal cord injury. *Exp Neurol* 247: 101–109, 2013. doi:10.1016/j.expneurol.2013.04.002.

Marchenko V, Ghali MG, Rogers RF. The role of spinal GABAergic circuits in the control of phrenic nerve motor output. *Am J Physiol Regul Integr Comp Physiol* 308: R916–R926, 2015. doi:10.1152/ajpregu.00244.2014.

McCrimmon DR, Zuperku EJ, Hayashi F, Dogas Z, Hinrichsen CF, Stuth EA, Tonkovic-Capin M, Krolo M, Hopp FA. Modulation of the synaptic drive to respiratory premotor and motor neurons. *Respir Physiol* 110: 161–176, 1997. doi:10.1016/S0034-5687(97)00081-9.

McPherson JG, Miller RR, Perlmutter SI. Targeted, activity-dependent spinal stimulation produces long-lasting motor recovery in chronic cervical spinal cord injury. *Proc Natl Acad Sci USA* 112: 12193–12198, 2015. doi:10.1073/pnas.1505383112.

Mercier LM, Gonzalez-Rothi EJ, Streeter KA, Posgai SS, Poirier AS, Fuller DD, Reier PJ, Baekey DM. Intraspinal microstimulation and diaphragm activation following cervical spinal cord injury. *J Neurophysiol* 117: 767–776, 2017. doi:10.1152/jn.00721.2016.

Mondello SE, Kasten MR, Horner PJ, Moritz CT. Therapeutic intraspinal stimulation to generate activity and promote long-term recovery. *Front Neurosci* 8: 21, 2014. doi:10.3389/fnins.2014.00021.

Moreno DE, Yu XJ, Goshgarian HG. Identification of the axon pathways which mediate functional recovery of a paralyzed hemidiaphragm following spinal cord hemisection in the adult rat. *Exp Neurol* 116: 219–228, 1992. doi:10.1016/0014-4886(92)90001-7.

Nantwi K, El-Bohy A, Schrimsher GW, Reier PJ, Goshgarian HG. Spontaneous recovery in a paralyzed hemidiaphragm following upper cervical spinal cord injury in adult rats. *Neurorehabil Neural Repair* 13: 225–234, 1999. doi:10.1177/154596839901300404.

Nishimura Y, Perlmutter SI, Eaton RW, Fetz EE. Spike-timing-dependent plasticity in primate corticospinal connections induced during free behavior. *Neuron* 80: 1301–1309, 2013. doi:10.1016/j.neuron.2013.08.028.

Pitts RF. The respiratory center and its descending pathways. *J Comp Neurol* 72: 605–625, 1940. doi:10.1002/cne.900720309.

Rejc E, Angeli C, Harkema S. Effects of lumbosacral spinal cord epidural stimulation for standing after chronic complete paralysis in humans. *PLoS One* 10: e0133998, 2015. doi:10.1371/journal.pone.0133998.

Rejc E, Angeli CA, Bryant N, Harkema S. Effects of stand and step training with epidural stimulation on motor function for standing in chronic complete paraplegics. *J Neurotrauma* 34: 1787–1802, 2017. doi:10.1089/neu.2016.4516.

Sandhu MS, Dougherty BJ, Lane MA, Bolser DC, Kirkwood PA, Reier PJ, Fuller DD. Respiratory recovery following high cervical hemisection. *Respir Physiol Neurobiol* 169: 94–101, 2009. doi:10.1016/j.resp.2009.06.014.

Satriotomo I, Dale EA, Dahlberg JM, Mitchell GS. Repetitive acute intermittent hypoxia increases expression of proteins associated with plasticity in the phrenic motor nucleus. *Exp Neurol* 237: 103–115, 2012. doi:10.1016/j.expneurol.2012.05.020.

Sayenko DG, Angeli C, Harkema SJ, Edgerton VR, Gerasimenko YP. Neuromodulation of evoked muscle potentials induced by epidural spinal-cord stimulation in paralyzed individuals. *J Neurophysiol* 111: 1088–1099, 2014. doi:10.1152/jn.00489.2013.

Sayenko DG, Atkinson DA, Floyd TC, Gorodnichev RM, Moshonkina TR, Harkema SJ, Edgerton VR, Gerasimenko YP. Effects of paired transcutaneous electrical stimulation delivered at single and dual sites over lumbosacral spinal cord. *Neurosci Lett* 609: 229–234, 2015. doi:10.1016/j.neulet.2015.10.005.

Shah PK, Sureddi S, Alam M, Zhong H, Roy RR, Edgerton VR, Gerasimenko Y. Unique spatiotemporal neuromodulation of the lumbosacral circuitry shapes locomotor success after spinal cord injury. *J Neurotrauma* 33: 1709–1723, 2016. doi:10.1089/neu.2015.4256.

Steinbusch HW. Distribution of serotonin-immunoreactivity in the central nervous system of the rat-cell bodies and terminals. *Neuroscience* 6: 557–618, 1981. doi:10.1016/0306-4522(81)90146-9.

Tai Q, Palazzolo KL, Goshgarian HG. Synaptic plasticity of 5-hydroxytryptamine-immunoreactive terminals in the phrenic nucleus following spinal cord injury: a quantitative electron microscopic analysis. *J Comp Neurol* 386: 613–624, 1997. doi:10.1002/(SICI)1096-9861(19971006)386:4<613::AID-CNE7>3.0.CO;2-5.

Tator CH, Minassian K, Mushahwar VK. Spinal cord stimulation: therapeutic benefits and movement generation after spinal cord injury. *Handb Clin Neurol* 109: 283–296, 2012. doi:10.1016/B978-0-444-52137-8.00018-8.

Widge AS, Moritz CT. Pre-frontal control of closed-loop limbic neurostimulation by rodents using a brain-computer interface. *J Neural Eng* 11: 024001, 2014. doi:10.1088/1741-2560/11/2/024001.

Zhou SY, Goshgarian HG. Effects of serotonin on crossed phrenic nerve activity in cervical spinal cord hemisected rats. *Exp Neurol* 160: 446–453, 1999. doi:10.1006/exnr.1999.7213.

Zhou SY, Goshgarian HG. 5-Hydroxytryptophan-induced respiratory recovery after cervical spinal cord hemisection in rats. *J Appl Physiol (1985)* 89: 1528–1536, 2000.

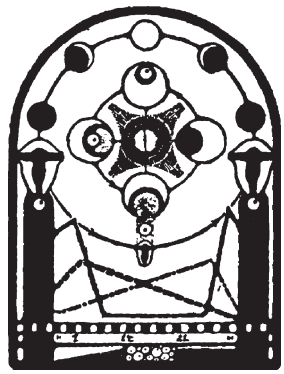

J Neurophysiol 117: 1014–1029, 2017.
First published December 14, 2016; doi:10.1152/jn.00638.2016.

RESEARCH ARTICLE | *Neural Circuits*

Coupling multielectrode array recordings with silver labeling of recording sites to study cervical spinal network connectivity

K. A. Streeter,[1] M. D. Sunshine,[1] S. R. Patel,[1] S. S. Liddell,[2] L. E. Denholtz,[2] P. J. Reier,[2] D. D. Fuller,[1] and D. M. Baekey[3]

[1]*Department of Physical Therapy, University of Florida, Gainesville, Florida;* [2]*Department of Neuroscience, University of Florida, Gainesville, Florida; and* [3]*Department of Physiological Sciences, University of Florida, Gainesville, Florida*

Submitted 10 August 2016; accepted in final form 12 December 2016

Streeter KA, Sunshine MD, Patel SR, Liddell SS, Denholtz LE, Reier PJ, Fuller DD, Baekey DM. Coupling multielectrode array recordings with silver labeling of recording sites to study cervical spinal network connectivity. *J Neurophysiol* 117: 1014–1029, 2017. First published December 14, 2016; doi:10.1152/jn.00638.2016.—Midcervical spinal interneurons form a complex and diffuse network and may be involved in modulating phrenic motor output. The intent of the current work was to enable a better understanding of midcervical "network-level" connectivity by pairing the neurophysiological multielectrode array (MEA) data with histological verification of the recording locations. We first developed a method to deliver 100-nA currents to electroplate silver onto and subsequently deposit silver from electrode tips after obtaining midcervical (C3–C5) recordings using an MEA in anesthetized and ventilated adult rats. Spinal tissue was then fixed, harvested, and histologically processed to "develop" the deposited silver. Histological studies verified that the silver deposition method discretely labeled (50-μm resolution) spinal recording locations between laminae IV and X in cervical segments C3-C5. Using correlative techniques, we next tested the hypothesis that midcervical neuronal discharge patterns are temporally linked. Cross-correlation histograms produced few positive peaks (5.3%) in the range of 0–0.4 ms, but 21.4% of neuronal pairs had correlogram peaks with a lag of ≥0.6 ms. These results are consistent with synchronous discharge involving mono- and polysynaptic connections among midcervical neurons. We conclude that there is a high degree of synaptic connectivity in the midcervical spinal cord and that the silver-labeling method can reliably mark metal electrode recording sites and "map" interneuron populations, thereby providing a low-cost and effective tool for use in MEA experiments. We suggest that this method will be useful for further exploration of midcervical network connectivity.

NEW & NOTEWORTHY We describe a method that reliably identifies the locations of multielectrode array (MEA) recording sites while preserving the surrounding tissue for immunohistochemistry. To our knowledge, this is the first cost-effective method to identify the anatomic locations of neuronal ensembles recorded with a MEA during acute preparations without the requirement of specialized array electrodes. In addition, evaluation of activity recorded from silver-labeled sites revealed a previously unappreciated degree of connectivity between midcervical interneurons.

spinal cord; phrenic motor output; cross-correlation; functional connectivity; metal deposition

MIDCERVICAL SPINAL INTERNEURONS form a complex and diffuse network that is synaptically coupled to both respiratory and nonrespiratory motor pools (Gonzalez-Rothi et al. 2015; Lane 2011; Lane et al. 2008b). Several groups have advanced the hypothesis that midcervical spinal interneurons can modulate phrenic motoneuron excitability and thereby influence the neural control of the diaphragm (Bellingham and Lipski 1990; Douse and Duffin 1993; Lane et al. 2008a,b; Palisses et al. 1989). Although there is some direct evidence to support this hypothesis (Marchenko et al. 2015; Sandhu et al. 2015), other studies have concluded the opposite (Duffin and Iscoe 1996). A significant hurdle in testing that specific hypothesis, or related hypotheses regarding cervical interneuronal circuits, is the difficulty of studying the "functional connectivity" in diffuse spinal cord networks. One of the foremost challenges is simultaneously recording numerous cells, and this can be addressed through the use of multielectrode arrays (MEAs). The MEA approach enables simultaneous recordings of multiple sites, but histologically identifying each recording location (vs. the electrode track) while also preserving tissue integrity poses a further challenge (Borg et al. 2015; Li et al. 2015; Nuding et al. 2015). Thus the initial thrust of the current work was modification and validation of a silver-labeling technique (Spinelli 1975) to enable postrecording deposition of a small amount of silver (i.e., for histological marking) from the tip of each electrode in an MEA. Additionally, we developed an electrical circuit to enable the use of small currents (100 nA) for silver electroplating and deposition to prevent tissue and electrode damage associated with high levels of current (Fung et al. 1998). Using the electroplated MEA, we recorded discharge from ensembles of neurons in the midcervical (C3–C5) spinal cord in adult rats and demonstrated a practical application of this technique by "matching" the array electrodes to the corresponding anatomic locations marked by silver.

The overall intent was to enable a better understanding of midcervical spinal discharge and "network-level" connectivity by pairing the neurophysiological MEA data with histological verification of the recording locations. Thus, using correlative techniques (Moore et al. 1970), we tested the hypothesis that the discharge patterns of midcervical (C3–C4) spinal neurons

Address for reprint requests and other correspondence: D. M. Baekey, Dept. of Physiological Sciences, Box 100144, 1333 Center Dr., Gainesville, FL 32610-0144 (e-mail: dbaekey@ufl.edu).

are temporally linked in time domains consistent with mono- and polysynaptic connections. In addition, midcervical neuronal discharge patterns were assessed relative to the endogenous inspiratory pattern, measured via bilateral phrenic nerve recordings, to determine whether bursting was temporally linked to phrenic motoneuron activity. To our knowledge, no prior study has comprehensively evaluated the temporal characteristics across multiple midcervical neurons using MEA technology. The results presented herein demonstrate a previously unappreciated degree of connectivity and indicate a high prevalence of temporally related discharge patterns between midcervical interneurons with characteristics consistent with mono- and polysynaptic connections and provide a comprehensive description of a cost-effective histological approach for validating anatomic locations of MEA recording sites.

MATERIALS AND METHODS

Animals. All experiments were conducted with adult Sprague-Dawley rats obtained from Envigo (formerly Harlan Laboratories). Most experiments ($n = 12$) were performed with untreated, spinal-intact rats. A subset of rats ($n = 2$) received a cervical spinal injury (C3/C4 lateralized contusion, force: 205 kDa, displacement: 1,225 μm; Infinite Horizon pneumatic impactor; Precision Systems and Instrumentation) using published methods from our group (Lane et al. 2012). Spinal-injured rats were allowed to recover for 12 wk before electrophysiology. Histological results from spinal-injured animals were used to determine effectiveness of silver labeling and to compare micromotor depths relative to silver-labeling depths. Since there is evidence suggesting neurophysiological properties such as connectivity may be altered following spinal cord injury (SCI; Lane et al. 2008b, 2009), analysis of neurophysiology was limited to spinal-intact animals ($n = 4$). All rats were housed in pairs in a controlled environment (12:12-h light-dark cycles) with food and water ad libitum. All experimental protocols were approved by the Institutional Animal Care and Use Committee at the University of Florida.

In vivo electrophysiology. All rats were anesthetized with 3% isoflurane (in 100% O_2) and transferred to a heated station where established surgical methods (Lee and Fuller 2010; Lee et al. 2009; Mahamed et al. 2011; Sandhu et al. 2015; Streeter and Baker-Herman 2014a,b; Strey et al. 2012) were used to set up electrophysiological experiments. Core body temperature was maintained at 37 ± 0.5°C with a servo-controlled heating device (model 700 TC-1000; CWE). A tail vein catheter was placed for in vivo delivery of urethane anesthesia and fluids. The trachea was cannulated (PE 240 tubing), and rats were pump-ventilated (Rodent Ventilator 683; Harvard Apparatus; volume: approximately 3-2.5 ml; frequency: 70/min). Once ventilated, CO_2 was added [fraction of inspired carbon dioxide (FI_{CO_2}): <3%] to maintain end-tidal CO_2 ($EtCO_2$) between approximately 40 and 50 mmHg throughout the protocol (Capnogard; Respironics). Tracheal pressure was monitored and lungs were periodically hyperinflated (2–3 breaths) to prevent atelectasis (~1/h). A bilateral vagotomy was performed. Rats were slowly converted (6 ml/h; Harvard Apparatus syringe pump) to urethane anesthesia (1.7 g/kg in vivo in distilled water), and isoflurane was withdrawn. A femoral arterial catheter (PE 50 tubing) was placed to monitor blood pressure (TA-100; CWE) and sample blood gases (i-STAT 1 Analyzer; Abbott) throughout the protocol. Using a dorsal approach, the left and right phrenic nerves were isolated, cut distally, and partially desheathed (~1/2 the length of the exposed nerve). A midline incision extending from the base of the skull to midthoracic region was made, and spinal vertebrae C3-T2 were exposed. Using a nose clamp and T2 spinous process, the rat was slightly elevated off the table to reduce ventilator-induced motion artifact and level the spinal cord. A laminectomy was performed from C3 to C6, the dura was cut and reflected back, and the pia was gently removed at the MEA insertion point. A unilateral pneumothorax was performed to decrease chest wall movement, and positive end-expiratory pressure (PEEP) of approximately 1–2 cm of water was applied to prevent atelectasis. Animals received the neuromuscular paralytic pancuronium bromide (2.5 mg/kg in vivo; Hospira) to eliminate spontaneous breathing efforts. Adequate depth of anesthesia was monitored by assessing blood pressure responses to toe pinch, and urethane supplements were given as necessary. Blood pressure and fluid homeostasis were maintained by a slow infusion of a 1:3 solution (8.4% sodium bicarbonate/Ringer lactate in vivo).

Bilateral phrenic nerve output was recorded using custom-made bipolar suction electrodes filled with 0.9% saline. Compound action potentials were amplified (20,000×; P511; Grass Instrument), band-pass filtered (3 Hz to 3 kHz), digitized [16-bit, 25,000 samples per second per channel; Power1401; Cambridge Electronic Design (CED), Cambridge, UK], and integrated (time constant: 20 ms) in Spike2 v8 software (CED). A custom-made MEA similar to that originally designed at the University of South Florida by Morris and colleagues (1996) and used in our previous report (Sandhu et al. 2015) was used to record bilateral midcervical (C3–C5) spinal activity (Fig. 1*A*). The array contained 16 tungsten electrodes coated with Epoxylite insulation (impedance: 10 ± 1 MΩ; shank diameter: 125 μm; tip diameter: ≤1 μm; cat. no. UEWLEGSE0N1E; FHC; Fig. 1*B*). A key feature of this array is the ability to control the depth of each of the electrodes independently using micromotors. This greatly improves the recording yield by allowing the experimenter to "hold" a recording on 1 electrode while continuing to search for neurons with other electrodes. The array was mounted on a stereotaxic frame, and 8 electrodes arranged in 2 staggered rows of 4 were placed into each hemicord at the dorsal root entry zone (Fig. 1*C*). The inner distance between the 2 sets of 8 electrodes was ~1 mm, whereas the distance between electrodes within each row was ~300 μm (Fig. 1*D*). Electrodes tips were

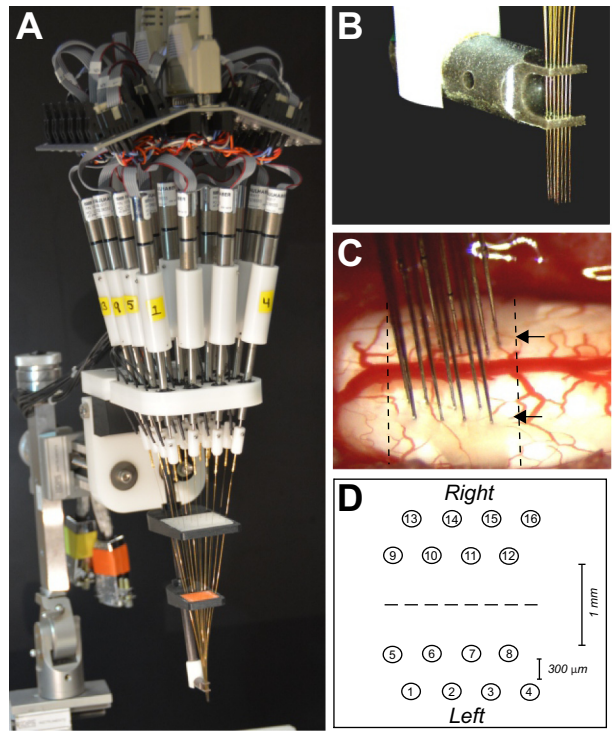

Fig. 1. Multielectrode array. *A*: multielectrode recording array containing 16 tungsten fine wire electrodes each controlled by micromotors and held in place by the array guide. *B*: high-resolution image of the electrode tips maintained in a "fixed matrix" by the array guide. *C*: image of the electrodes positioned in the dorsal C4 spinal cord at the dorsal root entry zone (e.g., black arrows). *D*: schematic of the recording matrix consisting of 8 electrodes arranged in 2 staggered rows of 4. The inner distance between the 2 sets of 8 electrodes was ~1 mm, and the distance between electrodes within each row was ~300 μm.

maintained in this "fixed matrix" by the array guide. One by one, electrodes were advanced into the spinal cord while audio was monitored until single units with ~3:1 signal-to-noise ratio were discriminated. Neural signals from single electrodes were amplified (5,000×), band-pass filtered (3-3 kHz), digitized (16-bit, 25,000 samples per second per channel; Power1401; CED), and recorded with Spike2 v8 software (CED). Once phrenic nerve activity and spinal discharge was stable, "baseline activity" was recorded with fraction of inspired oxygen ($F_{I_{O_2}}$) set to 0.50. Using experimental procedures similar to our previous studies (Sandhu et al. 2015; Strey et al. 2012), the inspiratory gas mixture was altered using adjustable flowmeters to expose rats to a 5-min period of hypoxia ($F_{I_{O_2}}$: 0.11) followed by 15 min of baseline oxygen levels ($F_{I_{O_2}}$: 0.50). Silver deposition was performed immediately after the neurophysiology protocol. An arterial blood gas was sampled during baseline and hypoxia to ensure blood gases were within physiological limits.

Analysis of electrophysiological signals. All electrophysiological data were collected and sorted using Spike2 v8 software (CED). Extracellular action potentials from individual neurons were extracted from continuous recordings and converted to waveforms using spike-sorting tools of the acquisition software. Briefly, spikes were clustered using at least 80% template matching and principal component analyses. Sorted spikes were exported and analyzed using custom MATLAB software (MathWorks R2015a). A standard set of analyses (spike interval histograms, cycle-triggered histograms, and spike-triggered averages) were performed to phenotype each neuron electrophysiologically. Interval histograms were created for each spike train to ensure only single-unit activity was represented in each waveform. Similar to previous studies (Galán et al. 2010; Sandhu et al. 2015), cycle-triggered histograms were used to assess the preferred respiratory modulation of each recorded neuron relative to the phase of the respiratory cycle defined by phrenic nerve activity (Cohen 1968). Using the integrated phrenic nerve output, the beginning and end of the inspiratory, and therefore expiratory, phases were calculated as a departure of phrenic nerve activity ≥15 standard deviations above the average activity during the expiratory phase. Cycle-triggered histograms were constructed for each neuron by dividing the respiratory period into 20 bins of equal size, and spikes were counted within each bin and summated over 50 consecutive breaths during baseline, hypoxia, and posthypoxia. To determine whether neurons were respiratory-modulated, the spikes occurring during bins of the inspiratory phase were separated from those occurring during the expiratory phase, and the Wilcoxon signed-rank test was used to test the null hypothesis (i.e., no difference between inspiration and expiration). Cervical spinal neurons were classified into four categories: *1*) neurons that discharged primarily during the inspiratory period (i.e., inspiratory-modulated; *waveform 1* in Fig. 7, *C* and *D*); *2*) neurons that discharged primarily during the expiratory period (i.e., expiratory-modulated; *waveform 1* in Fig. 7, *H* and *I*); *3*) neurons that discharged without respiratory modulation (i.e., tonic; *waveform 2* in Fig. 7, *C*, *D*, *H*, and *I*); and *4*) neurons that ceased firing at time points after baseline and were labeled as inactive at that time point.

Spike-triggered averaging of raw and rectified phrenic nerve activity was used to examine the temporal relationship of neuronal waveforms and phrenic motor output (Lipski et al. 1983). Short-latency, offset peaks in the raw and rectified phrenic nerve average provided evidence that the recorded neuron was a phrenic motoneuron (Christakos et al. 1994). If features were not detected using spike-triggered averaging, the recorded cell was classified as a spinal interneuron. Cross-correlation histograms were constructed for all possible pairs of simultaneously recorded neurons using a bin width of 0.2 ms to evaluate functional connectivity (Moore et al. 1970). Similar to published methods (Aertsen and Gerstein 1985), the detectability index (DI) was calculated for each cycle-triggered histogram as the peak relative to average background activity (calculated during the interval −15 to −3 ms before 0) divided by the standard deviation. Only significant features occurring with a positive lag (e.g., ≥0) were counted. Features were considered significant if the DI was ≥3 (Melssen and Epping 1987). Central peaks (0–0.4 ms) between a pair of neurons supported synchronous firing between neurons, whereas offset peaks (≥0.6 ms) indicated functional excitation between the trigger and target neurons.

Plating electrodes and depositing silver. Methods for electroplating and depositing silver described previously (Spinelli 1975) were adapted for use with MEA recordings. For each electrode, silver was electroplated (Fig. 2*A*) and deposited (Fig. 2*B*) using tightly controlled and monitored direct current (DC) circuits. The circuits consisted of an electrode selection interface (i.e., breakout box), two 9-V batteries, a custom-built μCurrent control device (Bare Electronics, Gainesville, FL), a μCurrent Precision nA Current Measurement Assistant v3 (cat. no. 882; EEVblog Adafruit Industries), and a digital multimeter (model 61-340; Ideal Industries) all connected with copper patch cables. Specifications of the μCurrent control circuit are provided in Fig. 2*C*. Before each experiment, 15 of the 16 fine wire tungsten electrodes were electroplated with dissolved silver cations in an electrolyte solution ($AgNO_3$/KCN), and an uninsulated silver wire (100 mm, 0.025-in. diameter; cat. no. 783500; A-M Systems) was used as the anode in the solution (Fig. 2*A*). The electrolyte solution was prepared by mixing equal parts of 1% potassium cyanide and 1% silver nitrate. The circuit was tested before each use by electroplating silver onto copper wire to ensure proper connections and current settings. Immediately following the testing procedure, the tip of each individual electrode was introduced to the electrolyte solution (as the cathode) for 100 s at 100 nA. Electrodes used to deposit silver were replated before each experiment. In a subset of experiments ($n = 3$), 2 of the 16 electrodes were coated with the lipophilic fluorescent dye 1,1′-dioctadecyl-3,3,3′,3′-tetramethylindocarbocyanine perchlorate ['DiI'; DiIC18(3); DiI; cat. no. D282; Thermo Fisher Scientific] after electrodes were electroplated with silver and before electrophysiology. Each electrode was repeatedly dipped (~10 times) in DiI (50 mg/ml in ethanol) and allowed to dry for 5 s between each dip (DiCarlo et al. 1996).

Subsequent to ensemble recordings of individual neurons, electrodes were left in place while the MEA was disconnected from the acquisition system and attached to the electrode selection interface (i.e., breakout box; Fig. 2*B*). Sites to be labeled were chosen based on the quality of the signals during the electrophysiological recordings. The circuitry was connected as in the plating procedure with the exception that *electrode 16* was used as the cathode and the individual electrode chosen for labeling was treated as the anode. Electroplated silver was released from the electrode tip using a 100-nA current for 10–100 s. Tissue was fixed approximately 15–30 min after silver was deposited (described below).

Tissue preparation. Animals were transcardially perfused with ice-cold saline followed by 4% paraformaldehyde (PFA; cat. no. 19210; Electron Microscopy Sciences) in 1× Dulbecco phosphate-buffered saline (DPBS; cat. no. 21-030-CV; Mediatech). Spinal tissue was harvested and postfixed in 4% PFA overnight at 4°C. The cervical spinal cord was subsequently blocked (C3-C6; approximately 8–9 mm of tissue) and cryoprotected in 30% sucrose in 1× DPBS overnight at 4°C. The spinal cord was embedded in optimal cutting temperature compound (OCT; cat. no. 23-730-571; Fisher Scientific), flash-frozen using 2-methylbutane and dry ice, and transversely cut at 40 μm on a cryostat (Microm HM 500; GMI). Sections for silver labeling were placed into 12-well trays (cat. no. 3737; Corning) containing Corning Netwell inserts (2 sections per well; 15-mm diameter, mesh size of 74 μm; cat. no. 3477; Corning) filled with glass-distilled water (~4 ml per well). Sections for immunohistochemistry were placed in 96-well plates containing 1× DPBS.

Silver staining protocol. Silver staining was performed immediately after sectioning. Because of the sensitivity of the reaction, all trays, glassware, and instruments used for staining protocol were thoroughly acid washed (1% HCl) before staining to eliminate contamination and remove nonspecific catalysts. Plastic 12-well trays

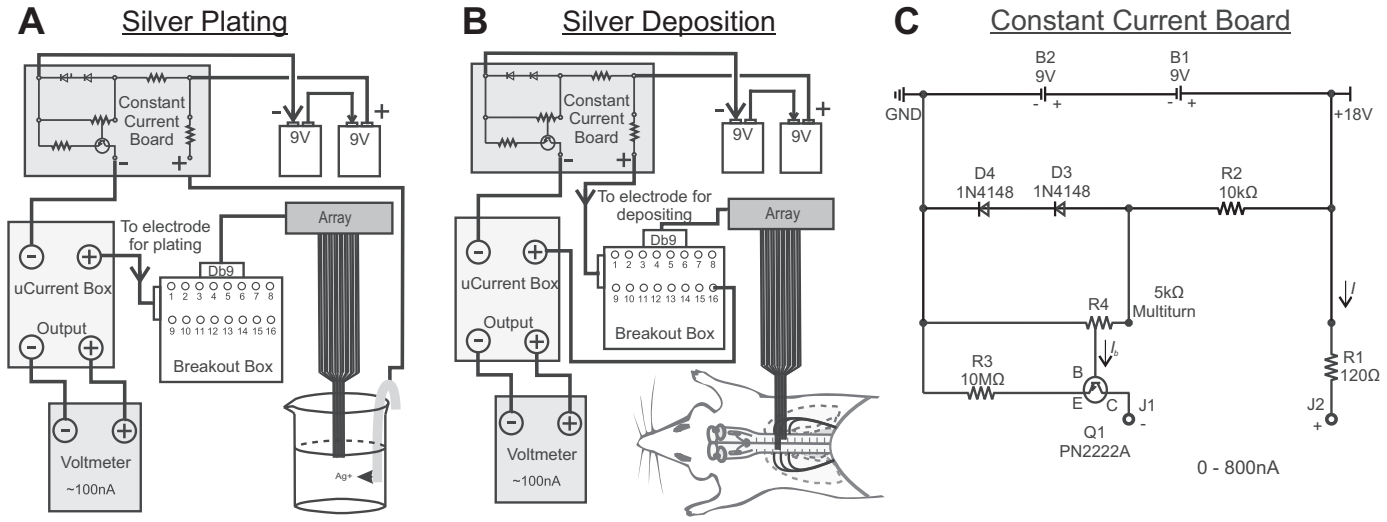

Fig. 2. Silver electroporation and deposition circuits. Both circuits consisted of an electrode selection interface (i.e., breakout box) connected to the array by a DB9 connector, 2 9-V batteries connected in series, a custom-built μCurrent control device (constant current board), a μCurrent Precision nA Current Measurement Assistant (uCurrent Box), and a digital multimeter connected via copper patch cables (thick black lines). *A*: for the silver electroplating circuit, the array was connected as the cathode to the electrode selection box (breakout box) while an uninsulated silver wire was placed in the electrolyte solution ($KCN/AgNO_3$) and used as the anode. The μCurrent box was connected to breakout box corresponding to the electrode to be plated (Ch1-15). *B*: for the silver deposition circuit, the polarity of the circuit was reversed with breakout box used to select the reference channel (cathode/Ch16) and the electrode to be deposited (anode/Ch1-15). *C*: the μCurrent control device uses an NPN transistor (Q1 PN2222A) to regulate current (*I*) from the power source (2 9-V batteries; B1 and B2) through a load between J1 (i.e., connector to μCurrent box) and J2 [i.e., connector to silver wire (*A*) or electrode (*B*)]. Two small-signal diodes, D3 and D4 (1N4148), provide a fixed voltage ($\sim$1.25 V_{DC}) used in parallel with voltage divider (R4). This adjustable voltage divider controls the base current (I_b) delivered to the transistor so that the emitter current of the transistor produces a stable current of 100 nA. As load between J1 and J2 changes, the transistor actively alters the voltage, and therefore current, drop across collector (C) to emitter (E), maintaining a constant voltage (across R3). Current was monitored by an EEVblog μCurrent Precision nA Current Measurement Assistant v3 with a consumer-grade multimeter and adjusted to maintain 100 nA.

containing the developer solution were discarded after used for a single tray of tissue, whereas all other trays were discarded after each animal. Netwell mesh inserts were soaked in bleach between each animal. The deposited silver was developed as previously described (Spinelli 1975). Briefly, stock solutions were prepared as outlined in Table 1. The hydrogen peroxide solution was covered in foil throughout the entire protocol due to its light sensitivity, and the hydroquinone and citric acid solution was made in the same bottle. The developer was made fresh for each 12-well tray of tissue by mixing the 3 stock solutions (acacia, silver nitrate, and hydroquinone/citric acid) 5 min before use (at the start of *step 9*). All steps were carried out in a fume hood, and light exposure was limited while mixing developer solution and during "developing" by turning off the fume hood light.

The solutions were poured into either 200-ml glass petri dishes (cat. no. 3160152BO; Corning) or 12-well plastic trays according to the step (see Table 1) and arranged in order of the staining sequence. To maintain precision during the staining protocol, staining was performed in "rounds," where each round contained 3 trays of tissue ($\sim$1-mm tissue per tray). Trays were staggered by 5 min, and all 3 trays of tissue were stained from start to finish. Rounds were repeated until all tissue was stained. The Netwell mesh inserts were transported through the staining sequence using a Netwell carrier kit with handles (cat. no. 3520; Corning) to allow simultaneous processing and ensure all wells were in each solution for the appropriate time. Following staining, tissue was stored at 4°C in Netwells filled with distilled water. Sections were mounted onto charged microscope slides (cat. no. 12-550-15; Fisher Scientific) using 1× PBS and allowed to dry for 48–72 h. Sections were counterstained with cresyl violet covered with mounting medium (cat. no. 4111; Thermo Scientific) and coverslipped. Images were captured with bright-field microscopy using a Microscope Axio Imager.A2 (Carl Zeiss Microscopy). Images were stitched and white balanced using Adobe Photoshop. Anatomic locations of the silver-labeled sites within the spinal laminae were identified using the *Atlas of the Spinal Cord* (Sengul et al. 2012). All representative spinal cord images reflect camera lucida-style drawings of our histological images or C4 spinal section in the same atlas. The depth of silver-labeled sites were determined using 10× photomicrographs and adjusted by 10% to account for tissue contraction during the fixation and histological processing based on estimates of prior investigations (Deutsch and Hillman 1977; Quester and Schröder 1997).

Immunohistochemistry. Initial immunohistochemistry (IHC) experiments determined the order in which IHC should be performed to achieve optimal fluorescent staining using tissue that did not contain deposited silver. IHC was performed either before or immediately after silver staining using two common markers (e.g., GFAP and NeuN). Using the optimal staining order, a subsequent experiment was performed with tissue containing deposited silver. All IHC was performed with free-floating sections in 96-well plates. All tissue was washed with 1× PBS with 0.2% Triton X-100 (3 × 5 min). For NeuN staining, tissue was incubated for 40 min at room temperature in 10% normal goat serum (NGS) in 1× PBS with 0.2% Triton X-100. Spinal sections were then incubated for 1 h at room temperature followed by 72 h at 4°C in the primary antibody solution: 10% NGS in 1× PBS with 0.2% Triton X-100 and NeuN (mouse anti-NeuN, 1:1,400; cat. no. MAB377; Millipore). Tissue was washed with 1× PBS (3 × 5 min) and incubated in the secondary antibody solution for 1 h at room temperature: 10% NGS in 1× PBS and Alexa Fluor 488 (goat anti-mouse, 1:500; cat. no. A11029; Invitrogen). Following incubation, tissue was washed with 1× PBS (3 × 5 min). For GFAP staining, tissue was incubated for 60 min at room temperature in 5% normal goat serum (NGS) in 1× PBS with 0.2% Triton X-100. Spinal sections were then incubated for 1 h at room temperature and overnight at 4°C in the primary antibody solution: 5% NGS in 1× PBS with 0.2% Triton X-100 and GFAP (mouse anti-GFAP, 1:200; G8393; Sigma-Aldrich). Tissue was washed with 1× PBS with 0.2% Triton X-100 (3 × 5 min) and then incubated in the secondary antibody solution for 1 h at room temperature: 5% NGS in 1× PBS with 0.2% Triton X-100 and Alexa Fluor 594 (goat anti-mouse, 1:500;

Table 1. *Silver staining protocol*

Dish no.	Contents	Time	Volume/Tray
1	**dH_2O**	**5 min**	**150 ml/dish**
2	**dH_2O**	**5 min**	**150 ml/dish**
*3**	1% $(NH_4)_2S$	5 min	48 ml/tray
4,†*	0.125% H_2O_2	5 min	48 ml/tray
5	**dH_2O**	**5 min**	**150 ml/dish**
6	**dH_2O**	**5 min**	**150 ml/dish**
*7**	**1% ascorbic acid**	**5 min**	**48 ml/tray**
8	**dH_2O**	**5 min**	**150 ml/dish**
9	**dH_2O**	**5 min**	**150 ml/dish**
10,†*	**Developer**	**8 min**	
	25% acacia		**16 ml (48 ml/tray)**
	2% hydroquinone, 5% citric acid		**16 ml (48 ml/tray)**
	1% $AgNO_2$		**16 ml (48 ml/tray)**
11	dH_2O	Quick rinse	150 ml/dish
12	dH_2O	Quick rinse	150 ml/dish
13	dH_2O	Quick rinse	150 ml/dish
14	1% $Na_2S_2O_4 \cdot 2H_2O$	3–4 min	150 ml/dish
15	dH_2O	Quick rinse	150 ml/dish

Sequence of solutions necessary to develop histologically the deposited silver adapted from Spinelli (1975). Solutions were prepared and arranged in the order of the staining sequence in either glass petri dishes or plastic trays. Volumes of solution were calculated for 1 12-well tray of tissue (24 sections; ~1 mm of tissue). Boldface text indicates the steps in which solutions were changed after processing 1 tray of tissue, and remaining steps indicate solutions were changed after processing 3 trays of tissue. Store in distilled water (dH_2O) at 4°C until ready to mount on charged slides, counterstain, and then cover with mounting medium. *Place solution in a 12-well tray. †Light-sensitive solutions. Change solution every 3 times except for boldface, which indicates change solutions every time.

cat. no. A11005; Life Technologies). Following incubation, tissue was washed with cold 1× PBS (3 × 5 min). Sections were mounted on positively charged glass slides (cat. no. 12-550-15; Fisher Scientific), covered with VECTASHIELD Antifade Mounting Medium (cat. no. H1-1200; Vector Laboratories), and coverslipped. Slides were air-dried and stored at 4°C. All fluorescent images were captured at ×10, ×20, and ×40 magnification with a Microscope Axio Imager.A2 (Carl Zeiss Microscopy).

RESULTS

Optimization of silver deposition from MEAs and subsequent histological development to enable visualization of recording locations. Initial experiments determined the parameters needed to deposit and identify silver in the spinal cord without emphasis on recording neuronal bursting from the electrodes. As the DC resistance of the commercially purchased recording electrodes was constant and the current used for electroplating silver onto the electrodes was standardized (as described in MATERIALS AND METHODS), we assessed the impact of two critical variables on the histological appearance of silver in the spinal cord: *1*) the duration of deposition current; and *2*) the duration of histological development. Figure 3 shows representative images of silver labeling obtained at different durations of deposition and histological development that demonstrate the variability of silver staining achieved by altering these parameters. Consistent and discrete labeling at a resolution between approximately 25 and 50 μm was obtained when current used to deposit silver was applied for 50 s and tissue was developed for 7–10 min (Fig. 3, *A* and *B*). When deposition current of <50 s was applied, few apparent labels were detected, presumably due to an inadequate amount of silver ions necessary for visualization. In contrast, deposition of 80–100 s resulted in a "halo effect" that increased the silver-labeled area to approximately 100–150 μm (Fig. 3, *C* and *D*), most likely due to a broad distribution of deposited silver. Similarly, histological development of <7 min was not long enough to "develop" the deposited silver required to visualize the label, whereas prolonged exposure to the developing solution tended to darken large areas of the section thus confounding differentiation due to insufficient contrast (data not shown).

We next verified that the sites of silver deposition represented the location of the tip (i.e., recording location) of a given electrode. In a subset of animals ($n = 2$ with silver processing, $n = 1$ unprocessed positive control), 2 of the 16 silver-plated electrodes were coated with the fluorescent lipophilic dye DiI to visualize the tracks associated with the electrode insertion (DiCarlo et al. 1996; Márton et al. 2016; Naselaris et al. 2005). Although DiI was readily detected in unprocessed tissue (data not shown), DiI could not be detected after the histological processing required for silver labeling. Therefore, we conclude these two techniques are not compatible. However, in several histological sections, an electrode track could be identified terminating at the silver-labeled site (Fig. 3*E*). This is consistent with the interpretation that the silver-labeled site is located at the tip of the electrode.

Another objective was to determine whether the silver-labeling method could be coupled with fluorescent immunohistochemistry (IHC) procedures. Accordingly, we performed IHC with two markers commonly used in the central nervous system (GFAP and NeuN) either before or immediately after histological processing for silver development. These markers were chosen due to their ability to label astrocytes (Bignami et al. 1972) and neurons (Wolf et al. 1996). Fluorescent staining was detected in both cases but was more robust when IHC was performed after the silver staining procedures (data not shown), indicating IHC (at least for these commonly used markers) is compatible with the histological processing steps necessary to develop the silver. Using this staining order, we determined the location of deposited silver relative to NeuN-positive cells. Representative photomicrographs from a C4 spinal section depicting positive silver labeling in the intermediate gray is shown in Fig. 4*A*. Fluorescent labeling of the same section stained with NeuN and 4′,6′-diamidino-2-phenylindole (DAPI) are shown in Fig. 4*B*. High-magnification images of the silver-labeled site suggest the recording electrode was in close proximity to a NeuN-positive neuron (Fig. 4*B*). These qualitative results demonstrate that the silver-labeling technique can be coupled with fluorescent IHC.

Using silver labeling to identify anatomic locations of metal array electrodes. In 6 animals ($n = 4$ spinal-intact and $n = 2$ SCI), we used the optimized deposition and development parameters discussed previously to label select electrodes. Overall, using this approach to identify the anatomic locations of the recording electrodes, we obtained positive labeling in 35 of 39 attempts. This indicates that the silver-labeling method can be used to identify the anatomic locations of array electrodes with a success rate of ~90%. Positive silver labeling was identified in the spinal gray matter between C3 and C5. The locations of each silver-labeled site in spinal-intact and SCI animals was plotted (unilaterally for simplicity) according to their anatomic locations (Fig. 5*A*). Silver-labeled sites were

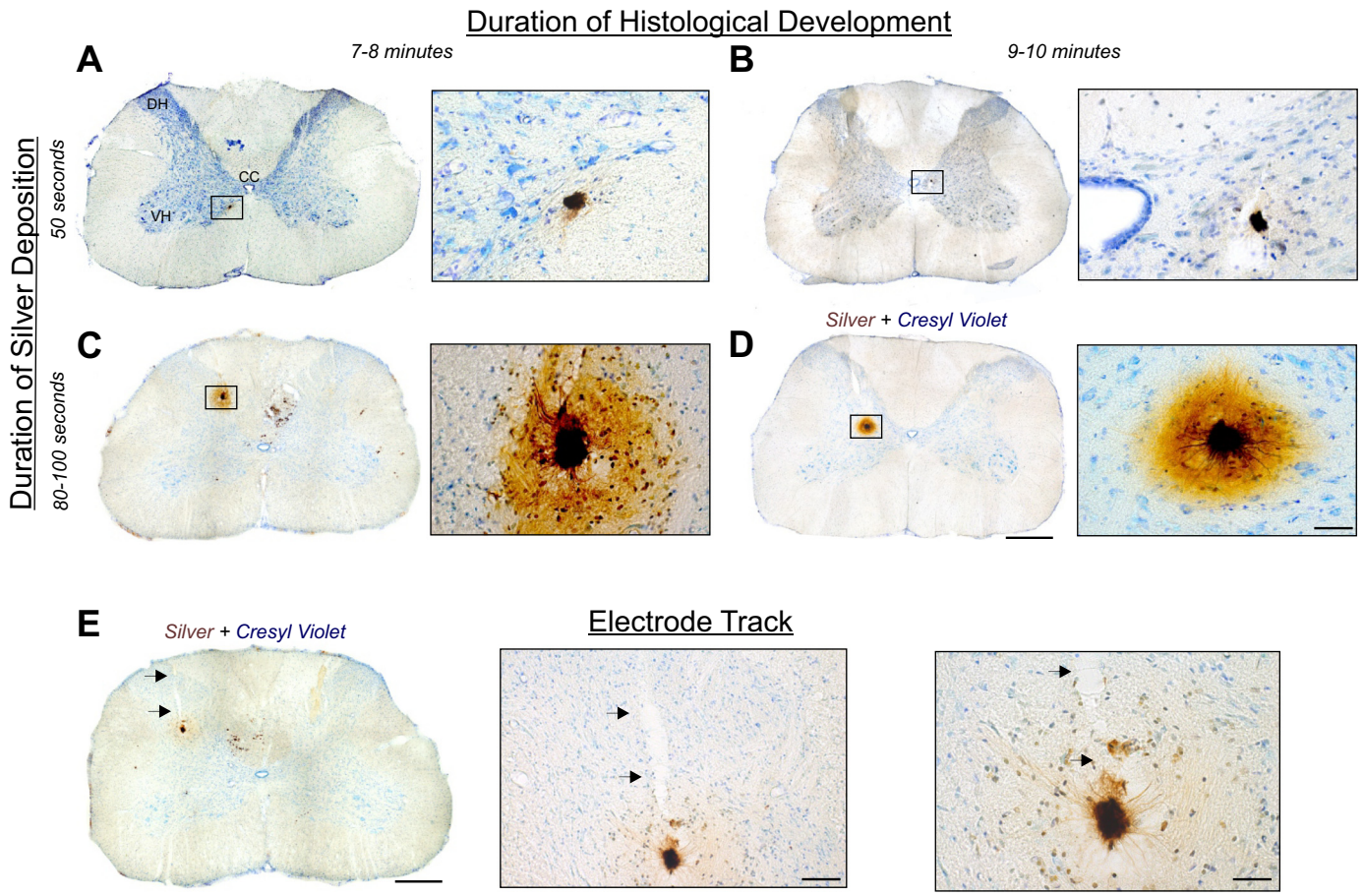

Fig. 3. Representative images of silver labeling. *A–D*: representative histological sections from the cervical spinal cord containing silver-labeled sites counterstained with cresyl violet and high-resolution images of the boxed areas. These images depict the variability of silver labeling at different durations of silver deposition (50–100 s) and histological development (7–10 min). *E*: images of a cervical spinal section depicting an electrode track (black arrows) coursing through the spinal tissue and terminating at the silver-labeled site. CC, central canal; DH, dorsal horn; VH, ventral horn. Scale bars: *A–D*: 0.5 mm and 50 μm (callouts); *E*: 0.5 mm, 100 μm, and 50 μm, respectively.

identified between laminae IV and X, with the greatest number found in lamina VII (Fig. 5*A*).

The success of the discrete silver labeling afforded the chance to compare the intended recording location (i.e., the micromotor coordinates used during the neurophysiology experiment) with the actual location of the labeling (Fig. 5, *B* and *C*). Each silver-labeled site was measured from the dorsal surface of the cord. Based on estimates of prior investigations regarding tissue shrinkage during paraformaldehyde fixation and subsequent tissue processing (Deutsch and Hillman 1977; Quester and Schröder 1997), the measured histological depth of each silver-labeled site was adjusted by 10%. This analysis indicated that the micromotor depth is likely to overestimate the actual depth of the electrode and perhaps even more importantly that this relationship is altered by SCI. Linear regression analysis indicated a significant relationship between recording coordinates and histological staining in spinal-intact animals (motor: 1.6 $\pm$ 0.04 mm; histological: 1.2 $\pm$ 0.05 mm; $P = 0.0003$) but not after chronic SCI (motor: 1.4 $\pm$ 0.07 mm; histological: 0.6 $\pm$ 0.05 mm; $P = 0.3014$; Fig. 5*B*). The depth of the silver-labeled site differed from the micromotor coordinate in both groups (Fig. 5*C*) but was significantly increased following SCI (0.8 $\pm$ 0.07 mm) compared with spinal-intact animals (0.4 $\pm$ 0.04 mm). These data highlight the need to identify multielectrode recording sites histologically, especially following experimental conditions such as SCI when tissue fibrosis and scarring can be expected to alter electrode movement within the central nervous system (CNS). Future studies can apply the linear fit as a proxy to calculate the actual depth of the electrode tips more accurately.

Coupling spinal discharge with anatomic locations. All silver-electroplated electrodes were capable of discriminating single units, indicating that the pretreatment had a minimal, if any, impact on the ability to record and discriminate extracellular signals. Three silver-labeled sites were identified within lamina IX of the ventral horn (Figs. 5*A* and 6*A*). Spike-triggered averaging (STA) of the raw and rectified phrenic nerve activity in relation to neuronal discharge produced a distinct peak with an average lag time of 0.45 $\pm$ 0.16 ms (Fig. 6*E*) and therefore indicated that the recorded discharge was from phrenic motoneurons (Christakos et al. 1994; Mitchell et al. 1992). All three of these cells were active primarily during the inspiratory phase (Fig. 6, *B* and *C*), which is the typical firing pattern of phrenic motoneurons in this preparation (Sandhu et al. 2015). The silver-labeling data verified that the recordings were from the region of the phrenic motor nucleus (Furicchia and Goshgarian 1987; Goshgarian and Rafols 1981; Kinkead et al. 1998; Mantilla et al. 2009; Prakash et al. 2000). This close matching between neurophysiological data and

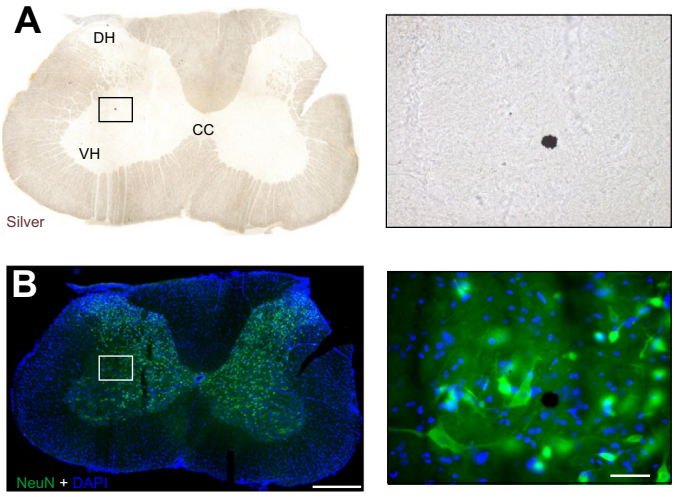

Fig. 4. Silver labeling coupled with fluorescent immunohistochemistry. *A*: representative cervical spinal section of positive silver labeling (brown/black) and high-resolution image of the boxed area. *B*: fluorescent labeling of neurons stained with NeuN (green) and nuclei stained with DAPI (blue) of the same section presented in *A*, and high-resolution image of the boxed area illustrating the silver-labeled site was in close proximity of a NeuN-positive cell. CC, central canal; DH, dorsal horn; VH, ventral horn. Scale bars: 0.5 mm and 50 μm (callouts).

anatomic data illustrates the effectiveness of the silver-labeling method.

The remaining silver-labeled sites were located between laminae IV and X (Fig. 7). Spike-triggered averaging provided no evidence of discharge synchrony in relation to phrenic motor output; thus these 28 recordings were considered to represent interneurons (Fig. 7, *E* and *J*). At baseline, most recorded interneurons (18/28 or 64%; Fig. 7*K*) fired tonically throughout the respiratory cycle (e.g., *waveform 2* in Fig. 7, *C*, *D*, *H*, and *I*). These tonically discharging cells were not restricted to a particular lamina but rather were recorded throughout the cervical gray matter (Fig. 7*L*). A smaller proportion of interneurons (5/28 or 18%; Fig. 7*K*) primarily fired during the inspiratory phase (*waveform 1* in Fig. 7, *C* and *D*), and these cells were found in laminae VI ($n = 1$), VII ($n = 3$), and X ($n = 1$). During hypoxia, 2 of these neurons (in laminae VII and X) switched to a tonic firing pattern but then resumed an inspiratory pattern posthypoxia. In addition, 1 inspiratory neuron in lamina VII was inspiratory-modulated during baseline and hypoxia but then assumed a tonic firing pattern posthypoxia. Similarly, during baseline conditions, 5 cells (5/28 or 18%; Fig. 7*K*) discharged primarily during the expiratory period (e.g., *waveform 1* in Fig. 7, *H* and *I*) and were located in laminae VIII ($n = 3$), IX ($n = 1$), and X ($n = 1$). During hypoxia, 3 of these neurons [in laminae VIII ($n = 2$) and IX ($n = 1$)] switched to a tonic firing pattern that was then maintained posthypoxia. In addition, 1 expiratory-modulated neuron in lamina VIII ceased bursting immediately posthypoxia. Therefore, due to phase switching, the proportion of tonic firing interneurons increased to 82% (23/28) during hypoxia and remained elevated posthypoxia (20/28 or 71%). Interneuron bursting patterns during baseline, hypoxia, and posthypoxia are summarized in Fig. 7*K*, and the corresponding anatomic locations are provided in Fig. 7*L*. In this sample of neurons, respiratory-related discharge was observed only in the ventral gray matter (i.e., laminae VI, VII, VII, IX, and X), and tonic discharge was recorded throughout the midcervical gray matter.

Mapping anatomic locations and quantitation of interneuronal discharge across midcervical spinal laminae are shown in Fig. 8. A representative example from 1 recording in which silver labeling was used to "map" the anatomic locations of the array electrodes and corresponding electrophysiological data is shown in Fig. 8, *A*–*C*. A camera lucida-style drawing of the anatomic locations of 8 silver-labeled electrodes was constructed (Fig. 8*B*). Numerical identification of the anatomic positions of each electrode corresponds to the schematic presented in Fig. 1*D* and defines the rostral-caudal and medial-lateral positions of the array electrodes. Corresponding midcervical spinal discharge and integrated phrenic nerve activity during baseline and hypoxia on the left and right hemicord is shown in Fig. 8*C*. The majority of these recordings were from tonic firing interneurons (*electrodes 3*, *8*, *9*, *11*, *12*, and *15*), and one represented a phase-switching (e.g., from tonic at baseline to expiratory during hypoxia) interneuron (*electrode 6*; Fig. 8*C*). Using this technique, a summary of the anatomic locations of all silver-labeled interneurons was constructed (Fig. 8*D*). In addition, the average discharge frequency of all silver-labeled interneurons was presented in Fig. 8*E*. The results indicate a dorsal-ventral discharge gradient, with higher discharge rates in laminae IV and X and lower values in laminae VIII and IX. This discharge map of the midcervical spinal network demonstrates the utility of using the silver-labeling technique to identify the anatomic locations of ensembles of interneurons recorded with a MEA. These results show the usefulness of using this technique to standardize the sampling distribution of recording locations across experimental groups.

Temporal relationships between cervical interneuron discharge. Anatomic data indicate that cervical interneurons are part of a diffuse and synaptically coupled propriospinal network (Lane et al. 2008b), but relatively little is known about functional connectivity between cervical interneurons. Therefore, initial analyses focused on all recorded neurons in spinal-intact rats (i.e., silver- and nonsilver-labeled neurons) to screen for short time scale (i.e., 0–10 ms) features (Aertsen and Gerstein 1985; Aertsen et al. 1989; Melssen and Epping 1987). Significant features were identified as departures in the cross-correlation histogram ≥3 standard deviations from the background noise (Melssen and Epping 1987). Using this approach, significant central (i.e., no lag time from 0) and offset correlogram peaks were detected (Fig. 9*A*). A summary of the latency of significant features relative to the trigger (i.e., *time 0*) are shown in Fig. 9*B*.

Inspection of the data suggested that latencies for correlogram peaks were distributed in 3 ranges: *1*) ≤0.4 ms; *2*) 0.6–2.8 ms; and *3*) ≥3.0 ms (discrete integers reflect 0.2-ms bins used to construct histograms; Fig. 9, *B* and *C*). Few correlations (37/704 or 5.3% of possible correlations) had a peak with latency ≤0.4 ms, which is consistent with excitation from a common synaptic input (Aertsen and Gerstein 1985; Kirkwood 1979; Kirkwood et al. 1991; Melssen and Epping 1987). A greater number of positive correlations had latencies between 0.6 and 2.8 ms and ≥3.0 ms (54/704 or 7.7% and 97/704 or 13.8%, respectively). Correlogram peaks with latencies >0.6 ms are consistent with the interpretation of functional excitation involving mono- or polysynaptic connections

(Aertsen and Gerstein 1985; Kirkwood 1979; Moore et al. 1970). We next evaluated the number of positive correlations relative to the recording locations. For this, neuronal pairs were classified as unilateral (i.e., recordings on the same side of the cord) or bilateral (i.e., recordings on opposite sides of the cord). Evaluation of unilateral pairs showed the average number of significant correlogram peaks was 20 ± 3.9 correlations per animal. A similar value was obtained for bilateral neuronal pairs (25 ± 7.5 correlations per animal; Fig. 9*D*). When normalized to the total number of possible unilateral (332) or bilateral (372) correlations, similar values were observed (24 ± 0.5 and 26 ± 5.5%, respectively; Fig. 9*E*). No significant differences in latencies were observed when data were separated into unilateral and bilateral neuronal pairs (data not shown).

Neuronal pairs with significant correlogram peaks that were also silver-labeled were used to construct correlation summary maps to illustrate the anatomic locations of each neuron (Fig. 10). The number of positive correlations within each lamina was normalized to the total number of neurons present in the corresponding lamina. Unilateral neuronal pairs are shown in Fig. 10*A*, and bilateral pairs are shown in Fig. 10*B*. Of the positive unilateral correlations, interneurons in dorsal lamina (i.e., IV, V, and VI) made and received the greatest number of excitatory connections (Fig. 10*A*). In contrast, when the trigger and target neuron were on opposite sides of the spinal cord, interneurons in laminae V, VIII, and IX made and received the most connections (Fig. 10*B*).

We also found 33 troughs in cross-correlograms that were significantly different from background activity using the same criteria used to detect peaks (data not shown). For comparison purposes, the number of troughs occurring ≤0.4 was 20/704 or 2.8%, whereas those between 0.6 and 2.8 ms was 1/704 or 0.1% and those ≥3.0 ms was 12/704 or 1.7%. Correlogram troughs with these latencies are generally thought to reflect functional inhibition (Aertsen and Gerstein 1985; Kirkwood 1979).

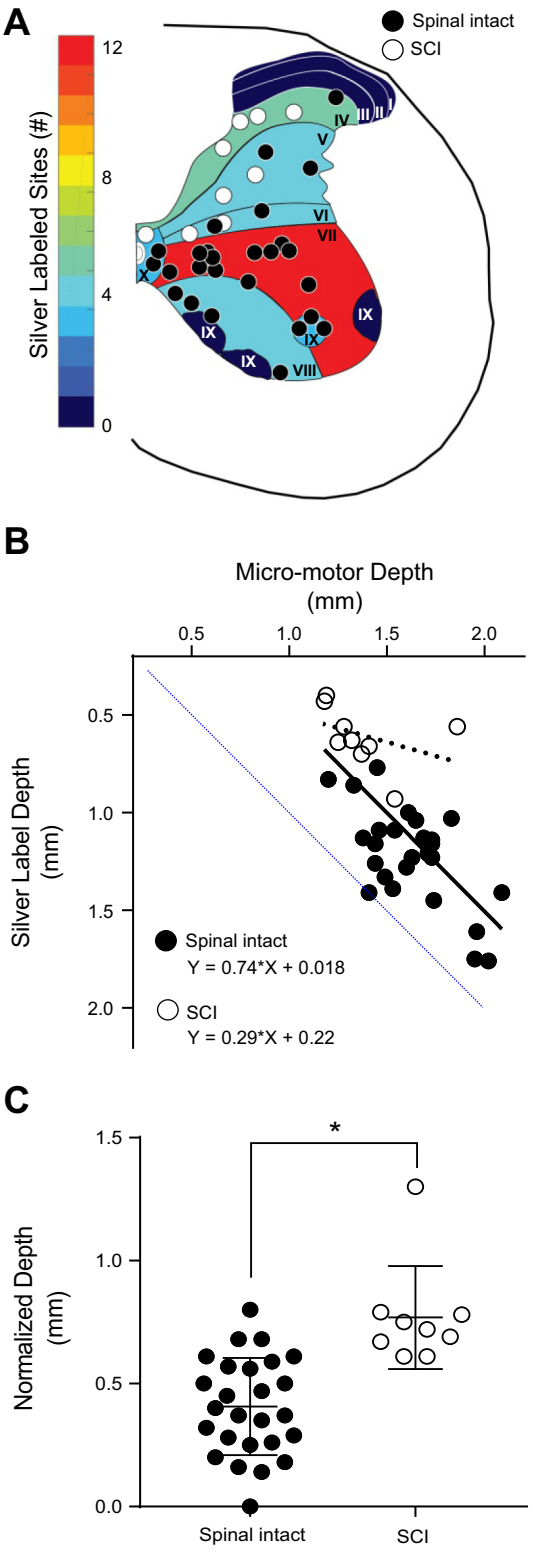

Fig. 5. Electrode and silver-labeled depth. *A*: representative C4 section of silver-labeled sites in spinally intact (●) and spinally injured (○) animals projected onto 1 side of the cord for simplicity. Each lamina was shaded according to the number (#) of silver-labeled sites within that lamina. *B*: scatter plot of the micromotor depths vs. the depths of the corresponding silver-labeled sites in spinally intact (●) and spinally injured (○) animals. Linear regression analysis was applied to determine the line of best fit and linear equation for each group. The line of identity is displayed to indicate the location where micromotor and silver-labeling depths are equal. *C*: normalized depth calculated as the difference between the micromotor depth silver-labeled site for spinally intact (●) and spinally injured (○) animals. *$P < 0.001$, unpaired *t*-test.

DISCUSSION

Here, we describe a silver-labeling technique that reliably identifies the position of MEA tips following in vivo neurophysiological recordings. The results indicate that silver labeling can be histologically identified with a resolution of ~50 μm while also preserving the structural integrity of the tissue with a 90% success rate. A practical application of this technique was demonstrated by matching the location of midcervical MEA recording sites with neuronal discharge to create maps of bursting patterns (e.g., Figs. 7 and 8). Moreover, using correlative techniques, we also provide to our knowledge the first neurophysiological evidence for the presence of extensive connections between interneurons in midcervical gray matter (e.g., Figs. 9 and 10). Coupling silver labeling with MEA neurophysiology provides a powerful tool to investigate network-level properties of the spinal cord.

Commentary regarding the silver-labeling method. The first challenge associated with adapting the silver-labeling method

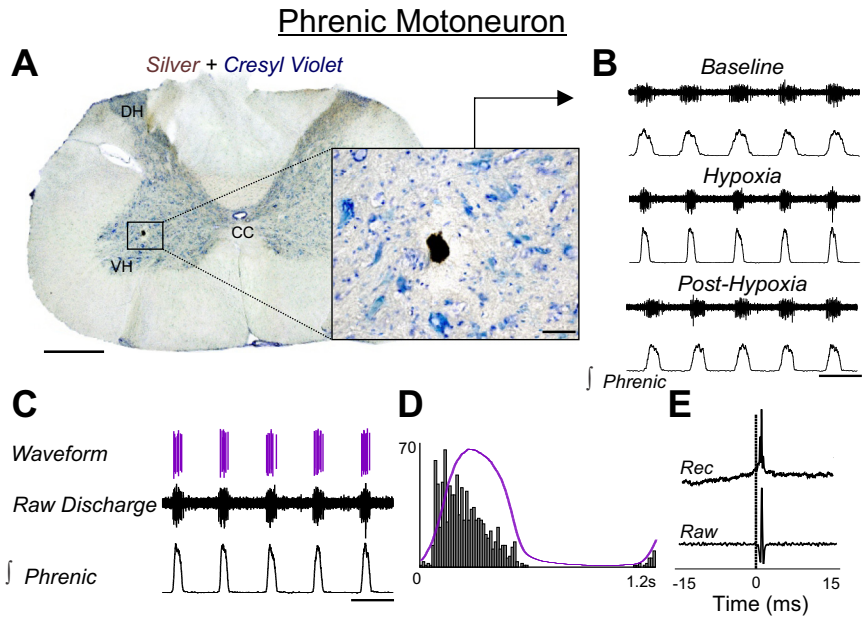

Fig. 6. Silver labeling of a phrenic motoneuron. *A*: representative C4 section containing a silver-labeled site counterstained with cresyl violet and high-resolution image containing the silver-labeled site located in the medial aspect of the ventral horn in lamina IX (callout). *B*: corresponding raw spinal discharge and integrated phrenic output during baseline, hypoxia, and posthypoxia depicting discharge during the inspiratory phase. *C*: integrated phrenic output, raw neuronal discharge, and sorted spikes (waveform) during hypoxia. *D*: cycle-triggered histogram during 50 consecutive breaths overlaid with the average integrated phrenic waveform during hypoxia. *E*: spike-triggered average of the raw and rectified (Rec) phrenic nerve depicting a delay of 0.76 ms. CC, central canal; DH, dorsal horn; VH, ventral horn. Scale bars: *A*: 0.5 mm and 50 μm (callout); *B* and *C*: 1.5 s.

(Spinelli 1975) for MEAs was accurately measuring the low currents (in nanoamperes) needed for electroplating and depositing silver from tungsten array electrodes. Although devices that measure low currents are commercially available (e.g., for patch-clamp/iontophoresis), they are expensive and not easily adapted to electroplating or electrodeposition. Additionally, multimeters cannot resolve currents in the nanoampere range and have limited accuracy due to voltage drop caused by current flow through the current-measuring device (i.e., "burden voltage"; Jones 2010). To overcome these limitations, we used an EEVblog μCurrent Precision Assistant that permits nanoampere currents to be measured on a standard multimeter and also improves the accuracy to 0.2% (Jones 2010). We also designed a μCurrent control device capable of generating 100 nA while also allowing current adjustments of $<$1 nA (circuit details provided in Fig. 2*C*). The ability to produce and control this current precisely was critical since passing higher currents can alter electrode impedance and recording characteristics (Fung et al. 1998). The current-generating system was specifically designed to be compatible with both single electrodes and MEAs.

Published methods for marking the location of MEAs include iontophoresis of neural tracers (Fekete et al. 2015; Haidarliu et al. 1999; Kovács et al. 2005), topical application of fluorescent dyes (DiCarlo et al. 1996; Naselaris et al. 2005), lesioning (Brozoski et al. 2006; Townsend et al. 2002), electrical imaging (Li et al. 2015), and imaging-based approaches (Borg et al. 2015; Fung et al. 1998; Koyano et al. 2011; Matsui et al. 2007). The silver-labeling method offers several advantages over these previous techniques. First, this technique can be used with the standard metal electrodes typically used with MEAs (Borg et al. 2015; Cogan 2008). This is in contrast to the specialized electrodes necessary for iontophoresis (Fekete et al. 2015; Kovács et al. 2005; Naselaris et al. 2005). Second, the silver-labeling method does not require implanted electrodes or expensive and often unavailable equipment such as MRI to visualize electrode placement (Borg et al. 2015; Fung et al. 1998; Koyano et al. 2011; Matsui et al. 2007). Third, the histologically identified silver deposition spanned an area of $\sim$50 μm, and this provides an $\sim$3$\times$ greater resolution compared to previously published techniques compatible with metal MEAs. For example, MRI-based approaches enable visualization of microelectrode sites at an in-plane resolution of 150–200 μm (Fung et al. 1998; Koyano et al. 2011; Matsui et al. 2007). Fluorescent dyes achieve resolutions between 50 and 400 μm but identify electrode track trajectories rather than discrete locations of electrode tips (DiCarlo et al. 1996; Naselaris et al. 2005). Finally, whereas lesioning techniques can damage surrounding tissues (Townsend et al. 2002), low current levels required for silver deposition preserve the integrity of the surrounding tissue. This is a particularly important point since it permits neurochemical phenotyping of neurons at or near the electrode tip.

One of the features enabling matching of electrophysiological signals with anatomic locations is that the relative position of each electrode was known since the electrodes exist in a fixed matrix (Fig. 1*D*). Nevertheless, with multiple silver-labeled sites in a relatively discrete area, matching each silver-labeled site with its corresponding recording electrode can pose a challenge. To overcome this hurdle, several safeguards were implemented. First, since recordings were performed with a bilateral recording array, a small longitudinal cut in the dorsal spinal cord was made before sectioning to demarcate the left vs. right hemicord. Second, the rostral-caudal orientation of spinal sections was maintained throughout the histological process by sectioning sequentially into 12-well plates. Most importantly, the histologically identified silver deposition was linked to the corresponding recording data by using the lateral-medial aspect of the electrode matrix. The phrenic motoneuron data provided further verification of the ability to match silver labeling with the neurophysiology data. The anatomic location of phrenic motoneurons is well-defined in rat (Goshgarian and Rafols 1981; Mantilla et al. 2009; Prakash et al. 2000; Zhan et al. 1989), and the electrophysiological analyses (e.g., STA) confirmed an appropriate match between the anatomic location of silver labeling (i.e., ventral gray matter, lamina IX) and the recording electrode. Moreover, cells with histological features consistent with phrenic motoneurons (Furicchia and Goshgar-

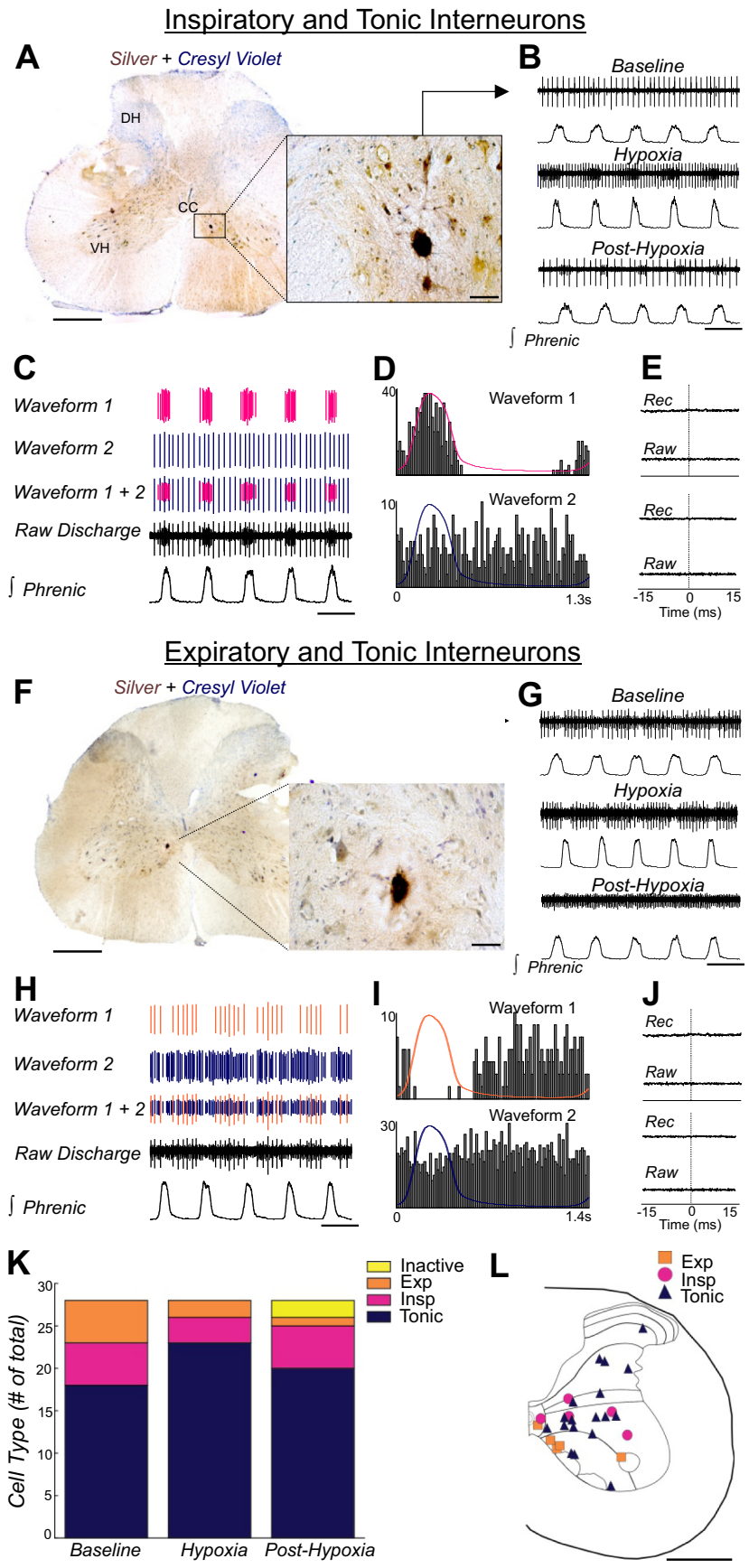

Fig. 7. Silver labeling of midcervical spinal interneurons. *A*: representative C4 section containing a silver-labeled site counterstained with cresyl violet and high-resolution image containing the silver-labeled site (callout). *B*: corresponding neuronal output and integrated phrenic output during baseline, hypoxia, and posthypoxia depicting a single tonic firing neuron at baseline and recruitment of a phasic inspiratory neuron during hypoxia and posthypoxia. *C*: integrated phrenic output, raw neuronal discharge, and sorted spikes (waveforms) during hypoxia. *D*: cycle-triggered histograms of both neurons during 50 consecutive breaths overlaid with the average integrated phrenic waveform during hypoxia. *E*: spike-triggered average of the raw and rectified phrenic nerve depicting a lack of positive features. *F*: representative C4 section containing a silver-labeled site counterstained with cresyl violet and high-resolution image containing the silver-labeled site (callout). *G*: corresponding neuronal output and integrated phrenic output during baseline, hypoxia, and posthypoxia depicting an expiratory and tonic firing neuron at baseline and hypoxia and only the tonic neuron posthypoxia. *H*: integrated phrenic output, raw neuronal discharge, and sorted spikes (waveforms) during hypoxia. *I*: cycle-triggered histograms of both neurons during 50 consecutive breaths overlaid with the average integrated phrenic waveform. *J*: spike-triggered average of the raw and rectified phrenic nerve depicting a lack of positive features. *K*: stacked bar graphs depicting the number of each cell type at baseline, hypoxia, and posthypoxia each normalized to the total number of interneurons ($n = 28$). *L*: anatomic location of each silver-labeled interneuron projected onto 1 side of the cord for simplicity, identified by the bursting pattern during baseline. Exp, expiratory; Insp, inspiratory; CC, central canal; DH, dorsal horn; VH, ventral horn. Scale bars: *A*, *F*, and *L*: 0.5 mm and 50 μm (callouts); *B*, *C*, *G*, and *H*: 1.5 s.

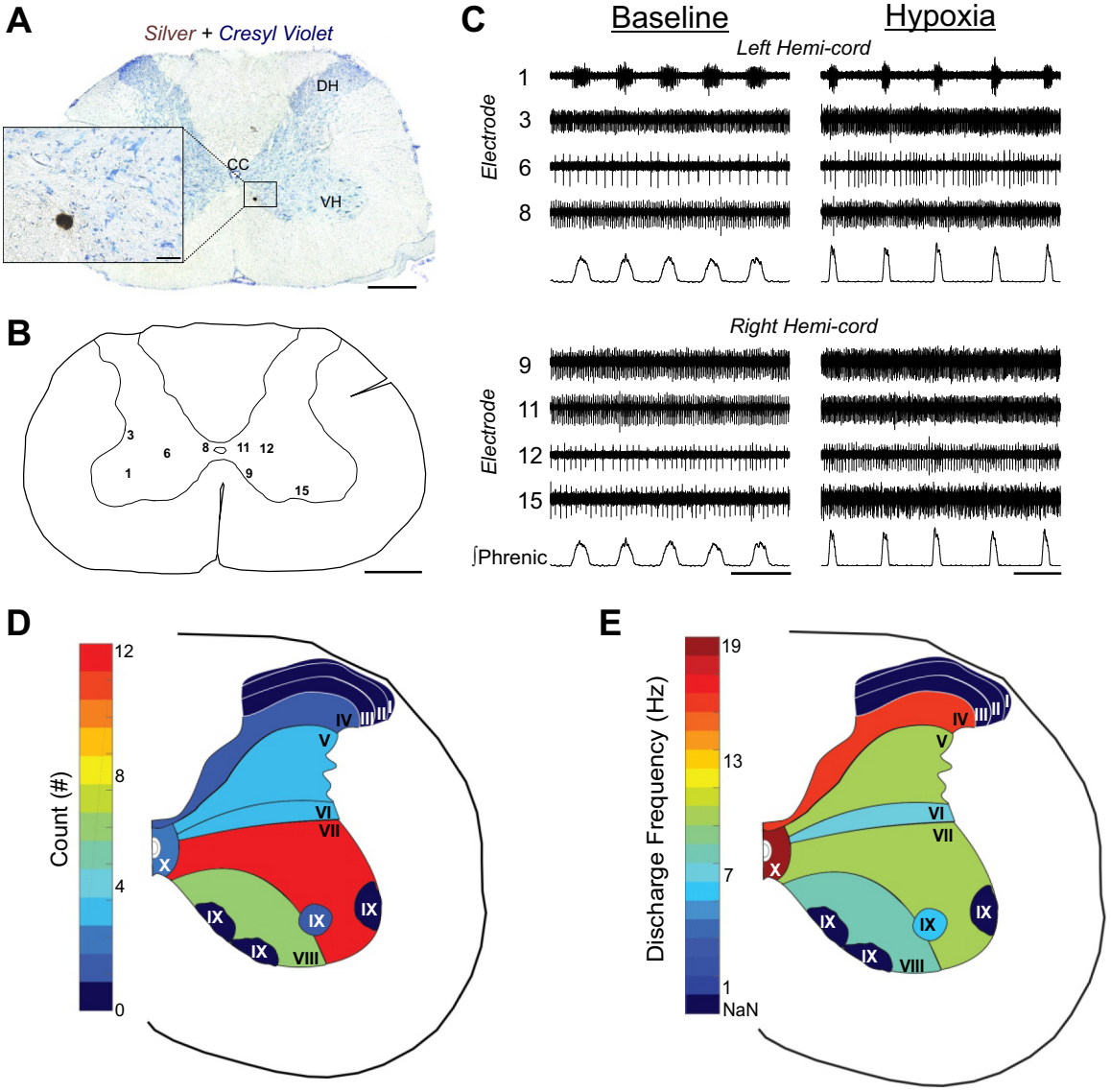

Fig. 8. Mapping anatomic locations of midcervical spinal neurons. *A*: representative photomicrograph of a C4 section containing a silver-labeled site (from *electrode 9*) counterstained with cresyl violet and high-resolution image of the silver-labeled site (callout). *B*: camera lucida-style drawing of the cervical spinal cord summarizing the anatomic locations of 8 silver-labeled sites obtained in 1 animal. *C*: integrated phrenic motor output and midcervical spinal discharge on the left and right hemicord corresponding to identified silver-labeled sites in *B* during baseline and hypoxia. *Electrode 1* recorded phrenic motoneuron discharge, and the remaining electrodes recorded interneuron discharge. *D*: representative C4 section summarizing the total number of silver-labeled interneurons within each lamina in spinal-intact animals. *E*: average discharge frequency of spinal interneurons within each lamina represented in *D*. CC, central canal; DH, dorsal horn; VH, ventral horn; NaN, no cells recorded. Scale bars: *A* and *B*: 0.5 mm and 50 μm (callout); *C*: 1.5 s.

ian 1987; Prakash et al. 2000) were clearly identified near the silver label (approximately 50–100 μm).

To ensure that our recordings (and silver-labeled sites) were from neurons (vs. fibers of passage) in the immediate vicinity of electrode, we used high-impedance tungsten wires coated with Epoxylite insulation with an exposed tip of $\leq$1 μm. We suggest that using these insulated high-impedance electrodes, the following assumptions are reasonable: *1*) the recorded neural discharge is of somatic origin (vs. axonal); and *2*) the amplitude of the recorded action potentials decreases with distance between the soma and the recording electrode tip. The reasons for these assumptions are as follows. Extracellular action potentials recorded from axons are very brief (i.e., 0.1–0.3 ms), small, and extremely sensitive to electrode movement (Bellingham and Lipski 1990; Kirkwood et al. 1988). In contrast, action potentials recorded in the current study were broad (i.e., $\geq$1 ms) and biphasic, and the recordings were stable as electrodes were moved up to 100 μm. These features are consistent with extracellularly recorded somatic action potentials (Bellingham and Lipski 1990; Nelson 1959). The literature indicates that the amplitude of extracellularly recorded action potentials is inversely proportion to the distance between the soma and the recording electrode (Kirkwood et al. 1988; Nelson 1959). Therefore, by achieving a 3:1 signal-to-noise ratio when placing each electrode, we can be confident that the electrode tip is close to the cell soma generating the largest action potential. Last, the electrode design described above reduces the surface area available for silver plating, and thus silver is deposited from only the ~1-μm plated length at each electrode tip.

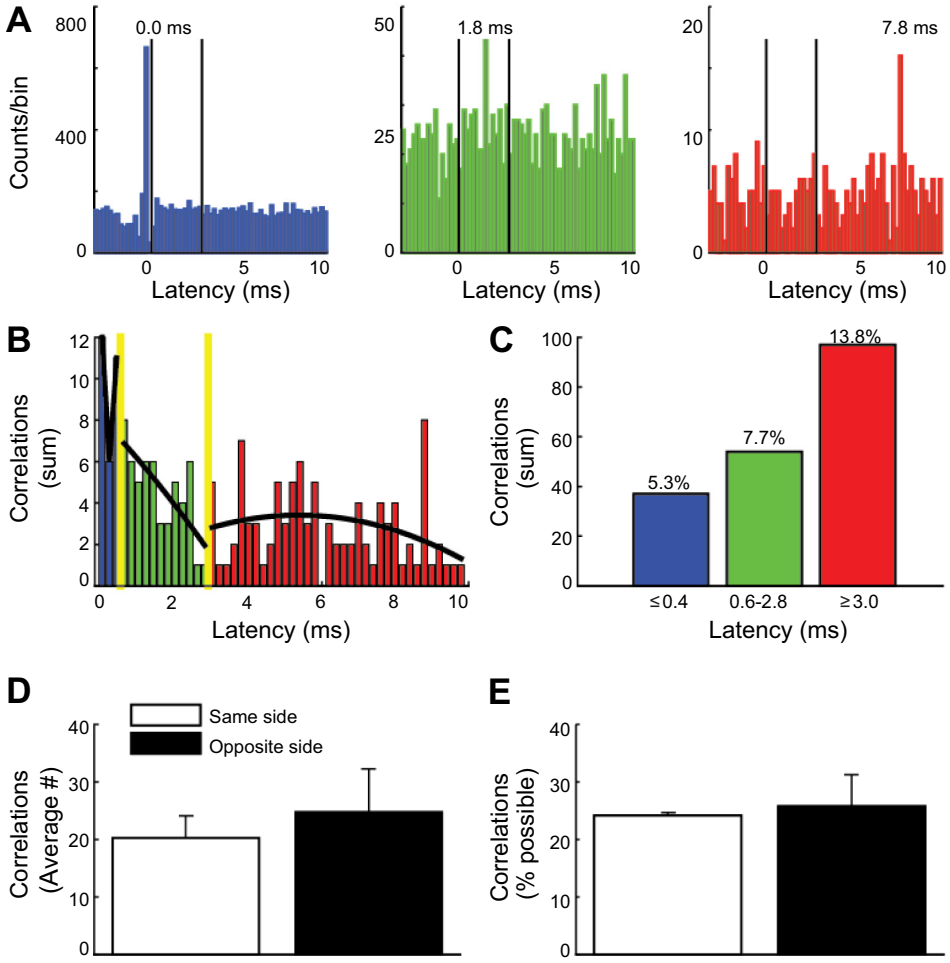

Fig. 9. Cross-correlation analysis of midcervical spinal interneurons. *A*: representative cross-correlations obtained from 3 pairs of neurons depicting a significant central peak (*left*), 1.8-ms offset peak (*middle*), and 7.8-ms offset peak (*right*). The number of trigger spikes for each correlation: 43,891; 39,208; and 3,928; and the detectability index of each correlation: 45.2; 4.3; and 5.3, respectively. Black lines plotted at 0.5 and 2.9 ms to indicate how data were grouped by latency (see *B*). *B*: a histogram of the latency relative to the trigger for all correlations with a significant peak. The 1st bar in the histogram is a count of the central peaks (0-ms latency), and each successive bar in the plot represents counts obtained in an increment of 0.2. Yellow bars plotted at 0.5 and at 2.9 ms indicate how data were grouped based on latency. Black lines are 2nd-order polynomial fit of the data. *C*: the sum of significant cross-correlations with latencies ≤0.4 ms, between 0.6 and 2.8 ms, and ≥3.0 ms. Percentages reflect the proportion of positive correlations out of the total possible ($n = 704$). *D*: the average number of positive correlations per animal when both recordings were on the same side of the cord (20 ± 3.9 positive correlations per animal) or on opposite sides of the cord (25 ± 7.5 positive correlations per animal). *E*: the number of significant correlations expressed as a percentage of total possible connections obtained when both recordings were on the same side of the cord (81/332 total possible) or on opposite sides of the cord (89/372 total possible).

The silver-labeling method was not 100% successful, and we suspect the small number of failures ($n = 4$ of 39 possible sites) occurred due to a lack of deposited silver or tissue damage during histological processing (e.g., tearing of sections or error during the placement of longitudinal notch in the spinal cord). A final methodological commentary relates to the difference between the histologically verified depth of the electrode and the coordinates used in the microdrive while placing each electrode (e.g., Fig. 5). The microdrive coordinates overestimated the actual depth of the recording and probably reflect some degree of "pillowing" of the tissue as the electrodes were advanced. The most salient point, however, is that the difference between histological and micromotor coordinates was increased in rats with chronic SCI (e.g., Fig. 5*C*). These data highlight the need to identify multielectrode recording sites histologically following SCI when tissue fibrosis and scarring can be expected to impede electrode movement within the spinal cord.

Midcervical spinal interneurons and respiratory motor output. Several laboratories have suggested that phrenic motoneuron discharge can be modulated by synaptic input from spinal interneurons (Bellingham and Lipski 1990; Davies et al. 1985; Sandhu et al. 2015). Anatomic studies show spinal interneurons are uniquely situated to modulate phrenic motor output since they are in close opposition with medullary projections (Davies et al. 1985; Fedorko et al. 1983; Hayashi et al. 2003; Lane et al. 2008b) and have synaptic connections to phrenic motoneurons (Dobbins and Feldman 1994; Lane et al. 2008b, 2009; Lois et al. 2009; Yates et al. 1999). Electrophysiological recordings in multiple species have demonstrated that cervical interneurons have respiratory-related discharge patterns (Bellingham and Lipski 1990; Duffin and Iscoe 1996; Marchenko et al. 2015; Palisses et al. 1989; Sandhu et al. 2015) and respond to respiratory stimuli such as phrenic afferent stimulation (Iscoe and Duffin 1996; Speck and Revelette 1987) and hypoxia (Sandhu et al. 2015). Our results add to this literature in two primary ways. First, to our knowledge, only one prior study (Marchenko et al. 2015) has combined neurophysiology with the histological identification of the anatomic location of respiratory-related spinal interneurons associated with the phrenic motor pool. Our data show that interneurons with respiratory-related discharge are located throughout laminae VI, VII, VII, IX, and X. Second, the current results provide new information regarding the impact of respiratory stimulation with hypoxia on midcervical interneuronal discharge patterns. Indeed, during/following hypoxia, ~29% of spinal interneurons alter their discharge in relation to the respiratory cycle. We noted that both inspiratory- and expiratory-modulated neurons had a tendency to adopt a tonic firing pattern during hypoxia. However, posthypoxia interneurons with baseline inspiratory discharge tended to resume an inspiratory firing pattern, whereas the expiratory interneurons maintained the tonic pattern. In addition, we found one example of a tonic firing interneuron during baseline and hypoxia that became

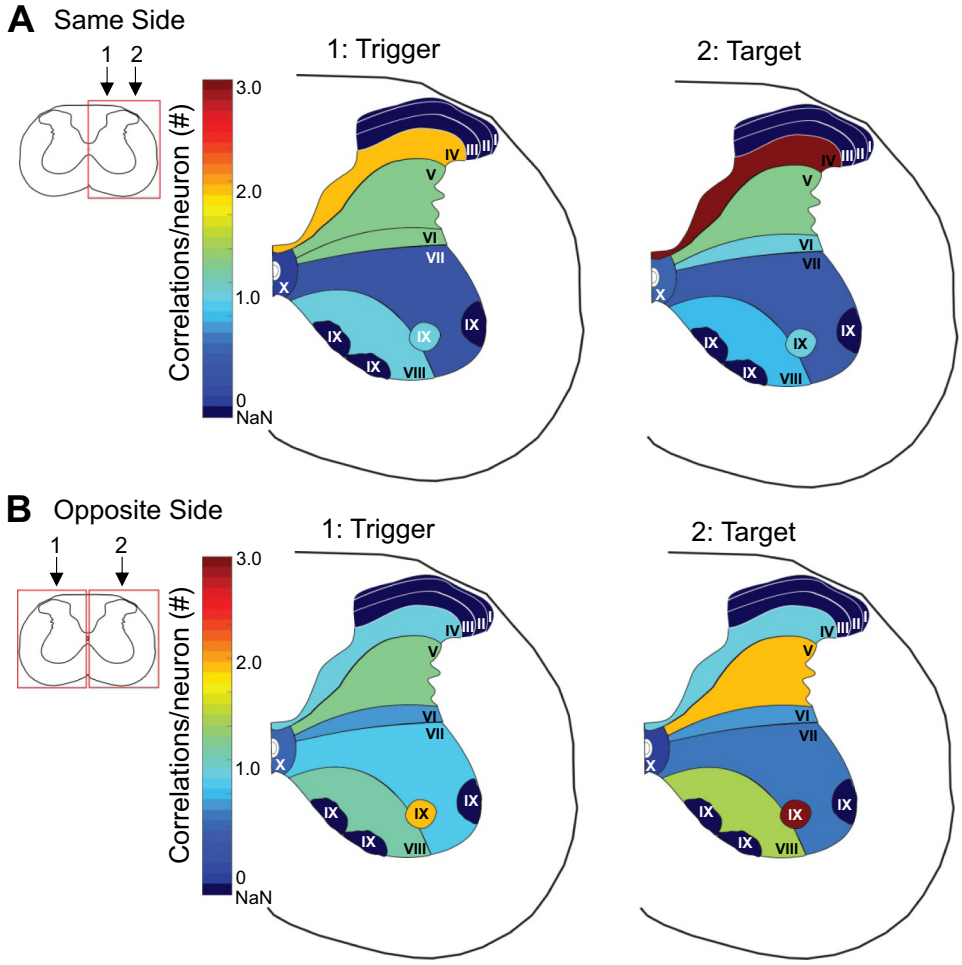

Fig. 10. Anatomic locations of functionally connected interneurons. Summary maps of silver-labeled interneurons with significant peaks in cross-correlograms. The number of positive correlations in each lamina was normalized to the number of neurons present in the lamina and shaded accordingly. *A*: when both trigger and target neurons were on the same side of the spinal cord (e.g., unilateral recordings), interneurons in dorsal lamina (i.e., IV, V, and VI) made and received the greatest number of excitatory connections. *B*: when the trigger and target neurons were on opposite sides of the spinal cord (e.g., bilateral recordings), interneurons in laminae V, VIII, and IX made and received the most connections.

inspiratory-modulated posthypoxia. Neurons exhibiting phase switching were located in intermediate and ventral laminae (i.e., VII, VIII, and X) rather than dorsal laminae. To our knowledge, this is the first report to describe hypoxia-induced phase switching of midcervical interneuron bursting patterns. When neuronal discharge frequency was evaluated relative to anatomic locations, higher frequencies were noted in laminae IV and X (e.g., Fig. 8*E*). These results again highlight the importance of matching anatomic location with discharge properties and show that midcervical interneuron discharge varies across cervical lamina, which is consistent with previous descriptions of lumbosacral neural activity (Borowska et al. 2013; Ruscheweyh and Sandkühler 2002).

Discharge synchrony between midcervical spinal interneurons. Despite both historical (Duffin and Iscoe 1996; Palisses et al. 1989) and recent publications (Lane 2011; Marchenko et al. 2015; Sandhu et al. 2015) related to cervical respiratory interneurons, the functional connectivity of midcervical spinal circuit remains largely unexplored. This can be attributed to the fact that studies investigating respiratory-related interneurons in the spinal cord have primarily used a single-unit recording approach (Bellingham and Lipski 1990; Lipski and Duffin 1986; Lipski et al. 1993) and have instead focused on connections between motor- and interneurons (Davies et al. 1985; Duffin and Iscoe 1996; Lipski et al. 1993). In the current study, we utilized cross-correlation analysis to characterize the functional connectivity of pairs of spinal interneurons. Similar to previous studies investigating spinal interneurons in nonrespiratory-related networks (Brown et al. 1979; Prut and Perlmutter 2003), we found relatively few examples of synchronous discharge consistent with a shared excitatory presynaptic input (Aertsen et al. 1989; Kirkwood 1979). That is, when interneuronal pairs were examined, correlogram peaks with latencies between 0 and 0.4 ms were only observed in 5.3% of recordings. In contrast, 21.4% of the total possible positive correlations had latencies ≥0.6 ms. These longer latency peaks are consistent with mono- and polysynaptic connections between cervical interneuron pairs. Of the positive correlations involving neurons on the same side of the spinal cord, interneurons in dorsal lamina (i.e., IV, V, and VI) made and received the greatest number of excitatory connections. In contrast, when the trigger and target neuron were on opposite sides of the spinal cord, interneurons in laminae V, VII, and IX made and received the most connections. Taken together, our results provide support for the hypothesis that cervical interneurons form a dynamic network that is capable of rapid reconfiguration and modulation of cervical motor outputs. We suggest that the MEA silver-labeling method will help advance our understanding of the functional and anatomic correlates of ensembles of spinal neurons.

Application to spinal cord injury. One potential application of MEA technology is to examine how SCI alters the cervical spinal networks. Spinal networks undergo substantial remodeling following SCI (Bareyre et al. 2004; Sperry and Goshgarian 1993), and interneurons have been implicated in SCI-

induced plasticity and motor recovery (Alilain et al. 2008; Bareyre et al. 2004; Harkema 2008). However, relatively little is known regarding their contribution to the spontaneous recovery of phrenic output following SCI (Lane et al. 2008b). In the current study, we performed recordings on $n = 2$ rats with chronic cervical SCI. The intent of these experiments was not to map changes in the spinal network postinjury but rather to confirm that the method developed herein could be effectively utilized in rats with SCI. We successfully deposited and detected silver labeling following SCI using the same parameters optimized in spinal-intact animals. However, we noted a greater discrepancy between micromotor and silver-labeling depth in spinal-injured animals (e.g., Fig. 5*C*). Although multiple factors may contribute to this disparity, structural changes resulting from fibrosis and scarring induced following injury (Cregg et al. 2014) may increase electrode drag, thereby reducing the effectiveness of utilizing the electrode micromotor to predict the actual depth of the electrode tips. Regardless of the specific cause, our results highlight the importance of histologically verifying the locations of recorded neurons, especially following experimental conditions such as SCI that may alter electrode movement within the CNS. We suggest that future studies utilizing the methods described here will shed light on the contribution of the propriospinal network to the recovery of function following SCI.

Conclusions. The methodology described here provides a solution to the fundamental limitation of using MEAs containing standard metal electrodes by identifying the discrete anatomic locations of the recording sites. Although prior studies have described methods to determine the approximate locations of MEA electrodes (Borg et al. 2015; Brozoski et al. 2006; DiCarlo et al. 1996; Fekete et al. 2015; Haidarliu et al. 1999; Kovács et al. 2005; Koyano et al. 2011; Naselaris et al. 2005; Townsend et al. 2002), to date labeling the discrete recording locations of nonspecialized metal array electrodes in an acute preparation while preserving the surrounding tissue has only been achieved with single-cell recordings. With MEA recordings, higher-order analyses can be used to investigate the functional connectivity of the neural network during physiological stimuli and following neurological injury (e.g., Figs. 9 and 10; also see: Aertsen and Gerstein 1985; Kirkwood 1979; Melssen and Epping 1987). In this regard, the current results are consistent with a high degree of synaptic connections between midcervical neurons. Collectively, our experiments show that: *1*) MEA silver-labeling method enables the electrophysiological output of neural networks to be coupled with histological verification of electrode locations; *2*) midcervical interneurons are capable of rapid phase switching of burst patterns relative to the respiratory cycle during and after hypoxia; and *3*) a high percentage of midcervical interneuronal pairs have temporally related discharge patterns.

ACKNOWLEDGMENTS

We thank Dave Doyle at Bare Electronics (Gainesville, FL), Dr. Nicole Tester, Alexis Caballero, and Kelly Schwanebeck for their technical assistance.

GRANTS

This work was supported by the National Institutes of Health Grants 1-R01-NS-080180-01A1 (D. D. Fuller), 1-F32-NS-095620-01 (K. A. Streeter), and T32-ND-043730 (M. D. Sunshine) and the Department of Defense Grant W81XWH-14-1-0625 (P. J. Reier).

DISCLOSURES

No conflicts of interest, financial or otherwise, are declared by the author(s).

AUTHOR CONTRIBUTIONS

K.A.S., P.J.R., D.D.F., and D.M.B. conceived and designed research; K.A.S., S.R.P., S.S.L., and L.E.D. performed experiments; K.A.S., M.D.S., S.R.P., S.S.L., L.E.D., and D.M.B. analyzed data; K.A.S., M.D.S., D.D.F., and D.M.B. interpreted results of experiments; K.A.S. and M.D.S. prepared figures; K.A.S. and D.M.B. drafted manuscript; K.A.S., D.D.F., and D.M.B. edited and revised manuscript; K.A.S., M.D.S., S.R.P., S.S.L., L.E.D., P.J.R., D.D.F., and D.M.B. approved final version of manuscript.

REFERENCES

Aertsen AM, Gerstein GL. Evaluation of neuronal connectivity: sensitivity of cross-correlation. *Brain Res* 340: 341–354, 1985.

Aertsen AM, Gerstein GL, Habib MK, Palm G. Dynamics of neuronal firing correlation: modulation of "effective connectivity." *J Neurophysiol* 61: 900–917, 1989.

Alilain WJ, Li X, Horn KP, Dhingra R, Dick TE, Herlitze S, Silver J. Light-induced rescue of breathing after spinal cord injury. *J Neurosci* 28: 11862–11870, 2008.

Bareyre FM, Kerschensteiner M, Raineteau O, Mettenleiter TC, Weinmann O, Schwab ME. The injured spinal cord spontaneously forms a new intraspinal circuit in adult rats. *Nat Neurosci* 7: 269–277, 2004.

Bellingham MC, Lipski J. Respiratory interneurons in the C5 segment of the spinal cord of the cat. *Brain Res* 533: 141–146, 1990.

Bignami A, Eng LF, Dahl D, Uyeda CT. Localization of the glial fibrillary acidic protein in astrocytes by immunofluorescence. *Brain Res* 43: 429–435, 1972.

Borg JS, Vu MA, Badea C, Badea A, Johnson GA, Dzirasa K. Localization of metal electrodes in the intact rat brain using registration of 3D micro-computed tomography images to a magnetic resonance histology atlas. *eNeuro* 2: pii: e0017, 2015.

Borowska J, Jones CT, Zhang H, Blacklaws J, Goulding M, Zhang Y. Functional subpopulations of V3 interneurons in the mature mouse spinal cord. *J Neurosci* 33: 18553–18565, 2013.

Brown PB, Koerber HR, Yezierski RP. Cross-correlation analysis of connectivities among cat lumbosacral dorsal horn cells. *J Neurophysiol* 42: 1199–1211, 1979.

Brozoski TJ, Caspary DM, Bauer CA. Marking multi-channel silicon-substrate electrode recording sites using radiofrequency lesions. *J Neurosci Methods* 150: 185–191, 2006.

Christakos CN, Cohen MI, Sica AL, Huang WX, See WR, Barnhardt R. Analysis of recurrent laryngeal inspiratory discharges in relation to fast rhythms. *J Neurophysiol* 72: 1304–1316, 1994.

Cogan SF. Neural stimulation and recording electrodes. *Annu Rev Biomed Eng* 10: 275–309, 2008.

Cohen MI. Discharge patterns of brain-stem respiratory neurons in relation to carbon dioxide tension. *J Neurophysiol* 31: 142–165, 1968.

Cregg JM, DePaul MA, Filous AR, Lang BT, Tran A, Silver J. Functional regeneration beyond the glial scar. *Exp Neurol* 253: 197–207, 2014.

Davies JG, Kirkwood PA, Sears TA. The detection of monosynaptic connexions from inspiratory bulbospinal neurones to inspiratory motoneurones in the cat. *J Physiol* 368: 33–62, 1985.

Deutsch K, Hillman H. The effect of six fixatives on the areas of rabbit neurons and rabbit and rat cerebral slices. *J Microsc* 109: 303–309, 1977.

DiCarlo JJ, Lane JW, Hsiao SS, Johnson KO. Marking microelectrode penetrations with fluorescent dyes. *J Neurosci Methods* 64: 75–81, 1996.

Dobbins EG, Feldman JL. Brainstem network controlling descending drive to phrenic motoneurons in rat. *J Comp Neurol* 347: 64–86, 1994.

Douse MA, Duffin J. Axonal projections and synaptic connections of C5 segment expiratory interneurones in the cat. *J Physiol* 470: 431–444, 1993.

Duffin J, Iscoe S. The possible role of C5 segment inspiratory interneurons investigated by cross-correlation with phrenic motoneurons in decerebrate cats. *Exp Brain Res* 112: 35–40, 1996.

Fedorko L, Merrill EG, Lipski J. Two descending medullary inspiratory pathways to phrenic motoneurones. *Neurosci Lett* 43: 285–291, 1983.

Fekete Z, Pálfi E, Márton G, Handbauer M, Bérces Zs, Ulbert I, Pongrácz A, Négyessy L. In vivo iontophoretic BDA injection through a buried microfluidic channel of a neural multielectrode. *Procedia Eng* 120: 464–467, 2015.

Fung SH, Burstein D, Born RT. In vivo microelectrode track reconstruction using magnetic resonance imaging. *J Neurosci Methods* 80: 215–224, 1998.

Furicchia JV, Goshgarian HG. Dendritic organization of phrenic motoneurons in the adult rat. *Exp Neurol* 96: 621–634, 1987.

Galán RF, Dick TE, Baekey DM. Analysis and modeling of ensemble recordings from respiratory pre-motor neurons indicate changes in functional network architecture after acute hypoxia. *Front Comput Neurosci* 4: pii: 131, 2010.

Gonzalez-Rothi EJ, Rombola AM, Rousseau CA, Mercier LM, Fitzpatrick GM, Reier PJ, Fuller DD, Lane MA. Spinal interneurons and forelimb plasticity after incomplete cervical spinal cord injury in adult rats. *J Neurotrauma* 32: 893–907, 2015.

Goshgarian HG, Rafols JA. The phrenic nucleus of the albino rat: a correlative HRP and Golgi study. *J Comp Neurol* 201: 441–456, 1981.

Haidarliu S, Sosnik R, Ahissar E. Simultaneous multi-site recordings and iontophoretic drug and dye applications along the trigeminal system of anesthetized rats. *J Neurosci Methods* 94: 27–40, 1999.

Harkema SJ. Plasticity of interneuronal networks of the functionally isolated human spinal cord. *Brain Res Rev* 57: 255–264, 2008.

Hayashi F, Hinrichsen CF, McCrimmon DR. Short-term plasticity of descending synaptic input to phrenic motoneurons in rats. *J Appl Physiol* 94: 1421–1430, 2003.

Iscoe S, Duffin J. Effects of stimulation of phrenic afferents on cervical respiratory interneurones and phrenic motoneurones in cats. *J Physiol* 497: 803–812, 1996.

Jones DL. *The μCurrent. A professional precision current adapter for Multimeters* (Online). http://alternatezone.com/electronics/ucurrent/uCurrentArticle.pdf, 2010.

Kinkead R, Zhan WZ, Prakash YS, Bach KB, Sieck GC, Mitchell GS. Cervical dorsal rhizotomy enhances serotonergic innervation of phrenic motoneurons and serotonin-dependent long-term facilitation of respiratory motor output in rats. *J Neurosci* 18: 8436–8443, 1998.

Kirkwood PA. On the use and interpretation of cross-correlation measurements in the mammalian central nervous system. *J Neurosci Methods* 1: 107–132, 1979.

Kirkwood PA, Munson JB, Sears TA, Westgaard RH. Respiratory interneurones in the thoracic spinal cord of the cat. *J Physiol* 395: 161–192, 1988.

Kirkwood PA, Schmid K, Otto M, Sears TA. Focal blockade of single unit synaptic transmission by iontophoresis of antagonists. *Neuroreport* 2: 185–188, 1991.

Kovács P, Dénes V, Kellényi L, Hernádi I. Microiontophoresis electrode location by neurohistological marking: comparison of four native dyes applied from current balancing electrode channels. *J Pharmacol Toxicol Methods* 51: 147–151, 2005.

Koyano KW, Machino A, Takeda M, Matsui T, Fujimichi R, Ohashi Y, Miyashita Y. In vivo visualization of single-unit recording sites using MRI-detectable elgiloy deposit marking. *J Neurophysiol* 105: 1380–1392, 2011.

Lane MA. Spinal respiratory motoneurons and interneurons. *Respir Physiol Neurobiol* 179: 3–13, 2011.

Lane MA, Fuller DD, White TE, Reier PJ. Respiratory neuroplasticity and cervical spinal cord injury: translational perspectives. *Trends Neurosci* 31: 538–547, 2008a.

Lane MA, Lee KZ, Fuller DD, Reier PJ. Spinal circuitry and respiratory recovery following spinal cord injury. *Respir Physiol Neurobiol* 169: 123–132, 2009.

Lane MA, Lee KZ, Salazar K, O'Steen BE, Bloom DC, Fuller DD, Reier PJ. Respiratory function following bilateral mid-cervical contusion injury in the adult rat. *Exp Neurol* 235: 197–210, 2012.

Lane MA, White TE, Coutts MA, Jones AL, Sandhu MS, Bloom DC, Bolser DC, Yates BJ, Fuller DD, Reier PJ. Cervical prephrenic interneurons in the normal and lesioned spinal cord of the adult rat. *J Comp Neurol* 511: 692–709, 2008b.

Lee KZ, Fuller DD. Preinspiratory and inspiratory hypoglossal motor output during hypoxia-induced plasticity in the rat. *J Appl Physiol (1985)* 108: 1187–1198, 2010.

Lee KZ, Reier PJ, Fuller DD. Phrenic motoneuron discharge patterns during hypoxia-induced short-term potentiation in rats. *J Neurophysiol* 102: 2184–2193, 2009.

Li PH, Gauthier JL, Schiff M, Sher A, Ahn D, Field GD, Greschner M, Callaway EM, Litke AM, Chichilnisky EJ. Anatomical identification of extracellularly recorded cells in large-scale multielectrode recordings. *J Neurosci* 35: 4663–4675, 2015.

Lipski J, Duffin J. An electrophysiological investigation of propriospinal inspiratory neurons in the upper cervical cord of the cat. *Exp Brain Res* 61: 625–637, 1986.

Lipski J, Duffin J, Kruszewska B, Zhang X. Upper cervical inspiratory neurons in the rat: an electrophysiological and morphological study. *Exp Brain Res* 95: 477–487, 1993.

Lipski J, Kubin L, Jodkowski J. Synaptic action of R beta neurons on phrenic motoneurons studied with spike-triggered averaging. *Brain Res* 288: 105–118, 1983.

Lois JH, Rice CD, Yates BJ. Neural circuits controlling diaphragm function in the cat revealed by transneuronal tracing. *J Appl Physiol* 106: 138–152, 2009.

Mahamed S, Strey KA, Mitchell GS, Baker-Herman TL. Reduced respiratory neural activity elicits phrenic motor facilitation. *Respir Physiol Neurobiol* 175: 303–309, 2011.

Mantilla CB, Zhan WZ, Sieck GC. Retrograde labeling of phrenic motoneurons by intrapleural injection. *J Neurosci Methods* 182: 244–249, 2009.

Marchenko V, Ghali MG, Rogers RF. The role of spinal GABAergic circuits in the control of phrenic nerve motor output. *Am J Physiol Regul Integr Comp Physiol* 308: R916–R926, 2015.

Márton G, Baracskay P, Cseri B, Plósz B, Juhász G, Fekete Z, Pongrácz A. A silicon-based microelectrode array with a microdrive for monitoring brainstem regions of freely moving rats. *J Neural Eng* 13: 026025, 2016.

Matsui T, Koyano KW, Koyama M, Nakahara K, Takeda M, Ohashi Y, Naya Y, Miyashita Y. MRI-based localization of electrophysiological recording sites within the cerebral cortex at single-voxel accuracy. *Nat Methods* 4: 161–168, 2007.

Melssen WJ, Epping WJ. Detection and estimation of neural connectivity based on crosscorrelation analysis. *Biol Cybern* 57: 403–414, 1987.

Mitchell GS, Sloan HE, Jiang C, Miletic V, Hayashi F, Lipski J. 5-Hydroxytryptophan (5-HTP) augments spontaneous and evoked phrenic motoneuron discharge in spinalized rats. *Neurosci Lett* 141: 75–78, 1992.

Moore GP, Segundo JP, Perkel DH, Levitan H. Statistical signs of synaptic interaction in neurons. *Biophys J* 10: 876–900, 1970.

Morris KF, Arata A, Shannon R, Lindsey BG. Long-term facilitation of phrenic nerve activity in cats: responses and short time scale correlations of medullary neurones. *J Physiol* 490: 463–480, 1996.

Naselaris T, Merchant H, Amirikian B, Georgopoulos AP. Spatial reconstruction of trajectories of an array of recording microelectrodes. *J Neurophysiol* 93: 2318–2330, 2005.

Nelson JR. Single unit activity in medullary respiratory centers of cat. *J Neurophysiol* 22: 590–598, 1959.

Nuding SC, Segers LS, Iceman KE, O'Connor R, Dean JB, Bolser DC, Baekey DM, Dick TE, Shannon R, Morris KF, Lindsey BG. Functional connectivity in raphé-pontomedullary circuits supports active suppression of breathing during hypocapnic apnea. *J Neurophysiol* 114: 2162–2186, 2015.

Palisses R, Persegol L, Viala D. Evidence for respiratory interneurones in the C3–C5 cervical spinal cord in the decorticate rabbit. *Exp Brain Res* 78: 624–632, 1989.

Prakash YS, Mantilla CB, Zhan WZ, Smithson KG, Sieck GC. Phrenic motoneuron morphology during rapid diaphragm muscle growth. *J Appl Physiol (1985)* 89: 563–572, 2000.

Prut Y, Perlmutter SI. Firing properties of spinal interneurons during voluntary movement. I. State-dependent regularity of firing. *J Neurosci* 23: 9600–9610, 2003.

Quester R, Schröder R. The shrinkage of the human brain stem during formalin fixation and embedding in paraffin. *J Neurosci Methods* 75: 81–89, 1997.

Ruscheweyh R, Sandkühler J. Lamina-specific membrane and discharge properties of rat spinal dorsal horn neurones in vitro. *J Physiol* 541: 231–244, 2002.

Sandhu MS, Baekey DM, Maling NG, Sanchez JC, Reier PJ, Fuller DD. Midcervical neuronal discharge patterns during and following hypoxia. *J Neurophysiol* 113: 2091–2101, 2015.

Sengul G, Watson C, Tanaka I, Paxinos G. *Atlas of the Spinal Cord*. San Diego, CA: Academic Press, 2012, p. 360.

Speck DF, Revelette WR. Attenuation of phrenic motor discharge by phrenic nerve afferents. *J Appl Physiol* 62: 941–945, 1987.

Sperry MA, Goshgarian HG. Ultrastructural changes in the rat phrenic nucleus developing within 2 h after cervical spinal cord hemisection. *Exp Neurol* 120: 233–244, 1993.

Spinelli DN. Silver tipped metal microelectrodes: a new method for recording and staining single neurones. *Brain Res* 91: 271–275, 1975.

Streeter KA, Baker-Herman TL. Decreased spinal synaptic inputs to phrenic motor neurons elicit localized inactivity-induced phrenic motor facilitation. *Exp Neurol* 256: 46–56, 2014a.

Streeter KA, Baker-Herman TL. Spinal NMDA receptor activation constrains inactivity-induced phrenic motor facilitation in Charles River Sprague-Dawley rats. *J Appl Physiol (1985)* 117: 682–693, 2014b.

Strey KA, Nichols NL, Baertsch NA, Broytman O, Baker-Herman TL. Spinal atypical protein kinase C activity is necessary to stabilize inactivity-induced phrenic motor facilitation. *J Neurosci* 32: 16510–16520, 2012.

Townsend G, Peloquin P, Kloosterman F, Hetke JF, Leung LS. Recording and marking with silicon multichannel electrodes. *Brain Res Brain Res Protoc* 9: 122–129, 2002.

Wolf HK, Buslei R, Schmidt-Kastner R, Schmidt-Kastner PK, Pietsch T, Wiestler OD, Blümcke I. NeuN: a useful neuronal marker for diagnostic histopathology. *J Histochem Cytochem* 44: 1167–1171, 1996.

Yates BJ, Smail JA, Stocker SD, Card JP. Transneuronal tracing of neural pathways controlling activity of diaphragm motoneurons in the ferret. *Neuroscience* 90: 1501–1513, 1999.

Zhan WZ, Ellenberger HH, Feldman JL. Monoaminergic and GABAergic terminations in phrenic nucleus of rat identified by immunohistochemical labeling. *Neuroscience* 31: 105–113, 1989.

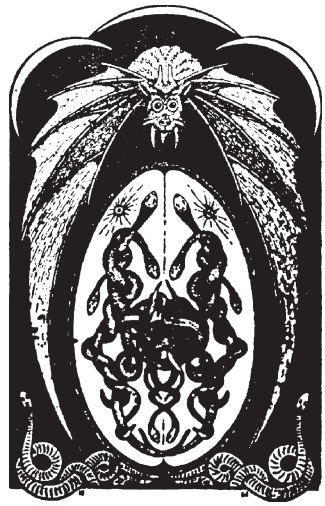

Development/Plasticity/Repair

Intermittent Hypoxia Enhances Functional Connectivity of Midcervical Spinal Interneurons

Kristi A. Streeter,[1,5]* Michael D. Sunshine,[1,5]* Shreya Patel,[1] Elisa J. Gonzalez-Rothi,[1,5] Paul J. Reier,[2,4,5] David M. Baekey,[3,5] and David D. Fuller[1,4,5]

[1]Departments of Physical Therapy, [2]Neuroscience, and [3]Physiological Sciences, [4]McKnight Brain Institute, and [5]Center for Respiratory Research and Rehabilitation, University of Florida, Gainesville, Florida 32610

Brief, intermittent oxygen reductions [acute intermittent hypoxia (AIH)] evokes spinal plasticity. Models of AIH-induced neuroplasticity have focused on motoneurons; however, most midcervical interneurons (C-INs) also respond to hypoxia. We hypothesized that AIH would alter the functional connectivity between C-INs and induce persistent changes in discharge. Bilateral phrenic nerve activity was recorded in anesthetized and ventilated adult male rats and a multielectrode array was used to record C4/5 spinal discharge before [baseline (BL)], during, and 15 min after three 5 min hypoxic episodes (11% O_2, H1–H3). Most C-INs (94%) responded to hypoxia by either increasing or decreasing firing rate. Functional connectivity was examined by cross-correlating C-IN discharge. Correlograms with a peak or trough were taken as evidence for excitatory or inhibitory connectivity between C-IN pairs. A subset of C-IN pairs had increased excitatory cross-correlations during hypoxic episodes (34%) compared with BL (19%; $p < 0.0001$). Another subset had a similar response following each episode (40%) compared with BL (19%; $p < 0.0001$). In the latter group, connectivity remained elevated 15 min post-AIH (30%; $p = 0.0002$). Inhibitory C-IN connectivity increased during H1–H3 (4.5%; $p = 0.0160$), but was reduced 15 min post-AIH (0.5%; $p = 0.0439$). Spike-triggered averaging indicated that a subset of C-INs is synaptically coupled to phrenic motoneurons and excitatory inputs to these "pre-phrenic" cells increased during AIH. We conclude that AIH alters connectivity of the midcervical spinal network. To our knowledge, this is the first demonstration that AIH induces plasticity within the propriospinal network.

Key words: **hypoxia; interneurons; network plasticity; neuroplasticity; respiratory; spinal cord**

Significance Statement

Acute intermittent hypoxia (AIH) can trigger spinal plasticity associated with sustained increases in respiratory, somatic, and/or autonomic motor output. The impact of AIH on cervical spinal interneuron (C-IN) discharge and connectivity is unknown. Our results demonstrate that AIH recruits excitatory C-INs into the spinal respiratory (phrenic) network. AIH also enhances excitatory and reduces inhibitory connections among the C-IN network. We conclude that C-INs are part of the respiratory, somatic, and/or autonomic response to AIH, and that propriospinal plasticity may contribute to sustained increases in motor output after AIH.

Introduction

Spinal interneurons can relay and modulate descending synaptic drive to motoneurons (Jankowska and Hammar, 2002), facilitate motoneuron recruitment (Renshaw, 1941; Hodson-Tole and Wakeling, 2009), and coordinate discharge between spinal motor pools (Lanuza et al., 2004). In the cervical cord, propriospinal neurons are synaptically coupled to respiratory motoneurons (Lane et al., 2008), limb motoneurons (Stepien et al., 2010), and sympathetic preganglionic neurons (Poree and Schramm, 1992). Many cervical interneurons (C-INs) respond to a brief period of reduced arterial oxygen (i.e., acute hypoxia) by altering discharge frequency (Sandhu et al., 2015; Streeter et al., 2017). The response of C-INs to repeated bouts of hypoxia [acute intermittent hypoxia (AIH)] is of interest because AIH can trigger spinal neuroplasticity and sustained increases in respiratory, autonomic, and/or somatic motor output (Dick et al., 2007; Lovett-Barr et al., 2012; Fuller and Mitchell, 2017). For these reasons, AIH is being actively explored as a therapeutic modality to promote motor recovery following neurologic disorders including spinal cord

Received April 12, 2017; revised June 20, 2017; accepted July 18, 2017.

Author contributions: K.A.S., P.J.R., D.M.B., and D.D.F. designed research; K.A.S., S.P., and E.J.G.-R. performed research; K.A.S., M.D.S., and D.D.F. analyzed data; K.A.S. and D.D.F. wrote the paper.

This work was supported by funding from the National Institute of Health, Grants 1RO1NS080180-01A1 (D.D.F.), 1F32NS095620-01 (K.A.S.), and T32-ND043730 (M.D.S.), and The Department of Defense, Grant W81XWH-14-1-0625 (P.J.R.).

*K.A.S. and M.D.S. contributed equally to this work.

The authors declare no competing financial interests.

Correspondence should be addressed to Dr. David Fuller, University of Florida, Department of Physical Therapy, P.O. Box 100154, Gainesville, FL 32610. E-mail: ddf@phhp.ufl.edu.

DOI:10.1523/JNEUROSCI.0992-17.2017

 0270-6474/17/378349-14$15.00/0

injury (Trumbower et al., 2012; Hayes et al., 2014; Tester et al., 2014; Gonzalez-Rothi et al., 2015) and amyotrophic lateral sclerosis (ALS; Nichols et al., 2013, 2015).

To date, studies of AIH-induced neuroplasticity have primarily used nerve or muscle recordings and mechanistic cellular models have focused on motoneurons (Gonzalez-Rothi et al., 2015). This is in part because the dogma in the field of respiratory neural control is that diaphragm activation on a breath-by-breath basis is driven by monosynaptic bulbospinal inputs to phrenic motoneurons (Lee and Fuller, 2011). However, the robust C-IN response to acute hypoxia (Sandhu et al., 2015; Streeter et al., 2017), and anatomical evidence that C-INs can be synaptically connected to phrenic motoneurons (Lane et al., 2008; Lane, 2011) raises the possibility that C-INs are part of a propriospinal network which can impact phrenic motor output. Further support for this idea comes from experiments showing that monosynaptic activation of phrenic motoneurons can rapidly switch to polysynaptic activation following serotonin release (Mitchell et al., 1992; Ling et al., 1994).

Here we used a multielectrode recording array to simultaneously monitor multiple C-INs during and following AIH. Our a priori hypothesis focused on network connectivity within the midcervical (C4/5) spinal cord. This was evaluated using cross-correlation analyses to examine the temporal relationship between discharging C-INs. We hypothesized that AIH would alter propriospinal connectivity as shown by an increase in the incidence of C-INs with temporally related discharge patterns. Testing this hypothesis also enabled us to determine how AIH altered the firing properties (e.g., discharge rate and pattern) of individual C-INs after AIH. Initial evaluation of our data revealed pre-phrenic C-INs which were synaptically coupled to phrenic motoneurons. Using *post hoc* analyses we therefore tested the additional hypothesis that AIH would alter the degree of functional connectivity between pre-phrenic C-INs and other C-INs. Collectively, the data provide the most comprehensive evaluation of C-IN discharge and functional connectivity to date. Our results indicate that AIH alters excitatory and inhibitory connectivity between C-INs and thus we conclude AIH induces plasticity in the cervical spinal network.

Materials and Methods

Animals. All neurophysiologic experiments were conducted with adult male ($n = 12$; 383 ± 8 g) Sprague-Dawley rats (Colony 217, ENVIGO Laboratories). Rats were housed in pairs in a controlled environment (12 h light/dark cycles) with food and water *ad libitum*. All experimental protocols were approved by the Institutional Animal Care and Use Committee at the University of Florida.

Neurophysiologic preparation. Rats were anesthetized with 3% isoflurane (in 100% O_2) and transferred to a heated surgical station where core body temperature was maintained at 37 ± 0.5°C (model 700 TC-1000, CWE). The trachea was cannulated and rats were pump-ventilated (Rodent Ventilator 683, Harvard Apparatus) and a bilateral vagotomy was performed. Inspired CO_2 was added to maintain end-tidal CO_2 between ~45 and 50 mmHg (Capnogard, Respironics). Tracheal pressure was continuously monitored and lungs were periodically hyperinflated via single breath occlusions (~1/h). A tail and femoral vein catheter were placed for intravenous delivery of urethane and fluids. Rats were slowly converted (6 ml/h; Harvard Apparatus syringe pump) to urethane anesthesia (1.7 g/kg, i.v.; 0.17 g/ml in distilled water) and isoflurane was withdrawn. A femoral arterial catheter was placed to monitor blood pressure and sample blood gases (i-STAT1 Analyzer, Abbot Laboratories). Using a dorsal approach, the left and right phrenic nerves were isolated, cut distally, and desheathed. A midline incision was made to expose spinal vertebrae C3–T2. A suture tied around the T2 spinous process was used to elevate and level the spinal cord. A laminectomy was performed from C3–C6 and the dura and arachnoid/pia over C4/5 were removed to prevent pillowing of the spinal cord as electrodes were inserted. Before neuronal recording, a pneumothorax was performed to decrease motion artifact associated with chest wall movement and positive end-expiratory pressure of 1–2 cm H_2O was applied to prevent atelectasis. Adequate depth of anesthesia was monitored by assessing arterial blood pressure responses to toe-pinch; urethane supplements (e.g., 0.2 ml bolus) were given if arterial pressure changed when the pinch was applied. Animals received the neuromuscular paralytic pancuronium bromide (2.5 mg/kg, i.v., Hospira) to prevent respiratory muscle contraction during the recording procedures. A continuous infusion (1–3 ml/h) of a 1:4 solution (8.4% sodium bicarbonate/lactated Ringer's solution, i.v.) was maintained during the experiment. A subset of rats ($n = 4$), received the nonsteroidal anti-inflammatory drug ketoprofen [(S)-(+)-ketoprofen, 12.5 mg/kg in 50% ETOH, *i.p.*; Sigma-Aldrich]. We did not detect any apparent differences between groups and therefore all data were combined.

Recordings. Bilateral phrenic nerve output was recorded using custom-made bipolar suction electrodes filled with 0.9% saline. Compound action potentials were amplified (×20 k, Grass Instruments, P511), analog bandpass filtered (3 Hz–3 kHz), digitized [16 bit, 25 k samples/s/channel; Power1401, Cambridge Electronic Design, (CED)], and integrated (time constant: 20 ms) with Spike2 software (CED). A custom-made multielectrode recording array containing 16 tungsten microelectrodes (impedance: 10 ± 1MΩ; shank diameter 125 μm; tip diameter ≤1 μm; Fred Haer) as previously described (Streeter et al., 2017) was used to record midcervical spinal discharge. Spinal recordings were performed using a unilateral ($n = 8$) or bilateral recording approach ($n = 4$) and data were pooled for analyses. The unilateral recording arrangement consisted of two staggered rows of eight microelectrodes spaced 300 μm apart and therefore extended ~2.5 mm. The bilateral recording arrangement had two sets of eight electrodes each consisting of two staggered rows of four. The inner two rows were separated by 1 mm and remaining electrodes were separated by 300 μm. In both arrangements, electrode tips were maintained in a "fixed matrix" in the medial-lateral and rostral-caudal dimension, by an array guide. The array was mounted on a stereotaxic frame and electrodes were inserted above the dorsal root entry zone at C4/5. Microelectrodes were advanced individually using micromotors until action potentials could be discriminated from background activity using an audio monitor. Recordings were amplified (×5 k), analog bandpass filtered (3 Hz–3 KHz), digitized (Power 1401, CED), and recorded (Spike2 software, CED). After recording stable baseline (BL) phrenic nerve activity and cervical spinal discharge (e.g., at least 10 min), animals were exposed to three 5 min episodes of hypoxia (FiO_2: 0.11; H1, H2, H3) separated by 5 min of hyperoxia (FiO_2: 0.50; PH1, PH2, PH3). A baseline arterial blood gas was obtained in 11/12 rats and verified that animals were well oxygenated (e.g., PaO_2 >95 mmHg) and normocapnic (e.g., 40–50 mmHg). In 9/12 animals an arterial blood sample was obtained during H1 and at 15 min posthypoxia.

Data and statistical analyses. All data were collected using Spike2.v8 software (CED). Action potentials were sorted into individual neurons and converted to waveforms using off-line spike-sorting analyses. Spikes were determined to represent a "single unit" based on (1) at least 80% template matching, (2) assessment of inter spike interval, and (3) principle component analysis. The "sorted spike" waveforms and phrenic nerve output were analyzed with custom MATLAB software (MathWorks, R2015a). All data were averaged over the stable portion (center 50 neural breaths) of each experimental time point. Statistical analyses were performed in GraphPad Prism 7 and MATLAB (see Table 1). For all comparisons using ANOVA, values during hypoxic episodes were compared with BL (e.g., BL, H1, H2, H3) and a separate ANOVA was used to examine non-hypoxic time points (e.g., BL, PH1, PH2, PH3, 15). The significance level was set to 0.05, except one instance in which it was set to 0.02 (discussed below).

Blood gas variables (e.g., PaO_2 and $PaCO_2$) were analyzed using a one-way ANOVA and individual comparisons were made using Fisher's least significant difference (LSD) *post hoc* test. Mean arterial pressure was compared using a one-way ANOVA and individual time point comparisons were determined using Fisher's LSD *post hoc* test.

Integrated phrenic amplitude was reported as amplitude (μV) and phrenic burst frequency was expressed as neural breaths per minute.

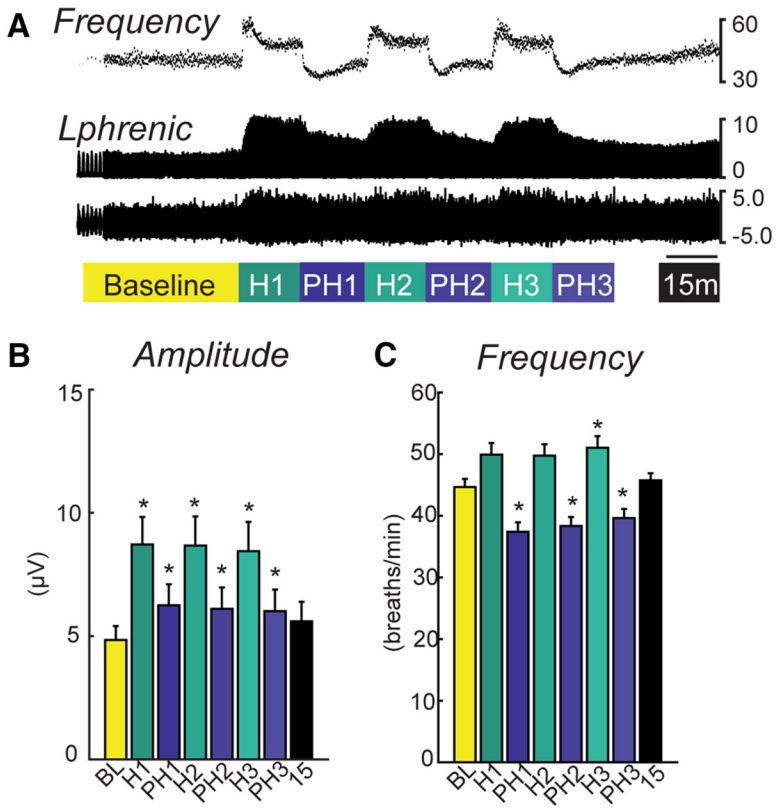

Figure 1. Phrenic nerve output before, during, and following acute intermittent hypoxia ***A***, Representative compressed raw and integrated left phrenic neurogram (μV), instantaneous burst frequency (per minute) before, during, and 15 min post-AIH. ***B***, ***C***, Average left phrenic burst amplitude (μV; ***B***), and frequency (neural breaths per minute; ***C***) during the center 50 breaths of each experimental time point. *Significantly different from BL. Scale bar, 5 min.

Differences in the left and right phrenic nerve burst amplitudes were indistinguishable at all time points ($p = 0.6470$); therefore, analysis of peak bursting focused on the left phrenic nerve. Using the integrated phrenic nerve output, the respiratory cycle was divided into inspiratory and expiratory phases. The beginning of the inspiratory phase and expiratory phase were identified as a departure of phrenic nerve activity ≥15 SD above the average activity during the expiratory phase. A two-way repeated-measure ANOVA was used to compare left and right phrenic nerve amplitude. For each phrenic nerve variable (i.e., amplitude and frequency) a one-way ANOVA with repeated-measures design was used for statistical comparisons and individual time point comparisons were determined by Fisher's LSD *post hoc* test.

Spike-triggered averaging (STA) of the phrenic nerve activity in relation to spinal neuron discharge was used to examine the temporal relationship of neuronal spikes and phrenic motor output (Lipski et al., 1983). Phrenic nerve activity was rectified and filtered with a two-pole Butterworth filter (250–3000 Hz) for all subsequent analyses. Left and right phrenic nerves were averaged separately using the sorted spikes (waveforms) of each recorded neuron as trigger events. Short-latency (e.g., <1.0 ms) peaks >5 SD from the average background (calculated over 6 ms before the trigger) were taken as evidence that the recorded neuron was a phrenic motoneuron (Mitchell et al., 1992; Sandhu et al., 2015). Identified phrenic motorneurons were excluded for all subsequent analyses.

If a short-latency feature was not detected in the STA, the recorded cell was classified as a C-IN. C-IN discharge during inspiration and expiration was compared using a one-way ANOVA. For each respiratory phase variable, a one-way ANOVA was used for statistical comparisons and individual time point comparisons were determined with Fisher's LSD *post hoc* test. Baseline frequency of activated versus inhibited C-INs was analyzed using a two-tailed unpaired *t* test.

To evaluate functional connectivity, cross-correlation histograms were constructed for all possible pairs of simultaneously recorded neurons using a bin width of 0.2 ms (Moore et al., 1970). The detectability index (DI; Aertsen and Gerstein, 1985) was calculated for each correlogram as the peak (or trough) relative to average background activity (calculated over 12 ms before the trigger), divided by the SD. Features were considered significant if the DI was >3 (Melssen and Epping, 1987), and only significant features in the positive direction were counted. Peaks or troughs are consistent with functional excitation or inhibition between the trigger and target neurons, respectively (Kirkwood, 1979; Aertsen and Gerstein, 1985). Summary graphs were expressed as the number of positive cross-correlogram features (CCs) expressed as a percentage of the total number of possible features (i.e., based on the total number of recorded cells at that time point). For statistical comparisons, the proportions of CCs were averaged during hypoxia episodes and during posthypoxia episodes. Using these values, separate χ^2 tests with Yates' correction (Hazra and Gogtay, 2016) were used to analyze differences in the proportion of CCs from BL.

Features in the phrenic nerve STA occurring with a lag time >1.0 ms were taken as evidence that the recorded cell was synaptically antecedent to the phrenic motoneuron pool (i.e., pre-phrenic C-IN; Lane et al., 2008). A 10 Hz high-pass filter was applied to the rectified phrenic signals used to construct pre-phrenic STAs. Features were considered significant if: (1) the STA was 2 SD from the mean activity before the trigger period (calculated in the interval −6 to 0 ms) and (2) the feature remained at this level for at least 0.75 ms. Offset STA features with positive deflections (peaks) were taken as evidence of excitatory pre-phrenic C-INs, whereas offset STA features with negative deflections (troughs) indicated inhibitory pre-phrenic C-INs. A two-tailed unpaired *t* test was used to analyze differences in STA parameters (e.g., time to onset and time to peak) between excitatory and inhibitory STA features. In subsequent analyses, cross-correlation histograms were constructed between identified pre-phrenic interneurons and other C-INs. For statistical comparisons, the proportions of CCs were averaged during hypoxia episodes and during posthypoxia episodes. Using these values, separate Fisher's exact tests were used to analyze differences in the proportion of CCs from BL. Linear regression analysis was used to examine the relationship between the proportion of second-order excitatory neurons to excitatory pre-phrenic C-INs during AIH.

Cycle-triggered histograms (Lindsey et al., 1992) were used to classify C-IN firing patterns relative to the respiratory cycle. Cycle-triggered histograms were constructed for each neuron by dividing each respiratory period into 20 bins. Neuronal spikes were then counted within each bin and summated over the respective bin across 50 consecutive breaths. The resulting histogram was overlaid with the averaged integrated phrenic waveform from the same 50 consecutive breaths, providing a visualization of neural discharge in relation to the respiratory cycle. To determine whether neurons were respiratory modulated, the cycle-triggered histograms were separated into inspiration and expiration and the Wilcoxon signed-rank test was used to test the null hypothesis (i.e., no difference between inspiration and expiration). Upon visual inspection of the data, the significance level was adjusted to 0.02 to reflect a physiologically meaningful modulation of neuronal firing with regard to the respiratory cycle. Neurons which were identified as respiratory modulated at BL were then categorized as inspiratory or expiratory modulated according to the phase of the respiratory cycle in which the cell was most active. Neurons not respiratory modulated (i.e., no significant difference if activity between inspiration and expiration) were classified as tonic. Those which were not active during BL were classified as recruited.

Table 1. Output of all statistical tests

	Comparison	Test	Test output	p
Fig. 1	L vs R phrenic amp	Two-way RM ANOVA	$F_{(1, 22)} = 0.2156$	0.647
	L phrenic amp: hypoxia	One-way RM ANOVA	$F_{(1.205, 12.25)} = 28.34$	0.0001
	L phrenic amp: posthypoxia	One-way RM ANOVA	$F_{(1.555, 17.11)} = 7.218$	0.0082
	Phrenic frequency: hypoxia	One-way RM ANOVA	$F_{(1.154, 12.69)} = 5.438$	0.0330
	Phrenic frequency: posthypoxia	One-way RM ANOVA	$F_{(1.514, 16.65)} = 20.08$	<0.0001
Fig. 3	Activated vs inhibited C-INs BL firing rate inspiration	Unpaired t test (two-tailed)	$t_{(72)} = 2.46$	0.0163
	Activated vs inhibited C-INs BL firing rate expiration	Unpaired t test (two-tailed)	$t_{(70)} = 0.9673$	0.3367
	Activated C-INs inspiration: hypoxia	One-way ANOVA	$F_{(3, 226)} = 4.184$	0.0066
	Activated C-INs inspiration: posthypoxia	One-way ANOVA	$F_{(4,228)} = 0.3296$	0.8579
	Activated C-INs expiration: hypoxia	One-way ANOVA	$F_{(3,221)} = 2.799$	0.0409
	Activated C-INs expiration: posthypoxia	One-way ANOVA	$F_{(4,227})) = 0.4648$	0.7615
	Inhibited C-INs inspiration: hypoxia	One-way ANOVA	$F_{(3,75)} = 3.061$	0.0333
	Inhibited C-INs inspiration: posthypoxia	One-way ANOVA	$F_{(4,80)} = 4.623$	0.0021
	Inhibited C-INs expiration: hypoxia	One-way ANOVA	$F_{(3,68)} = 2.726$	0.0508
	Inhibited C-INs expiration: posthypoxia	One-way ANOVA	$F_{(4,71)} = 3.781$	0.0076
Fig. 4	All excitatory CCs: BL vs hypoxia	χ^2 with Yates' correction	$\chi^2_{1,N=696)} = 0.2061$	0.6498
	All excitatory CCs: BL vs posthypoxia	χ^2 with Yates' correction	$\chi^2_{1,N=673)} = 5.621$	0.0177
	All excitatory CCs: BL vs 15 min	χ^2 with Yates' correction	$\chi^2_{1,N=534)} = 3.142$	0.0763
	≤1 hypoxia Excitatory CCs: BL vs hypoxia	χ^2 with Yates' correction	$\chi^2_{1,N=696)} = 17.56$	<0.0001
	≤1 hypoxia Excitatory CCs: BL vs posthypoxia	χ^2 with Yates' correction	$\chi^2_{1,N=673)} = 3.637$	0.0565
	≤1 hypoxia Excitatory CCs- BL vs 15 min	χ^2 with Yates' correction	$\chi^2_{1,N=534)} = 2.14$	0.1435
	≤1 posthypoxia Excitatory CCs: BL vs hypoxia	χ^2 with Yates' correction	$\chi^2_{1,N=696)} = 0.5925$	0.4415
	≤1 posthypoxia Excitatory CCs: BL vs posthypoxia	χ^2 with Yates' correction	$\chi^2_{1,N=673)} = 36.05$	<0.0001
	≤1 posthypoxia Excitatory CCs- BL vs 15 min	χ^2 with Yates' correction	$\chi^2_{1,N=534)} = 13.52$	0.0002
Fig. 5	All inhibitory CCs: BL vs hypoxia	χ^2 with Yates' correction	$\chi^2_{1,N=696)} = 0.2108$	0.6462
	All Inhibitory CCs: BL vs posthypoxia	χ^2 with Yates' correction	$\chi^2_{1,N=673)} = 3.467$	0.0626
	All Inhibitory CCs: BL vs 15 min	χ^2 with Yates' correction	$\chi^2_{1,N=534)} = 4.062$	0.0439
	≤1 hypoxia Inhibitory CCs: BL vs hypoxia	χ^2 with Yates' correction	$\chi^2_{1,N=696)} = 5.801$	0.0160
	≤1 hypoxia Inhibitory CCs: BL vs posthypoxia	χ^2 with Yates' correction	$\chi^2_{1,N=673)} = 0.2163$	0.6419
	≤1 hypoxia Inhibitory CCs: BL vs 15 min	χ^2 with Yates' correction	$\chi^2_{1,N=534)} = 1.142$	0.2852
	≤1 posthypoxia Inhibitory CCs: BL vs hypoxia	χ^2 with Yates' correction	$\chi^2_{1,N=696)} = 0.0150$	0.9023
	≤1 posthypoxia Inhibitory CCs: BL vs posthypoxia	χ^2 with Yates' correction	$\chi^2_{1,N=673)} = 0.1263$	0.7223
	≤1 posthypoxia Inhibitory CCs: BL vs 15 min	χ^2 with Yates' correction	$\chi^2_{1,N=534)} = 0.1522$	0.6965
Fig. 6	Excitatory vs inhibitory pre-phrenic onset STA	Unpaired t test (two-tailed)	$t_{(6)} = 0.4851$	0.6448
	Excitatory vs inhibitory pre-phrenic STA peak	Unpaired t test (two-tailed)	$t_{(6)} = 0.8584$	0.4236
Fig. 7	2nd order C-INs to excitatory pre-phrenic C-INs- BL vs hypoxia	Fisher's exact test	$n = 44$	0.4803
	2nd order C-INs to excitatory pre-phrenic C-INs: BL vs posthypoxia	Fisher's exact test	$n = 40$	0.0896
	2nd order C-INs to excitatory pre-phrenic C-INs: BL vs 15 min	Fisher's exact test	$n = 35$	>0.9999
	2nd order C-INs to excitatory pre-phrenic C-INs: hypoxia	Linear Regression	$F_{(1,2)} = 108.9$	0.0091
	2nd order C-INs to excitatory pre-phrenic C-INs: posthypoxia	Linear Regression	$F_{(1,3)} = 0.1538$	0.7211
Table 2	PaO_2	One-way ANOVA	$F_{(2,26)} = 120.6$	<0.0001
	$PaCO_2$	One-way ANOVA	$F_{(2,26)} = 0.6328$	0.5391
	MAP: hypoxia	One-way ANOVA	$F_{(3,37)} = 3.266$	0.0320
	MAP: posthypoxia	One-way ANOVA	$F_{(4,46)} = 0.1974$	0.9385

MAP, Mean arterial pressure.

Table 2. Average arterial PO_2, PCO_2, and MAP before, during, and 15 min after AIH

	BL	H1	15	PH1	H2	PH2	H3	PH3
PaO_2	228 ± 7	40 ± 2*	188 ± 14*					
$PaCO_2$	46.6 ± 1.3	44.8 ± 1.9	47.2 ± 1.3					
MAP	128 ± 9	95 ± 12*	89 ± 11	121 ± 11	88 ± 11*	121 ± 11	87 ± 11*	123 ± 11

*Significantly different from BL. MAP, Mean arterial pressure.

Results of all statistical analyses are provided in Table 1. In the Results section, relevant p values from *post hoc* tests are included to illustrate significant differences between individual time points.

Results

Blood gases and arterial pressure

Arterial blood gas data and blood pressure are summarized in Table 2. Baseline arterial blood samples confirmed rats were well oxygenated and normocapnic (Table 2). As expected, PaO_2 was decreased during H1 ($p < 0.0001$). Rats remained well oxygenated at 15 min post-AIH, but this value was reduced compared with BL ($p = 0.0034$). $PaCO_2$ values were not different from BL during H1 or 15 min after AIH ($p = 0.5391$). As previously reported in this preparation (Bavis and Mitchell, 2003), the mean arterial blood pressure was decreased during each bout of hypoxia relative to BL (H1: $p = 0.0369$; H2: $p = 0.0121$; H3: $p = 0.0116$), but was not different from BL at any time point posthypoxia (all $p > 0.9385$).

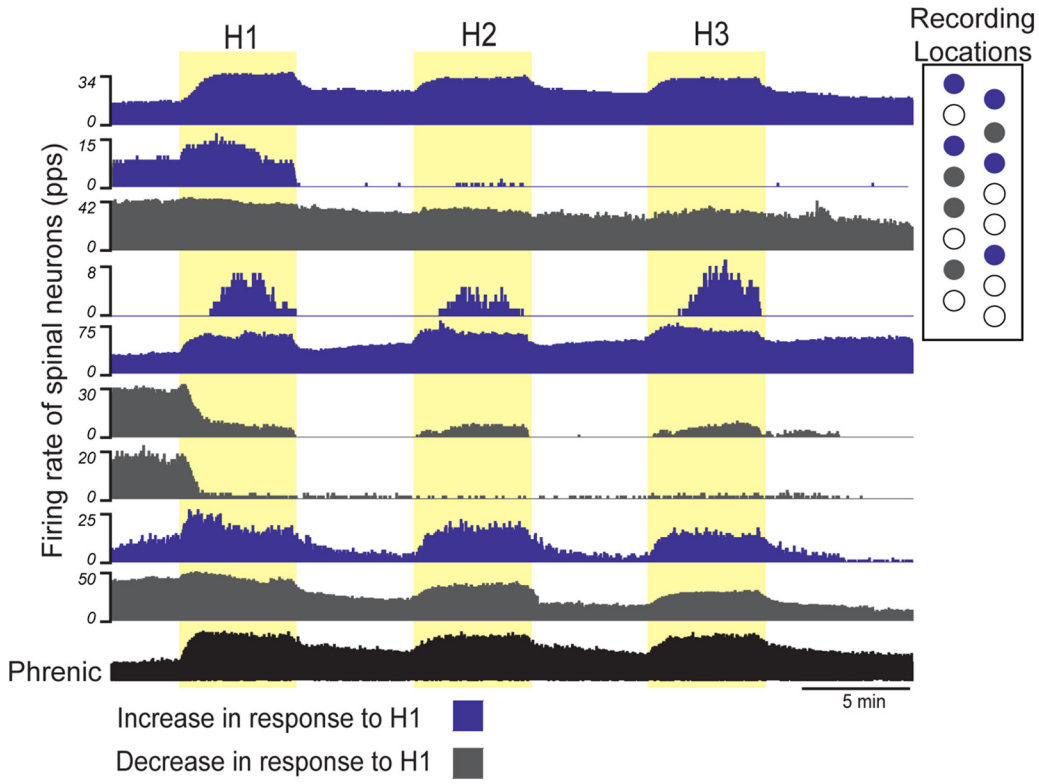

Figure 2. C-IN activity before, during, and following acute intermittent hypoxia. Representative compressed firing rate traces (pulses per second), corresponding locations of C-INs, and integrated phrenic neurogram from one experiment before, during, and 15 min post-AIH.

Phrenic nerve activity during AIH

Representative phrenic neurogram and instantaneous burst frequency are shown in Figure 1*A*. Average rectified, integrated burst amplitude before, during, and 15 min post-AIH is shown in Figure 1*B*. As expected, amplitude increased during each bout of hypoxia (H1: $p < 0.0001$; H2: $p = 0.0002$; H3: $p = 0.0004$) compared with BL. Burst amplitude remained elevated during each posthypoxic period (PH1: $p = 0.0039$; PH2: $p = 0.0126$; PH3: $p = 0.0288$), but was not different from BL at 15 min posthypoxia ($p = 0.0951$). Average burst frequency before, during, and 15 min post-AIH is shown in Figure 1*C*. Phrenic burst frequency tended to increase during H1 and H2, and was significantly increased from BL during H3 ($p = 0.0176$). A decrease in burst frequency occurred following each bout of hypoxia (PH1: $p = 0.0025$; PH2: $p = 0.0031$; PH3: $p = 0.0144$); however at 15 min post-AIH, frequency was not different from BL ($p = 0.3695$).

C-IN discharge during AIH

Representative C-IN firing rate histograms and phrenic neurogram from one animal are shown in Figure 2. To characterize the response to AIH, neurons were separated into two groups based on their firing rate during the first episode of hypoxia (e.g., H1). C-INs increasing firing rate during H1 were classified as "hypoxia activated" and cells which decreased firing rate were considered "hypoxia inhibited". During the first episode of hypoxia, 73% of C-INs increased firing rate, and 21% decreased firing rate during the inspiratory phase. A similar proportion of neurons increased (71%) and decreased (19%) firing rate during the expiratory phase. The average increase in firing rate (from BL) for hypoxia-activated C-INs was 10.6 ± 1.0 pps, whereas hypoxia-inhibited cells decreased by 8.6 ± 2.1 pps.

Heat maps illustrating the firing rate of individual C-INs as well as average rate during the inspiratory and expiratory phases are shown in Figure 3, *A* and *B*, respectively. At BL hypoxia-activated neurons had a significantly lower firing rate during the inspiratory phase (9.5 ± 1.3 pps) compared with hypoxia-inhibited neurons (15.8 ± 2.3 pps; $p = 0.0163$; Fig. 3*A*). During the inspiratory phase, hypoxia-activated C-INs increased firing rate by an average of 6.7 ± 2.2% during H1 ($p = 0.0028$), 7.1 ± 2.3% during H2 ($p = 0.0020$), and 5.8 ± 2.3% during H3 ($p = 0.0091$). However, the firing rate of these cells was not persistently altered following AIH, and returned to BL values after 15 min ($p = 0.9059$). Hypoxia-inhibited C-INs decreased firing rate during the inspiratory phase by an average of 5.9 ± 2.8% during H1 ($p = 0.0435$), 6.2 ± 2.8% during H2 ($p = 0.0337$), and 8.1 ± 2.8% during H3 ($p = 0.0062$). Cells classified as hypoxia inhibited had a decreased firing rate following all hypoxia episodes (PH1: $p = 0.0108$; PH2: $p = 0.0021$; PH3: $p = 0.0004$), which remained below BL 15 min post-AIH ($p = 0.0034$). Similar changes in discharge frequency during the expiratory phase were noted for both hypoxia-activated and -inhibited C-INs (Fig. 3*B*). Together, these results indicate that: (1) the majority of C-INs (>90%) alter firing rate in response to hypoxia, (2) hypoxia-activated C-INs had a lower BL firing rate compared with hypoxia-inhibited C-INs, and (3) hypoxia-inhibited C-INs showed a persistent inhibition with discharge rates remaining below BL at 15 min post-AIH.

Functional connectivity of C-INs during AIH

Cross-correlation analysis was used to evaluate short time scale (i.e., 0–10 ms) discharge synchrony among C-INs before, during, and after AIH. Significant features (i.e., peaks and troughs) were

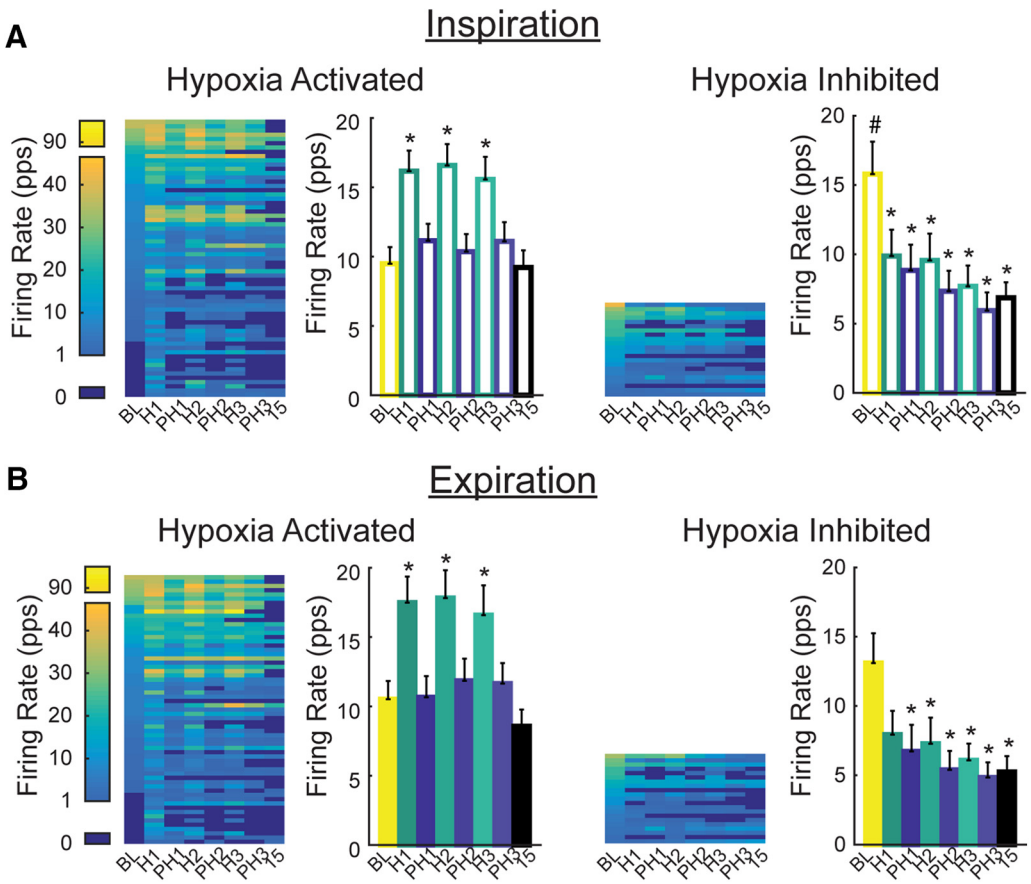

Figure 3. C-IN activity before, during, and following acute intermittent hypoxia. ***A***, ***B***, Firing rate heat maps summarizing firing rate of individual neurons and average firing rate (pulses per second) before, during, and 15 min post-AIH for hypoxia-activated and -inhibited neurons during inspiration (***A***, open bars) and expiration (***B***, shaded bars). For all heat maps, each row represents the firing rate of one C-IN and is organized according to BL firing rate. *Significantly different from BL. #Significantly different from hypoxia-activated BL.

identified as departures in the cross-correlation histogram >3 SD above the background (Aertsen and Gerstein, 1985; Melssen and Epping, 1987; Aertsen et al., 1989). Positive (Fig. 4*A*) and negative (Fig. 5*A*) correlogram features were taken as evidence for excitatory or inhibitory connectivity, respectively (Kirkwood, 1979; Aertsen and Gerstein, 1985). Heat maps derived from the cross-correlation analysis illustrate connectivity among C-IN pairs. For all heat maps, each row represents a pair of neurons. When no correlogram feature was detected the position in the matrix was colored dark purple; when a feature was present, the position was colored according the proportion of C-INs that showed a feature at that time point. Thus, the color of each column illustrates the proportion of functional connections observed at each time point. The proportion of positive correlogram features was expressed relative to the total number of possible connections (i.e., based on the total number of recorded cells at that time point).

The average proportion of excitatory connections is shown in Figure 4. During BL, excitatory connections were detected among 32% of C-IN pairs (Fig. 4*B*). When all C-INs with an excitatory connection were examined, we detected an increase in the average number of positive correlograms following hypoxia (PH1, PH2, PH3) compared with BL (41%, $p = 0.0177$). Excitatory connectivity was slightly elevated 15 min posthypoxia, but this did not reach the threshold for statistical significance ($p = 0.0763$ vs BL). Neuronal pairs for which a correlogram peak was present during one or more hypoxia or posthypoxia periods are summarized in Figure 4, *C* and *D*, respectively. In C-INs with positive correlogram features during hypoxia, the average number of excitatory connections was 19% at BL, and this was increased to 34% during hypoxia (Fig. 4*C*; $p < 0.0001$). In those neuronal pairs which showed positive correlogram features following hypoxia, the average number of excitatory connections was increased during the initial posthypoxia period (41%; $p < 0.0001$ vs BL) and remained increased 15 min post-AIH ($p = 0.0002$). These data show for the first time that AIH enhances excitatory connectivity among C-INs.

In contrast to the number of excitatory connections, comparatively few inhibitory connections (4%) were detected at BL (Fig. 5). Overall, the number of inhibitory connections did not change during hypoxia ($p = 0.6462$) or following hypoxia ($p = 0.0626$), but was significantly reduced at 15 min post-AIH ($p = 0.0439$). In C-INs functionally connected during hypoxia, the average number of inhibitory connections during hypoxia was increased to 34% compared with 19% at BL (Fig. 4*C*; $p = 0.0160$). No significant changes were detected in the subset of neurons that were functionally connected during at least one posthypoxia (Fig. 4*D*). These results indicate that inhibitory connections were enhanced in a subset of C-INs during hypoxia exposure, and reduced 15 min following the AIH paradigm. Together, these data show that AIH alters excitatory and inhibitory connectivity, leading to a more excited propriospinal network.

"Pre-phrenic" C-INs during AIH

In 8% of recordings, STA of the rectified phrenic nerve activity in relation to neuronal discharge produced a broad feature with a delay >1 ms (Fig. 6). This delay suggests that the cell was synap-

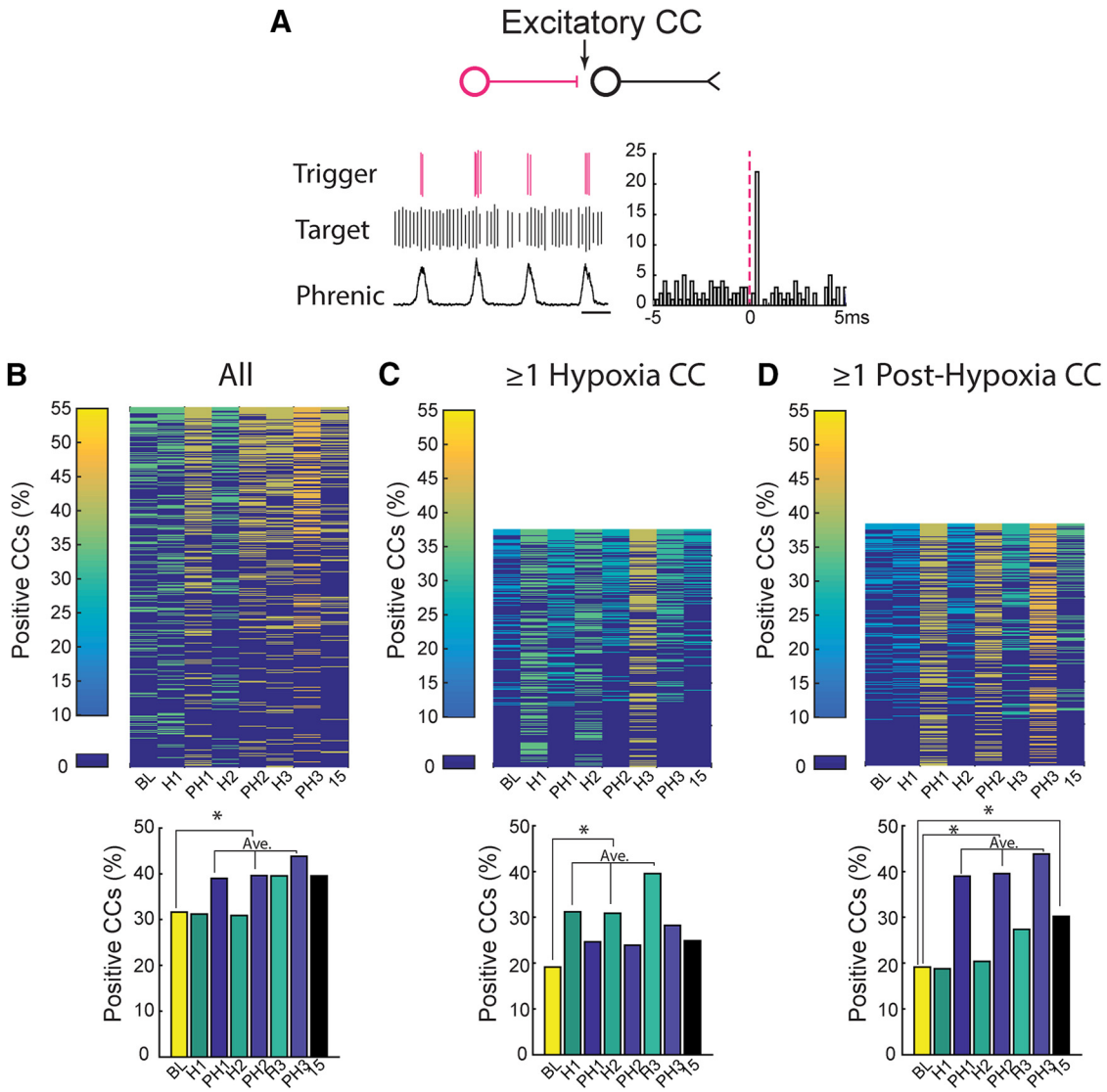

Figure 4. Excitatory connectivity of C-INs before, during, and following acute intermittent hypoxia. ***A***, Representative example of integrated phrenic output and activity from a pair of C-INs and resulting excitatory CC. ***B–D***, Using cross-correlation analysis, heat maps for excitatory correlograms were constructed before, during, and for 15 min post-AIH for all C-IN pairs. For all heat maps, each row represents a neuronal pair. When no correlogram feature was detected the position in the matrix was colored dark purple and when a feature was present, the position was colored according the proportion of C-INs that showed a feature at that time point. The color of each column represents the proportion of positive CCs (as a percentage of possible connections) during each time point. Neuronal pairs with a connection during at least one hypoxia (***C***), and neuronal pairs with a connection during at least one posthypoxia (***D***). The proportion of excitatory connections (as a percentage of possible connections) during each time point is shown below each heat map. *Significantly different from BL.

tically coupled to the phrenic motoneuron pool, as the latency is greater than synaptic delay (e.g., 1.0 ms; Borst et al., 1995); these neurons were classified as pre-phrenic C-INs (Lane et al., 2008). Offset STA peaks were taken as evidence of excitatory pre-phrenic C-INs (Fig. 6*A*), whereas offset troughs indicated inhibitory pre-phrenic C-INs (Fig. 6*B*). With this approach, a total of five excitatory and two inhibitory pre-phrenic interneurons were identified (Table 3). Of these seven cells, three were ipsilateral to the phrenic nerve in which the STA was detected. In addition, two excitatory and one inhibitory pre-phrenic interneuron produced an STA in the phrenic nerve contralateral to the recording location, consistent with a commissural connection. One inhibitory pre-phrenic interneuron was active during expiration produced an STA for both the left and right phrenic nerve, indicating it was functionally coupled to both the left and right phrenic motor pools. All excitatory pre-phrenic C-INs fired with either a tonic or inspiratory pattern (Fig. 6*C*), whereas both inhibitory pre-phrenic C-INs had an expiratory pattern (Fig. 6*D*). The average time to STA onset, and STA peak for excitatory and inhibitory pre-phrenic C-INs are shown in Figure 6, *E* and *F*, and was no different between groups (onset: $p = 0.6448$; peak: $p = 0.4236$).

We next identified C-INs that were functionally connected to pre-phrenic C-INs; these neurons were operationally defined as "second order" (Fig. 7). The relationship between the number of excitatory connections from second-order C-INs to either excitatory pre-phrenic neurons or inhibitory pre-phrenic neurons was quantified (Fig. 7*C*,*D*), and examined using linear regression (Fig. 7*E*,*F*). A strong, positive relationship was present between the number of excitatory connections ($n = 24$) from second-order neurons to excitatory pre-phrenic interneurons ($n = 5$) during ($R^2 = 0.982$; $p = 0.0091$), but not after hypoxia ($R^2 = 0.048$; $p = 0.7211$; Fig. 7*E*). We did not detect a sufficient number of inhibitory pre-phrenic interneurons ($n = 2$) to enable a similar statistical test, but data are shown in Figure 7*F*. These results

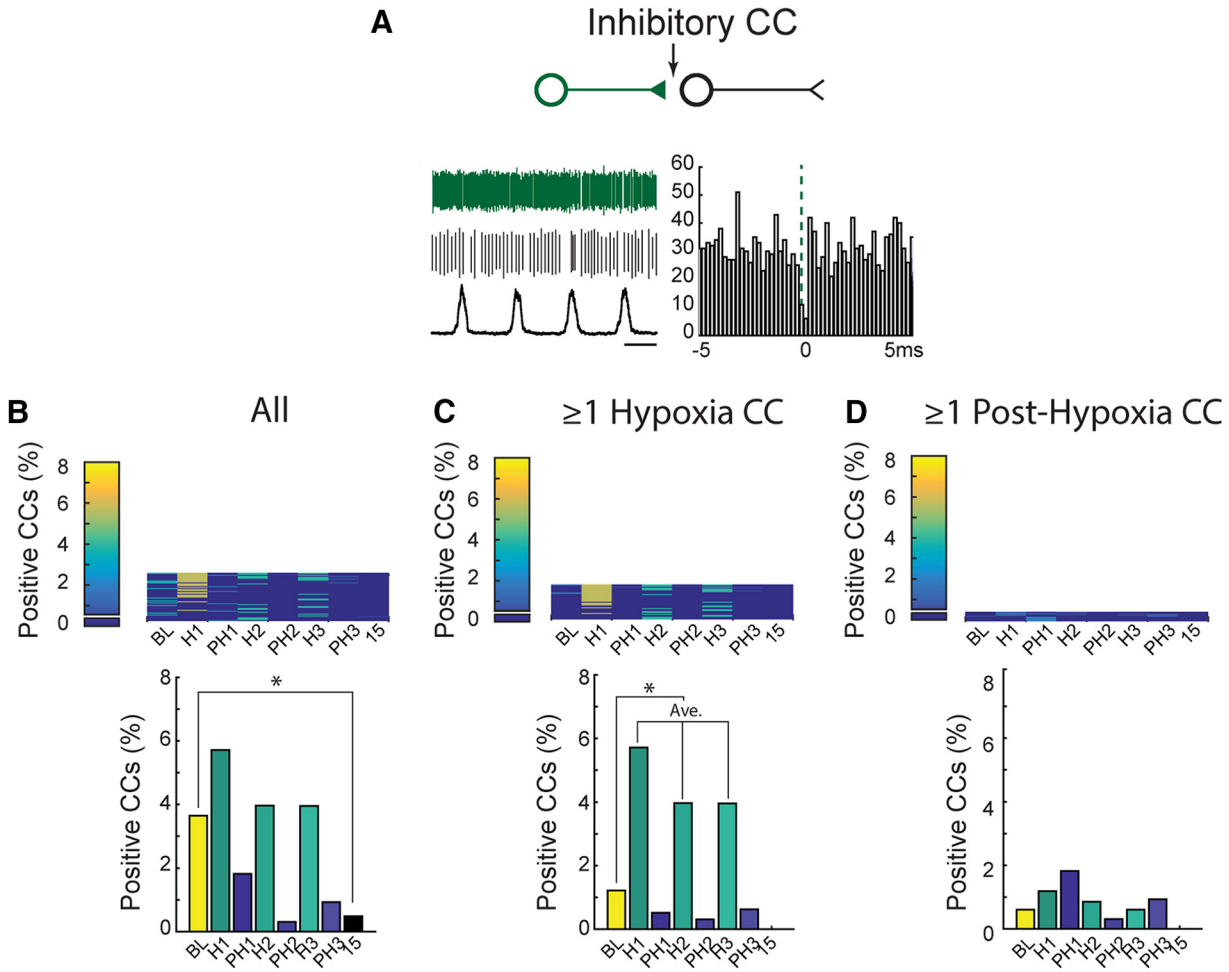

Figure 5. Inhibitory connectivity of C-INs before, during, and following acute intermittent hypoxia. ***A***, Representative example of integrated phrenic output and activity from a pair of C-INs and resulting inhibitory CC. ***B–D***, Using cross-correlation analysis, heat maps for inhibitory correlograms were constructed before, during, and 15 min post-AIH for all C-IN pairs. For all heat maps, each row represents a neuronal pair. When no correlogram feature was detected the position in the matrix was colored dark purple and when a feature was present, the position was colored according the proportion of C-INs that showed a feature at that time point. The color of each column represents the proportion of positive CCs (as a percentage of possible connections) during each time point. Neuronal pairs with a connection during at least one hypoxia (***C***), and neuronal pairs with a connection during at least one posthypoxia (***D***). The proportion of inhibitory connections (as a percentage of possible connections) during each time point is shown below each heat map. *Significantly different from BL.

provide evidence that the number of excitatory connections between C-INs and excitatory pre-phrenic interneurons is enhanced during hypoxia. Thus we conclude that C-INs are an integral part of the neural network that controls the diaphragm, and that the strength of synaptic connections in this network may be altered during and after AIH. A schematic summarizing the connections from second-order C-INs to excitatory and inhibitory pre-phrenic C-INs is shown in Figure 7, *G* and *H*.

Stratification of C-IN firing patterns according to the respiratory cycle

For a final evaluation, we phenotypically stratified C-INs as tonic (T), inspiratory (I), expiratory (E), or recruited (R) based on their BL discharge pattern (Fig. 8). Recruited neurons were defined as cells which were "off" (e.g., did not fire) during BL, but began firing at a later time point. In addition, a portion of C-INs was active during BL and turned off at a subsequent time point. Representative examples of the firing rate and cycle triggered histograms for phenotypically defined C-IN (e.g., T, I, E, and R) are shown in Figure 8, *A* and *B*.

We next examined whether bursting patterns are altered during or after AIH. Heat maps of C-IN firing patterns are shown in Figure 8*C*. For all heat maps, each row represented one neuron and its bursting pattern at defined by color. As illustrated by this figure, C-INs switch which respiratory phase they fire during in response to AIH defined as phase switching. In addition, some C-INs adopted a respiratory-related firing pattern (e.g., inspiratory/expiratory) in response to hypoxia. A summary of the number of C-INs across the experimental time points stratified by firing pattern is presented in Figure 8*C*. At each time point, the majority of recorded C-INs (54 ± 2) fired tonically through the respiratory cycle. The average number of C-INs with an inspiratory firing pattern was similar during hypoxia (12 ± 2) compared with posthypoxia (13 ± 1). In contrast, a greater number of expiratory neurons were active during each bout of hypoxia (10 ± 2) compared with posthypoxia (5 ± 0). On average, more C-INs (80 ± 2) were active during hypoxia than posthypoxia (72 ± 3), indicating C-INs were recruited during hypoxic episodes.

The approximate anatomical location of each recording was determined using the micromotor coordinates of each electrode. These data were used to create a map of the locations of each cell in respect to the firing patterns across the experiment (Fig. 9). These images show the recording locations spanned the gray mat-

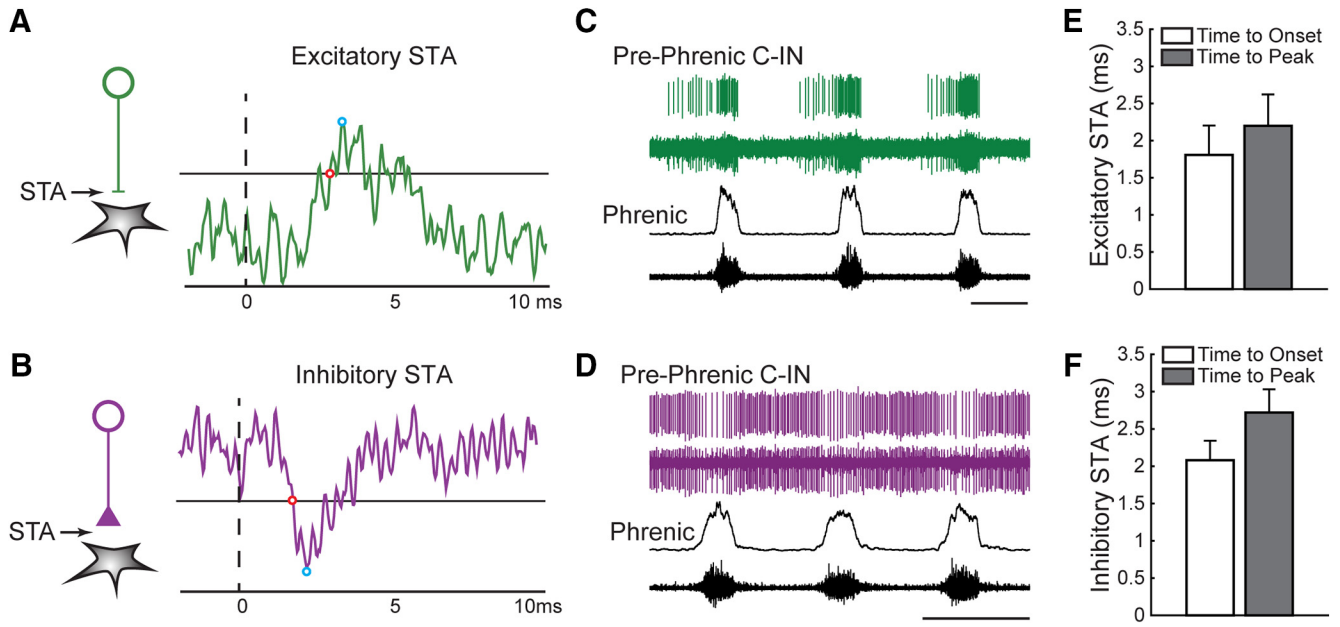

Figure 6. Pre-phrenic C-INs synaptically coupled to phrenic motoneurons. ***A***, ***B***, Representative STA of the rectified phrenic nerve activity in relation to neuronal discharge depicting a broad peak (***A***) and trough (***B***) with a latency >1 ms and > 2SD from the mean activity (solid line). Open red circle denotes STA onset, open blue circle denotes STA peak. ***C***, ***D***, Raw pre-phrenic C-IN and sorted spikes and raw and integrated phrenic nerve activity from an excitatory (***C***) and inhibitory (***D***) pre-phrenic C-IN used to construct STAs in ***A*** and ***B***, respectively. ***E***, ***F***, Average time between pre-phrenic discharge and STA onset (ms) and STA peak (ms) for excitatory (***E***) and inhibitory (***F***) pre-phrenic C-INs. Scale bar, 1 s.

Table 3. Summary of excitatory and inhibitory pre-phrenic C-INs bursting pattern, time point in which the neuron was active, and presence of a STA of the rectified ipsilateral and/or contralateral phrenic nerve activity in relation to neuronal discharge

	Firing pattern	Time with activity	Ipsilateral STA	Contralateral STA
Excitatory	Tonic	All	X	
	Tonic	All		X
	Tonic	H1		X
	Inspiratory	All	X	
	Inspiratory	PH1, PH2, PH3, 15 min	X	
Inhibitory	Expiratory	All		X
	Expiratory	All	X	X

ter and show little stratification with regard to C-IN busting pattern. Of note, tonic C-INs showed the greatest dorsal ventral distribution and phrenic motoneurons were located ventral to C-INs.

Discussion

Here we demonstrate that the incidence of excitatory and inhibitory connectivity among C-INs was persistently altered by AIH, indicating AIH induces plasticity in the propriospinal network. Specifically, following AIH we detected a sustained decrease in inhibitory connections as well as increase in excitatory connectivity between C-INs. Successive bouts of hypoxia also caused a progressive increase in the incidence of excitatory connections to C-INs which were synaptically coupled to phrenic motoneurons (i.e., pre-phrenic C-INs). Collectively, the comprehensive evaluation of C-IN bursting presented herein leads us to conclude that the spinal impact of AIH extends beyond motoneurons. AIH-induced alterations in C-IN discharge and associated changes in propriospinal network connectivity may contribute to respiratory, somatic, or autonomic responses and to neuroplastic changes in these motor outputs.

C-INs and hypoxia

In the midcervical spinal cord, C-INs show both inspiratory- and expiratory-related discharge (Palisses et al., 1989; Bellingham and Lipski, 1990; Iscoe and Duffin, 1996). We observed respiratory-related C-IN discharge, but also a high prevalence of tonic firing C-INs, some of which were synaptically coupled to phrenic motoneurons. In regards to hypoxia, we previously reported changes in both the rate and pattern of C-IN discharge. Specifically, following a single hypoxic episode, 40% of the recorded C-INs continued to fire at rates above prehypoxia values (Sandhu et al., 2015) and 29% altered their discharge pattern during or following hypoxia (Streeter et al., 2017). Here we observed that >90% of recorded C-INs had altered firing rates during or following hypoxia. We also provide the following new information regarding C-IN phenotype and the response to hypoxia. First, baseline C-IN firing rate was significantly different between cells which were activated versus inhibited during hypoxia, indicating the initial discharge pattern may predict the response to hypoxia exposure. Second, following AIH cells which were activated by hypoxia rapidly returned to BL firing rate, whereas C-INs which were inhibited by hypoxia had persistent decreases in firing rate, suggesting AIH has a differential impact on populations of C-INs. Last, we noted that C-INs which were initially active across the entire respiratory cycle (i.e., tonic) can rapidly switch to a respiratory-related firing pattern (e.g., inspiratory/expiratory) upon exposure to hypoxia. This provides further evidence that the cervical propriospinal network is responding to hypoxia in a manner that is coordinated with the respiratory network. Overall, the data indicate that hypoxia responsiveness is a general property of C-INs, but that this can manifest in numerous ways.

The mechanisms which cause C-INs to alter their firing rate and pattern in response to hypoxia are unknown, but several potential explanations are available. C-INs receive synaptic input from brainstem nuclei associated with both respiratory (Fedorko et al., 1983; Davies et al., 1985; Hayashi et al., 2003; Lane et al., 2008) and sympathetic control (Guyenet, 2000). These brainstem

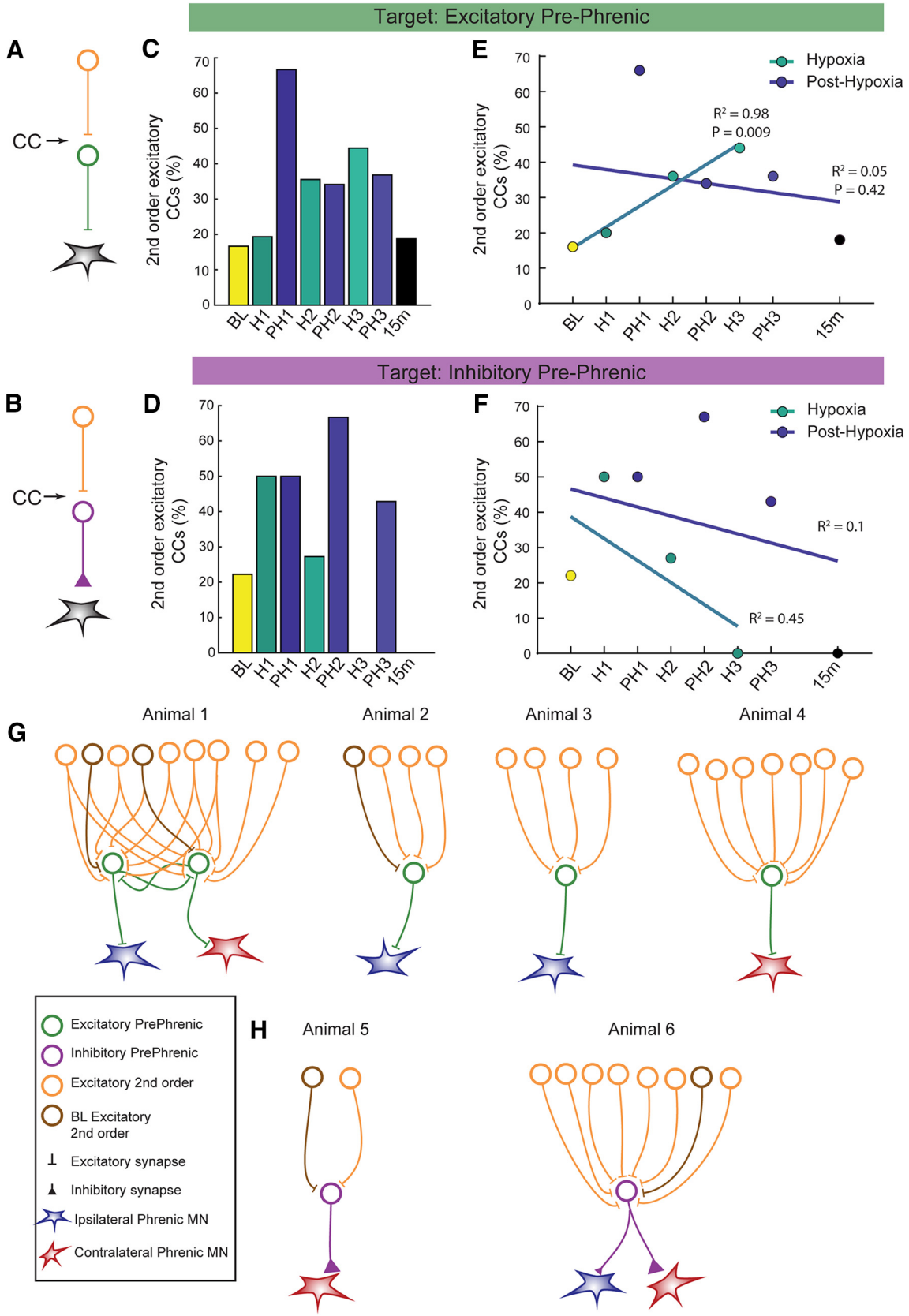

Figure 7. C-INs temporally linked to pre-phrenic neurons before, during, and following acute intermittent hypoxia. ***A***, ***B***, Schematic of second-order excitatory C-IN projecting to excitatory pre-phrenic (***A***) and inhibitory pre-phrenic C-IN (***B***). ***C***, ***D***, Excitatory C-INs (as a percentage of possible connections) temporally linked to excitatory pre-phrenic C-INs (***C***) and inhibitory (***D***) pre-phrenic C-INs. ***E***, ***F***, Linear regression analysis of the proportion of second-order excitatory connections to excitatory (***E***) and inhibitory (***F***) pre-phrenic C-INs. ***G***, ***H***, Schematic summarizing second-order excitatory C-INs projecting to excitatory (***G***) and inhibitory (***H***) pre-phrenic interneurons at BL (brown) and recruited (orange) during intermittent hypoxia.

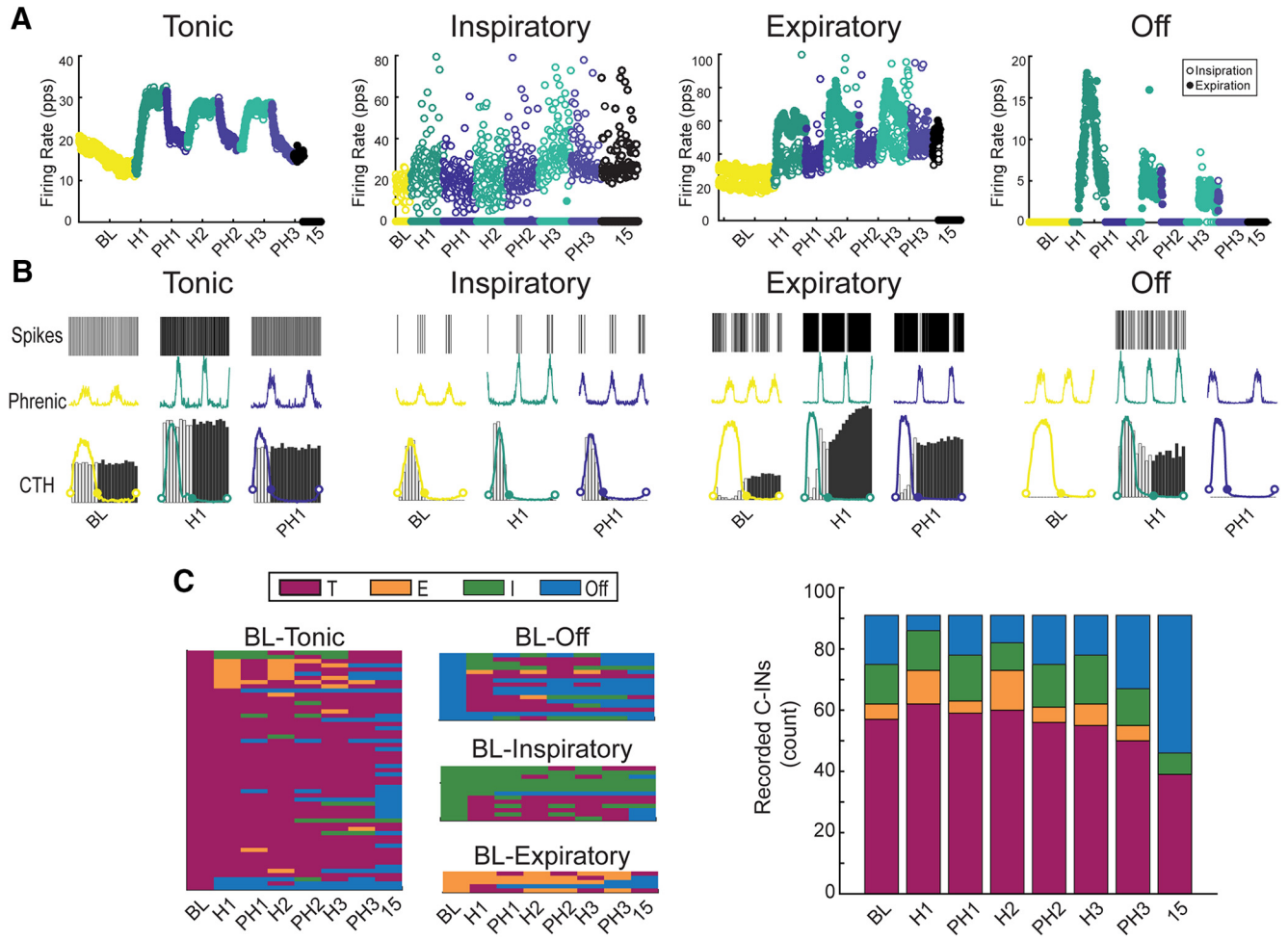

Figure 8. Characterization of C-IN firing patterns before, during, and following acute intermittent hypoxia. ***A***, Representative examples of the firing rate (pulses per second) during inspiration (open circles) and expiration (filled circles) of phenotypically stratified C-INs (e.g., T, I, E, and off) before, during, and 15 min post-AIH. ***B***, Representative examples of C-INs firing patterns depicting sorted spikes (top trace), integrated phrenic nerve output (middle trace), and cycle-triggered histogram (CTH; bottom trace) during 50 consecutive breaths overlaid with the average integrated phrenic waveform. Open circles denote the beginning of the inspiratory phase; closed circles denote the end of the inspiratory phase/beginning of the expiratory phase. Open bars in CTH depict activity during the inspiratory phase and shaded bars depict activity during the expiratory phase. ***C***, Heat maps summarizing firing patterns before, during, and 15 min post-AIH. For all heat maps, each row represents one neuron and are organized according to BL cell type (T, E, I, off). Stacked bar graph depicts the number of C-INs with each firing pattern before, during, and 15 min post-AIH and posthypoxia.

regions are robustly activated by hypoxia (Hirooka et al., 1997), and may therefore drive the C-IN response via bulbospinal synaptic inputs. The observed switch from tonic to phasic respiratory bursting during hypoxia indicates that at least a subset of C-INs are receiving synaptic inputs related to the endogenous respiratory cycle. An alternative possibility is that C-INs directly sense oxygen. Indeed, oxygen-sensing neurons are found in various brain regions (Neubauer and Sunderram, 2004), and recent evidence suggests a subpopulation of C-INs sense changes in oxygen in lieu of brainstem input (Wilson et al., 2015).

Pre-phrenic C-INs

Several laboratories have suggested that C-INs are functionally connected to phrenic motoneurons (Palisses et al., 1989; Bellingham and Lipski, 1990; Douse and Duffin, 1993; Sandhu et al., 2009). Neuroanatomical evidence indicates that pre-phrenic C-INs have the potential to relay information from medullary neurons to phrenic motoneurons (Lane et al., 2008), or serve as spinal commissural connections (Lois et al., 2009). Our data are consistent with both suggestions because we show pre-phrenic C-INs can modulate ipsilateral and contralateral phrenic output. We add to our current understanding of pre-phrenic C-INs by showing both excitatory and inhibitory inputs to phrenic motoneurons. Whereas excitatory pre-phrenic C-INs fired with either a tonic pattern, or burst in phase with inspiration, inhibitory pre-phrenic C-INs had an expiratory firing pattern. In the medulla, pre-inspiratory/inspiratory neurons (i.e., those that start before and continue firing into inspiration) are critical for respiratory rhythm generation (Smith et al., 2013). Whether inspiratory pre-phrenic C-INs have rhythmogenic properties is unknown, but there is evidence suggesting that spinal networks can produce oscillations in phrenic output (Viala and Freton, 1983). The pre-phrenic C-IN data presented here support the hypothesis that the cervical propriospinal network is capable of modulating the output of the phrenic motor nucleus on a breath-by-breath basis.

Our data also show that AIH alters the effective connections between second-order excitatory C-INs and pre-phrenic C-INs. Thus, AIH may trigger *de novo* recruitment of C-INs into propriospinal network which is coupled to the phrenic motor nucleus. Due to the short time scale in which this occurs, this likely reflects activation of existing, but previously silent synaptic connec-

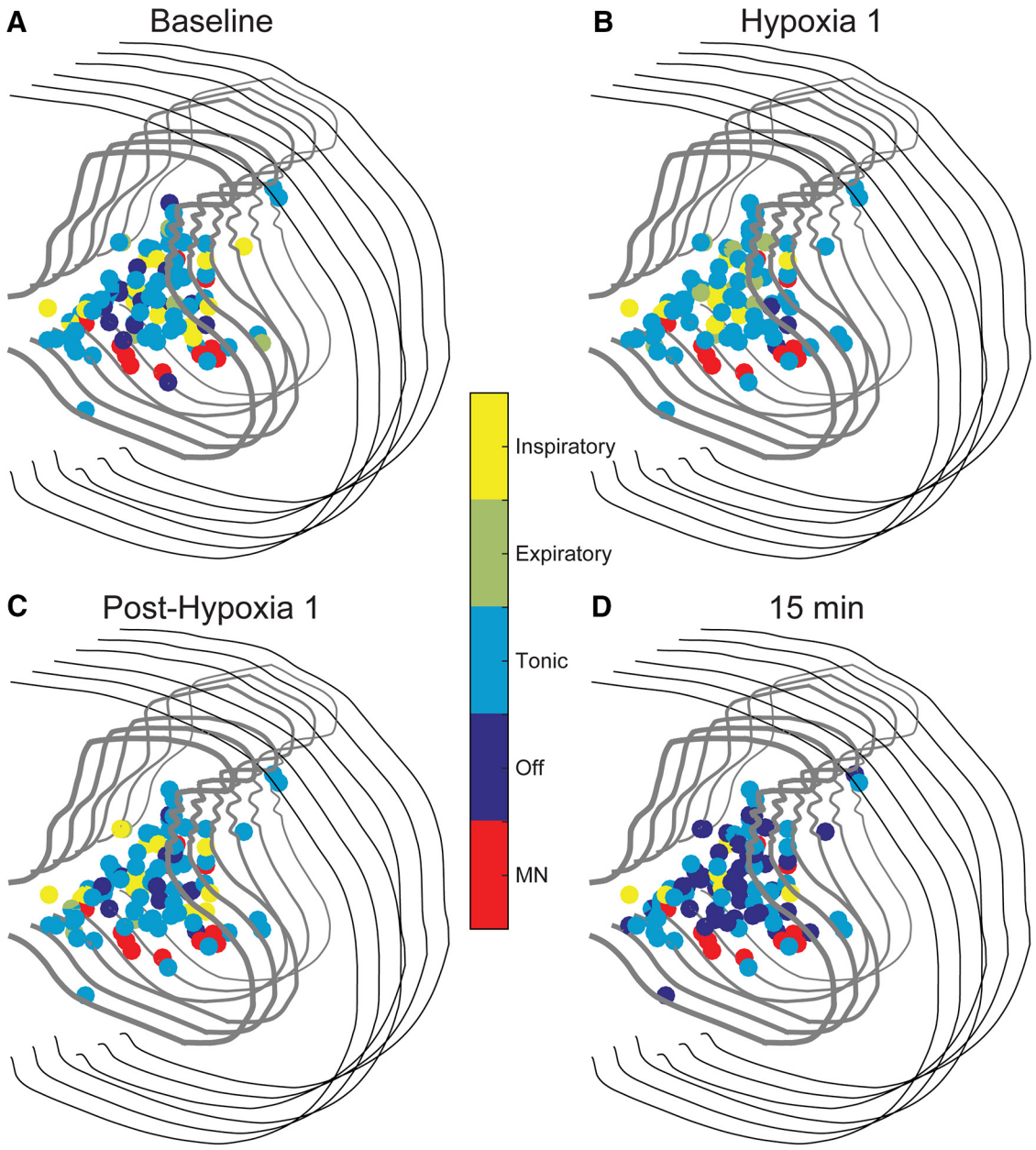

Figure 9. Locations of recorded neurons stratified by firing pattern. ***A–D***, Summary of locations of recorded C-INs and phrenic motoneurons (MN) during BL (***A***), hypoxia 1 (***B***), posthypoxia 1 (***C***), and 15 min post-AIH (***D***).

tions. One established mechanism underlying this phenomenon is serotonin release (Li and Zhuo, 1998). Several prior studies show that serotonin can rapidly activate polysynaptic spinal pathways to phrenic motoneurons (Mitchell et al., 1992; Ling et al., 1994). Because serotonin is released during hypoxia (Kinkead et al., 2001), we hypothesize that serotonin may be involved in shaping the response of the cervical propriospinal network to AIH.

AIH, C-INs, and spinal cord plasticity

AIH induces plasticity in sympathetic (Dick et al., 2007), somatic (Lovett-Barr et al., 2012; Trumbower et al., 2012), and respiratory motor output (Baker et al., 2001). To date, studies of AIH-induced spinal plasticity have primarily used recordings of nerve and/or muscle activity as outcome measures, but provide little to no insight regarding propriospinal networks. Data from Mitchell and colleagues suggest that AIH-induced phrenic motor plasticity requires mechanisms within phrenic motoneurons. Specifically, delivery of relevant siRNA molecules (e.g., TrkB or PKCθ) to the intrapleural space and subsequent knockdown of TrkB or PKCθ in phrenic motoneurons attenuates AIH-induced plasticity (Devinney et al., 2015; Dale et al., 2017). These observations indicate that motoneuron plasticity is a fundamental component of the response to AIH, but do not preclude a role for C-INs in the expression of phrenic motor plasticity. Our data confirm that the cervical propriospinal network is responding to acute hypoxia, and show persistent changes in network excitability post-AIH. C-INs may therefore be a fundamental part of the neural substrate driving AIH-induced motor plasticity in respiratory and other systems. There is precedent that chemoafferent stimulation can alter network connectivity in brainstem structures. Specifically, Morris et al. (2000) showed that carotid chemoreceptor stimulation (i.e., mimicking hypoxia) can alter synaptic connec-

tions in medullary neural networks. However, our data are the first to show that changes in excitatory and inhibitory connectivity among C-INs are evoked by AIH. Determining the functional impact of these changes is challenging due to the complexity of propriospinal networks (Jankowska, 2001), and likely will require genetic and/or viral approaches to selectively inhibit or activate specific populations of C-INs. However, based on the current data showing rapid and sustained changes in propriospinal connectivity, we propose that that C-INs are an integral part of the neuronal substrate orchestrating the respiratory, somatic, and autonomic neuroplastic responses to AIH.

Significance

It is well established that propriospinal neurons play a critical role in shaping motor output along the spinal neuraxis (Cherniak et al., 2017). In regards to the cervical spinal cord and breathing, prior work establishes that some C-INs are synaptically coupled to spinal respiratory motoneurons (Lane, 2011), and that C-INs can show respiratory-related discharge patterns. However, the functional impact of the cervical propriospinal network on phrenic (diaphragm) motor output is less clear. In this context, the current data establish a few significant points. First, AIH can cause persistent changes in connectivity within the overall propriospinal network. AIH is firmly established to be a powerful trigger of spinal respiratory neuroplasticity (Fuller and Mitchell, 2017), and these results indicate that C-INs are an important component of the neuroplastic response to AIH. This may be particularly important in the context of using AIH as a "neurorehabilitation modality" (Gonzalez-Rothi et al., 2015), because AIH exposure can promote functional recovery of respiratory as well as nonrespiratory motor output following spinal cord injury in animal models and humans (Trumbower et al., 2012; Hayes et al., 2014; Tester et al., 2014; Gonzalez-Rothi et al., 2015). Indeed, remodeling of propriospinal networks is an important component of motor recovery after incomplete spinal cord injury (Bareyre et al., 2004) and AIH may facilitate this process. Second, these data show that C-INs which are pre-phrenic (i.e., synaptically coupled to phrenic motoneurons) have excitatory and inhibitory inputs to phrenic motoneurons, and that excitatory input to excitatory C-INs increases during AIH. Thus, C-INs may have a more important role in controlling the phrenic motor pool and the diaphragm than is currently appreciated. Together, our data indicate that the midcervical spinal cord contains a network that responds dynamically to acute hypoxia, and that AIH alters the overall connectivity of the interneuronal network.

References

Aertsen AM, Gerstein GL (1985) Evaluation of neuronal connectivity: sensitivity of cross-correlation. Brain Res 340:341–354. CrossRef Medline

Aertsen AM, Gerstein GL, Habib MK, Palm G (1989) Dynamics of neuronal firing correlation: modulation of "effective connectivity". J Neurophysiol 61:900–917. Medline

Baker TL, Fuller DD, Zabka AG, Mitchell GS (2001) Respiratory plasticity: differential actions of continuous and episodic hypoxia and hypercapnia. Respir Physiol 129:25–35. CrossRef Medline

Bareyre FM, Kerschensteiner M, Raineteau O, Mettenleiter TC, Weinmann O, Schwab ME (2004) The injured spinal cord spontaneously forms a new intraspinal circuit in adult rats. Nat Neurosci 7:269–277. CrossRef Medline

Bavis RW, Mitchell GS (2003) Intermittent hypoxia induces phrenic long-term facilitation in carotid-denervated rats. J Appl Physiol 94:399–409. CrossRef Medline

Bellingham MC, Lipski J (1990) Respiratory interneurons in the C5 segment of the spinal cord of the cat. Brain Res 533:141–146. CrossRef Medline

Borst JG, Helmchen F, Sakmann B (1995) Pre- and postsynaptic whole-cell recordings in the medial nucleus of the trapezoid body of the rat. J Physiol 489:825–840. CrossRef Medline

Cherniak M, Anglister L, Lev-Tov A (2017) Shaping the output of lumbar flexor motoneurons by sacral neuronal networks. J Neurosci 37:1294–1311. CrossRef Medline

Dale EA, Fields DP, Devinney MJ, Mitchell GS (2017) Phrenic motor neuron TrkB expression is necessary for acute intermittent hypoxia-induced phrenic long-term facilitation. Exp Neurol 287:130–136. CrossRef Medline

Davies JG, Kirkwood PA, Sears TA (1985) The detection of monosynaptic connexions from inspiratory bulbospinal neurones to inspiratory motoneurones in the cat. J Physiol 368:33–62. CrossRef Medline

Devinney MJ, Fields DP, Huxtable AG, Peterson TJ, Dale EA, Mitchell GS (2015) Phrenic long-term facilitation requires PKCθ activity within phrenic motor neurons. J Neurosci 35:8107–8117. CrossRef Medline

Dick TE, Hsieh YH, Wang N, Prabhakar N (2007) Acute intermittent hypoxia increases both phrenic and sympathetic nerve activities in the rat. Exp Physiol 92:87–97. CrossRef Medline

Douse MA, Duffin J (1993) Axonal projections and synaptic connections of C5 segment expiratory interneurones in the cat. J Physiol 470:431–444. CrossRef Medline

Fedorko L, Merrill EG, Lipski J (1983) Two descending medullary inspiratory pathways to phrenic motoneurones. Neurosci Lett 43:285–291. CrossRef Medline

Fuller DD, Mitchell GS (2017) Respiratory neuroplasticity: overview, significance and future directions. Exp Neurol 287:144–152. CrossRef Medline

Gonzalez-Rothi EJ, Lee KZ, Dale EA, Reier PJ, Mitchell GS, Fuller DD (2015) Intermittent hypoxia and neurorehabilitation. J Appl Physiol (1985) :jap 00235 02015.

Guyenet PG (2000) Neural structures that mediate sympathoexcitation during hypoxia. Respir Physiol 121:147–162. CrossRef Medline

Hayashi F, Hinrichsen CF, McCrimmon DR (2003) Short-term plasticity of descending synaptic input to phrenic motoneurons in rats. J Appl Physiol 94:1421–1430. CrossRef Medline

Hayes HB, Jayaraman A, Herrmann M, Mitchell GS, Rymer WZ, Trumbower RD (2014) Daily intermittent hypoxia enhances walking after chronic spinal cord injury: a randomized trial. Neurology 82:104–113. CrossRef Medline

Hazra A, Gogtay N (2016) Biostatistics series module 4: comparing groups–categorical variables. Indian J Dermatol 61:385–392. CrossRef Medline

Hirooka Y, Polson JW, Potts PD, Dampney RA (1997) Hypoxia-induced Fos expression in neurons projecting to the pressor region in the rostral ventrolateral medulla. Neuroscience 80:1209–1224. CrossRef Medline

Hodson-Tole EF, Wakeling JM (2009) Motor unit recruitment for dynamic tasks: current understanding and future directions. J Comp Physiol B 179:57–66. CrossRef Medline

Iscoe S, Duffin J (1996) Effects of stimulation of phrenic afferents on cervical respiratory interneurones and phrenic motoneurones in cats. J Physiol 497:803–812. CrossRef Medline

Jankowska E (2001) Spinal interneuronal systems: identification, multifunctional character and reconfigurations in mammals. J Physiol 533:31–40. CrossRef Medline

Jankowska E, Hammar I (2002) Spinal interneurones; how can studies in animals contribute to the understanding of spinal interneuronal systems in man? Brain Res Brain Res Rev 40:19–28. CrossRef Medline

Kinkead R, Bach KB, Johnson SM, Hodgeman BA, Mitchell GS (2001) Plasticity in respiratory motor control: intermittent hypoxia and hypercapnia activate opposing serotonergic and noradrenergic modulatory systems. Comp Biochem Physiol A Mol Integr Physiol 130:207–218. CrossRef Medline

Kirkwood PA (1979) On the use and interpretation of cross-correlation measurements in the mammalian central nervous system. J Neurosci Methods 1:107–132. CrossRef Medline

Lane MA (2011) Spinal respiratory motoneurons and interneurons. Respir Physiol Neurobiol 179:3–13. CrossRef Medline

Lane MA, White TE, Coutts MA, Jones AL, Sandhu MS, Bloom DC, Bolser DC, Yates BJ, Fuller DD, Reier PJ (2008) Cervical prephrenic interneurons in the normal and lesioned spinal cord of the adult rat. J Comp Neurol 511:692–709. CrossRef Medline

Lanuza GM, Gosgnach S, Pierani A, Jessell TM, Goulding M (2004) Genetic identification of spinal interneurons that coordinate left-right locomotor activity necessary for walking movements. Neuron 42:375–386. CrossRef Medline

Lee KZ, Fuller DD (2011) Neural control of phrenic motoneuron discharge. Respir Physiol Neurobiol 179:71–79. CrossRef Medline

Li P, Zhuo M (1998) Silent glutamatergic synapses and nociception in mammalian spinal cord. Nature 393:695–698. CrossRef Medline

Lindsey BG, Hernandez YM, Morris KF, Shannon R (1992) Functional connectivity between brain stem midline neurons with respiratory-modulated firing rates. J Neurophysiol 67:890–904. Medline

Ling L, Bach KB, Mitchell GS (1994) Serotonin reveals ineffective spinal pathways to contralateral phrenic motoneurons in spinally hemisected rats. Exp Brain Res 101:35–43. Medline

Lipski J, Kubin L, Jodkowski J (1983) Synaptic action of $R_{[beta]}$ neurons on phrenic motoneurons studied with spike-triggered averaging. Brain Res 288:105–118. CrossRef Medline

Lois JH, Rice CD, Yates BJ (2009) Neural circuits controlling diaphragm function in the cat revealed by transneuronal tracing. J Appl Physiol 106: 138–152. CrossRef Medline

Lovett-Barr MR, Satriotomo I, Muir GD, Wilkerson JE, Hoffman MS, Vinit S, Mitchell GS (2012) Repetitive intermittent hypoxia induces respiratory and somatic motor recovery after chronic cervical spinal injury. J Neurosci 32:3591–3600. CrossRef Medline

Melssen WJ, Epping WJ (1987) Detection and estimation of neural connectivity based on crosscorrelation analysis. Biol Cybern 57:403–414. CrossRef Medline

Mitchell GS, Sloan HE, Jiang C, Miletic V, Hayashi F, Lipski J (1992) 5-Hydroxytryptophan (5-HTP) augments spontaneous and evoked phrenic motoneuron discharge in spinalized rats. Neurosci Lett 141:75–78. CrossRef Medline

Moore GP, Segundo JP, Perkel DH, Levitan H (1970) Statistical signs of synaptic interaction in neurons. Biophys J 10:876–900. CrossRef Medline

Morris KF, Baekey DM, Shannon R, Lindsey BG (2000) Respiratory neural activity during long-term facilitation. Respir Physiol 121:119–133. CrossRef Medline

Neubauer JA, Sunderram J (2004) Oxygen-sensing neurons in the central nervous system. J Appl Physiol 96:367–374. CrossRef Medline

Nichols NL, Gowing G, Satriotomo I, Nashold LJ, Dale EA, Suzuki M, Avalos P, Mulcrone PL, McHugh J, Svendsen CN, Mitchell GS (2013) Intermittent hypoxia and stem cell implants preserve breathing capacity in a rodent model of amyotrophic lateral sclerosis. Am J Respir Crit Care Med 187:535–542. CrossRef Medline

Nichols NL, Satriotomo I, Harrigan DJ, Mitchell GS (2015) Acute intermittent hypoxia induced phrenic long-term facilitation despite increased SOD1 expression in a rat model of ALS. Exp Neurol 273:138–150. CrossRef Medline

Palisses R, Perségol L, Viala D (1989) Evidence for respiratory interneurones in the C3–C5 cervical spinal cord in the decorticate rabbit. Exp Brain Res 78:624–632. Medline

Poree LR, Schramm LP (1992) Interaction between medullary and cervical regulation of renal sympathetic activity. Brain Res 599:297–301. CrossRef Medline

Renshaw B (1941) Influence of discharge of motoneurons upon excitation of neighboring motoneurons. J Neurophysiol 4:167–183.

Sandhu MS, Dougherty BJ, Lane MA, Bolser DC, Kirkwood PA, Reier PJ, Fuller DD (2009) Respiratory recovery following high cervical hemisection. Respir Physiol Neurobiol 169:94–101. CrossRef Medline

Sandhu MS, Baekey DM, Maling NG, Sanchez JC, Reier PJ, Fuller DD (2015) Midcervical neuronal discharge patterns during and following hypoxia. J Neurophysiol 113:2091–2101. CrossRef Medline

Smith JC, Abdala AP, Borgmann A, Rybak IA, Paton JF (2013) Brainstem respiratory networks: building blocks and microcircuits. Trends Neurosci 36:152–162. CrossRef Medline

Stepien AE, Tripodi M, Arber S (2010) Monosynaptic rabies virus reveals premotor network organization and synaptic specificity of cholinergic partition cells. Neuron 68:456–472. CrossRef Medline

Streeter KA, Sunshine MD, Patel SR, Liddell SS, Denholtz LE, Reier PJ, Fuller DD, Baekey DM (2017) Coupling multi-electrode array recordings with silver labeling of recording sites to study cervical spinal network connectivity. J Neurophysiol 117:1014–1029. CrossRef Medline

Tester NJ, Fuller DD, Fromm JS, Spiess MR, Behrman AL, Mateika JH (2014) Long-term facilitation of ventilation in humans with chronic spinal cord injury. Am J Respir Crit Care Med 189:57–65. CrossRef Medline

Trumbower RD, Jayaraman A, Mitchell GS, Rymer WZ (2012) Exposure to acute intermittent hypoxia augments somatic motor function in humans with incomplete spinal cord injury. Neurorehabil Neural Repair 26:163–172. CrossRef Medline

Viala D, Freton E (1983) Evidence for respiratory and locomotor pattern generators in the rabbit cervico-thoracic cord and for their interactions. Exp Brain Res 49:247–256. Medline

Wilson R, Derakhshan F, Roy A, Baghdadwala M, McDonald F, Scheibli E, Harris M, Dutschmann M (2015) Spinal oxygen sensors (SOS) drive sympathetic activity that precedes, predicts and outlives phrenic gasps during hypoxia in the absence of the brainstem. FASEB J 29:859.7.

Contents lists available at ScienceDirect

Experimental Neurology

journal homepage: www.elsevier.com

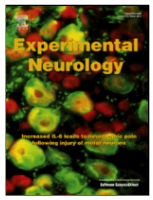

Research Paper

Intraspinal microstimulation for respiratory muscle activation

Michael D. Sunshine[a, b, c, *, 1], Comron N. Ganji[a, b], Paul J. Reier[d], David D. Fuller[c, e], Chet T. Moritz[a, b, f, g]

[a] Rehabilitation Medicine, University of Washington, Seattle, WA, United States
[b] Center for Sensorimotor Neural Engineering (CSNE), Seattle, WA, United States
[c] Physical Therapy and McKnight Brain Institute, University of Florida, Gainesville, FL, United States
[d] Neuroscience, University of Florida, Gainesville, FL, United States
[e] Center for Respiratory Research and Rehabilitation, University of Florida, Gainesville, FL, United States
[f] Physiology & Biophysics, University of Washington, Seattle, WA, United States
[g] University of Washington Institute for Neuroengineering (UWIN), University of Washington, Seattle, WA, United States

ARTICLE INFO

Keywords:
Intraspinal microstimulation
Respiration
Phrenic motoneurons

ABSTRACT

A complex propriospinal network is synaptically coupled to phrenic and intercostal motoneurons, and this makes it difficult to predict how gray matter intraspinal microstimulation (ISMS) will recruit respiratory motor units. We therefore mapped the cervical and high thoracic gray matter at locations ~~which~~ ISMS activates diaphragm (DIA) and external intercostal (EIC) motor units. Respiratory muscle electromyography (EMG) was recorded in anesthetized female spinally intact adult rats while a stimulating electrode was advanced ventrally into the spinal cord in 600 μm increments. At each depth, single biphasic stimuli were delivered at 10–90 μA during both the inspiratory and expiratory phase independently. Twenty electrode tracks were made from C2-T1 at medial and lateral gray matter locations. During inspiration, ISMS evoked DIA and EIC activity throughout C2-T1 gray matter locations, with mutual activation occurring at 17 ± 9% of sites. During inspiratory phase ISMS the average latency for DIA activation was 4.40 ± 0.70 ms. During the expiratory phase, ISMS-induced DIA activation required electrodes to be in close proximity to the phrenic motoneuron pool, and average activation latency was 3.30 ± 0.50 ms. We conclude that appropriately targeted ISMS can co-activate DIA and EIC motor units, and endogenous respiratory drive has a powerful impact on ISMS-induced respiratory motor unit activation. ~~The~~ long latency diaphragm motor unit activation ~~latency~~ suggests the presence of a complex propriospinal network that can modulate phrenic motor output.

1. Introduction

Intraspinal microstimulation (ISMS) of gray matter is a technique in which microwires are placed into the spinal cord and microampere electrical currents are used to activate spinal neurons. ISMS was pioneered as a potential treatment following spinal cord injury (SCI) or other central nervous system injury. The method can directly produce forelimb (Moritz et al., 2007; Nishimura et al., 2013; Sunshine et al., 2013; Zimmermann and Jackson, 2014) or hindlimb movement (Giszter et al., 1993; Lemay and Grill, 2004; Mushahwar et al., 2000; Tresch and Bizzi, 1999) and can also trigger neuroplasticity associated with restoration of limb function (Kasten et al., 2013; McPherson et al., 2015). ISMS has also been used to restore autonomic function following SCI in humans (Nashold et al., 1981).

A particular advantage of ISMS is that selectively placed microwires can activate intraspinal networks (Jankowska and Roberts, 1972) which produce coordinated or "synergistic" patterns of muscle activation (Mushahwar et al., 2002; Sunshine et al., 2013). These synergies have also been termed "motor primitives" that enable co-active muscle groups to be recruited simultaneously (Overduin et al., 2014). ISMS can also activate entire motor pools via activation of sensory afferent neurons (Gaunt et al., 2006) and has the distinct advantage of evoking natural recruitment order (Mushahwar and Horch, 1998) and activating fatigue resistant muscle fibers (Bamford et al., 2005). Collectively, the literature establishes that ISMS can effectively activate forelimbs and hindlimbs, in coordinated patterns of muscle activation. To date, however, the impact of ISMS on respiratory muscle activation has not been systematically evaluated throughout the cervical and high thoracic cord regarding co-activation. Prior work establishes that intraspinal stimulation in the mid- to high cervical spinal cord can evoke

Abbreviations: ISMS, intraspinal microstimulation; DIA, diaphragm; EIC, external intercostal; SCM, sternocleidomastoid; WGA, wheat germ agglutinin; StTA, stimulus triggered average.

* Corresponding author at: Department of Rehabilitation Medicine, University of Washington, Seattle, WA 98195, United States.
Email address: mdsunshi@ufl.edu (M.D. Sunshine)
[1] Graduate Student, Rehabilitation Sciences PhD ProgramDepartment of Physical Therapy, University of Florida, Gainesville FL 32610, United States

https://doi.org/10.1016/j.expneurol.2017.12.014
Received 18 July 2017; Received in revised form 20 December 2017; Accepted 26 December 2017
Available online xxx
0014-4886/

robust phrenic motoneuron and/or diaphragm activation (Fuller et al., 2003; Ling et al., 1995; Mercier et al., 2017), but to our knowledge, the ability of intraspinal stimulation to activate multiple respiratory motor pools using low (microampere) currents has not been rigorously evaluated across the cervical and high thoracic spinal cord.

Application of ISMS for respiratory motoneuron activation must consider several unique features of the spinal respiratory networks. Foremost, the spinal cord contains a dense population of propriospinal neurons, many of which are synaptically coupled to respiratory circuits including phrenic and intercostal motoneurons (Billig et al., 2000; Cregg et al., 2017; Lane et al., 2008; Lipski and Duffin, 1986; Marchenko et al., 2015). In the thoracic spinal cord, neurophysiological studies establish that interneurons can relay medullary inspiratory drive to intercostal motoneurons (de Almeida and Kirkwood, 2013; Merrill and Lipski, 1987). Mid-cervical interneurons are also synaptically coupled to phrenic motoneurons (Lane et al., 2008; Lois et al., 2009), and can modulate phrenic motor output (Cregg et al., 2017; Marchenko et al., 2015; Sandhu et al., 2015). In regards to ISMS, the salient point is that activation of propriospinal neurons may be an effective way to recruit respiratory motoneurons (Cregg et al., 2017; DiMarco and Kowalski, 2013) Activation of propriospinal neurons may be more effective at co-activating multiple spinal respiratory motor pools vs. direct motoneuron stimulation. Another fundamental consideration is that spinal respiratory motoneurons receive a volley of excitatory synaptic inputs during the inspiratory phase, and are actively inhibited during the expiratory phase (Berger, 1979; Merrill and Fedorko, 1984; Sears, 1964). Thus, the ability of ISMS to activate respiratory motoneurons, either directly or through interneuron networks, is likely to vary with the phase of the endogenous respiratory cycle.

Our primary purpose was to systematically map the cervical (C2-C7) and high thoracic (T1) gray matter locations at which ISMS could activate spinal respiratory motoneurons. In doing so we tested three hypotheses. Our first two hypotheses derived from observations that inspiratory phrenic motoneuron activation appears to occur primarily via monosynaptic inputs (Lee and Fuller, 2011), whereas inspiratory intercostal motoneuron activation may involve a propriospinal relay (Kirkwood et al., 1988; Saywell et al., 2011) We therefore hypothesized that ISMS would most readily activate diaphragm motor units at short latencies consistent with monosynaptic inputs to phrenic motoneurons, and that activation of external intercostal motor units would be most prominent at longer latencies. Our third hypothesis was based on the work of Berger and others (Berger, 1979; Hayashi and Fukuda, 1995) demonstrating active inhibition of phrenic motoneurons during the expiratory period. We therefore hypothesized that the impact of ISMS on respiratory muscle activation would vary across the respiratory cycle. In cases of complete spinal transection injuries, concerns regarding phase-dependence of ISMS would be moot; however, most spinal injuries are functionally incomplete and even ventilator dependent individuals with spinal cord injury can have residual synaptic input to respiratory motoneurons (McDonald et al., 2002). Thus, we directly compared the impact of ISMS during the inspiratory vs. expiratory phase on respiratory motor unit activation.

The work focused on two primary inspiratory muscles, the diaphragm (DIA) and external intercostal (EIC), with a major emphasis on locating ISMS locations that could activate both muscles. We also recorded from an accessory respiratory muscle that typically does not exhibit rhythmic respiratory activity, the sternocleidomastoid (SCM). The sternocleidomastoid was included to determine if ISMS sites that activated primary respiratory muscles could also activate accessory respiratory muscles.

2. Methods

2.1. Overview

ISMS was delivered between the second cervical (C2) and the first thoracic (T1) segment (Fig. 1A, B) and evoked respiratory muscle activity was recorded in six adult female Long-Evans rats (267 ± 21 g). Somatotopic maps of ISMS-evoked responses were obtained during the in-

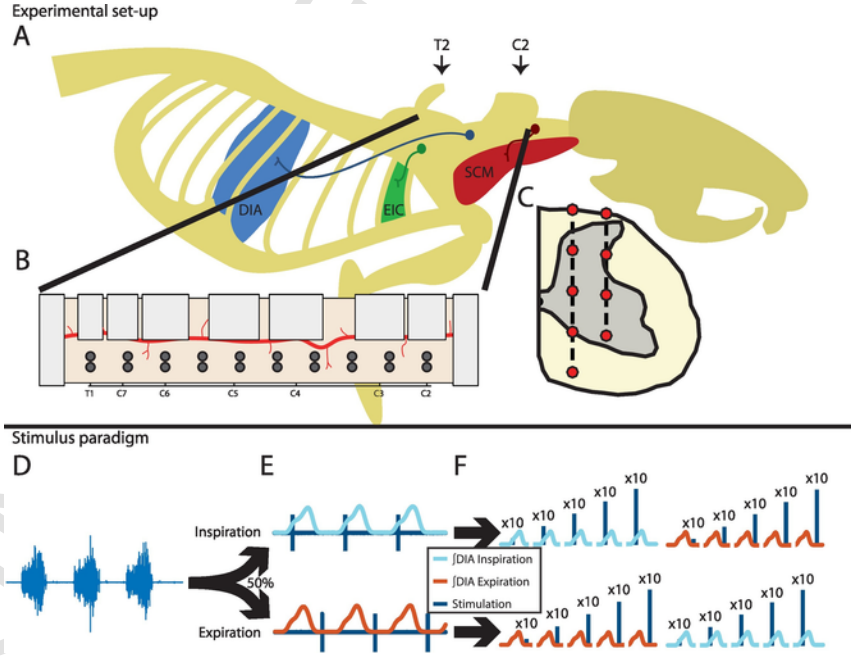

Fig. 1. Experimental set-up. A) Rodent respiratory anatomy including schematic of spinal innervation to key respiratory muscles. EMG recording electrodes were placed in the Diaphragm (DIA), External Intercostal (EIC) and Sternocleidomastoid (SCM) muscles. B) Dorsal view of the exposed spinal cord. Gray circles indicate the position where each of the 20 stimulation tracks began on the dorsal surface of the spinal cord in an example animal. C) Coronal view illustrating electrode tracks (dashed lines) and stimulus locations (red circles). Stimulus paradigm. D) Diaphragm EMG prior to the start of stimulation. E) Diaphragm EMG is rectified and integrated with a sliding-average window. For each stimulation site, there was a 50% probability of first triggering stimulation during either inspiration or expiration. F) Ten stimuli delivered at 10–90 μA in steps of 20 μA. After all stimulus intensities are delivered during one phase of respiration, stimulation is then delivered during the opposite respiratory phase at each intraspinal location. (For interpretation of the references to color in this figure legend, the reader is referred to the web version of this article.)

spiratory phase and the expiratory phase of the respiration cycle. Ten stimuli were delivered during both the inspiratory and expiratory phase at each of five amplitudes ranging from 10 to 90 μA in steps of 20 μA (Fig. 1D–F). Prior to the ISMS procedure, respiratory muscles were injected with fluorescently conjugated wheat germ agglutinin (WGA) to determine the relationship between the anatomical location of the motoneurons and the locations with which they can be activated with ISMS. Animals were housed in a photo-shifted room (12 h dark, 12 h light; lights off at 10 am and on at 10 pm) and surgeries began at 8:23 am ± 1.81 h (mean ± SD). All procedures were approved by the University of Washington Institutional Animal Care and Use Committee.

2.2. Surgical procedure-wheat germ agglutinin injection

Three days prior to the ISMS mapping procedure, rats were anesthetized with either an intraperitoneal injection of ketamine (80 mg kg^{-1}; Pfizer) and xylazine (10 mg kg^{-1}; Lloyd) or 2% isoflurane. Small incisions were made in the skin over the sternocleidomastoid and rostral intercostal. Additionally, the pectoralis muscle was incised to allow for a more accurate injection of 2.5% WGA (25-50 μl; reconstituted in 0.9% saline). WGA was conjugated to Alexa-Fluor 555 or 594 and injected into the sternocleidomastoid and external intercostal respectively. An injection of 2.5% WGA conjugated to Alexa-Fluor 488 (ThermoFisher Scientific W11261) was administered intrapleurally to label the motoneurons of the diaphragm (Buttry and Goshgarian, 2015). Muscles and skin were sutured in layers and buprenorphine (0.05 mg kg^{-1}) was administered to suppress sensation during anesthesia and recovery.

2.3. Surgical procedure-mapping

Three days after WGA injection, rats were anesthetized with intraperitoneal injections of ketamine (80 mg kg^{-1}; Pfizer) and xylazine (10 mg kg^{-1}; Lloyd). Supplemental doses of ketamine were given as needed to maintain a stable plane of sedation throughout the procedure. Hydration was maintained with 0.9% saline solution delivered subcutaneously (Baxter). All surgical procedures were performed on a water recirculating heating pad to maintain body temperature.

An incision was made on the dorsal surface through the skin, and muscles overlying cervical segments C1-C7 and the thoracic segments T1-T2 were dissected away from the vertebral columns and lamina. A right hemi-laminectomy was performed from C2-T1 which exposed 13.7 ± 1.2 mm (mean ± SD) of the spinal cord. The dura was incised to permit electrode insertion without dimpling of the dorsal spinal cord surface (Fig. 1B). Separate incisions were made in the skin in order to place bipolar electromyography (EMG) electrodes in the sternocleidomastoid (SCM) and external intercostal (EIC). An additional incision was made through the skin and rectus abdominus to access the costal region of the diaphragm (DIA). EMG wires consisted of 50 μm tungsten wires (A-M systems; 797,500). Electrode placement was verified by observing regular synchronized bursting of the inspiratory muscles diaphragm and external intercostal during breathing with no phasic activity of the sternocleidomastoid (Fig. 2A). A final incision was made on the ventral surface in the skin to access the trachea. A tracheotomy was then performed which allowed for ventilation with oxygen (100%) during the mapping procedure which consisted of ISMS delivered in 20 tracks throughout the cervical and high thoracic spinal cord.

2.4. Intraspinal microstimulation mapping

Stimuli were delivered using a single epoxy coated tungsten microelectrode (part number: UEWSFESEBN3F; impedance 300–500 kΩ; Fred Haer) positioned by a stereotaxic manipulator (Kopf Instruments) mounted on a custom spinal fixation frame. Constant current stimuli consisted of a single symmetric biphasic square-wave pulse with a duration of 300 μs per phase. Current returned through a distant bare

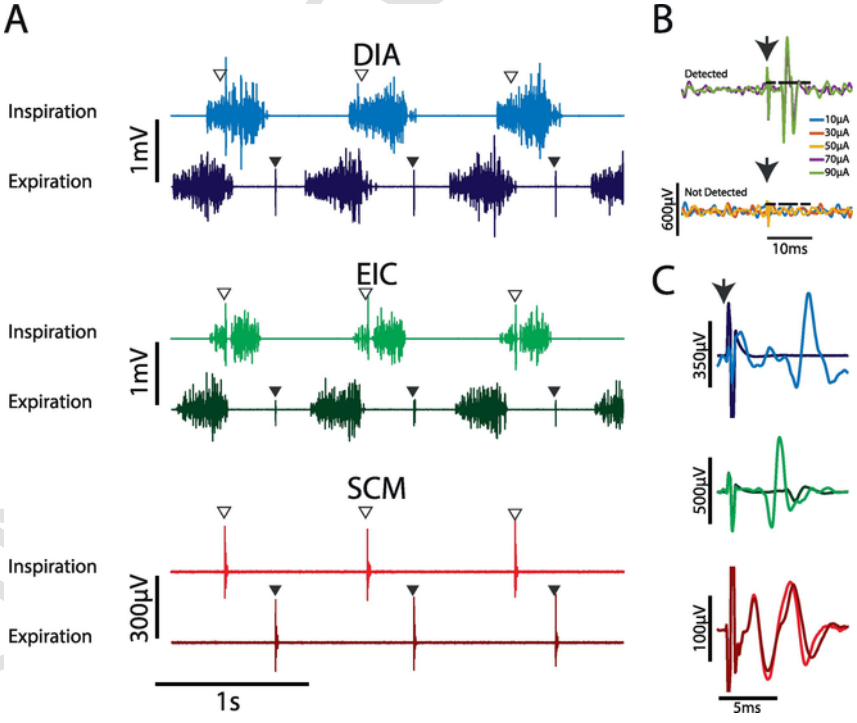

Fig. 2. Example EMG traces and stimulus triggered averages. A) Electromyography recordings from the sternocleidomastoid (SCM), external intercostal (EIC), and diaphragm (DIA) muscles showing stimulation during inspiration (open arrowhead) and expiration (closed arrowhead). B) Expanded stimulus triggered average of evoked responses in the diaphragm when stimulation was delivered during inspiration illustrating that the evoked response was easily discernible from the background activity. Dashed line indicated threshold. C) Stimulus triggered averages (StTAs) reveal the dynamic excitation during inspiration (light colors) compared to expiration (dark colors) for the DIA and EIC. Arrow indicates the delivery of the single pulse ISMS stimulus.

wire electrode placed under the skin above the hindquarters. Stimulation was delivered with an analog stimulus isolator (model 2200; A-M systems) controlled by 1401 Power3 (Cambridge Electronic Design) using custom Spike2 software. Stimulus amplitudes ranged from 10 to 90 μA in increments of 20 μA. A total of ten stimulation pulses at each of the five amplitudes were produced during inspiration and expiration, with the order of delivery randomized (Fig. 1D–F). To reduce bias associated with the duration of the procedure, the starting positions of ISMS tracks were randomized in the anterior –posterior and medial-lateral directions between each animal.

The exposed C1-T2 spinal cord was measured and divided into an evenly spaced 10 × 2 grid. This resulted in ten uniformly spaced stimulation sites along the rostrocaudal axis from C1-T2. At each of these sites, 2 locations were stimulated, designated as medial (0.5 mm from spinal midline) and lateral (1.0 mm from midline). Electrodes were advanced ventrally from the surface of the spinal cord in increments of 600 μm to a total depth of 2400 μm and 1800 μm for the medial and lateral tracks, respectively (Fig. 1C). The order of each stimulation track was randomized prior to the mapping procedure for each animal. This approach enabled an unbiased and reproducible "mapping" of responses to electrical stimulation along the extent of the cervical and high thoracic spinal cord. Based on published descriptions of the "transition points" between spinal cord segments in the rat (Padmanabhan and Singh, 1979) we estimate that the 10 stimulation sites (i.e., in the 10 × 2 grid) were: mC2, rC3, rC4, cC4, cC5, cC6, cC7, mC8, mT1, mT2 (m = middle, r = rostral, c = caudal). Throughout the text, when segments are mentioned (e.g. C2) this refers the vertebral bones, not the spinal segments, as those were not directly assessed in this procedure.

2.5. EMG recording

ISMS-evoked electromyography (EMG) was recorded using a differential amplifier (A-M systems 1700). Data were digitized using a 16 channel data acquisition unit (1401-Power3) and custom Spike2 acquisition software. Integrated diaphragm EMG activity was used to trigger stimulation during either expiration or inspiration, and an example of this is shown in Fig. 1. EMG data were recorded at 20,000 samples per second and analog band-pass filtered between 300 and 2000 Hz and saved to disk for offline filtering and analysis (see Data analysis section).

2.6. Tissue slicing and image processing

At the conclusion of the mapping procedure, animals were euthanized with an intraperitoneal injection of beuthanasia (200 mg kg^{-1}) and transcardially perfused with saline followed by 10% formalin. A fiducial mark was made at the center of the C2 vertebral bone to standardize the comparison between electrophysiological data and histology. Tissue was post-fixed overnight in 10% formalin then placed in 30% sucrose for cryoprotection. Spinal cord tissue from all animals was sliced (60 μm) in the coronal plane, using a cryostat (Leica CM1850).

Coronal sections were photographed using an inverted widefield microscope (LEICA DM IRB/E) with a 10 × primary objective. Images were processed using custom MATLAB software where slice and gray-white borders were traced and motoneurons were manually identified. There was an average of 753 ± 172 μm between analyzed sections.

2.7. Data analysis

Evoked muscle activity was low [illegible] filtered at 5 kHz to remove extraneous frequencies and anti-alias the data which was then compiled into stimulus triggered averages (StTAs, Fig. 2B–C) using custom MATLAB software (The MathWorks). Sweeps with significant EMG response were identified and the amplitude of and time to response were quantified (Sunshine et al., 2013). A significant EMG response in the StTA was defined as an event starting after the resolution of the stimulus artifact that crossed a threshold greater than ± 50 μV for longer than 1 ms (Sunshine et al., 2013).

2.8. Data pooling

We stimulated at 5 medial depths and 4 lateral depths at each of the 10 coordinates along the C2-T1 rostro-caudal axis. Within each individual animal the percentage of sites (out of the 90) that elicited an evoked potential for each muscle was determined and an average across all animals was created by standardizing the location on the 10 × 2 spinal cord grid (Fig. 3). The relative likelihood of activating a given muscle or pair of muscles was determined by calculating the percentage of the nine possible stimulus sites at each segmental location that produced the particular activation pattern (Fig. 4). This was calculated within each animal and then averaged between animals to form the contours in Fig. 4. These contours do not represent the lowest possible stimulus current to activate any muscle but rather the lowest stimulus current to produce the muscle represented in the contour.

The amplitude of the evoked response was calculated at the lowest stimulus current to produce an evoked response. This was done for all sites within an animal where an evoked response could be elicited. Evoked response amplitude was then averaged within and between animals (Fig. 5). The onset of ISMS induced muscle activation was measured as the duration from stimulus to response, and was determined at each of the stimulus locations. This was assessed for each muscle and then averaged across animals (Fig. 6).

2.9. Statistics

All statistical analyses were performed in MATLAB or in GraphPad Prism 7. A Lilliefors test was used to determine if the data sets were normally distributed. For data that were not normally distributed, a Wilcoxon rank-sum test was used to determine significance. Normally distributed data were tested using a Student's *t*-test. When data were collected using the same amplitude stimulation a paired Student's t-test was used (Sunshine et al., 2013). Synaptic delays were analyzed using an ordinary two-way analysis of variance (ANOVA); Individual comparisons were performed with Fisher's Least Significant Difference (LSD) post hoc test. Activation onsets for each muscle group were analyzed using an ordinary one-way analysis of variance (ANOVA), and individual comparisons were performed with Fisher's Least Significant Difference (LSD) post hoc test. All values stated in text are mean ± standard deviation (SD) unless otherwise noted.

3. Results

3.1. Impact of electrode location and respiratory phase on ISMS-induced respiratory muscle activation

A representative map of ISMS locations from a single animal is presented in Fig. 3A. Note that the anatomical locations at which ISMS activated a particular muscle tended to cluster together across multiple segments. Independent muscle activation (i.e., without any co-activation) occurred at a relatively low number of locations, and was more likely to occur during expiratory vs. inspiratory phase ISMS (Fig. 3B). Overall, significantly more sites elicited independent muscle activation during expiratory (25 ± 8%) compared to inspiration-triggered ISMS (18 ± 4%; $p = 0.03$). In contrast, activating two muscles via a single ISMS pulse (i.e., co-activation) was more likely to occur during the inspiratory phase (51 ± 12% of sites) as compared to the expiratory phase (25 ± 11%; $p < 0.001$). The mean co-activation data are shown in Fig. 3C. Note that significantly greater co-activation of all muscle pairs occurred during inspiratory vs. expiratory stimulation. We also

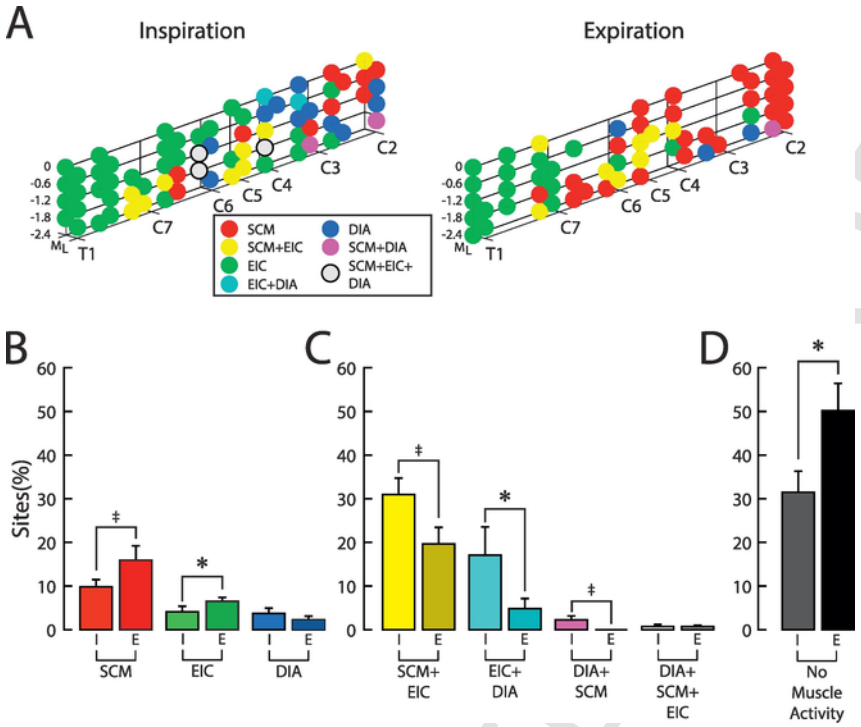

Fig. 3. ISMS-evoked respiratory muscle activation & co-activation. A) Stimulus locations activating respiratory muscles during inspiration (left) and expiration (right) at the lowest stimulus current to elicit EMG activity in a representative animal, the center of the vertebral bones is noted along the x-axis. Colors denote individual muscles or combinations of muscles. Abbreviations as in Fig. 2B–D) EMG response observed as a percentage of the total sites tested at the lowest current to elicit EMG activity in any muscle (mean + SEM). Each figure displays the type of muscle activity or co-activity during inspiration ('I'; light shading) and expiration ('E'; dark shading). ‡ denotes $p < 0.1$, * denotes $p < 0.05$. Diaphragm (DIA), External Intercostal (EIC) and Sternocleidomastoid (SCM).

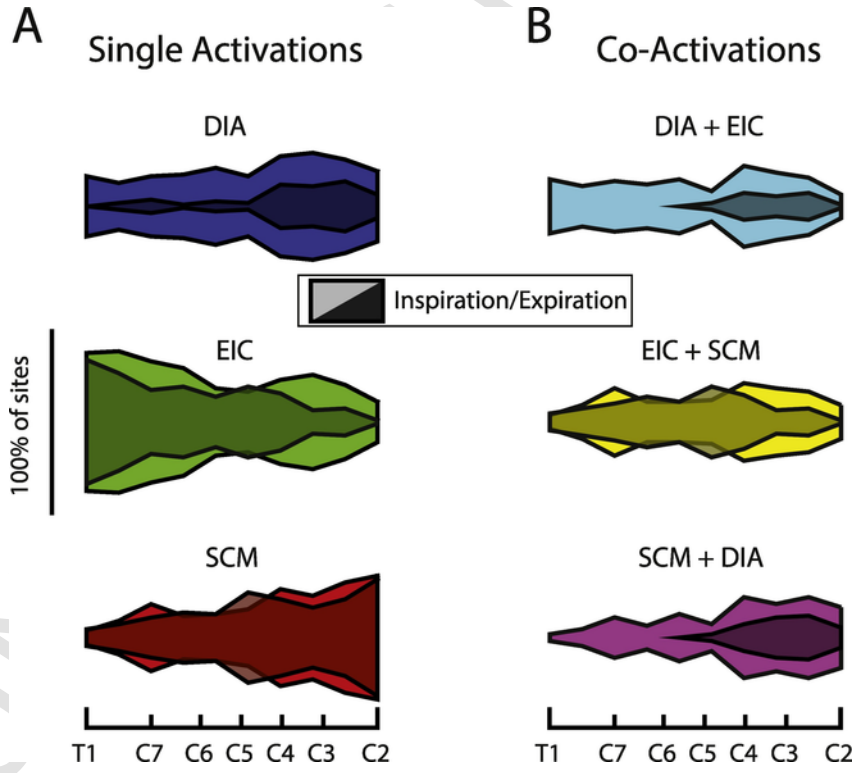

Fig. 4. Rostrocaudal distribution of muscle activations. A) Average distribution from all animals showing the likelihood of single muscle activation via ISMS. B) Average distribution from all animals showing the likelihood of co-active muscle activation via ISMS, the average location of each vertebral bone is noted on the x-axis. Light contours represent the activation likelihood during inspiration whereas dark contours depict activation during expiration. Note: each contour represents the lowest stimulus intensity which activated the muscle. Diaphragm (DIA), External Intercostal (EIC) and Sternocleidomastoid (SCM).

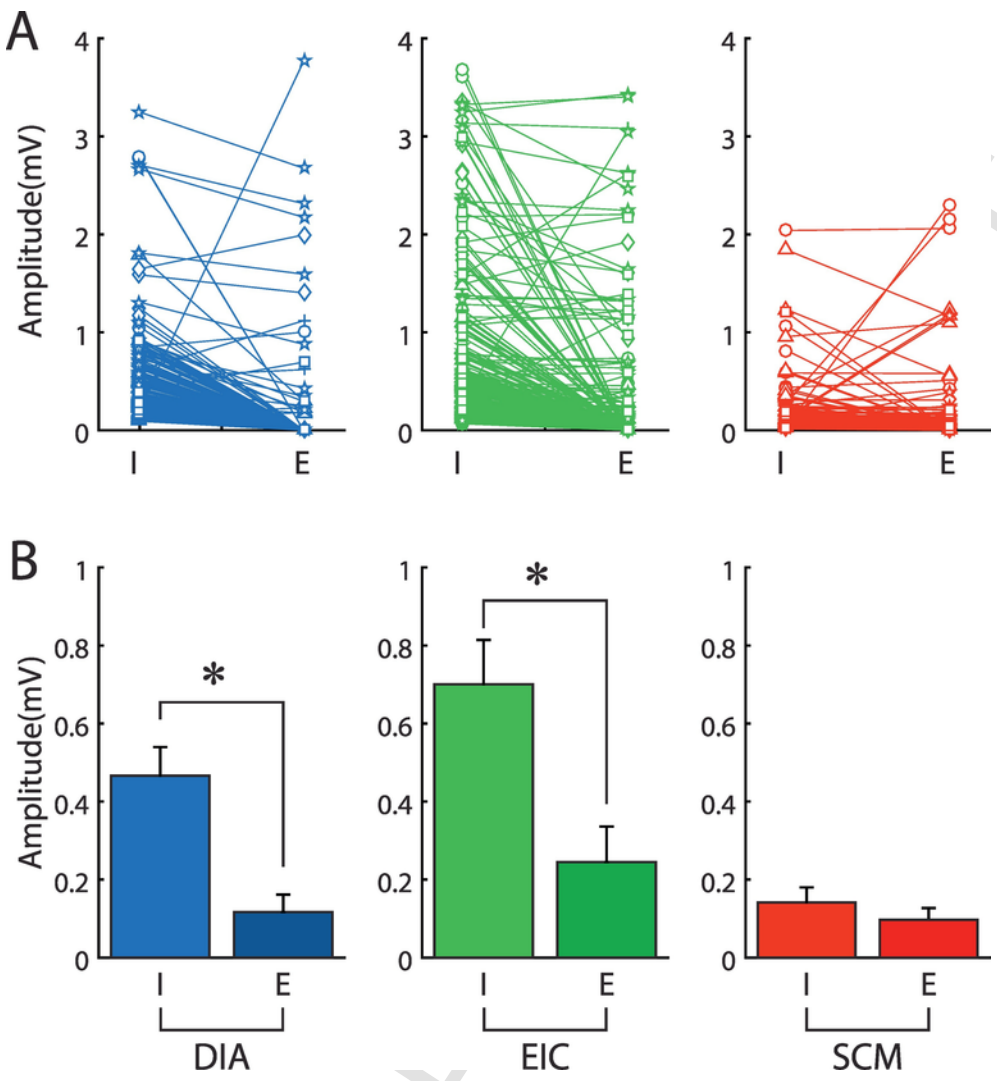

Fig. 5. Amplitude of muscle activation at inspiratory stimulus threshold. A) Individual activations between inspiration ('I') and expiration ('E') are connected by lines. Individual animals are indicated by different symbols. B) Average muscle activation for inspiration and expiration (mean + SEM) are significantly different for the principal respiratory muscles (DIA and EIC) but not for the accessory muscle (SCM), * denotes $p < 0.05$. Diaphragm (DIA), External Intercostal (EIC) and Sternocleidomastoid (SCM).

observed a considerable number of ISMS locations at which no muscle activation could be evoked, and as shown in Fig. 3D this was more prominent during expiration when approximately 50% of locations failed to evoke muscle activity. The average stimulation threshold to evoke a response ranged from 46 to 55 μA and this value was not different between muscles, nor was it altered by the respiratory phase (two-way ANOVA interaction $p = 0.4492$).

Maps showing the rostrocaudal distribution of ISMS locations that produced muscle activation across all animals are shown in Fig. 4. During inspiration-triggered ISMS, selective activation of diaphragm motor units occurred at locations throughout the cervical and high thoracic spinal cord, but was more likely to occur in the mid-cervical region (light shading in Fig. 4A, top panel). During expiration-triggered stimulation, selective diaphragm activation was rare unless the electrodes were placed in the immediate vicinity of the phrenic motoneuron pools (i.e. C3-4 vertebral segments, dark shading in Fig. 4A, top panel). In comparison to the diaphragm response, the ability to selectively activate the external intercostal and sternocleidomastoid muscles was less sensitive to the respiratory phase (Fig. 4A, middle and bottom panels; note the overlap between light and dark shading). However, as with the diaphragm, the probability of selectively activating each of these muscles increased with proximity to the respective motoneuron pool.

The rostrocaudal distribution of ISMS locations at which a single pulse produced respiratory muscle co-activation are shown in Fig. 4B. Co-activation of diaphragm and external intercostals was evoked at locations from C2-T1, with a tendency to occur more often at C3-C4 (Fig. 4B, top panel). There was a strong impact of the respiratory cycle on co-activation of these two muscles (Fig. 4B, compare light and dark shading). The external intercostal and sternocleidomastoid were co-activated at ISMS locations from C2-T1, and there was relatively little impact of the respiratory cycle on this response (Fig. 4B, middle panel). Co-activating the sternocleidomastoid and diaphragm was more likely to occur during inspiratory phase ISMS, and at locations rostral to C5 (Fig. 4B, lower panel).

We also examined the impact of respiratory phase on the amplitude of ISMS-evoked EMG compound action potentials (Fig. 5). These comparisons of peak-to-peak EMG amplitude (see Fig. 2B–C for example waveforms) were made using the minimum ISMS current that was necessary to activate each muscle. Inspiratory- and expiratory phase comparisons were made at each of the electrode positions (Fig. 5A). A location was excluded from further analysis if a response could not be evoked at relatively low currents (≤ 90 μA; which was the maximum current used in this study, to reduce the spread of current away from the location of the tip of the electrode) during inspiration-triggered

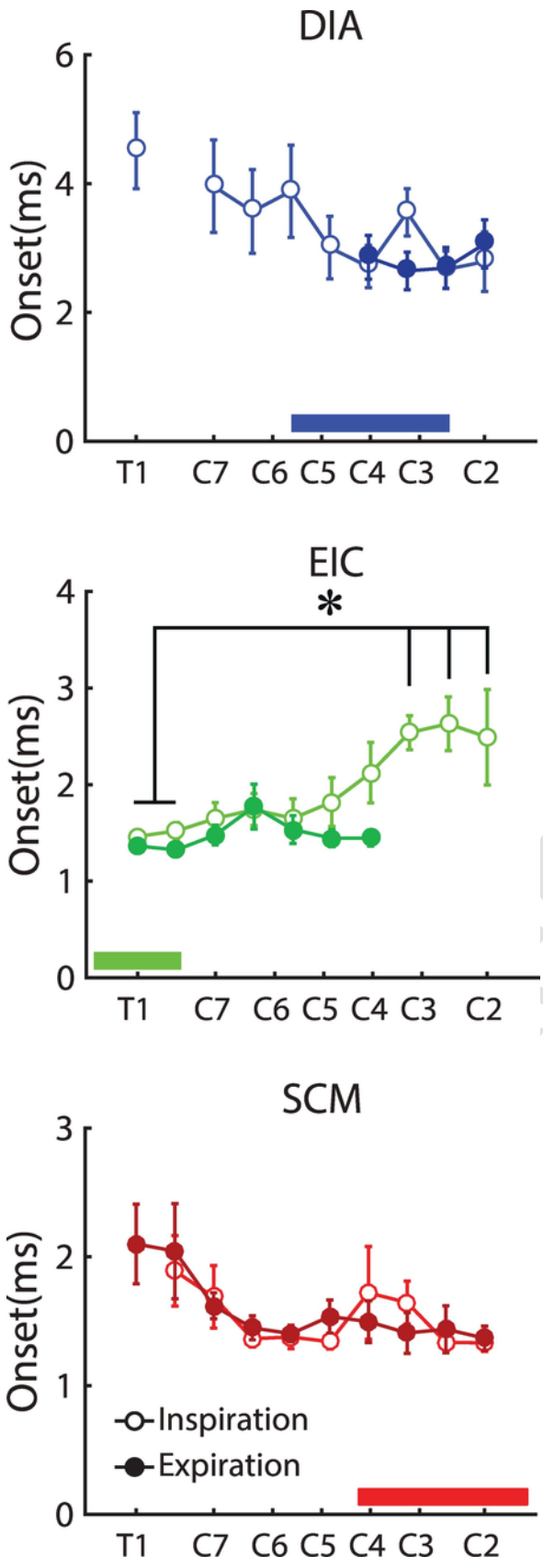

Fig. 6. Onset of ISMS-induced respiratory muscle activation. The shortest time to muscle activation at each rostrocaudal position along the spinal cord (mean ± SEM), the average location of each vertebral bone is noted on the x-axis. Open symbols mark inspiration, closed symbols expiration. Colored bar in each panel indicates the location where efferent nerve exits the spinal cord as an approximate marker of motor neuron pools or direct activation of ventral roots. (* denotes $p < 0.009$). Diaphragm (DIA), External Intercostal (EIC) and Sternocleidomastoid (SCM).

stimulation. With these guidelines, inspiratory phase ISMS activated the external intercostal at 51 ± 11% of stimulus locations, and the diaphragm responded at 41 ± 24% of sites. As shown in Fig. 5B, both ~~of~~ these muscles had a substantial decrease in evoked potential amplitude when ISMS was delivered during the expiratory phase. Specifically, during expiration the diaphragm evoked response decreased by 76 ± 18% ($p = 0.002$), and the external intercostal response decreased by 68 ± 24% ($p = 0.01$, Fig. 5B). The sternocleidomastoid could be activated at 37 ± 8% of the sites tested during the inspiratory phase, but there was no apparent impact of the respiratory cycle on this response (Fig. 5B).

3.2. Activation latency

Fig. 6 shows the shortest latency between delivery of the ISMS pulse and the subsequent evoked respiratory muscle EMG response; these latencies were then averaged between animals. The shortest latencies observed along these curves were consistent with direct motoneuron activation (Gustafsson and Jankowska, 1976), and occurred at locations close to the spinal ventral roots innervating the respective muscles. There was no impact of the respiratory cycle on onset latency for any of the three muscles tested (compare open vs. filled symbols in Fig. 6). Diaphragm onset latency tended to be shorter when the electrode was in the mid-cervical cord, but no statistically significant differences in latencies were detected across the cervical and high thoracic spinal cord (Fig. 6, top panel). The external intercostal onset latency was greater when stimulation was applied at the three most rostral locations in the cervical spinal cord (Fig. 6, middle panel, $p < 0.009$). Sternocleidomastoid onset latency tended to be lower when ISMS was applied rostral to C6, but this was not statistically significant (Fig. 6, lower panel).

3.3. Histological verification of motoneuron distribution relative to microwire placement

The spinal cord location of each motoneuron pool was histologically confirmed using retrograde neuronal labeling as shown in Fig. 7. These experiments were completed to validate the conclusions regarding placement of the ISMS electrodes in relation to each of the three respective pools (e.g., Figs. 4, 6, 8). Sternocleidomastoid and external intercostal motoneurons were labeled by intramuscular WGA injection. For phrenic motoneuron labeling, WGA was delivered to the in~~traplural~~ space to target the diaphragm (Buttry and Goshgarian, 2015; Mantilla et al., 2009).

Based on morphological appearance and location of the labeled neurons, we conclude that spinal cord WGA labeling was restricted to motoneurons and did not occur in segmental interneurons (Fig. 7A–D). That observation is consistent with a prior study of spinal cord intact rats using WGA tracing (Buttry and Goshgarian, 2015). Retrograde transsynaptic transport of WGA did occur, however, with brainstem labeling observed in 2 of 6 rats following external intercostal tracing, 3 of 6 rats following sternocleidomastoid tracing, and 3 of 6 rats following diaphragm tracing (Table 1). Consistent with a prior report, brainstem WGA labeling was noted in the nucleus ambiguous following diaphragm application (Buttry and Goshgarian, 2015).

WGA labeling of sternocleidomastoid motoneurons was observed across the length of the ventro-lateral cervical spinal cord with peak labeling 4–6 mm rostral to the center of C2 (Fig. 7E). Intrapleural injections resulted in clear phrenic motoneuron labeling in the mid-cervical cord, but the distribution of labeled cells extended slightly into the high thoracic spinal cord (fewer than 2 cells per segment) as previously

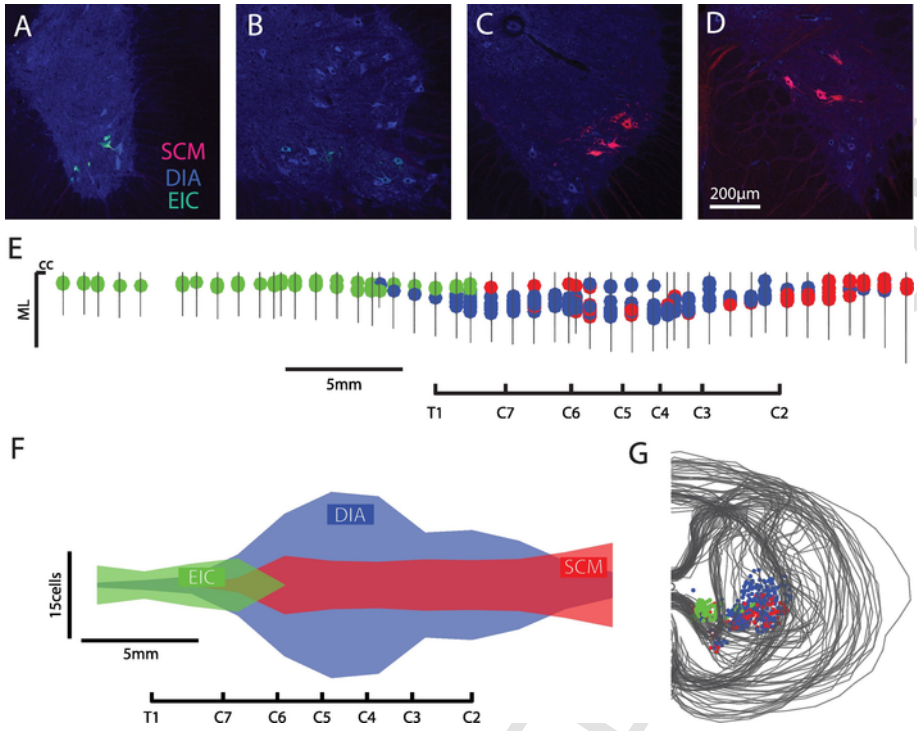

Fig. 7. Coronal images of WGA labeled motor neurons. Coronal sections from spinal segments T5 (A) and C5 (B) depict EIC and DIA motor neurons. Sections from spinal segments C4 (C) and C2 (D) illustrating the location of DIA and SCM motor neurons. Locations are as expected based on established anatomy. WGA labeling was pseudo-colored to match previous figures rather than intrinsic fluorophore. Summary of WGA-labelled motor neuron locations. E) Motor neuron labeling of SCM (red), DIA (blue), and EIC (green) displayed in a top down longitudinal view from an example animal. 'cc' indicates location of central canal, the location of each vertebral bone is noted on the x-axis spanning the region that was investigated with intrapsinal microstimulation. F) 2D contour of the average WGA labeling across all animals ($N = 6$). Neuron counts were averaged across 2 mm of tissue, the average location of each vertebral bone is noted on the x-axis. G) Coronal view from the same animal. Outlines indicate gray matter and spinal border for each segment superimposed Diaphragm (DIA), External Intercostal (EIC) and Sternocleidomastoid (SCM). (For interpretation of the references to color in this figure legend, the reader is referred to the web version of this article.)

reported (Buttry and Goshgarian, 2015). However, as shown in Fig. 7E the vast majority of WGA labeled cells were located between C4 and C5 confirming the location of the phrenic motor nucleus (Buttry and Goshgarian, 2015; Goshgarian and Rafols, 1981; Lane et al., 2008). Following external intercostal application, WGA labeled motoneurons were observed in the low cervical cord (C6) through the rostral thoracic (T1) spinal cord (Fig. 7E). A scaled map showing the spinal cord distribution of WGA labeling for each motor neuron pool is provided in Fig. 7G.

3.4. Supplemental analyses

The latencies of all recorded evoked responses ($n = 3187$ across all experiments) are summarized in Fig. 8. The histogram plot in Fig. 8A indicates a multi-modal distribution of activation latency with the earliest detectable EMG responses occurring 1.2 ms after the stimulus. The latency distributions were next used to classify the activation of individual muscles during inspiratory- (Fig. 8B) and expiratory-phase ISMS (Fig. 8C). During inspiration, the average number of short latency (< 2.6 ms) diaphragm activations was relatively low. The greatest number of diaphragm activations occurred at latencies ≥ 3.9 ms (Fig. 8B). In contrast to the diaphragm, both the external intercostal and sternocleidomastoid were more likely to be activated at latencies ≤ 2.5 ms (Fig. 8B). Fig. 9 provides a representative map showing the rostrocaudal distribution of the onset latency of ISMS-induced muscle activation from one experiment. Note the profound contrast between diaphragm activation during inspiratory vs. expiratory phase ISMS (Fig. 9, top panel). This example also illustrates that the ISMS coordinates associated with short latency activation of the sternocleidomastoid and external intercostal aligned closely with the respective location of the motoneuron pool for each muscle (Fig. 9) these locations are based on the stereotaxic coordinates, and we cannot rule out a certain amount of current spread throughout the tissue.

4. Discussion

Our results show that ISMS during spontaneous breathing can co-activate the diaphragm and external intercostal muscles, and therefore has promise as a potential respiratory neuroprosthesis. Co-activation of these potentially synergistic muscles did not require electrode placement in discrete regions, but rather could be induced at locations throughout the cervical cord. In addition, both the co-activation patterns and motor unit potential amplitude were substantially different during inspiratory- versus expiratory ISMS. Thus, the phase of the respiratory cycle must be taken into account during ISMS. Evaluation of ISMS electrode location relative to motor unit activation latency suggests the presence of a complex propriospinal network that can modulate respiratory motor output as proposed by prior authors (Cregg et al., 2017; Kirkwood et al., 1988; Lane et al., 2008).

4.1. Impact of respiratory phase on motor unit activation

Our results demonstrate the importance of considering the respiratory phase when using electrical stimulation to activate respiratory circuits. Since phrenic motoneurons are actively inhibited during expiration (Berger, 1979), we predicted that there would be a difference in the amplitude of the ISMS evoked response across the respiratory cycle. As expected, stimulating in phase with inspiration activated motor units in the external intercostal and diaphragm (e.g., Fig.4B top panel, light vs. dark regions). In addition, an important clinical consideration is that inspiration triggered ISMS produced more co-activation of these potentially synergistic muscle groups.

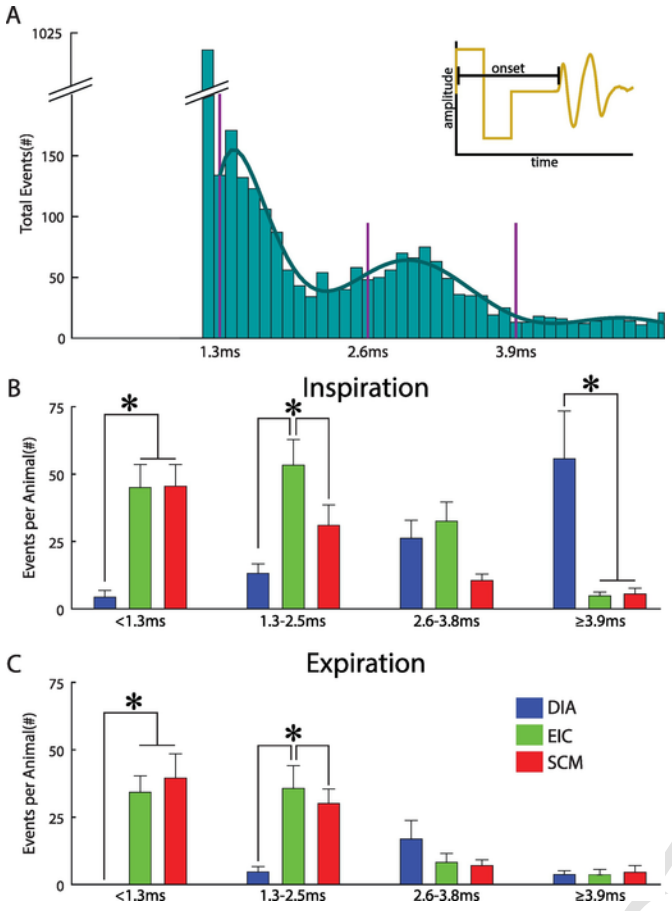

Fig. 8. Synaptic delays following ISMS stimulation A) Pooled data from all trials with ISMS-evoked EMG responses (3187/16200). Histogram (0.1 ms resolution) demonstrates the quantal pattern of synaptic delays. Dark green line indicates polynomial fit, purple lines indicate how data were divided into putative direct, monosynaptic, disynaptic and polysynaptic activations. B) Muscle activation synaptic delays resulting from stimulation delivered during the inspiratory phase. C) Muscle activation synaptic delays resulting from stimulation delivered during the expiratory phase. (* denotes $p < 0.05$). Diaphragm (DIA), External Intercostal (EIC) and Sternocleidomastoid (SCM). (For interpretation of the references to color in this figure legend, the reader is referred to the web version of this article.)

Table 1
WGA labeling in the nucleus ambiguus. WGA labeling from at least one of the injected muscles was observed to have been retrogradely transported to the nucleus ambiguus in five of the six rats. Muscles are intercostal (IC), sternocleidomastoid (SCM) and diaphragm (DIA).

Rat	IC	SCM	DIA
1	+	−	−
2	+	+	−
3	−	+	+
4	−	−	−
5	−	+	+
6	−	−	+

Another point of consideration is that long latency diaphragm activations – consistent with polysynaptic pathway activation – were more prominent when ISMS was delivered during the inspiratory versus the expiratory phase. The respiratory phase dependence of these long-latency activations may reflect more than just inspiratory-expiratory oscillations in phrenic motoneuron excitability (Berger, 1979). Respiratory-related bursting patterns are often reported in cervical interneurons (Duffin and Iscoe, 1996; Hayashi et al., 2003; Hilaire et al., 1986; Lane et al., 2009; Palisses and Viala, 1987; Sandhu et al., 2015; Streeter et al., 2017b) and at least a portion of these cells can have direct input from the ventral respiratory group in the medulla (Duffin and Iscoe, 1996). Thus, oscillations in the excitability of the cervical propriospinal network, and specifically increased excitability during the inspiratory phase, may enable polysynaptic activations during inspiratory ISMS.

4.2. ISMS as a possible respiratory neuroprosthesis

Optogenetic stimulation has been previously investigated as a method of central nervous stimulation system to modulate respiratory volume/frequency in awake rats (Burke et al., 2014; Kanbar et al., 2010). ISMS provides an alternative, as electrical stimulation can be delivered via relatively simple circuits and fully-implanted systems (Troyk et al., 2012). Additionally, the tight temporal precision of ISMS makes it an ideal intervention for closed loop stimulation (McPherson et al., 2015; Nishimura et al., 2013; Zimmermann and Jackson, 2014). Other types of electrical spinal stimulation (epidural) have been investigated in particular for the activation of intercostal muscles; these methods may also provide alternatives to diaphragmatic pacing, however, these approaches require separate electrodes for intercostal and diaphragm activation (DiMarco et al., 1987; DiMarco et al., 2004). Clinical closed loop electrical stimulators already exist for disorders such as epilepsy (Sun and Morrell, 2014), and custom multi-channel stimulators are under development (Yi-Kai Lo et al., 2016) that will expand the potential to deliver ISMS for a range of conditions following CNS injury.

Our data also indicate that respiratory phase specific stimulation could be incorporated into diaphragmatic pacing strategies if endogenous respiratory drive is partially maintained (e.g., after incomplete cervical spinal cord injury). In this case, stimulation putatively delivered to the muscle, acts via depolarizing the nerve to evoke muscle contractions. In fact diaphragm pacing is only effective if the phrenic nerve and phrenic motor pool are intact (Onders et al., 2009). Future use of ISMS to activate respiratory circuits in a synergistic and context-dependent manner may provide functional activation of respiratory muscles and aid in ventilator weaning (Levine et al., 2008; Smuder et al., 2016). Importantly, current diaphragmatic pacers are largely open loop systems and do not have the ability to leverage the phase-dependent information which may enhance their effect when coupled with ISMS.

4.3. Spinal networks and ISMS

Many research groups have suggested that propriospinal networks can regulate respiratory motoneuron output (Cregg et al., 2017; Hudson et al., 2017; Lane et al., 2008), and we therefore evaluated the latency between ISMS and respiratory muscle activation to provide indirect evidence of synaptic connectivity. Factors such as variability in EMG electrode placement and/or ISMS electrode placement will impact the latency data. However, by pooling > 3000 evoked responses, we were able to evaluate the latency data in a manner that at least partially mitigates these influences. Evaluating the large number of evoked responses revealed a multi-modal distribution of the latency data (e.g., Fig. 8). If the contribution of each potential synapse is estimated to be ~ 1.3 ms (Borst et al., 1995; Borst and Sakmann, 1996; Meinrenken et al., 2003), the multi-modal distribution suggests the presence of direct, mono-, di- and polysynaptic activation of motoneurons during ISMS (see x-axis on Fig. 8A). The longer latency activations are consistent with prior reports indicating that ISMS preferentially activates spinal motoneurons via polysynaptic interneuronal pathways (Gustafsson and Jankowska, 1976; Jankowska and Roberts, 1972).While we did not directly measure synaptic connectivity in the spinal cord, we feel this analysis is informative, particularly in light of the rapidly increasing interest in spinal interneurons and activation of respiratory motoneurons (Cregg et al., 2017; Fuller, 2017; Hudson et al., 2017).

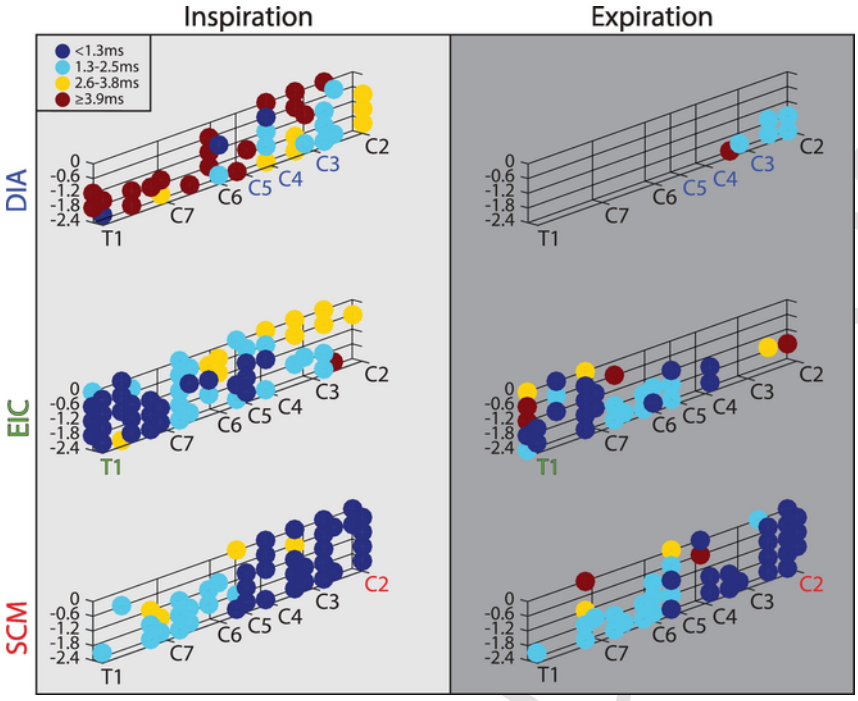

Fig. 9. Locations of ISMS activation latency. Data from an example animal illustrating that those activations with shorter latencies of ISMS occur near the location of each motor pool during inspiration the location of each vertebral bone is noted on the x-axis, the distance from the dorsal surface of the spinal cord is indicated on the z-axis in millimeters. There is also a dramatic reduction of polysynaptic (≥ 3.9 ms) activations between inspiration and expiration, suggesting that ISMS activates complex spinal networks preferentially during inspiration. Diaphragm (DIA), External Intercostal (EIC) and Sternocleidomastoid (SCM).

Diaphragm motor unit activation at latencies below 2.6 ms occurred only when ISMS electrodes were in close proximity to the phrenic motor pool. Inspiratory phrenic motoneuron depolarization appears to be primarily driven by monosynaptic, excitatory bulbospinal inputs (Ellenberger and Feldman, 1988; Ellenberger et al., 1990), and ISMS activation of these pathways is likely to account for these short latency diaphragm activations (e.g., Fig. 8B). Across all experiments, we observed only a relatively small number of short latency diaphragm activations. In contrast, ISMS at sites throughout the cervical cord produced diaphragm activation at latencies > 3.9 ms. These longer latencies are consistent with activation of polysynaptic excitatory pathways (Borst et al., 1995; Borst and Sakmann, 1996; Meinrenken et al., 2003). Polysynaptic spinal activation of phrenic motoneurons is plausible since both neurophysiological (Marchenko et al., 2015; Sandhu et al., 2015; Streeter et al., 2017b) and anatomical data (Dobbins and Feldman, 1994; Lane et al., 2008; Lois et al., 2009) have shown mid cervical interneurons which are synaptically coupled with the phrenic motor pool. There is currently relatively little evidence, however, that cervical interneurons convey brainstem "respiratory drive" to phrenic motoneurons during spontaneous breathing (Duffin and Iscoe, 1996). It is worth emphasizing, however, that conclusions in this regard have been drawn almost exclusively from studies of anesthetized and immobile experimental animals. Data from humans (Butler et al., 2014; Hudson et al., 2017) as well as recent multi-electrode recordings in animals (Sandhu et al., 2015; Streeter et al., 2017a) raise the possibility of a propriospinal contribution to respiratory-related control of phrenic motoneurons. Another possibility is that rather than conveying respiratory drive, the propriospinal network primarily functions to coordinate the activation of the diaphragm with other muscles (e.g., intercostal, trunk muscles) during breathing and/or postural movements (Bellingham, 1999; Decima et al., 1967). Indirect support for this hypothesis comes from studies showing that intercostal muscle activation can alter phrenic activity (Bellingham, 1999; Remmers, 1973) and also anatomical studies confirming that cervical interneurons can be synaptically linked to both the intercostal and phrenic motor pools (Lane et al., 2008). Collectively, our results confirm that diaphragm and external intercostal muscle co-activation occurs at ISMS locations throughout the cervical spinal cord, and the latency data are consistent with the possibility that activation of polysynaptic spinal networks can drive diaphragm recruitment.

In regards to somatotopy, a prior study in primates surprisingly failed to identify a clear relationship between cervical ISMS location and the pattern of forelimb activation (Moritz et al., 2007). In contrast, a clear spatial relationship between motoneuron recruitment and stimulus location was identified in our subsequent study of ISMS and forelimb muscles in rats (Sunshine et al., 2013). In the current study, there was not a strict somatotopy per se, but nevertheless a clear relationship existed between the location of the ISMS electrode and the evoked responses. For example, the clusters of activation shown in Fig. 3A aligned with the expected somatotopic organization of the motoneuron pools as shown by prior data (Buttry and Goshgarian, 2015; Lane et al., 2008) and the WGA tracing data reported here. Somatotopy was less apparent for polysynaptic activation of phrenic motoneurons, as these pathways were activated throughout the cervical spinal cord (e.g., Fig. 9).

5. Conclusion

We report the first comprehensive mapping of ISMS locations in the cervical and high thoracic spinal cord and the associated evoked respiratory muscle responses. Our findings demonstrate that respiratory phase is a fundamentally important consideration when designing ISMS protocols and suggest ISMS-induced activation of polysynaptic spinal pathways can effectively recruit inspiratory muscles. These data will inform the development of implanted devices not only for neuroprosthetics to drive ventilation after neurologic injury, but also for ISMS-based approaches for targeted neuroplasticity to restore endogenous function. While not directly addressed here, spinal cord stimulation shows promise as a therapeutic modality following spinal cord injury (Kasten et al., 2013; McPherson et al., 2015). Similar applications of

ISMS to promote plasticity and rewiring of the respiratory circuits have exciting potential to modernize treatments for neurological disorders affecting ventilation.

Author contributions

MS and CG conceived of the study design. MS and CG collected and MS analyzed the data. PR, DF and CT provided feedback on data interpretation and financial support. MS and CG drafted manuscript and DF edited the document. PR and CT also provided substantial review of manuscript. All experiments were performed in the lab of CT. The authors have no conflicts of interest to report.

Acknowledgments

The authors would like to thank Spencer Boyer for his help with the real-time EMG processing, and members of the Moritz lab for comments on the manuscript. W81XWH-14-1-0625 (PJR), Center for Sensorimotor Neural Engineering (CSNE), National Science Foundation Engineering Research Center (EEC-1028725), 1RO1NS080180-01A1 (DDF).

References

de Almeida, A.T., Kirkwood, P.A., 2013. Specificity in monosynaptic and disynaptic bulbospinal connections to thoracic motoneurones in the rat. J. Physiol. 591, 4043–4063.
Bamford, J.A., Putman, C.T., Mushahwar, V.K., 2005. Intraspinal microstimulation preferentially recruits fatigue-resistant muscle fibres and generates gradual force in rat. J. Physiol. 569, 873–884.
Bellingham, M.C., 1999. Synaptic inhibition of cat phrenic motoneurons by internal intercostal nerve stimulation. J. Neurophysiol. 82, 1224–1232.
Berger, A.J., 1979. Phrenic motoneurons in the cat: subpopulations and nature of respiratory drive potentials. J. Neurophysiol. 42, 76–90.
Billig, I., Foris, J.M., Enquist, L.W., Card, J.P., Yates, B.J., 2000. Definition of neuronal circuitry controlling the activity of phrenic and abdominal motoneurons in the ferret using recombinant strains of pseudorabies virus. J. Neurosci. 20, 7446–7454.
Borst, J.G., Sakmann, B., 1996. Calcium influx and transmitter release in a fast CNS synapse. Nature 383, 431–434.
Borst, J.G., Helmchen, F., Sakmann, B., 1995. Pre- and postsynaptic whole-cell recordings in the medial nucleus of the trapezoid body of the rat. J. Physiol. 489 (Pt 3), 825–840.
Burke, P.G., Abbott, S.B., Coates, M.B., Viar, K.E., Stornetta, R.L., Guyenet, P.G., 2014. Optogenetic stimulation of adrenergic C1 neurons causes sleep state-dependent cardiorespiratory stimulation and arousal with sighs in rats. Am. J. Respir. Crit. Care Med. 190, 1301–1310.
Butler, J.E., Hudson, A.L., Gandevia, S.C., 2014. The neural control of human inspiratory muscles. Prog. Brain Res. 209, 295–308.
Buttry, J.L., Goshgarian, H.G., 2015. WGA-Alexa transsynaptic labeling in the phrenic motor system of adult rats: intrapleural injection versus intradiaphragmatic injection. J. Neurosci. Methods 241, 137–145.
Cregg, J.M., Chu, K.A., Hager, L.E., Maggard, R.S.J., Stoltz, D.R., Edmond, M., Alilain, W.J., Philippidou, P., Landmesser, L.T., Silver, J., 2017. A latent propriospinal network can restore diaphragm function after high cervical spinal cord injury. Cell Rep. 21, 654–665.
Decima, E.E., von Euler, C., Thoden, U., 1967. Spinal intercostal-phrenic reflexes. Nature 214, 312–313.
DiMarco, A.F., Kowalski, K.E., 2013. Activation of inspiratory muscles via spinal cord stimulation. Respir. Physiol. Neurobiol. 189, 438–449.
DiMarco, A.F., Altose, M.D., Cropp, A., Durand, D., 1987. Activation of the inspiratory intercostal muscles by electrical stimulation of the spinal cord. Am. Rev. Respir. Dis. 136, 1385–1390.
DiMarco, A.F., Connors, A.F., Kowalski, K.E., 2004. Gas exchange during separate diaphragm and intercostal muscle breathing. J. Appl. Physiol. 96, 2120–2124, (1985).
Dobbins, E.G., Feldman, J.L., 1994. Brainstem network controlling descending drive to phrenic motoneurons in rat. J. Comp. Neurol. 347, 64–86.
Duffin, J., Iscoe, S., 1996. The possible role of C5 segment inspiratory interneurons investigated by cross-correlation with phrenic motoneurons in decerebrate cats. Exp. Brain Res. 112, 35–40.
Ellenberger, H.H., Feldman, J.L., 1988. Monosynaptic transmission of respiratory drive to phrenic motoneurons from brainstem bulbospinal neurons in rats. J. Comp. Neurol. 269, 47–57.
Ellenberger, H.H., Vera, P.L., Haselton, J.R., Haselton, C.L., Schneiderman, N., 1990. Brainstem projections to the phrenic nucleus: an anterograde and retrograde HRP study in the rabbit. Brain Res. Bull. 24, 163–174.
Fuller, D.D., 2017. Spinal Decision Making for Respiratory Muscle Recruitment?, (J Physiol).
Fuller, D.D., Johnson, S.M., Olson, E.B., Mitchell, G.S., 2003. Synaptic pathways to phrenic motoneurons are enhanced by chronic intermittent hypoxia after cervical spinal cord injury. J. Neurosci. 23, 2993–3000.
Gaunt, R.A., Prochazka, A., Mushahwar, V.K., Guevremont, L., Ellaway, P.H., 2006. Intraspinal microstimulation excites multisegmental sensory afferents at lower stimulus levels than local alpha-motoneuron responses. J. Neurophysiol. 96, 2995–3005.
Giszter, S.F., Mussa-Ivaldi, F.A., Bizzi, E., 1993. Convergent force fields organized in the frog's spinal cord. J. Neurosci. 13, 467–491.
Goshgarian, H.G., Rafols, J.A., 1981. The phrenic nucleus of th albino rat: a correlative HRP and Golgi study. J. Comp. Neurol. 201, 441–456.
Gustafsson, B., Jankowska, E., 1976. Direct and indirect activation of nerve cells by electrical pulses applied extracellularly. J. Physiol. 258, 33–61.
Hayashi, F., Fukuda, Y., 1995. Electrophysiological properties of phrenic motoneurons in adult rats. Jpn. J. Physiol. 45, 69–83.
Hayashi, F., Hinrichsen, C.F., McCrimmon, D.R., 2003. Short-term plasticity of descending synaptic input to phrenic motoneurons in rats. J. Appl. Physiol. 94, 1421–1430.
Hilaire, G., Khatib, M., Monteau, R., 1986. Central drive on Renshaw cells coupled with phrenic motoneurons. Brain Res. 376, 133–139.
Hudson, A.L., Gandevia, S.C., Butler, J.E., 2017. Task-Dependent Output of Human Parasternal Intercostal Motor Units Across Spinal Levels, (The Journal of Physiology).
Jankowska, E., Roberts, W.J., 1972. An electrophysiological demonstration of the axonal projections of single spinal interneurones in the cat. J. Physiol. 222, 597–622.
Kanbar, R., Stornetta, R.L., Cash, D.R., Lewis, S.J., Guyenet, P.G., 2010. Photostimulation of Phox2b medullary neurons activates cardiorespiratory function in conscious rats. Am. J. Respir. Crit. Care Med. 182, 1184–1194.
Kasten, M.R., Sunshine, M.D., Secrist, E.S., Horner, P.J., Moritz, C.T., 2013. Therapeutic intraspinal microstimulation improves forelimb function after cervical contusion injury. J. Neural Eng. 10.
Kirkwood, P.A., Munson, J.B., Sears, T.A., Westgaard, R.H., 1988. Respiratory interneurones in the thoracic spinal cord of the cat. J. Physiol. 395, 161–192.
Lane, M.A., White, T.E., Coutts, M.A., Jones, A.L., Sandhu, M.S., Bloom, D.C., Bolser, D.C., Yates, B.J., Fuller, D.D., Reier, P.J., 2008. Cervical prephrenic interneurons in the normal and lesioned spinal cord of the adult rat. J. Comp. Neurol. 511, 692–709.
Lane, M.A., Lee, K.Z., Fuller, D.D., Reier, P.J., 2009. Spinal circuitry and respiratory recovery following spinal cord injury. Respir. Physiol. Neurobiol. 169, 123–132.
Lee, K.Z., Fuller, D.D., 2011. Neural control of phrenic motoneuron discharge. Respir. Physiol. Neurobiol. 179, 71–79.
Lemay, M.A., Grill, W.M., 2004. Modularity of motor output evoked by intraspinal microstimulation in cats. J. Neurophysiol. 91, 502–514.
Levine, S., Nguyen, T., Taylor, N., Friscia, M.E., Budak, M.T., Rothenberg, P., Zhu, J., Sachdeva, R., Sonnad, S., Kaiser, L.R., Rubinstein, N.A., Powers, S.K., Shrager, J.B., 2008. Rapid disuse atrophy of diaphragm fibers in mechanically ventilated humans. N. Engl. J. Med. 358, 1327–1335.
Ling, L., Bach, K.B., Mitchell, G.S., 1995. Phrenic responses to contralateral spinal stimulation in rats: effects of old age or chronic spinal hemisection. Neurosci. Lett. 188, 25–28.
Lipski, J., Duffin, J., 1986. An electrophysiological investigation of propriospinal inspiratory neurons in the upper cervical cord of the cat. Exp. Brain Res. 61, 625–637.
Lois, J.H., Rice, C.D., Yates, B.J., 2009. Neural circuits controlling diaphragm function in the cat revealed by transneuronal tracing. J. Appl. Physiol. 106, 138–152.
Mantilla, C.B., Zhan, W.Z., Sieck, G.C., 2009. Retrograde labeling of phrenic motoneurons by intrapleural injection. J. Neurosci. Methods 182, 244–249.
Marchenko, V., Ghali, M.G., Rogers, R.F., 2015. The role of spinal GABAergic circuits in the control of phrenic nerve motor output. Am. J. Physiol. Regul. Integr. Comp. Physiol. 308, R916–926.
McDonald, J.W., Becker, D., Sadowsky, C.L., Jane, J.A., Conturo, T.E., Schultz, L.M., 2002. Late recovery following spinal cord injury. Case report and review of the literature. J. Neurosurg. 97, 252–265.
McPherson, J.G., Miller, R.R., Perlmutter, S.I., 2015. Targeted, activity-dependent spinal stimulation produces long-lasting motor recovery in chronic cervical spinal cord injury. Proc. Natl. Acad. Sci. U. S. A. 112, 12193–12198.
Meinrenken, C.J., Borst, J.G., Sakmann, B., 2003. Local routes revisited: the space and time dependence of the Ca2 + signal for phasic transmitter release at the rat calyx of Held. J. Physiol. 547, 665–689.
Mercier, L.M., Gonzalez-Rothi, E.J., Streeter, K.A., Posgai, S.S., Poirier, A.S., Fuller, D.D., Reier, P.J., Baekey, D.M., 2017. Intraspinal microstimulation and diaphragm activation after cervical spinal cord injury. J. Neurophysiol. 117, 767–776.
Merrill, E.G., Fedorko, L., 1984. Monosynaptic inhibition of phrenic motoneurons: a long descending projection from Bötzinger neurons. J. Neurosci. 4, 2350–2353.
Merrill, E.G., Lipski, J., 1987. Inputs to intercostal motoneurons from ventrolateral medullary respiratory neurons in the cat. J. Neurophysiol. 57, 1837–1853.
Moritz, C.T., Lucas, T.H., Perlmutter, S.I., Fetz, E.E., 2007. Forelimb movements and muscle responses evoked by microstimulation of cervical spinal cord in sedated monkeys. J. Neurophysiol. 97, 110–120.
Mushahwar, V.K., Horch, K.W., 1998. Selective activation and graded recruitment of functional muscle groups through spinal cord stimulation. Ann. N. Y. Acad. Sci. 860, 531–535.
Mushahwar, V.K., Collins, D.F., Prochazka, A., 2000. Spinal cord microstimulation generates functional limb movements in chronically implanted cats. Exp. Neurol. 163, 422–429.
Mushahwar, V.K., Gillard, D.M., Gauthier, M.J., Prochazka, A., 2002. Intraspinal micro stimulation generates locomotor-like and feedback-controlled movements. IEEE Trans. Neural Syst. Rehabil. Eng. 10, 68–81.
Nashold Jr, B.S., Friedman, H., Grimes, J., 1981. Electrical stimulation of the conus medullaris to control the bladder in the paraplegic patient. A 10-year review. Appl. Neurophysiol. 44, 225–232.
Nishimura, Y., Perlmutter, S.I., Fetz, E.E., 2013. Restoration of upper limb movement via artificial corticospinal and musculospinal connections in a monkey with spinal cord injury. Front. Neural. Circuits. 7, 57.
Onders, R.P., Elmo, M., Khansarinia, S., Bowman, B., Yee, J., Road, J., Bass, B., Dunkin, B., Ingvarsson, P.E., Oddsdóttir, M., 2009. Complete worldwide operative experience in laparoscopic diaphragm pacing: results and differences in spinal cord injured patients and amyotrophic lateral sclerosis patients. Surg. Endosc. 23, 1433–1440.

Overduin, S.A., d'Avella, A., Carmena, J.M., Bizzi, E., 2014. Muscle synergies evoked by microstimulation are preferentially encoded during behavior. Front. Comput. Neurosci. 8, 20.

Padmanabhan, R., Singh, S., 1979. Observations on the topographical relations of spinal nerve roots in the rat. Acta Anat. (Basel) 105, 378–380.

Palisses, R., Viala, D., 1987. Existence of respiratory interneurons in the cervical spinal cord of the rabbit. C. R. Acad. Sci. III 305, 321–324.

Remmers, J.E., 1973. Extra-segmental reflexes derived from intercostal afferents: phrenic and laryngeal responses. J. Physiol. 233, 45–62.

Sandhu, M.S., Baekey, D.M., Maling, N.G., Sanchez, J.C., Reier, P.J., Fuller, D.D., 2015. Midcervical neuronal discharge patterns during and following hypoxia. J. Neurophysiol. 113, 2091–2101.

Saywell, S.A., Ford, T.W., Meehan, C.F., Todd, A.J., Kirkwood, P.A., 2011. Electrophysiological and morphological characterization of propriospinal interneurons in the thoracic spinal cord. J. Neurophysiol. 105, 806–826.

Sears, T.A., 1964. The slow potentials of thoracic respiratory motoneurones and their relation to breathing. J. Physiol. 175, 404–424.

Smuder, A.J., Gonzalez-Rothi, E.J., Kwon, O.S., Morton, A.B., Sollanek, K.J., Powers, S.K., Fuller, D.D., 2016. Cervical spinal cord injury exacerbates ventilator-induced diaphragm dysfunction. J. Appl. Physiol. 120, 166–177, (1985).

Streeter, K., Sunshine, M., Patel, S., Reier, P., Baekey, D., Fuller, D., 2017. Intermittent Hypoxia Enhances Connectivity Between Cervical Spinal Interneurons, (in prep).

Streeter, K.A., Sunshine, M.D., Patel, S.R., Liddell, S.S., Denholtz, L.E., Reier, P.J., Fuller, D.D., Baekey, D.M., 2017. Coupling multielectrode array recordings with silver labeling of recording sites to study cervical spinal network connectivity. J. Neurophysiol. 117, 1014–1029.

Sun, F.T., Morrell, M.J., 2014. Closed-loop neurostimulation: the clinical experience. Neurotherapeutics 11, 553–563.

Sunshine, M.D., Cho, F.S., Lockwood, D.R., Fechko, A.S., Kasten, M.R., Moritz, C.T., 2013. Cervical intraspinal microstimulation evokes robust forelimb movements before and after injury. J. Neural Eng. 10.

Tresch, M.C., Bizzi, E., 1999. Responses to spinal microstimulation in the chronically spinalized rat and their relationship to spinal systems activated by low threshold cutaneous stimulation. Exp. Brain Res. 129, 401–416.

Troyk, P.R., Mushahwar, V.K., Stein, R.B., Suh, S., Everaert, D., Holinski, B., Hu, Z., DeMichele, G., Kerns, D., Kayvani, K., 2012. An implantable neural stimulator for intraspinal microstimulation. In: Conference proceedings: Annual International Conference of the IEEE Engineering in Medicine and Biology Society. pp. 900–903, (IEEE Engineering in Medicine and Biology Society. Annual Conference 2012).

Yi-Kai Lo, C.-W.C., Kuan, Yen-Cheng, Culaclii, Stanislav, Kim, Brian, Chen, Kuanfu, Gad, Parag, Reggie Edgerton, V., Liu, Wentai, 2016. A 176-Channel 0.5 cm3 0.7 g wireless implant for motor function recovery after spinal cord injury. In: IEEE International Solid-State Circuits Conference.

Zimmermann, J.B., Jackson, A., 2014. Closed-loop control of spinal cord stimulation to restore hand function after paralysis. Front. Neurosci. 8, 87.

Plasticity and Activation of Spared Intraspinal Respiratory Circuits Following Spinal Cord Injury

W81XWH-14-1-0625 (UNCLASSIFIED)
SC120209

PI: Paul J. Reier, Ph.D. **Org:** University of Florida Coll. Med. and McKnight Brain Institute **Total Award Amount:** $415,556.23

Study/Product Aim(s)

- **Aim 1:** To determine whether physiologically-based ISMS (intraspinal microstimulation) below a C3/4 lateralized contusion or C2 hemisection will enhance the respiratory activity of PhMNs and the diaphragm.
- **Aim 2:** To demonstrate with neuroanatomical and electrophysiological methods that patterned electrical stimulation of spinal circuitry, caudal to the site of injury, will promote altered connectivity in conjunction with changes in PhMN and diaphragm function.

Approach

This project is to assess the effects of epidural stimulation vs. ISMS on phrenic motoneuron/diaphragm function and phrenic circuit connectivity following cervical spinal cord injury. Terminal electrophysiological experiments will first be performed to map the phrenic motor circuit in rats 1-2 months post C3/4 contusions using microarray assemblies. Terminal electrophysiological comparisons will then be obtained of epidural and ISMS stimulation on activation of the phrenic motor circuit after chronic C2 hemisection (C2Hx; one month post-SCI). The studies will then move to in vivo tests following C2Hx and C3/4 contusions. ISMS will entail open- and closed-loop stimulation.

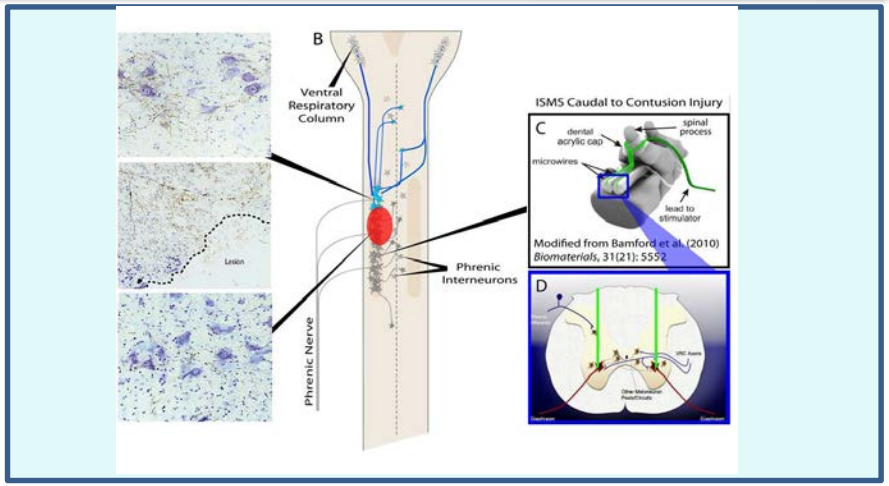

Illustrated here is the overall goal of the project testing spinal stimulation on recovery of diaphragm function following interruption of descending respiratory drive pathways to the phrenic nucleus.

Timeline and Cost

Activities CY	15	16	17	
Administrative Task 1				
Major Tasks 1-5				
Major Tasks 6-11				
Estimated Budget ($K)	**$174***	**$175***	**EWOF**	

* Direct Cost

Current Budget Report Interval: 10/16/2015 – 1-15-2017

Goals/Milestones:

CY15 Goal –

- ☐ Admin. Task 1: obtain IACUC and ACURO approvals
- ☐ Major Tasks 1-2: To map phrenic circuit discharge patterns following a C3/4 lateralized contusion injury and terminal electrophysiological comparison of epidural stimulation and ISMS after chronic C2 hemisection
- ☐ Major Task 3: Analysis of Tissue Responses to Microwire Implantation
- ☐ Major Task 4: Prepare for respiratory studies
- ☐ Major Task 5: Phase I of closed-loop intraspinal stimulation of phrenic motor neurons (PhMNs) after C2Hx.

CY16 Goal –

- ☐ Major Tasks 6-11: Open- and closed loop studies in spinal-contused rats. Replication of most promising stimulation approach with follow up neuroanatomical studies.

Comments/Challenges/Issues/Concerns

- Given the labor-intensive nature of this project, the scope of the work had to be reduced. An EWOF also was necessary, and the last Major Tasks are now being pursued under another funding mechanism.
- Several publications have nonetheless emerged from this work.

Budget Expenditure as of 4-13-2017

Cumulative TDC expenditures: $342,078.82 (including U.Wash. Subcontract)